

Implementation of Novel Technologies in HTPD

(Bio-) 3D-Printing and Microfluidics

zur Erlangung des akademischen Grades eines
DOKTORS DER INGENIEURWISSENSCHAFTEN (Dr.-Ing.)

der Fakultät für Chemieingenieurwesen und Verfahrenstechnik des
Karlsruher Instituts für Technologie (KIT)

genehmigte
DISSERTATION

von
Dipl.-Ing. Carsten Philipp Radtke
aus Karlsruhe

Referent: Prof. Dr. Jürgen Hubbuch

Korreferent: Prof. Dr. Matthias Franzreb

Tag der mündlichen Prüfung: 26.01.2018



This document is licensed under a Creative Commons Attribution-ShareAlike 4.0 International License (CC BY-SA 4.0): <https://creativecommons.org/licenses/by-sa/4.0/deed.en>

CHAPTER 1

Abstract

The investigation of complex interactions and the multitude of influencing parameters in biotechnological processes requires a huge number of single experiments. To increase the amount of information gained from the available sample volume, approaches of miniaturizing the investigated unit operations are developed. Also the time invested in experimentation is reduced by parallelized procedures and the manual effort is drastically decreased by the application of robotic instrumentation such as liquid-handling stations (LHS). LHS are widely used tools in the field of bioprocess development. Their ability of automated handling of liquids and miniaturized reaction vessels (e.g. multiwell plates) enables high-throughput screening of a variety of experimental conditions. These miniaturized, parallelized and automated investigations are a central element of high-throughput process development (HTPD) and are well-established in biotechnological research in academia as well as in industry.

Only recently the established process development has been further improved by new concepts. These include e.g. *in silico* approaches for the automated data handling and the modeling of processes as well as the reorganization of workflows and unit operations. However, for the generation of innovative approaches and their fast integration into process development, novel technologies are to be implemented in HTPD.

The scope of this thesis is to broaden the ambit of LHS as toolbox for process development. For this purpose, new technological strategies are to be combined and integrated in automated experimental workflows on LHS. A key element in this work is the application of 3D-printing techniques. 3D-printing is defined as the layerwise built-up of three dimensional objects. Currently, multiple printing techniques are available with a huge amount of different printing materials. The availability of 3D-printer in the entry-level segment and furthermore the possibility of ordering 3D-printed parts from service providers opens a broad circle of users access to 3D-printing. The simple usability in comparison with conventional fabrication methods allows also laypersons the fast realization of technical concepts. This strategy is most commonly referred to as rapid prototyping.

In this thesis, rapid prototyping was used to develop new approaches for the implementation of microfluidics and bioprinting in LHS-based high-throughput experimentation. In the first part, the applicability of the 'microfluidics-on-liquid handling station' (μ F-on-LHS) system for different biotechnological areas was investigated. This system has been developed as a preparatory work for this dissertation. It combines the advantages of experiments

executed in microfluidic channels with the automated workflow of a LHS.

The μ F-on-LHS system was further developed and now covers an analytic bottleneck in the biopharmaceutical development. In LHS-based experimentation, the method of choice for qualitative and quantitative analysis of samples are absorption measurements. Due to the detection limits of the integrated spectrophotometers, the sample concentration has to be adapted which demands error-prone dilution steps. To overcome this issue of error and to simplify the measurement, a disposable microfluidic device was designed allowing the absorption measurements of protein solutions in a concentration range from 0.1 to 100 mg/mL in a high-throughput format. Each of the 96 channels of one device consists of four measurement chambers with distinct channel height, increasing from 100 to 1500 μ m. This setup enables a four point measurement of 36 μ L samples with various optical path lengths for the direct calculation of calibration curves and the determination of protein concentrations. The device was validated according to ICH-guidelines and the applicability was demonstrated by its integration in a microscale chromatography screening performed on a LHS. The developed microfluidic device will simplify process development and increase the process robustness.

The second example for the application of the μ F-on-LHS system covers the field of chemical synthesis. Here, the advantageous application of microfluidic flow-through experiments performed on LHS was shown for the fabrication of polymer nanoparticles. The photopolymerization of miniemulsions is a promising approach for the production of nanoparticles and nanocapsules from biofunctional polymers. Miniemulsions provide mild reaction conditions for sensitive biomaterials and monomer droplets of a miniemulsion behave as separate reaction compartments. However, the targeted total monomer conversion depends on many influencing factors. The developed microfluidic device allows the screening of these factors in an automated screening procedure. In a design of experiments approach, the influence on the monomer conversion was investigated by varying miniemulsion compositions and irradiation conditions. This resulted in the classification of cause variables in a large parameter space with only small sample consumption.

The connectivity of the μ F-on-LHS system with other microfluidic approaches was demonstrated by the integration of microfluidic biofilm flowcells in a fully automated procedure. This platform was applied for the execution of fluorescence *in situ* hybridization (FISH) as well as catalyzed reporter deposition fluorescence *in situ* hybridization (CARD-FISH). These methods are powerful tools for the identification of single species in complex microbial communities as is present in biofilms. Custom made cartridges enabled the processing of up to nine flowcells in parallel. Besides the automated execution of every process step of the CARD-FISH protocol, also a semi-quantitative read-out of the fluorescence signal of the stained species was established. The procedure was successfully applied to single- and mixed-species biofilms of *E. coli* and *B. subtilis*. The repeatability and reproducibility was enhanced and the required manual work was significantly reduced which increases the possible throughput of cultivation flowcells in one working day.

The second part of this work describes the linkage of the three dimensional printing of biomaterials and biocompatible materials, referred to as bioprinting, and automated screening procedures on LHS. For this, different printing techniques were investigated

regarding their applicability in the production of multiwell plate compatible three dimensional hydrogel structures. The integration of these structures in multiwell plates enables their implementation in automated experiments executed by LHS. This strategy allows for high-throughput investigations of various printing materials and their effect on the interactions between the different components of the bioinks with the liquid surroundings.

The driving force behind bioprinting is the vision of printing spare parts for the human body which is referred to as tissue engineering. The research in this field demands strict requirements to the printing devices applied. For example, the devices have to be operated in sterile conditions and simple first printing trials are mostly hard to execute due to stringent operation regimentation. These circumstances hamper the application spectrum of bioprinting techniques in research areas besides tissue engineering. To overcome this shortcoming, entry-level bioprinting devices are a promising approach. As such devices are not commercially available, one aim of this thesis was the construction and establishment of an entry-level device capable of extrusion-based bioprinting. This was achieved by the modification of a conventional fused filament fabrication printer. The open source pedigree of this printer allowed the fast adaption of customized extension parts which were partly fabricated by the printer itself. Besides the construction of a syringe extrusion unit and the replacement of the original wooden housing parts with custom-fit acrylic glass parts, an user friendly user interface was established to simplify the control of the printer and the printing process. This setup is capable of printing simple geometrical structures into the wells of multiwell plates and, furthermore, the fabrication of more complex 3D-structures. Printing in multiwell plates is a prerequisite for the implementation of bioprinted structures in HTPD. The feasibility of the concept was demonstrated by the execution of a biocatalysis case study on a LHS. For this purpose, a two step printing procedure was applied to encapsulate the enzyme β -galactosidase in hollow hydrogel cylinders which were directly fabricated in multiwell plates. Subsequently, an activity assay of the encapsulated enzyme was executed and analyzed on a LHS. Thus, optimal parameters for a hydrogel-based β -galactosidase process could be determined, which is an important step towards the use of functional hybrid materials in biocatalysis. It was shown that the presented device allows a simple first access to bioprinting and bioprinting materials and opens new ways in process development by the implementation of bioprinted structures in high-throughput approaches.

Bioprinted structures are also applied as carrier modules for controlled drug-delivery. Thereby, the uptake and release kinetics of the drug molecule is affected by the physical and chemical properties of the printed structures, the utilized materials and the condition of the surrounding liquid. To investigate these interrelations, a screening procedure was established. For the fabrication of multiwell compatible bioprinted structures, a stereolithography-based 3D-printer was applied. Stereolithography is the spatially controlled photopolymerization of low viscous precursor solutions. To establish bioprinting with an entry-level stereolithography printer, the ideal adjustment of bioink composition and printing parameters have been investigated. This allowed the fabrication of hollow hydrogel cylinders of various compositions which could be placed in the wells of a 48 well plate. These structures were examined with regard to their uptake and release behavior

under varying buffer conditions in a LHS-based screening procedure. Lysozyme was used as model substance. The resulting pH and salt dependent uptake and release profiles showed the successful application of this concept. The presented setup provides another beneficial approach for the implementation of bioprinted structures in automated screening procedures for the support of bioprinting material development.

In summary, it can be said that technological approaches for the advantageous combination of microfluidics and bioprinting with LHS have been established and thoroughly investigated in this work. The μ F-on-LHS system has been successfully integrated into automated procedures for various applications. A microfluidic chip has been developed that eliminates a bottleneck in the concentration determination in bioprocess development. Furthermore, the performance of flow-through polymerization experiments in combination with statistical experimental design in the field of chemical synthesis has been established. In addition, the μ F-on-LHS system has been further developed and expanded and now allows the automated analysis of biofilms by FISH. Besides that, structures fabricated using bioprinting techniques were successfully integrated into HTPD. Two different printing techniques have been established for the production of these structures. The suitability of this concept has been demonstrated for biocatalysis and drug-delivery case studies. The technologies developed offer new powerful approaches to extend the range of applications for the development of future-proof LHS-based high-throughput processes.

CHAPTER 2

German Abstract - Zusammenfassung

Die Untersuchung komplexer Wechselwirkungen und einer Vielzahl von Einflussgrößen in biotechnologischen Prozessen erfordert zahlreiche Einzelversuchen. Durch Miniaturisierung der gängigen einzelnen Prozessschritte wird die Menge an Informationen die aus dem verfügbaren Probenvolumen gewonnen werden kann gesteigert. Mit dem Einsatz von Robotertechnik wie z. B. Liquid-Handling Stationen (LHS) wird der manuelle Aufwand drastisch reduziert. Der Einsatz von LHS ist in der Bioprozessentwicklung weit verbreitet. Sie ermöglichen die automatisierte Handhabung von Flüssigkeiten und miniaturisierten Reaktionsgefäßen (wie z. B. Multiwell-Platten) und erlauben somit das Hochdurchsatz-Screening einer Vielzahl experimenteller Bedingungen. Diese miniaturisierten, parallelisierten und automatisierten Untersuchungen sind ein zentrales Element der Hochdurchsatz-Prozessentwicklung (High-Throughput Process Development, HTPD) und sind in der biotechnologischen Forschung sowohl im akademischen Bereich als auch in der Industrie etabliert.

Erst in jüngster Zeit wird die bestehende Prozessentwicklung durch neue Konzepte weiter verbessert. Dazu gehören z. B. *in silico* Ansätze für die automatisierte Datenverarbeitung und die Prozessmodellierung sowie die Reorganisation von Arbeitsabläufen und Prozessschritten. Um innovative Ansätze und deren schnelle Einbindung in die Prozessentwicklung zu verwirklichen sollen neuartige Technologien in HTPD integriert und angewendet werden.

Der Fokus dieser Arbeit liegt daher in der Erweiterung des Anwendungsbereichs von LHS als Basis für die Prozessentwicklung. Dazu sollen neue technologische Strategien kombiniert und in automatisierte experimentelle Arbeitsabläufe auf LHS integriert werden. Ein Schlüsselement dieses Ansatzes ist die Anwendung von 3D-Drucktechniken. 3D-Druck ist definiert als der schichtweise Aufbau dreidimensionaler Objekte. Gegenwärtig stehen mehrere Drucktechniken mit einer Vielzahl von unterschiedlichen Druckmaterialien zur Verfügung. Die Verfügbarkeit von 3D-Druckern im Einstiegssegment und die Möglichkeit 3D-Druckteilen bei Dienstleistern zu bestellen ermöglicht einem breiten Nutzerkreis den Zugang zum 3D-Drucken. Die im Vergleich zu herkömmlichen Fertigungsmethoden einfache Bedienbarkeit von 3D-Druckern ermöglicht zudem auch Laien die schnelle Umsetzung von technischen Konzepten. Diese Strategie wird häufig als Rapid Prototyping bezeichnet.

In dieser Arbeit wird Rapid Prototyping verwendet, um neuen Ansätze zu entwickeln, welche die Einbindung von Mikrofluidik und Bioprinting in LHS-gestützte Hochdurchsatz-Experimente ermöglichen soll. Im ersten Teil dieser Arbeit wurde die Anwendbarkeit des

'microfluidics-on-liquid handling station' (μ F-on-LHS) Konzepts für verschiedene biotechnologische Bereiche untersucht. Dieses System wurde als Vorarbeit für diese Dissertation entwickelt. Es verbindet die Vorteile von Experimenten in mikrofluidischen Kanälen mit dem automatisierten Workflow von LHS.

Eine Weiterentwicklung des μ F-on-LHS Konzepts schließt eine analytische Lücke in der biopharmazeutischen Prozessentwicklung. In auf LHS durchgeführten Experimenten sind Absorptionsmessungen die Methode der Wahl für die qualitative und quantitative Analyse von Proben. Aufgrund der Detektionsgrenzen der integrierten Spektralphotometer muss die Probenkonzentration angepasst werden, was fehleranfällige Verdünnungsschritte erfordert. Um diese Fehlerquelle zu beseitigen und die Messung zu vereinfachen, wurde ein Einweg-Mikrofluidikchip entwickelt. Dieser Chip ermöglicht Absorptionsmessungen von Proteinlösungen in einem Konzentrationsbereich von 0.1 bis 100 mg/mL im Hochdurchsatzformat. Jeder der 96 Kanäle eines Chips besteht aus vier Messkammern mit unterschiedlicher Kanalhöhe, die zwischen 100 und 1500 μ m variieren. Dieser Aufbau ermöglicht eine Vier-Punkt-Messung einer Probe von 36 μ L mit mehreren optischen Weglängen für die direkte Erstellung von Kalibrierkurven und die Bestimmung von Proteinkonzentrationen. Der Chip wurde nach ICH-Richtlinien validiert und seine Anwendbarkeit wurde in einem miniaturisierten Chromatographie-Screening auf einer LHS nachgewiesen. Der entwickelte mikrofluidische Chip wird die Prozessentwicklung vereinfachen und die Robustheit der Prozesse erhöhen.

Das zweite Beispiel für die Anwendung des μ F-on-LHS Systems betrifft den Bereich der chemischen Synthese. Hier zeigte sich die vorteilhafte Anwendung der mikrofluidischen Experimente im Durchfluss auf LHS zur Herstellung von Polymer-Nanopartikeln. Die Photopolymerisation von Miniemulsionen ist für die Herstellung von Nanopartikeln und Nanokapseln aus biofunktionellen Polymeren ein vielversprechender Ansatz. Miniemulsionen bieten milde Reaktionsbedingungen für empfindliche Biomaterialien und die Monomertropfen einer Miniemulsion verhalten sich als separate Reaktionskompartimente. Die angestrebte vollständige Umwandlung des Monomers hängt jedoch von vielen Einflussfaktoren ab. Der entwickelte mikrofluidische experimentelle Aufbau ermöglicht das Screening dieser Faktoren in einem automatisierten Verfahren. Mit Hilfe statistischer Versuchsplanung wurde der Einfluss von unterschiedlichen Miniemulsionszusammensetzungen und Bestrahlungsbedingungen auf die Monomerumwandlung untersucht. Dieses Vorgehen erlaubte die Klassifizierung von Einflussgrößen in einem großen Parameterraum bei nur geringem Probenverbrauch.

Die Kompatibilität des μ F-on-LHS Systems mit anderen mikrofluidischen Methoden wurde durch die Integration von mikrofluidischen Biofilm-Flusszellen in ein vollautomatisches Verfahren gezeigt. Diese Kombination ermöglichte die automatisierte Durchführung der Fluoreszenz *in situ* Hybridisierung (FISH) sowie der 'catalyzed reporter' Fluoreszenz *in situ* Hybridisierung (CARD-FISH). Beide Methoden sind leistungsfähige Werkzeuge zur Identifizierung einzelner mikrobieller Spezies in komplexen Gemeinschaften, wie sie in Biofilmen vorkommen. Speziell angefertigte Transportkassetten ermöglichen die parallele Prozessierung von bis zu neun Flusszellen. Neben der automatisierten Ausführung aller Prozessschritte des (CARD)-FISH Protokolls wurde auch ein semi-quantitatives Auslesen

des Fluoreszenzsignals der angefärbten Proben etabliert. Das Verfahren wurde durch die automatisierte Durchführung von FISH-Experimenten mit Biofilmen bestehend aus nur einer oder mehrerer Spezies und anschließender Analyse mittels Fluoreszenzspektroskopie im integrierten Plattenleser validiert. Die Wiederholbarkeit und Reproduzierbarkeit wurde durch die Automatisierung gesteigert, gleichzeitig wurde der nötige manuelle Arbeitsaufwand stark reduziert.

Der zweite Teil dieser Arbeit beschreibt die Verknüpfung des dreidimensionalen Drucks von Biomaterialien und biokompatiblen Materialien, das so genannte Bioprinting, und automatisierte Screeningverfahren auf LHS. Hierzu werden verschiedene Drucktechniken auf ihre Anwendbarkeit bei der Herstellung von Multiwellplatten-kompatiblen dreidimensionalen Hydrogelstrukturen untersucht. Die Integration solcher Strukturen in Multiwellplatten ermöglicht deren Einbindung in automatisierte, von LHS durchgeführte Experimente. Diese Strategie ermöglicht die Hochdurchsatzuntersuchung von variablen Zusammensetzungen der Druckmaterialien als auch der umgebenden Flüssigkeit und die Auswirkungen dieser Variationen auf die Interaktionen zwischen den verschiedenen Komponenten der Biotinten.

Die treibende Innovationskraft hinter Bioprinting ist die Vision, Ersatzteile für den menschlichen Körper zu drucken, das so genannte Tissue Engineering. Die Forschung auf diesem Gebiet stellt hohe Anforderungen an die eingesetzten Druckgeräte. So müssen die Geräte z.B. steril betrieben werden und einfache Druckversuche sind aufgrund der strengen Betriebsvorschriften meist nur schwer durchführbar. Diese Umstände erschweren das Anwendungsspektrum von Bioprinting-Techniken in Forschungsgebieten neben dem Tissue Engineering. Bioprinting-Geräte im Einstiegssegment sind ein vielversprechender Ansatz um diesen Nachteil auszugleichen. Da solche Geräte nicht kommerziell erhältlich sind, waren der Aufbau und die Etablierung eines Einstiegsgerätes für den extrusionsgestützten Biodruck ein Ziel dieser Arbeit. Dies wurde durch den Umbau eines konventionellen Fused-Filament-Fabrication-Druckers erreicht. Der Open Source Gedanke auf dem der Drucker beruht ermöglichte die schnelle Adaption von speziell angefertigten Erweiterungsteilen, die zum Teil vom Drucker selbst hergestellt wurden. Neben dem Bau einer Extrusionseinheit und dem Austausch der originalen Holzgehäuseteile durch passgenaue Acrylglasteile wurde auch eine benutzerfreundliche Bedienoberfläche etabliert, um die Steuerung des Druckers und des Druckprozesses zu vereinfachen. Mit diesem Aufbau ist es möglich, einfache geometrische Strukturen in die Wells von Multiwellplatten zu drucken und auch komplexere 3D-Strukturen herzustellen. Durch den Druck in Multiwellplatten ist die Implementierung von Bio-3D-Strukturen in HTPD möglich. Die Umsetzbarkeit des Konzepts wurde durch die Durchführung einer Biokatalyse-Fallstudie auf einer LHS nachgewiesen. Zu diesem Zweck wurde ein zweistufiges Druckverfahren angewendet, um das Enzym β -Galactosidase in hohlen, direkt in Multiwellplatten hergestellten, Hydrogelzylindern zu verkapseln. Anschließend wurde ein Aktivitätsassay des verkapselten Enzyms auf einer LHS durchgeführt und analysiert. So konnten optimale Prozessparameter für einen Hydrogel basierten β -Galactosidase Prozess bestimmt werden. Dies ist ein wichtiger Schritt in Richtung der Verwendung von funktionellen Hybridmaterialien in der Biokatalyse. Somit wurde gezeigt, dass der entwickelte Drucker einen einfachen ersten Einstieg in Bioprinting und Biodruck-

materialien ermöglicht und durch die Implementierung von mit Bioprinting-Techniken gedruckte Strukturen in Hochdurchsatz-Experimente neue Wege in der Prozessentwicklung eröffnet.

Diese Bio-3D-Strukturen werden auch als Trägermatrizen für die kontrollierte Wirkstoffabgabe eingesetzt. Dabei wird die Aufnahme- und Freisetzungskinetik des Wirkstoffmoleküls durch die physikalischen und chemischen Eigenschaften der gedruckten Strukturen und die in der umgebenden Flüssigkeit herrschenden Bedingungen beeinflusst. Um diese Zusammenhänge genauer zu untersuchen wurde ein Screeningverfahren etabliert. Für die Herstellung von Multiwell-kompatiblen Hydrogel-Strukturen wurde bei dieser zweiten Studie ein Stereolithographiedrucker eingesetzt. Die Stereolithographie ist die räumlich gesteuerte Photopolymerisation niederviskoser Monomerlösungen. Um das Bioprinting mit einem Stereolithographiedrucker der Einstiegsklasse zu etablieren, wurde die ideale Abstimmung der Biotintenzusammensetzung und Druckparametern untersucht. Dies ermöglichte die Herstellung von hohlen Hydrogelzylindern, die in Wells einer 48 Well-Platte eingesetzt werden konnten. Diese Strukturen wurden in einem LHS-basierten Screeningverfahren auf ihr Aufnahme- und Freisetzungsverhalten unter unterschiedlichen Pufferbedingungen untersucht. Dabei diente Lysozym als Modellmolekül. Die resultierenden pH- und salzabhängigen Aufnahme- und Freisetzungsprofile zeigten die erfolgreiche Anwendung des entwickelten Verfahrens. Die hier vorgestellte Studie zeigt einen weiteren vorteilhaften Ansatz auf, welcher die Implementierung von mit Bioprinting-Techniken gedruckter Strukturen in automatisierte Screeningverfahren ermöglicht.

Zusammenfassend kann gesagt werden, dass in dieser Arbeit technologische Ansätze für die vorteilhafte Verknüpfung von Mikrofluidik und Bioprinting mit automatisierten LHS-Experimenten etabliert und eingehend untersucht wurden. Das $\mu\text{F-on-LHS}$ System wurde erfolgreich in automatisierte Verfahren für verschiedene Anwendungsbereiche integriert. Es wurde ein mikrofluidischer Chip entwickelt der den Engpass der Konzentrationsbestimmung in der Hochdurchsatz-Bioprozessentwicklung beseitigt. Weiterhin wurde die Durchführung von Polymerisationsexperimenten im Durchfluss in Kombination mit statistischer Versuchsplanung im Bereich der chemischen Synthese etabliert. Darüber hinaus wurde das System weiterentwickelt und erweitert und erlaubt nun die automatisierte Analyse von Biofilmen in mikrofluidischen Kultivierungschips durch FISH. Außerdem wurden mit Bioprinting-Techniken hergestellte Strukturen erfolgreich in die Hochdurchsatz-Prozessentwicklung integriert. Für die Herstellung dieser Strukturen wurden zwei verschiedene Drucktechniken etabliert. Die Eignung dieses Konzepts wurde für Biokatalyse- und Drug-Delivery-Fallstudien gezeigt.

Die entwickelten Technologien bieten neue leistungsfähige Ansätze, um das Anwendungsspektrum von LHS für die Entwicklung von zukunftsfähigen Hochdurchsatz-Prozessen zu erweitern.

Contents

1	Abstract	c
2	German Abstract - Zusammenfassung	g
3	Introduction	1
3.1	High-Throughput Experimentation	2
3.2	Microfluidics	4
3.3	The Microfluidics on Liquid-Handling Station System	5
3.4	3D-Printing	6
3.4.1	Conventional 3D-printing techniques	7
3.4.2	Bioprinting	7
4	Research proposal	11
5	Publications & Manuscripts	14
5.1	Implementation of a Microfluidic Device for the quantification of protein concentrations	16
5.2	Photoinitiated Miniemulsion Polymerization in Microfluidic Chips	34
5.3	Fully Automated Method for Fluorescence <i>in situ</i> Hybridization for Biofilm Analysis	56
5.4	The <i>Biomaker</i> : An entry-level bioprinting device for biotechnological applications	76
5.5	Assessment of hydrogels using a combination of 3D printing and high-throughput screening	94
6	Conclusion & Outlook	113
	Bibliography	115
	Appendix	144
A	Publications	144

CHAPTER 3

Introduction

The human urge to understand the processes in nature has always driven researchers and explorers to new findings. Universal scholars and specialists have accumulated a broad knowledge which nowadays can be imparted in schools and universities to educate the young scientists. This allows the training of specialized professionals with sound expertise. The research of these professionals lead to a deeper understanding and a high information density in their specific area. To increase the creativity and for the recognition of scientific gaps to bridge, a scientific exchange has to take place between the several disciplines. This interdisciplinary communication is able to address new challenges implied by scientific progress [1].

An example for a interdisciplinary research area is biotechnology. This area combines life sciences, like biology and chemistry, and the engineering principles like mathematics, material science and technical processes [2]. The aim of biotechnological research is not only to fully understand the processes of nature, but to make them technically feasible and usable. The adaptations of these processes are made on the macroscopic and microscopic level. The adapted processes are applied for the controlled production of specific molecules. These target molecules range from simple molecules [3–5] as well as complex biomolecules such as antibodies for biopharmaceutical use [6, 7]. An optimization of the production of these molecules can be achieved by the determination of ideal environmental growth and process conditions or by specific manipulations of lifelike processes and organisms [8]. The large multiplicity of possible conditions, variations and combinations engendered challenges hardly to be mastered with conventional lab work. In order to cope with increasing experimental effort, methods and technologies have been adapted and developed. Promising approaches to increase the throughput of samples and reactions have been found in the automation and parallelization of experiments and the reduction of the needed sample volume through miniaturization [9]. For this purpose, new devices have been developed which enable the implementation of these features in the experimental workflow.

In the following sections, the devices and techniques applied in this doctoral thesis for the execution of experiments are described. Besides the microwell plates, liquid-handling stations and microfluidics which allow automated and miniaturized experimentation also the combinatorial concept of μ F-on-LHS is introduced.

The lead time for the implementation of novel scientific concepts and their application is mostly long due to constructive effort. By adapting rapid prototyping technologies for the manufacturing of lab equipment, the time to application was significantly reduced [10, 11]. Rapid prototyping methods have contributed to the fast optimization and adaption of

laboratory equipment [12, 13]. By including biological or biocompatible materials in rapid prototyping production processes, new areas of biotechnology are explored. This approach was taken in biomedical research for the additive fabrication of hybrid materials and functional 3D-tissues [14]. The technological advances in bioprinting for tissue engineering in terms of methods, materials and devices have also inspired further biotechnological sectors to new, innovative applications. This includes the incorporation of algae [15] and bacterial cells [16] in bioprinting processes.

At the end of this chapter, an overview about 3D-printing and bioprinting is given. The application of these technologies is set into the context of this work.

3.1 High-Throughput Experimentation

In Hungary of the early 1950s, laboratory equipment was scarce and influenza broke out, which motivated Gyula Takácsy to develop novel laboratory tools. As reported by the Hungarian National Center for Epidemiology, the hungarian microbiologist Takácsy developed one of the first approaches on the replacement of separate reaction tubes. One of his developments is the first prototype of what will be known as multiwell plate or microplate. He prepared a piece of acrylic glass with 8 x 12 cavities for the simplified preparation of multiple simultaneous serial dilutions.[17] This invention was soon be adapted from other researchers and further developed [18]. With the production of disposable plates containing up to 96 cavities, the multiwell plate was available for researchers in large quantities. The possibility of parallel experimentation with a scaled-down sample volume accelerated the investigation and execution of various experiments. With the standardization of the well and plate dimensions promoted by the Society for Biomolecular Sciences (ANSI/SBS 1-2004 to ANSI/SBS 4-2004) the automated handling of these plates became possible [19].

The transfer and merging of liquids is one of the most essential tasks in life science research. In order to increase the throughput of experiments and minimize the manual effort, the handling of the microplates and further the handling of liquids had to be automated. To accomplish this purpose, liquid-handling stations (LHS) were developed which are able to process several thousands of samples. Such extensive test series are referred to as high-throughput screening (HTS) or high-throughput experimentation (HTE).[20]

The automated sample handling and the ability to mix and dilute liquid reagents in a broad volume range with a high reproducibility led to an intensified utilization of these LHS in various industrial and scientific procedures. The application of the LHS support rapid scientific progress for labour-intensive research projects, such as the human genome project [21, 22] or drug discovery [23]. In order to meet the increasingly complex requirements, the LHS can be expanded modularly. Robotic liquid handling arms with options up to 384 pipetting tips facilitate the integration of microplates with 384 and 1536 wells in automated processes. Various lab devices were implemented to enable more process steps to be automated and novel scale-down approaches have been developed to take advantage of the available potential offered by the LHS. The properties described here and the successful implementation of many process steps make the LHS a workhorse in bioprocess development and biotechnological research [20, 24]. In the following section, selected examples of HTE applications on LHS are described.

Applications of HTE in Bioprocess Development

The higher laboratory efficiency which was achieved by the execution of LHS-based high-throughput experimentation has led to the establishment of LHS as integral part in various research areas. Technical extensions which allow the manipulation of samples beyond the transfer of liquids extended the spectrum of applications. The sample preparation and processing was further automated by the integration of e.g. centrifuges, shaker platforms, tempering conditioning systems and filtration units in the automated workflows [20]. Furthermore, the integration of spectrophotometric plate readers allowed the simple and fast sample UV/Vis absorption based sample analysis. The benefits of automated sample processing were employed e.g. in biocatalysis research [25] and genomics [26]. One of the major application areas of LHS-based biochemical experimentation is in the high-throughput process development (HTPD) of the biopharmaceutical research. The flexibility of the LHS allowed the miniaturization of various process steps of pharmaceutical production including upstream, downstream and formulation operations [23, 27]. Huber et al. integrated a microscale cultivation device in a robotic platform to generate high-content data for biological production systems [28]. Furthermore, a combination with small-scale downstream procedures is possible. Such scale-down approaches have been developed for a variety of process steps. The published applications range from protein crystallization [29], precipitation [30] and refolding studies [31] to the investigation of alternative purification procedures like aqueous two-phase systems in microplate format [32, 33]. Investigations for chromatography-based purification were made in terms of resin screening studies [34, 35] and miniaturized chromatography procedures [36–38] as can be seen in figure 3.1. The reduced volume of samples required for a miniaturized experimental approach is ideal for the small amount of target molecules available in the early phase of drug discovery.

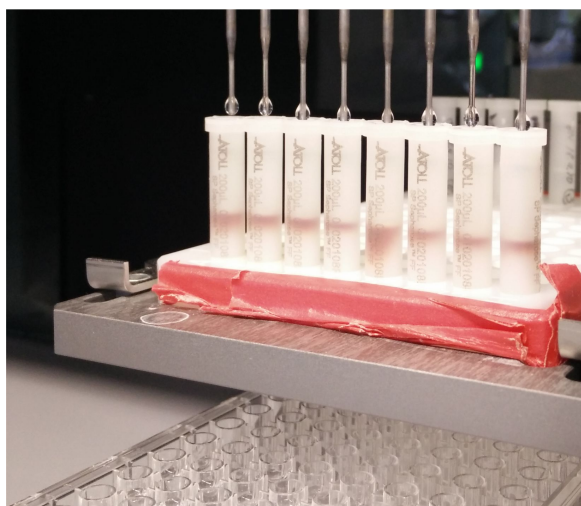


Figure 3.1: Microscale chromatography executed on a liquid-handling station

3.2 Microfluidics

Microfluidics is described as the manipulation of small volumes of liquid in the range from few microliters to even nanoliters. Comparable with the development and application of microplates, the technological development of microfluidics has also been driven by the need of an increased throughput with decreased sample consumption [39]. The assembly of microfluidic channels is called microfluidic chip or device. Through networks of these small channels, liquids are transported by active or passive pumping. The throughput of samples is increased by multiplexing or parallelization of channel systems. Thus, various assays and complex flows can be realized in microfluidic devices on compact space. The applications range from simple flow-through experiments to elaborate mixing tasks and single cell investigations.[40–42] The small scale of the channels implies changes in the fluid dynamics compared to the macro scale. In microfluidic systems a laminar flow is established. Due to the small channel diameters, turbulences which are difficult to control are avoided. The laminar flow also has the effect that the mixing of liquids is driven exclusively by diffusion. Additionally, it enables the generation of multiphase streams and droplets.[43] Operations like mixing or sorting are accomplished by the integration of special fluidic elements [44–46], microvalves and micropumps [47, 48].

For the fabrication of sophisticated microfluidic devices, a range of production techniques and materials are in use.[49, 50] The production techniques for these channel systems originally derived from the semiconductor industry and micro-electromechanical devices. With methods like etching and photolithography microfluidic channels were produced in glass and silicon parts.[51] With the rising demand of disposable devices, the fabrication in glass and silicon got too expensive. This led to the implementation of new materials and designs in the microfluidic device fabrication process [52–54]. Nowadays, silicone and other polymers are applied for the fabrication of microfluidic devices. The selection of techniques for the production include one-step and two-step manufacturing methods [49]. Also micromilling [55] and 3D-printing are applied for the production of casting molds as well as the direct fabrication of microfluidic devices [13, 56].

Microfluidic Applications in Life Science and Biotechnology

In the past, various microfluidic applications have been developed for biomedical and biological research and diagnostics [40, 41, 57]. The ability of precise fluid handling and flow-through applications have made microfluidics an alternative to conventional experimentation [58].

As already mentioned, the microfluidic research was driven by application in genomics like DNA synthesis [59] or flow-through PCR [60]. The size of microfluidic structures allows single cell investigations in stem cell research [61] just as studies of cell communities as in biofilms [62, 63]. The integration of cross-sections in the microfluidic networks allows the specific generation of droplets [64], which are used as microreactors [65] or cell vehicles [66]. Further, this droplet generation devices are applied for polymerization studies [67, 68]. The laminar flow behavior of fluids in microfluidic channels comes into effect by the generation of aqueous two-phase systems for the separation of cells [69–71] and proteins [72, 73]. Further protein separation approaches are investigated by the implementation of liquid

chromatography procedures on microfluidic devices [74].

Despite the great number of scientific publications on microfluidics, only a few microfluidic approaches have been developed beyond the proof-of-concept status and toward marketability [58, 75]. This commercialized approaches are for example lab-on-disk devices where transport and distribution of the liquids is controlled by centrifugal forces (Gyros xPlore™) and microfluidic capillary electrophoresis systems (PerkinElmer LabChip®).

3.3 The Microfluidics on Liquid-Handling Station System

Although few microfluidic-based applications have been commercialized, the breakthrough as standard method in industry and academia is still lacking. The available devices are designed for specific applications and microfluidic channel layouts. A common standard for an easy transfer and application of microfluidic methods is an ongoing topic of discussion [75–77]. Besides the standardization of connectivities, the integration in automated workflows is also a desirable feature [76, 78].

In preliminary works of this thesis, an approach of combining liquid-handling stations and microfluidic devices was developed [79]. This 'microfluidics on liquid-handling stations' system (μ F-on-LHS) enables the execution of microfluidic experiments by a LHS compatible interface (see figure 3.2).

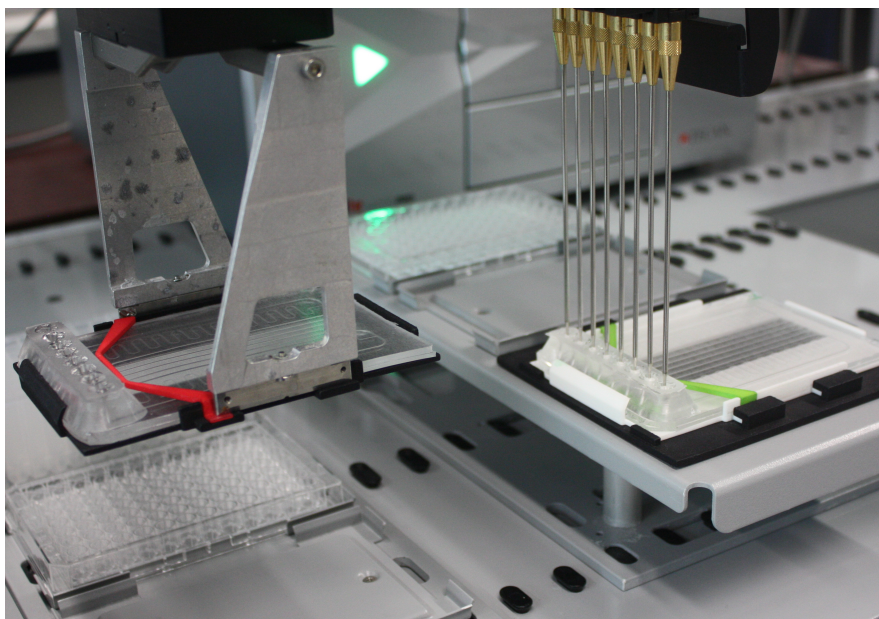


Figure 3.2: Photograph of μ F-on-LHS devices in an automated procedure on a liquid-handling station.

The peripheral equipment needed for microfluidic experiments like pumps, valves and control units is provided by the LHS. The dimensions of the used microfluidic devices are in agreement with the standard dimensions of microwell plates. Therefore, the chips can be transferred by the robotic manipulator arm and integrated functional devices such as integrated spectrophotometer can be part of the workflow. The microfluidic chips are

fabricated using silicone molding procedure [49]. The shape of the channel structures is defined by an replication master which can be freely adapted to the intended application. The connection of the LHS tips to the microfluidic channels is reversible, which allows the fully automated handling of the chips on the LHS.

3.4 3D-Printing

With the invention of the printing press by Johannes Gutenberg in 1440, a rapid and precise reproduction of letters, words and pictures became possible. For his invention, Gutenberg misused the already existing screwpress and adapted this machine to a new purpose. In the process of time, the printing press was continuously improved, modified and further adaptations to new emerging needs and developments were carried out. With the rising popularity of personal computers and inkjet printers since the middle of the 20th century, the creation and reproduction of texts and pictures could be accessed by the population at large. In the 1980s, similar to the approach of Gutenberg, scientists rededicated the known method of photopolymerization to an new application. They developed an apparatus for the build up of three-dimensional objects based on photopolymerization. With the patent of this apparatus filed by Chuck Hull in 1986, the era of additive manufacturing (AM), mostly referred as 3D-Printing, began [80]. AM describes manufacturing technologies which build up objects by layer-wise addition of material. On the contrary, traditional methods like milling, turning and drilling are now described as subtractive manufacturing. Within the umbrella term of additive manufacturing, in addition to stereolithography further techniques have been developed in the following years (see overview in section 3.4.1). In the case of 3D-printing, the expiry of patents and subsequently the dropping prices of 3D-printing machines drastically increased the popularity and number of employed 3D-printers in industrial, academic or private workshops.[81, 82]

At the moment, rapid prototyping is the most widely used application of 3D-printing. Thus, 3D-printed prototypes accelerate the development of the final product compared to conventional production or prototyping methods, like machining and injection molding. Furthermore, for small-batch production, customer-specific adjustments and manufacturing of functional pre-serial parts 3D-printing provides as an ideal fabrication technology, particularly because of the elimination of investments for tooling.[83, 84]

Due to these advantages of 3D-printing in comparison with other techniques a variety of industrial fields make use of 3D-printing [83, 85]. In medium-sized companies or in scientific laboratories 3D-printing is applied to supplement mechanical workshops.

The application of 3D-Printers for rapid prototyping tasks in the academic research has lead to improvements of existing technologies or methods (e.g. syringe pumps [86], custom bottle caps and multiwell plates [87], culture systems [88]). Furthermore, the production methods offered through 3D-printing support the development of novel scientific tools which are tough to realize with conventional methods [89, 90]. Through the free availability of computer-aided design (CAD) software and databases with 3D-files, online tutorials, the ever-growing 3D-printing community and the numerous specialized 3D-printing providers, everyone has access to 3D-printing.

3.4.1 Conventional 3D-printing techniques

In preparation for all printing techniques, a digital, three-dimensional file of the object to build has to be designed and further processed into thin layers. The thickness of the layers depends on the possible resolution of the 3D-printer. These layers are then translated in a command set which can be interpreted by the 3D-printer for the layer-by-layer conversion of the digital into a haptic model.

The first patented 3D-printing technology was stereolithography (SLA, see figure 3.3 middle). This technique is based on the light-induced polymerization of monomers. The light source for this applied photopolymerization can either be a laser (laser-based SLA) or a so called digital light processing unit like a projector (DLP-based SLA). Both systems have in common, that the directed light induces a spatial controlled polymerization of liquid photopolymer resin. This resin is provided in a vat in which a build platform is immersed. The resin-filled gap between the bottom of the vat and the build platform or the last build layer defines the layer height. The laser beam scans the image of the current layer to build and solidifies the shape of the model. [91]

A variation of this technique is the multi-jet modeling as depicted in figure 3.3 (bottom). Here, a print-head distributes the resin comparable to an inkjet process. The resin is UV-polymerized by passing light sources mounted on the print-head. [92, 93] In case of the binder jetting technology, not the material itself but a binder liquid is distributed by the print head. The defined application of binder onto layer-wise provided powder material generates the models [94].

Another fabrication technology for three-dimensional objects is selective laser sintering (SLS) [95]. Powder material is layer-wise piled up and melted by a laser. With this technique, also metal containing powders can be processed which enables the print of metal parts [96].

The most popular 3D-printing technique is the fused deposition modeling (FDM) or fused filament fabrication (FFF). With this method, melted thermoplastic material is extruded in several lines to build up every layer (see 3.3, top). The popularity of this technique is based upon the low prices for the printers and the printing material, but also the open-source pedigree and support through user-communities are a big advantage of FFF. As the concept printing procedure is very straightforward and allows a lot of tuning possibilities, a huge amount of various materials is available, including flexible, carbon fiber reinforced and metal or wood infused materials [97, 98].

3.4.2 Bioprinting

A particular application of 3D-printing techniques can be found in the field of bioprinting. The concept of bioprinting describes the coating or printing of biomaterials like cells or proteins, biocompatible materials or other biological relevant materials [99]. The bioprinting development was originally driven by the visionary idea of reproducing organs by 3D-printing techniques [100]. First steps were made by the modification of inkjet printers for the two dimensional patterning of biologically active components [101]. The build-up of three dimensional structures could be achieved by the modification of stereolithographic

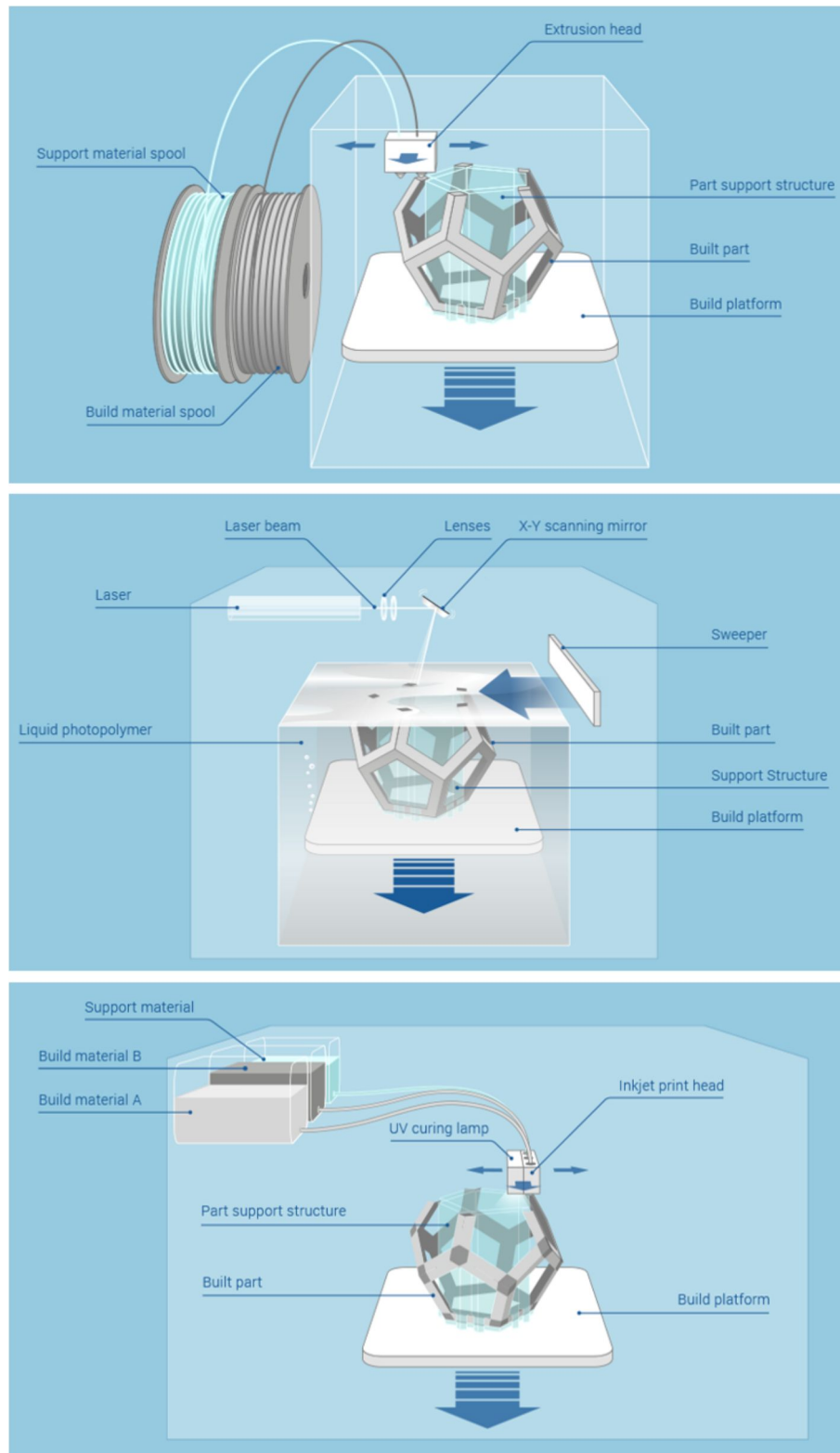


Figure 3.3: Schematic representation of the 3D-printing techniques fused filament fabrication, stereolithography and multi-jet modeling (from top to bottom, illustrations taken from: www.additively.com)

methods and the development of extrusion-based bioprinters. Most of the bioprinting research has been made in the fields of tissue engineering and regenerative medicine. The focus lies on the coordination of printing material and printing techniques for the production of complex structures able to mimic living tissues. The printed structures are applied for bone regeneration, transplantable tissues or as models for drug testing. The biological components are implemented directly in the printing material or are seeded afterwards on printed matrices. The challenge of a successful integration of sensitive biological material in the printing process is the preservation of the biological integrity of the components. This requires the provision of mild printing conditions with regard to material, printing environment and printing technique. Therefore, physical and chemical parameters like printing temperature, occurring shear stress and toxicity have to be considered. Malda et al. emphasized the adjustment of the printing parameters in the so called 'biofabrication window' to balance shape fidelity, stiffness and cell culture abilities [102]. The most applied techniques for bioprinting processes are deposition-based methods like inkjet and extrusion printing. The inkjet bioprinting techniques are adopted from conventional thermal or piezoelectric print heads. The printing material is forced through small orifices and low volume droplets are generated and deposited. [103, 104] The extrusion-based printing techniques were derived from paste extrusion instrumentation. Compressed air or piston generated pressure pushes the printing material through dispensing tips of varying geometrical dimensions [105]. An schematic representation of these techniques is shown in figure 3.4.

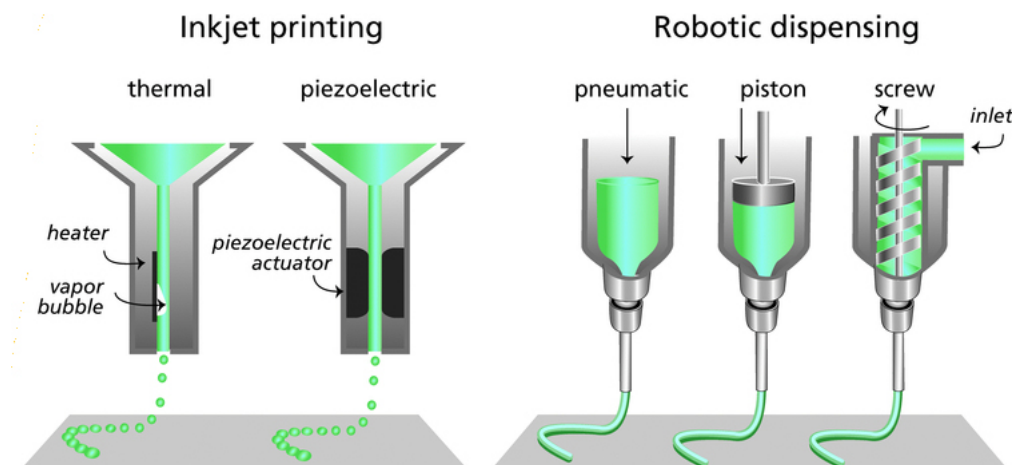


Figure 3.4: Deposition-based bioprinting methods for the fabrication of three dimensional structures of bioinks. Illustration adapted with permission. [102]

Commercially available bioprinter are most commonly equipped with several options for cell bioprinting like special print heads and cell-friendly environments. Since the variety of devices currently on the market is very small and these are in a very high price segment, there is an urgent need for flexible and inexpensive entry-level devices [106]. The beneficial application of these devices is seen in biotechnological research areas beyond tissue engineering. The reduced costs and comprehensible operational sequences eases the

access and lower the hurdle of device manipulation in comparison to costly commercial devices. Furthermore, by the reduction or even renunciation of the implementation of living cells in printing processes, entry-level bioprinting devices are a promising tool for an easy first access to bioprinting in research and education.

The materials used in bioprinting processes are mostly referred to as bioinks. The base component of bioinks are polymers or their precursors, some of which have already shown their suitability in other biotechnological applications like for example enzyme encapsulation or DNA and protein release studies [107–110]. Besides the basic material also biological components and auxiliary materials for the optimization of the printing process and the print results are added. For the incorporation of biological components in polymeric networks a high content of water is preferable to maintain biological activity by mimicking native environments. [102]

In the case of extrusion-based bioprinting, the use of hydrogels as printing material is well established. Hydrogels are biocompatible polymers that show the ability to absorb and retain large quantities of water within the network structures. Hydrogel networks generate a mechanical supportive environment [102]. Hydrogels are therefore suitable for providing mild conditions for encapsulated biological components whilst protecting them from harmful surroundings. The polymers used for the fabrication of hydrogels are either of natural or synthetic origin. The state of network stability is related to the cross-linking strategy. This allows the generation of reversible or covalently bonded networks structures, dependent on physical or chemical cross-linking.[110] Through the variation of bioink components and cross-linking strategies, the characteristics of precursor solutions and resulting polymeric networks are tuned [102, 107, 111]. Further porosity, swelling behavior and therefore diffusivity of the hydrogels can be tuned [110]. Setting up the right combination of printing device, bioink formulation and overall printing process is one of the major challenges in bioprinting [100].

CHAPTER 4

Research proposal

The process development in the biotechnological and chemical sector often requires labor intensive screening studies to optimize relevant parameters. Numerous independent experiments are needed to determine the optimal conditions for the individual process. However, the required manual work and time decreases the possible experimental throughput on a working day. Therefore, suitable automation of such operations is worthwhile to achieve in order to increase experimental throughput. Furthermore, the outcome of the methods, particularly of sensitive assays, would benefit from a good repeatability and comparability. To date, the automation of multiwell plate based assays can be readily accomplished by the use of commercially available and widely used liquid handling stations. However, beyond these well-established methods the degree of automation in biotechnological labs is still low.

Within the scope of this doctoral thesis, the implementation of applications from the interdisciplinary area of biotechnology into automated experimental workflows is investigated. The focus hereby lies on the development of techniques and processes by integrating the fields of microfluidics as well as 3D bioprinting to industrial relevant instrumentation.

The first goal, the automation of microfluidic experiments, should be achieved by adapting the concept of microfluidics on liquid handling stations (μ F-on-LHS). This μ F-on-LHS concept was developed in preliminary works to this thesis. The presented interface between microfluidic channels and the tips of a liquid handling station combines the advantages of both systems for flow through investigations in an automated experimental workflows. In order to demonstrate the broad applicability of this concept, examples from the field of material synthesis, microbiology and analysis in bioprocess development are to be investigated.

For various approaches in the biological or biochemical area biocompatible polymer networks are applied. The polymers provide functional surfaces or serve as encapsulation material for biological components. The size of the polymer structures range from monoliths in the range of few centimeters to particles in the nanometer range. One applied method for the generation of polymer nanoparticles is the photoinitiated polymerization of miniemulsions. The outcome of a polymerization process depends on the influence of several cause variables. The knowledge of the effects of these variables is essential for the production of tailor-made particles. A strategy for the systematical investigation of

these interdependencies is highly desirable. For the execution of the variables screening an automated process management and low sample consumption is beneficial. To enable reliable experimental workflows and the gaining of a large information quantity from one single batch of miniemulsion the concept of μ F-on-LHS is to be applied.

The study of complex multi-species biofilms is of interest not only in terms of caused issues in everyday life but also in terms of the potential benefits that may arise from their targeted integration in bioprocesses. For the deeper understanding of the interactions and processes taking place in biofilms, the identification of the species involved is a key factor. For this task, fluorescence *in situ* hybridization (FISH) is the method of choice in microbiological research. The FISH-procedure as well as the subsequent microscopic imaging are time- and work-consuming. The automation of this workflow is a worthwhile development towards better comparability of individual experiments with the additional benefit of less manual effort. The adaption of cultivation flowcells to the μ F-on-LHS interface is to perform to enable automated experimentation. Besides the automation of the diverse protocol steps also the quantitative fluorescence analysis of the processed flowcells in the integrated plate reader is to be investigated.

UV/Vis spectroscopy in plate readers plays a central role in bioprocess development. Here, the key factors of process control are the yield of the target molecule and the concentration of potential contaminants. The assessment of the performance of respective process steps is dependent on the quality of the analysis. The method of choice for qualification and quantification of these performance indicators is the spectrophotometric absorption measurement. The raising challenge for the employed device is the wide concentration range to be covered. Increasing titers in purification processes exceed the detection limits of conventional photometers. The available devices capable of this concentration range are either not high throughput compatible or need extra space for the implementation in automated workflows. Therefore, a tool is supposed to be developed which allows the absorption measurements of samples with reduced volumes and increased concentration range compared to microplate based measurements. Ideally, this tool is suitable for manual use as well as fully integratable in automated workflows with standard LHS equipment.

Besides the investigation of beneficial applications of the μ F-on-LHS in biotechnological context it is the aim of this work to investigate the integration of bioprinting techniques in automated screening procedures. Bioprinting is of increasing interest in the field of tissue engineering and regenerative medicine. However, the available bioprinter are cost intensive and complex which reduces the acceptance and their integration in other biotechnological areas. Beyond tissue engineering, 3D bioprinting offers the potential of enabling completely new approaches for biotechnology. By the systematical use of "nature's toolbox", novel application possibilities may be established beyond natural systems. The addressed topics are the integration of biocatalysts for artificial reaction cascades and the investigation of interactions between printed hydrogels and their liquid surrounding. Therefore, to access the possibilities of printable biology for the next generation of biotechnology new approaches have to be explored to adapt and modify conventional 3D printers for bioprinting. These

approaches shall enable entry-level access in bioprinting research. Furthermore strategies to integrate 3D-printed structures in automated screening studies in order to optimize relevant process parameters should be developed.

CHAPTER 5

Publications & Manuscripts

5.1 Implementation of an Analytical Microfluidic Device for the Quantification of Protein Concentrations in a High-Throughput Format16

This article presents a microfluidic device for the high-throughput compatible absorption measurements in a wide concentration range. The applicability of this device was shown in a miniaturized chromatography case study. The developed device provides a beneficial supplement in high-throughput process development on liquid-handling stations.

published in Engineering in Life Sciences (DOI: 10.1002/elsc.201500185)

5.2 Photoinitiated Miniemulsion Polymerization in Microfluidic Chips on Automated Liquid Handling Stations: Proof of Concept34

In this paper, the application of the μ F-on-LHS system for a flow-through miniemulsion photopolymerization study is presented. By means of a design of experiments approach, the affect of various parameters on the residual monomer content was investigated. This allowed for the determination finding of the ideal parameter combination for a total monomer conversion.

published in Engineering in Life Sciences (DOI: 10.1002/elsc.201500186)

5.3 Fully Automated Method for Fluorescence *in situ* Hybridization (FISH) for Biofilm Analysis.....56

This study describes the development of an automated execution of the FISH protocol for biofilms grown in microfluidic cultivation flowcells. Up to 9 flowcells in parallel can be handled on a liquid-handling station. Furthermore, the semi-quantitative read-out of fluorescence signals in the integrated plate reader was established.

original manuscript is edited and extended for a publication in a wider context

5.4 The *Biomaker*: An entry-level bioprinting device for biotechnological applications 76

This article presents an entry-level bioprinting device. This device is based on a conventional fused filament 3D printer and was modified for extrusion based bioprinting. This user friendly printer allows the structuring of bioinks in high-throughput compatible labware. Thus, a simple integration of bioprinted structures in automated screening experimentation is enabled.

published in Journal of Chemical Technology and Biotechnology (DOI: 10.1002/jctb.5429)

5.5 Assessment of hydrogels for biopharmaceutical purposes using a combination of 3D printing and high-throughput screening94

This manuscript describes the application of stereolithography for the three dimensional build-up of multiwell plate compatible hydrogel cylinders. These structures are then investigated on their interactions with the model protein lysozyme regarding uptake and release behaviour. The integration in automated workflows allows the screening of various influencing parameters such as pH and ionic strength.

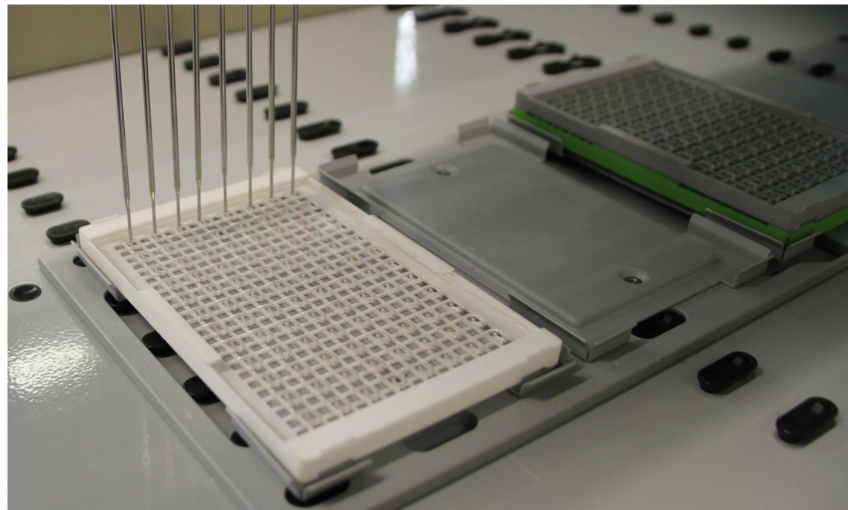
manuscript under preparation

5.1 Implementation of an analytical microfluidic device for the quantification of protein concentrations in a high-throughput format

Carsten P. Radtke*, Marie-Therese Schermeyer*, Yün Claudia Zhai, Jacqueline Göpper and Jürgen Hubbuch

Institute of Engineering in Life Sciences, Section IV: Biomolecular Separation Engineering, Karlsruhe Institute of Technology (KIT), 76131 Karlsruhe, Germany

* *These authors contributed equally to this work.*



published in *Engineering in Life Sciences* 16 (2016): 515–524.
DOI: 10.1002/elsc.201500185

Abstract

Nowadays the performance of experiments in automated microliter scale format are common practice in the biopharmaceutical process development. The increased number of experiments, reduced sample volumes and usage of robotic platforms require the adjustment of photometric measurements to determine the protein concentration. This work presents the qualification and usage of a disposable measurement device which can be used with conventional microplate photometers. The application of the microfluidic device (μ F-device) allows absorption measurements of protein concentrations from around 0.1 to 100 mg/mL with an accuracy of 99.2 % dependent on given protein extinction coefficients. The integrated four measurement chambers of increasing height (100 – 1500 μ m) allow the direct calculation of calibration curves and the determination of protein concentrations independent of used optical path lengths with a sample volume of 36 μ L. This study contains the validation of the analytical μ F-device according to ICH Guidelines as well as a representative case study. A salt gradient screening with chromatography columns in microliter scale performed on a liquid-handling station presents the usability of the μ F-device. It is shown that an improvement of the repeatability and accuracy of the chromatograms could be achieved by μ F-device implementation in comparison to photometric measurements performed in microtiter plates.

Keywords: *absorption measurement; high protein concentration; high-throughput experimentation; microfluidic*

Introduction

The market of biopharmaceuticals is steadily growing especially the commercialization of monoclonal antibody drug substances [112]. This trend requires the development of new process steps as well as the optimization of established ones. The purification development of the complex molecules is regarded as the most cost and time intensive step due to high investment and material costs [113]. To face these disadvantages the downstream development focusses on statistically based design of experiments [114] as well as automated sample handling and analysis [23] at an early phase. At this early phase of product development only a low amount of target molecules are available. To gain the highest amount of information out of the given low sample volume the execution of high throughput screening procedures in microliter scale is the method of choice [24, 115]. Many process steps are already established in an automated microscale format, like microliter scale chromatography [36] or precipitation screenings [116]. Unfortunately they are not used to their full potential due to limited integrated analytical methods. Implemented analytical methods are often time consuming, do need high sample volumes and are not specialized to the extended determination range tested in the high throughput format. One of the most important parameters to be tested is the product yield and the impurity concentration. The method of choice to determine these parameters are photometric measurements. Dependent on the tested process step, the concentrations to be determined vary from around 0.01 mg/mL to more than 100 mg/mL. Thus, the analytical method has to cover a wide concentration range. Since conventional photometric methods do not cover this range the samples have to be diluted. The dilution of the samples increase the inaccuracy of the measurement and requires a rough knowledge of the initial concentration of the molecule to be measured. Aggravating this situation in some cases, not only one specific type of molecule has to be quantified but also samples with different types of molecules, with varying extinction coefficients and concentrations. One example is the determination of target molecule and impurity concentrations of fractions collected from chromatography runs. The selection of the optimal dilution requires previous knowledge of expected protein content to avoid measurement inaccuracy for one type of the molecules to be determined. Every photometric detector has a specific absorption limit depending on given device properties. Based on the Lambert Beer Law (equation 5.1), the absorption A and therefore the maximum measurable protein concentration c is linearly dependent on the extinction coefficient ε_λ and the path length d of the measurement cell.

$$A = c * \varepsilon_\lambda * d \tag{5.1}$$

The extinction coefficient ε_λ is dependent on the amino acids on the protein surface which absorb light at the set wave length and therefore specific for every protein. The parameter which can be manipulated by the developers is the path length d . The linear relation of d to A led to the implementation of novel instruments with lower or flexible path lengths. One example therefore is the Nanodrop spectrophotometer series from Thermo Scientific (Waltham, USA) [117]. With these tools one to eight sample drops with a volume of 2 μ L

are contained by surface tension between two planar surfaces. The instruments can generate path lengths between 1 and 0.05 mm. The low sample consumption, easy usage and the relatively high protein concentration which can be measured directly, explain the sales volume of these instruments. The Solo VPE from C. Technologies Inc. (Bridgewater, USA) is able to change the optical path length from 0.01 mm to 15 mm via a movable optical fiber (Fibrette™). From the variable path length data the slope m can be calculated ($m = \Delta A / \Delta d$). With m and known ε_λ the protein concentration can be determined. Due to many measurement points over a wide path length range the tool is very precise and covers a huge protein concentration range [118]. Disadvantages of described tools are the manual operation and the limited number of samples which can be measured simultaneously (one sample (Nanodrop 2000c and Solo VPE) to eight samples (Nanodrop 8000)). Thus they are hardly automatable nor high throughput compatible. An instrument which meets the high throughput needs of the biopharmaceutical process development is the DropSense™ 96 UV/VIS droplet reader from Trinean (Gentbrugge, Belgium). This instrument also has a very small sample consumption of 2 μL and is equipped with 96-well robotic compatible measurement units. Here the protein absorption is measured in two chambers of differing heights. This two point measurement does not allow the application of the slope technique implemented with the SoloVPE. The microfluidic device (μF -device) presented in the current study is an approach to combine the advantages of the instruments described above. The μF -device and its channel structures are constructed according to the microplate format. The specific design of the channel structures, each with four measurement chambers of different height, allow the application of the slope method for an increased measurement accuracy and a direct four-point calibration of every measured sample. Especially to be emphasized is the accurate measurement in a wide protein concentration range enabled by the provided path lengths. Furthermore, microplate photometers already implemented in the lab can be used so that no investment in a new instrument has to be done.

Materials and Methods

Design and manufacturing of the μF -device

Materials The two component curing silicone Elastosil®RT 601 (Wacker Chemie, Burghausen, Germany), a polydimethylsiloxane (PDMS), was used for manufacturing the μF -device. The replication master for the μF -device was designed in-house and manufactured by Proform AG (Marly, Switzerland). This master served as inverted structure in the molding cavity and therefore defined the channels of the molded μF -device. The master was designed according to the microwell plate standard. A total of 96 channel structures are evenly distributed on the master. The inlets of the channel structures are vertical cylinders which are aligned such as wells of a 96-well plate (see figure 5.1).

Connected to the inlet, a circular channel with four oval chambers and a vertical outlet on the end was designed. The four chambers have different heights (100, 600, 1000 and 1500 μm) and are arranged in the pattern of the wells of a 384-well plate. This allows a simple read out of the chambers in the microplate photometer. To improve the stability and the automated handling of the μF -device on the liquid handling station (LHS), the silicone μF -device was placed inside a specially designed, 3D printed cartridge (Sculpteo, Villejuif, France). This cartridge allowed the handling by the robotic manipulator arm

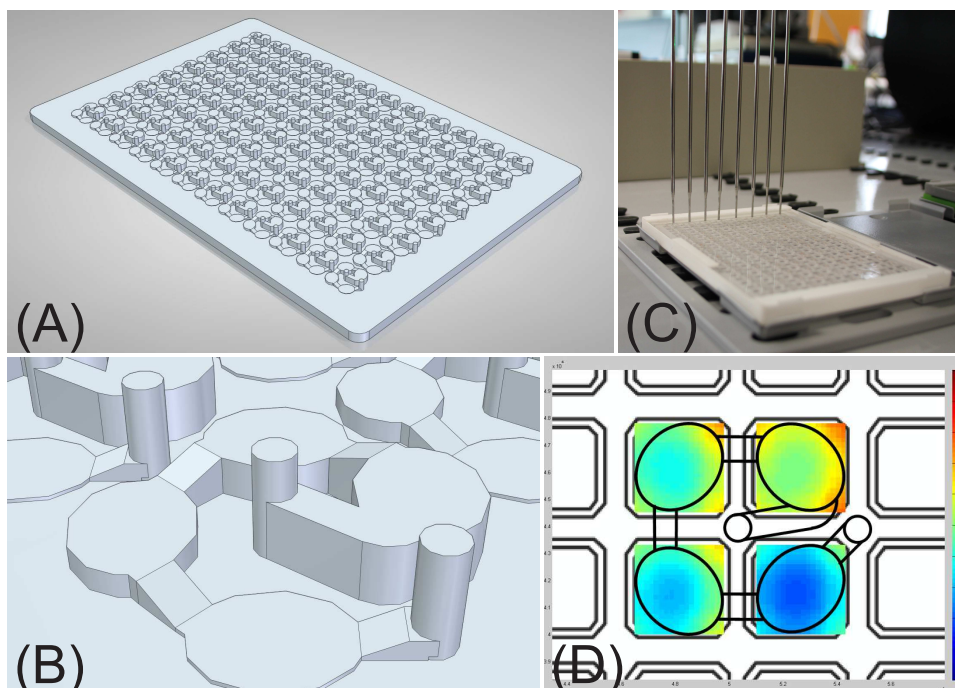


Figure 5.1: (A) CAD model of the replication master for the manufacturing of the μ F-device. (B) Magnified channel structure with the four measuring chambers of varying channel height (100, 600, 1000, and 1500 μ m) (C) Photograph of the assembled device on the deck of the liquid handling station. The LHS-tips dispense the samples directly into the channel structures eight at a time. (D) Visualization of the absorption data gained in the four measuring chambers of one channel structure to illustrate the absorption gradient due to the differing channel heights.

of the LHS. The measurement in the microplate photometer was possible through 384 perforations which were arranged evenly according to the microplate standard.

Methods The molding process of the μ F-device was executed as described by Wald-baur et al. [79]. Only the spacer part of the molding tool was replaced. To obtain a clear and plain surface, a flat piece of polished stainless steel was employed instead.

Qualification of the μ F-device

Materials Lysozyme from Chicken egg white was purchased in solid form from Hampton Research (Aliso Viejo, USA). Acetic acid and sodium acetate for buffer preparation were purchased from Merck KGaA (Darmstadt, Germany). Ultrapure water (ISO 3696) was used to prepare all solutions. Protein solutions for μ F-device qualification were prepared in 20 mM acetate buffer at pH 5 with a nominal mass concentration of 50 mg/mL. A buffer exchange of the protein solution with Sephadex media from GE Healthcare (Buckinghamshire, Great Britain) was performed to remove buffer salts or other components present in the purchased protein preparations. The size exclusion chromatography (SEC) column was manually packed with a diameter of 2.5 cm and a bed height of 23 cm. The

fractions were concentrated to a protein concentration of 100 mg/mL with the help of 20 mL Vivaspin ultra filtration spin columns (Sartorius, Goettingen, Germany) with a molecular weight cut off of 3000 Da. For liquid handling a Tecan Freedom Evo 200 (Tecan, Crailsheim, Germany) LHS equipped with 1 mL syringes was used. The LHS was equipped with an Infinite® M200 pro plate reader (Tecan, Crailsheim, Germany) and controlled by Magellan 7.1, both provided by Tecan. The LHS was controlled by Evoware 2.5 also provided by Tecan. To compare the absorption results of the μ F-device with an established method, measurements of protein absorption at 280 nm in the Nanodrop 2000 (Thermo Scientific, Waltham, USA) were performed.

Methods The buffer exchange of the lysozyme solution was conducted at an ÄktaPrime plus system from GE Healthcare. A total of 5 mL of lysozyme solution with a concentration of 50 mg/mL was purified. The protein was fractionated in 10 mL Falcon tubes and the concentration measured with an extinction coefficient of 22 L/(g*cm) with the Nanodrop 2000. The concentration of the dilute protein concentration was performed with Vivaspins and a rotational speed of 8000 rad/sec. A protein dilution series from 100 mg/mL to 0.1 mg/mL with acetate buffer was prepared. The μ F-device was automatically handled and filled on the robotic platform. The absorption at 280 nm of protein solutions and buffer blanks were measured in the μ F-device in quadruplicate. For the calculation of protein concentration the Lambert-Beer Law was applied

$$c = \frac{A}{\varepsilon_{\lambda} * d} \quad (5.2)$$

With the absorption A, the concentration c [mg/mL], the extinction coefficient ε_{λ} [mL/mg*cm] and the path length d [cm]. Additionally the slope m, which results of the absorptions plotted against the four given path lengths was determined. With this slope the calculation of protein concentrations with increased measurement accuracy became possible.

$$c = \frac{m}{\varepsilon_{\lambda}} \quad (5.3)$$

The evaluation of gained results and consequently the validation of the μ F-device followed the International Conference on Harmonisation (ICH) harmonized tripartite guideline Q2(R1) (Validation of analytical procedures: text and methodology) [119]. Following these guidelines the accuracy, repeatability and measuring range of absorption results gained with the developed analytical μ F-device were studied. To prove the precision of the analytical device lysozyme solution with a concentration of 5 mg/mL was prepared and measured in four measurement units of the μ F-device. The deviation of the absorption measurements were calculated. To determine the absorption range of the μ F-device, lysozyme solutions in a concentration range of 0.1 and 100 mg/mL were prepared and measured in quadruplicate.

Case Study

Materials For the chromatography runs the buffer described in section 2.1 was used (Buffer A). By adding 1.25 M sodium chloride (NaCl) (Merck, Darmstadt, Germany) to Buffer A the high salt buffer (Buffer B) was prepared. Purified monoclonal antibody (mAb) solution was provided by Synthron (Nijmegen, Netherlands). Cytochrome C (CytC) was purchased as lyophilized powder from Sigma-Aldrich (St. Louis, USA). The mAb stock solution was buffer exchanged and concentrated to 65 mg/mL by 20 mL Vivaspins with a molecular weight cut off of 50000 Da. For fraction collection, fraction volume determination and UV absorption measurements, half area UV-MTPs were used. For the preparation of high salt buffers and the dilution of elution fractions two 96 deep well square plates (DWP) (VWR, Germany) with a volumetric capacity of 2 mL were used. RoboColumns[®] prepacked with 200 μ L SP Sepharose FF were purchased from Atoll GmbH (Weingarten, Germany). Column chromatography in high throughput experimental mode using RoboColumns[®] was performed on a Tecan Freedom Evo 200 LHS, additionally equipped with a Te-Chrom column carrier.

Methods To prepare the elution buffers, two different troughs with Buffer A and Buffer B were assigned to the robotic platform. These components were mixed automatically in a DWP to achieve four salt gradients with respectively 10 salt steps resulting in different end concentrations. The gained end salt concentrations were 1.25 M, 1 M, 0.75 M and 0.5 M NaCl. CytC was dissolved in acetate buffer and transferred to the mAb solution to reach a starting protein concentration of 60 mg/mL mAb and 3 mg/mL CytC. This solution was transferred to eight Eppendorf Tubes (Eppendorf, Hamburg, Germany) and also placed in designated carriers on the robotic platform. A detailed description of parallelized chromatography performed automated on an LHS has been published by Wiendahl et al. [37]. In this case study an exemplary salt gradient screening was performed. Therefore, four gradients of varying slopes were tested to separate mAb molecules from CytC via cation-exchange chromatography (CEX). The salt gradients had a length of ten column volumes respectively 2 mL with different end salt concentrations which resulted in four different salt gradient slopes. For every tested salt gradient twenty elution fractions with a set volume of 100 μ L were collected in half area UV-MTP. After measuring the absorption at 900 and 990 nm to gain information of the precise fraction volumes following the method published by McGown et al. [120] and Lampinen et al. [121], 38 μ L of the samples were transferred to the presented analytical μ F-device. A volume of 20 μ L of the samples for the 1:50 dilution and 33 μ L for the 1:15 dilution were transferred to DWPs. To reach the respective dilution low salt buffer was added to every sample (980 μ L respectively 467 μ L), mixed and transferred to a full area UV-MTP. Afterwards the absorption at 280 nm and 410 nm was measured of undiluted samples transferred to the μ F-device and diluted samples transferred to the UV-MTPs. Every cation-exchange run was executed and analyzed in duplicate.

Results

 Qualification of the μ F-device

According to the ICH Q2 guidelines the μ F-device has been tested in regard to accuracy, precision (repeatability), linearity and range. For the qualification a lysozyme solution series from 0.1 – 100 mg/mL was prepared. After the preparation the theoretical lysozyme concentration was verified by fourfold absorption measurements with the Nanodrop 2000. The determined concentration values can be found in figure 5.2.

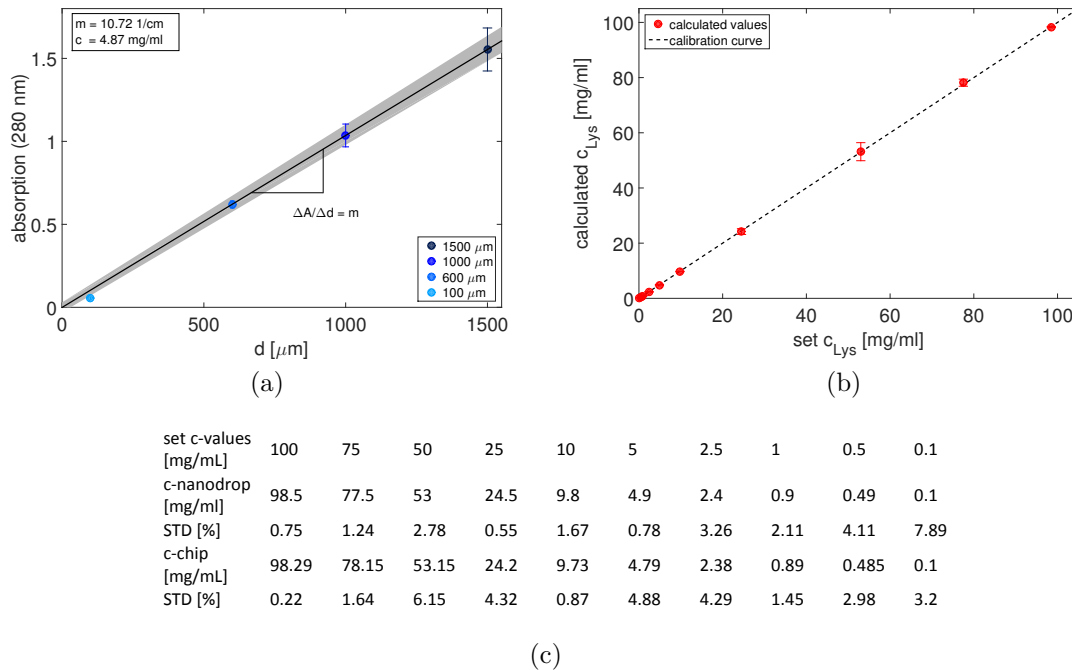


Figure 5.2: (a) Lysozyme absorption values measured in the μ F-device plotted against the channel height. Exemplarily determination of the slope m of the regression line. The reference concentration of this sample measured in Nanodrop 2000 was 4.9 mg/mL. (b) Calculated lysozyme concentrations based on μ F-device absorption data plotted against set concentration values with corresponding standard deviations. (c) Tabular listing of theoretical lysozyme concentrations, concentrations based on Nanodrop measurements and concentrations based on μ F-device measurements with corresponding standard deviations.

For qualification the absorption of every sample was determined in four channel structures. Additionally a buffer blank was measured and subtracted from the protein absorption values. The absorption values were plotted against the height of the four measuring chambers synonymous to the optical path length. The resulting values and the zero value were fitted with a linear regression. Values deviating from the regression line by more than 3 % were excluded from the regression of the second fit calculation. Thereupon, the slope m of the optimized regression was calculated for every measured sample. With m and ε_{280} (equation 5.3) the concentration could be calculated. In figure 5.2a the described method is exemplarily shown for a protein sample containing 4.9 mg/mL lysozyme. For

this measurement the slope m with a value of 10.71 1/cm was calculated which resulted in a protein concentration of 4.87 mg/ml (see equation 5.3). For measurements in the areas of the upper and lower detection limits the concentration can directly be calculated with the application of the Lambert-Beer law (equation 5.2). Here only the highest or lowest channel height was suitable for the exact absorption measurement. For the used photometer the range of detection was between 0.001 and 2.3 OD. Calculated lysozyme concentrations can be found in the tabular listing in figure 5.2c. For the visualization of the gained results, the lysozyme concentrations and related standard deviations determined with the μ F-device are plotted against set concentration values determined by Nanodrop measurements in figure 5.2b.

Case Study

The presented analytical μ F-device enables direct protein absorption measurements in a wide concentration range implementable on a liquid handling station. In order to demonstrate the applicability of the μ F-device it was implemented in a HTE (high throughput experimentation) process development step. For this, HTE chromatography was performed with a binary protein solution containing mAb with a starting concentration of 65 mg/mL and CytC with a starting concentration of 3 mg/mL. The actual aim of the chromatography screening was to find the optimal salt gradient to separate these two proteins. For this, four gradients of varying slope and end salt concentration were tested in duplicate. Important for the selection of the best suited gradient was the proper determination of protein concentration in the collected elution fractions. The elution fractions were analyzed directly in the channel structures of the μ F-device respectively in four chambers of differing heights and after dilution of the fractions in MTPs for comparison. The absorption values of every single fraction are displayed as round symbols in figure 5.3 and figure 5.4. The absorption values of the mAb and CytC molecules were separated with the help of the also measured absorption at 410 nm wavelength. At this wavelength CytC has a second absorption maximum whereas mAb does not absorb light. With the known absorption ratio of 280 nm and 410 nm of CytC (0.24, data not shown) the detected 280 nm sum signal could be divided in mAb and CytC specific absorption. The absorption values of the 20 elution fractions formed the basis of a nonlinear Gaussian fit for the preparation of chromatograms describing the elution of the molecules. In figure 5.3 the absorption values at 280 nm from mAb and CytC are plotted against the elution volume.

The fitted chromatogram represents the run with the steepest salt gradient with absorption values measured in the measuring chambers from 100 μ m to 1500 μ m path length in the μ F-device. With decreasing channel height the absorption values decreased. The mAb represented by the blue symbols eluted first over an elution volume of 1000 μ L. CytC, represented by the red symbols, starts to elute at around 650 μ L and over an elution volume of 850 μ L. No baseline separation could be achieved. Independent on the chamber height the curve progression was similar. Only the absorption signals of CytC measured with a path length of 100 μ m did not show a significant absorption peak. Depending on the salt gradient slope the chromatograms showed varying resolutions. The plot set in figure 5.4 a-d illustrates the influence of the varying salt gradients on the resolution of the chromatographic runs.

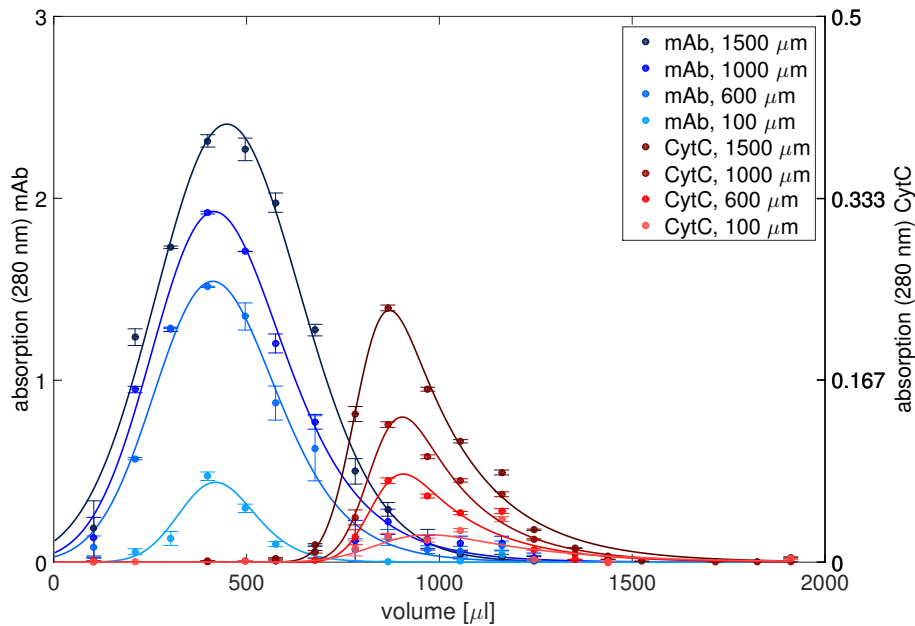


Figure 5.3: Elution profiles of mAb and CytC with a gradient from 0–1.25 mM NaCl in 10 CV. Plotted are absorption values at 280 nm measured in the μ F-device in the four respective measuring chambers with a height of 100, 600, 1000 and 1500 μ m. Absorption values of mAb are plotted as blue circles, absorption values of CytC are plotted as red circles. The absorption values were fitted with a nonlinear Gaussian fit (blue and red lines).

The graphs contain the absorption values measured in the channels at a path length of 1000 μ m and absorption values measured in a UV MTP. For the measurement in the MTP the fractions had to be diluted. Depending on the expected protein content the samples were diluted in a ratio of 1:50 (fraction 1-12) respectively in a ratio of 1:15 (fraction 13-20). The shown absorption values of the MTP are standardized to a dilution of 1:50. With decreasing slope of the salt gradient the detected elution peaks of both protein types widened. Additionally the elution points were shifted to higher volumes and the resolution of the separation declined. In figure 5.4d the run with the lowest gradient is depicted. Here the elution peak of the mAb overlays the CytC elution peak. The absolute absorption values of the MTP were lower in the order of magnitude of around 75 % in comparison to absorption values measured in the 1000 μ m chamber of the μ F-device. With decreasing slope of the salt gradient the chosen nonlinear Gaussian fit did get less precise independent on measurement device. In figure 5.4a fraction 4, 9 and 13 (F4, F9 and F13) are highlighted in yellow. For these fractions the approach to calculate protein concentrations from μ F-device absorption data is shown for both proteins (figures 5.5a and 5.5b) and compared to the calculated protein concentrations based on MTP absorption data (figure 5.5a).

In figure 5.5a and 5.5b the mAb respectively CytC absorption values of F4, F9 and F13 are plotted against the path lengths of the measuring chambers of the μ F-device.

5.1 Implementation of a Microfluidic Device for the quantification of protein concentrations

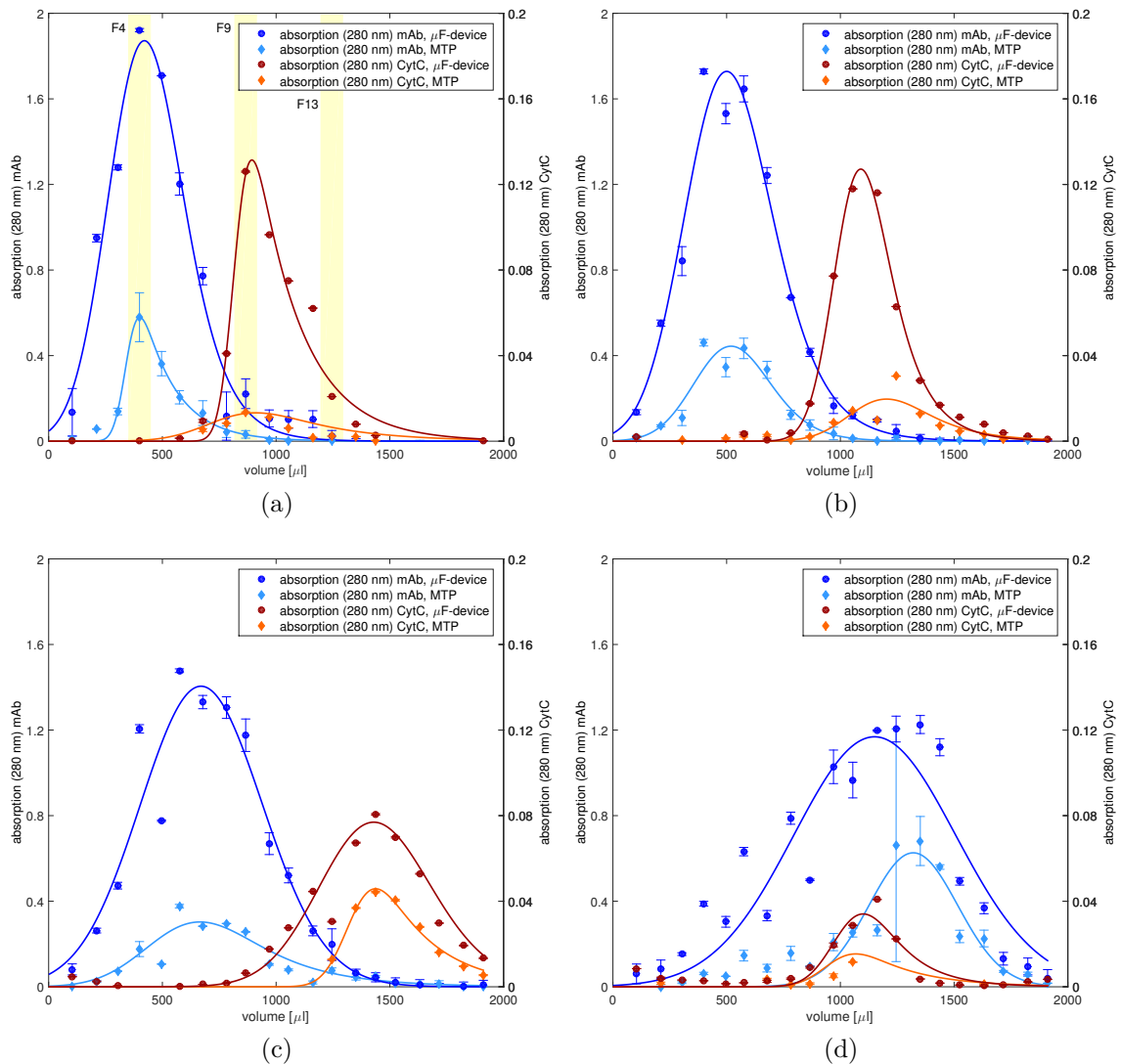


Figure 5.4: Chromatograms of the four screened elution gradients of mAb and CytC absorption values. Illustrated are absorption values with related standard deviations measured in the μ F-device in a measuring chamber height of 1000 μ m and absorption values measured in MTP after dilution. (a) Gradient from 0 – 1.25 mM NaCl in 10 CV, highlighted are fraction 4, 9 and 13 which have been further investigated; (b) gradient from 0 – 1 mM NaCl in 10 CV; (c) gradient from 0 – 0.75 mM NaCl in 10 CV; (d) gradient from 0 – 0.5 mM NaCl in 10 CV.

The regression lines were calculated based on at least 3 measured values of one channel structure in duplicate. Measurement values which deviated from this regression by more than 3 % were not included in the calculation of the slope m . The mAb absorption value for F4 determined with a path length of 1500 μ m was eliminated from further calculations due to this deviation as well as the CytC absorption value of F9 which was determined with a chamber height of 1500 μ m and F13 which was determined with a chamber height

5.1 Implementation of a Microfluidic Device for the quantification of protein concentrations

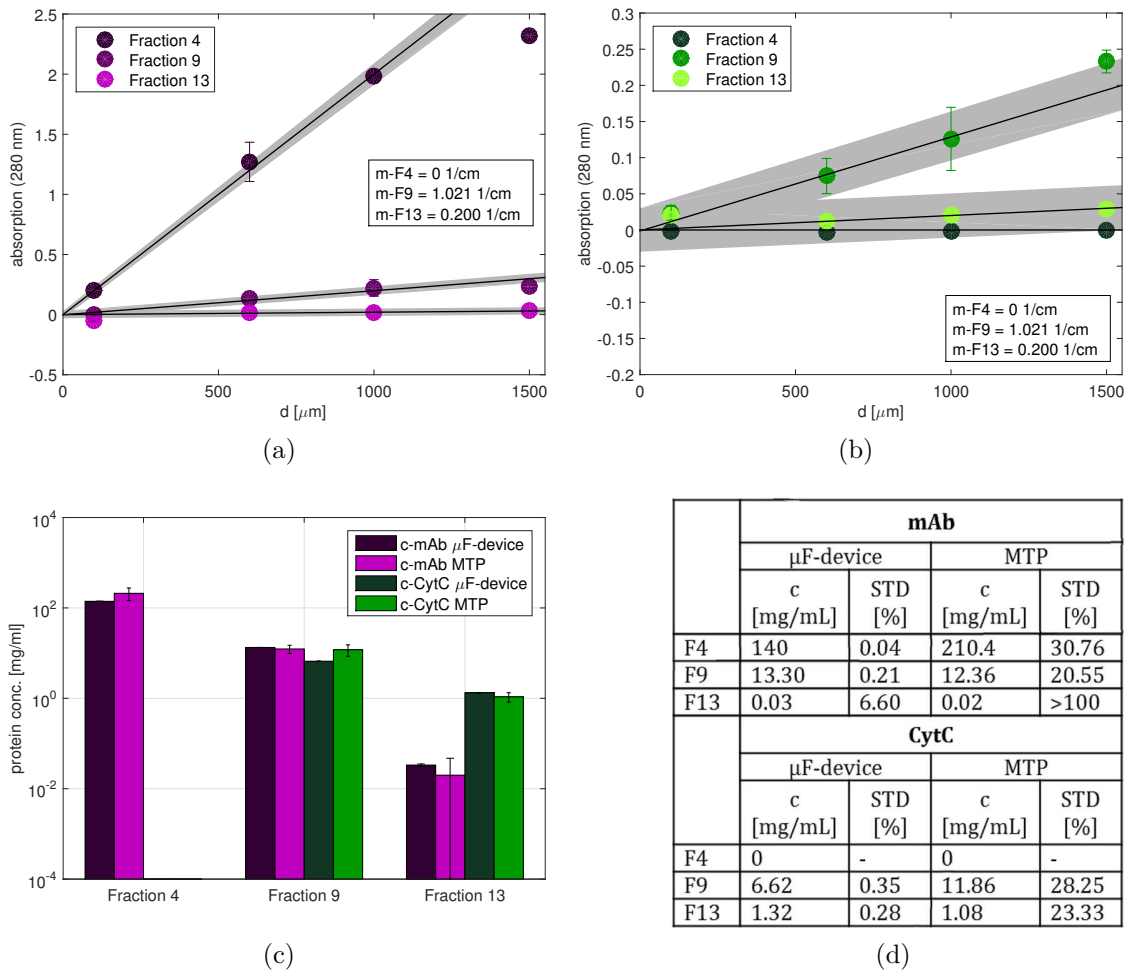


Figure 5.5: Absorption values with related standard deviations of fraction 4, 9 and 13 from mAb (a) and CytC (b) measured in the μF -device plotted against channel height with regression lines and related slope values m . The grey area depicts the allowed deviation of 3%. (c, d) Protein concentrations with related standard deviations of F4, F9 and F13 calculated based on μF -device absorption values (dark colored) and based on MTP absorption values (light colored). The concentrations based on absorption values measured in the μF -device were calculated with the slope method (equation 5.3).

of $100 \mu\text{m}$. This exclusion criteria is illustrated by the grey area in figures 5.5a and 5.5b. The calculated regression coefficients (R^2) for shown data all had a value above 0.996. The corresponding protein concentrations were determined following equation 5.3. The protein concentrations of similar fractions were also determined based on absorption measurements conducted in MTPs. The so calculated mAb and CytC concentrations are compared to μF -device results in figure 5.5c. To display the wide protein concentration range of chosen fractions in one plot, a logarithmic scale was selected. The highest mAb concentration could be found in F4 with a value of 140 mg/mL based on data of the μF -device and

a standard deviation of 0.04 % and 210 mg/mL based on MTP data with a standard deviation of 30.1 %. In F9 both molecules were present at a comparable concentration. In F13 the lowest mAb concentration was detected with a value of 0.02 – 0.03 mg/mL. All calculated protein concentrations with associated standard deviations can be found in a tabular listing in figure 5.5d.

Discussion

Qualification of the μ F-device

In this section the validation of the presented analytical tool according to accuracy, repeatability, linearity and range as prescribed by the ICH guideline Q2 (R1) is discussed. The comparison between measured protein concentrations determined with the μ F-device and the reference concentration values determined with the Nanodrop 2000 (see figure 5.2) illustrates an excellent consistency. In accordance to ICH guidelines this complies the validation criterion of accuracy. The determined accuracy was 99.02 % in a concentration range of 0.5 – 10 mg/mL (equation 5.3) and 99.92 % in a range of 0.1 – 0.5 mg/mL and 10 – 100 mg/mL Lysozyme. The obtained measurement deviations can be explained by the manual manufacturing of the μ F-device and the used silicone material with relatively low stiffness. With known protein concentration the applied slope method and so fitted calibration curve can be used to calculate the extinction coefficient with only one protein sample respectively one starting concentration. Nonetheless, with the fourfold measurement of ten different lysozyme concentrations an excellent repeatability could be determined expressed by an average standard deviation of 3.1 %. The linearity of gained results could be shown both for plotting the absorption values over path length ($R^2 = 0.988$) and plotting calculated concentration over reference concentration values ($R^2 = 0.9998$) (see figure 5.2).

Case Study

The aim of the executed case study was to separate the mAb molecules with a relatively high starting concentration of 65 mg/mL from CytC molecules with a starting concentration of 3 mg/mL. To find an optimal separation with CEX a screening of four salt gradients differing in slope and end salt concentration were performed in microliter scale on a LHS. As assumed the mAb molecules with an isoelectric point (pI) of 7.9 eluted prior to CytC molecules with a pI of 10.4 for all performed runs with the exception of the run presented in figure 5.4d (this phenomenon will be discussed within the next paragraph). The explanation for this elution order can be found in the stronger electrostatic interaction of CytC with negatively charged ligands in comparison with weaker adsorption of mAb molecules on the resin. Thus, a higher salt concentration is necessary to desorb the CytC molecules from the resin what implies a later elution. With decreasing gradient slope the peaks were shifted to later elution volumes. In figure 5.4d it seems that CytC is eluting with the mAb molecules but taking the mass balance of CytC molecules into account, it can be expected that the main peak of CytC elutes outside the set fraction range. The elution of CytC at comparatively low salt concentrations are potentially caused by a specific interaction with the mAb and thus a co-elution of CytC molecules. The best chromatographic resolution could be found with the steepest gradient and an end salt concentration of 1.25 mM NaCl.

To further optimize the run with the aim of a baseline separation, a step elution with a step height of 0.4 mM NaCl hold for 5 CV for mAb elution and a second step with 1.25 mM NaCl hold for 4 CV to elute CytC from the column is recommended, based on the results of the gradient screening. In the next paragraph the absorption values of μ F-device measurements will be discussed and compared to MTP absorption measurements. Fractions analyzed with the analytical device have a mean standard deviation of 3.5 % compared to MTP measurements with a mean standard deviation of 8.2 % (see figure 5.3 and 5.4). The higher accuracy of absorption measurements executed with the μ F-device can be explained by direct analysis of all fractioned samples without the need of dilution. In figure 5.3 the absorption measurements of every measuring chamber is plotted. The decrease of absorption values with decreasing path length respectively height of measuring chamber is in good agreement with the Lambert Beer law (equation 5.1). The selected nonlinear Gaussian fit represents the absorption values very precise. This not only implies that the absorption values can be fitted with a characteristic chromatographic elution curve but also that the absorption values actually represents the eluting protein amount. The CytC peak cannot be depicted well by the fit of results of the 100 μ m measuring chamber. Here, the measured absorption values of CytC are close to the buffer blank absorption what may explain the weak fit results. In figure 5.4 the influence of the salt gradient on the elution profile measured in the μ F-device and in the MTP is shown. The absolute absorption values of the MTP and the μ F-device varied due to divergent path length and the dilution of the fractions for MTP measurements. In principal the curve progressions of chromatograms obtained by absorption results of the μ F-device and MTP are comparable as well as elution starting points, absorption maxima and elution end points. Deviations traceable to the measurement system are obtained with CytC peaks and were especially significant at the flattest tested gradient (see figure 5.4d). One explanation may be the chosen dilution rate of 1:50 for the fractions F1-F12. Due to the low amount of CytC in these fractions the error caused by dilution had a higher impact. Contributing to this assumption the comparability of CytC peaks was better for a flatter gradient depicted in figure 5.4c. Here, CytC molecules elute where the fractions have been diluted in a ratio of 1:15 what gives a better precision of the results. In all displayed graphs the measured absorption values oscillate around the fit curve for measurements executed in μ F-device and MTP. The oscillatory movement is periodical and due to the practical implementation of the chromatographic run on the LHS. The dispensing of the buffers is not continuous as in common chromatographic runs but subsequently. This potentially cause a longer holding time of the proteins on the column. This phenomenon had an increased impact on fit results with decreasing salt gradient slope. To increase fit accuracy the step size as well as the fraction size should be decreased. To depict the dependencies of specific path length of the measuring chambers on the absorption values the linear relation is shown in figure 5.5a and 5.5b for three exemplarily chosen fractions (F4, F9, and F13). The regression coefficient of 0.996 proves the linearity of the adsorption values gained with different chamber heights. The mAb absorption value of F4 measured in the chamber with a height of 1500 μ m was excluded from further calculations due to the exceedance of the determined absorption limit of 2.3 OD. The same reasoning applies to the CytC absorption value of F13 measured in a chamber of 100 μ m height. At this point the

quantification limit was reached. This explanation does not hold true for the deviation of the CytC absorption value of F9 measured in the 1500 μm chamber height. Here the deviation is potentially due to a measurement error in the channel structure caused by small air bubbles. With the help of the slope of the discussed regression lines the concentrations of mAb and CytC in the respective fractions could be calculated. These calculated concentrations were compared to the concentrations determined with MTP absorption values and are displayed in figure 5.5c. The calculated values represent the expected concentrations of mAb and CytC when taking the related chromatograms of figure 5.4a into account. In direct comparison, deviations between MTP and μF -device results of more than 60 % were detected for both protein species. One explanation of these high discrepancies can be found in the extent of calculated standard deviations. The standard deviations of determined mean protein concentrations measured in the microfluidic channels had a maximum value of 0.06 mg/mL. The comparatively low standard deviations of these measurements prove the reliability of the developed μF -device. In contrast, the standard deviations of protein concentrations determined with MTP were between 1.08 and 64.71 mg/mL (20 – >100 %). These standard deviations were so high that the standard deviation error also covered concentrations calculated with μF -device absorption results. The high standard deviations of the concentrations calculated based on MTP results could be explained with dilution errors, additional required liquid handling steps and the potential formation of a meniscus in the wells of the MTP. The angle of this meniscus is highly dependent on protein concentration and buffer compositions. The consideration of this phenomenon is complex especially when measuring varying concentrations at varying liquid levels during one screening, such as occurred in this case study. The deviations potentially caused by meniscus can be excluded by application of the μF -device due to the completely filled channel structures. Including the discussed standard deviations the calculated concentrations based on μF -device and MTP results are comparable and support the statement that the presented μF -device is applicable for absorption measurements. In the discussed case study the target molecule (mAb) and the impurity (CytC) could be quantified due to the second absorption maximum of Cytochrome C at 410 nm. To distinguish between target molecule and impurities having similar absorption characteristics the spectral method published by Hansen et al. [38, 122] may be transferred to the presented μF -device. This possible application will be part of future investigations.

Concluding Remarks

The presented analytical μF -device could be validated according to ICH guidelines. In the course of this validation the accuracy, repeatability and linearity was proven for a concentration range from 0.1 – 100 mg/mL, with lysozyme as model protein. This qualification permits the application of the μF - device for protein absorption measurements in the biopharmaceutical process development. The case study demonstrated a successful application of the μF -device on a liquid handling station. The analytical μF -device was simple to implement in an existing automated development step. Furthermore, the absorption of elution fractions measured with the presented μF -device resulted in comprehensible characteristic elution profiles. Consequently, the μF -device presented in this study is a promising alternative or supplement to existing devices combining a wide

measurement range with high throughput compatibility.

Acknowledgments

This research work is part of the project „Molecular Interaction Engineering: From Nature’s Toolbox to Hybrid Technical Systems“, which is funded by the German Federal Ministry of Education and Research (BMBF), funding code 031A095B and the project “Euro Trans Bio”, also funded by the BMBF, funding code 031607B. The authors bear the complete responsibility for the content of this publication. Special thanks go to Gang Wang for the modeling support.

References

23. Bhambure, R., Kumar, K., and Rathore, A. S. 'High-throughput process development for biopharmaceutical drug substances'. *Trends in Biotechnology*, vol. 29(3) (2011), pp. 127–135 (cit. on pp. 2, 3, 18).
24. Hertzberg, R. P. and Pope, A. J. 'High-throughput screening: new technology for the 21st century'. *Current Opinion in Chemical Biology*, vol. 4(4) (2000), pp. 445–451 (cit. on pp. 2, 18, 97).
36. Bensch, M., Schulze Wierling, P., Lieres, E. von, and Hubbuch, J. 'High Throughput Screening of Chromatographic Phases for Rapid Process Development'. *Chemical Engineering & Technology*, vol. 28(11) (2005), pp. 1274–1284 (cit. on pp. 3, 18, 97).
37. Wiendahl, M., Schulze Wierling, P., Nielsen, J., Fomsgaard Christensen, D., Krarup, J., Staby, A., and Hubbuch, J. 'High Throughput Screening for the Design and Optimization of Chromatographic Processes - Miniaturization, Automation and Parallelization of Breakthrough and Elution Studies'. *Chemical Engineering & Technology*, vol. 31(6) (2008), pp. 893–903 (cit. on pp. 3, 22).
38. Hansen, S. K., Skibsted, E., Staby, A., and Hubbuch, J. 'A label-free methodology for selective protein quantification by means of absorption measurements.' *Biotechnology and bioengineering*, vol. 108(11) (2011), pp. 2661–2669 (cit. on pp. 3, 30).
79. Waldbaur, A., Kittelmann, J., Radtke, C. P., Hubbuch, J., and Rapp, B. E. 'Microfluidics on liquid handling stations (μ F-on-LHS): an industry compatible chip interface between microfluidics and automated liquid handling stations'. *Lab on a Chip*, vol. 13(12) (2013), pp. 2337–2343 (cit. on pp. 5, 20, 37, 38, 59, 60, 68, 78).
112. Walsh, G. 'Biopharmaceutical benchmarks 2014'. *Nature Biotechnology*, vol. 32(10) (Oct. 2014), pp. 992–1000 (cit. on p. 18).
113. Lowe, C. R., Lowe, A. R., and Gupta, G. 'New developments in affinity chromatography with potential application in the production of biopharmaceuticals'. *Journal of Biochemical and Biophysical Methods*, vol. 49(1) (2001), pp. 561–574 (cit. on p. 18).
114. Nfor, B. K., Verhaert, P. D., Wielen, L. A. van der, Hubbuch, J., and Ottens, M. 'Rational and systematic protein purification process development: the next generation'. *Trends in Biotechnology*, vol. 27(12) (2009), pp. 673–679 (cit. on p. 18).
115. Nfor, B. K., Ahamed, T., Dedem, G. W. van, Wielen, L. A. van der, Sandt, E. J. van de, Eppink, M. H., and Ottens, M. 'Design strategies for integrated protein purification processes: challenges, progress and outlook'. *Journal of Chemical Technology & Biotechnology*, vol. 83(2) (2008), pp. 124–132 (cit. on p. 18).
116. Wiendahl, M., Völker, C., Husemann, I., Krarup, J., Staby, A., Scholl, S., and Hubbuch, J. 'A novel method to evaluate protein solubility using a high throughput screening approach'. *Chemical Engineering Science*, vol. 64(17) (2009), pp. 3778–3788 (cit. on p. 18).

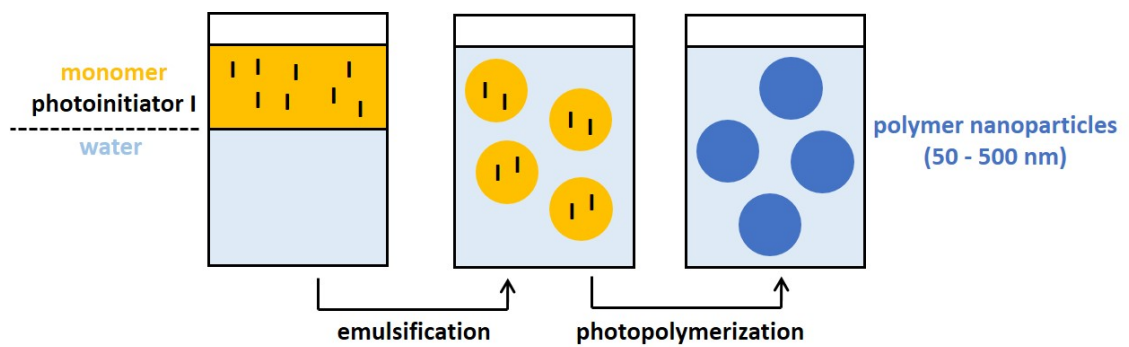
117. Robertson, C. 'Liquid photometer using surface tension to contain sample'. US6628382 B2. 2003 (cit. on p. 18).
118. Thakkar, S. V., Allegre, K. M., Joshi, S. B., Volkin, D. B., and Middaugh, C. R. 'An Application of Ultraviolet Spectroscopy to Study Interactions in Proteins Solutions at High Concentrations'. *Journal of Pharmaceutical Sciences*, vol. 101(9) (2012), pp. 3051–3061 (cit. on p. 19).
119. Baber, N. 'International conference on harmonisation of technical requirements for registration of pharmaceuticals for human use (ICH).' *British Journal of Clinical Pharmacology*, vol. 37(5) (May 1994), pp. 401–404 (cit. on p. 21).
120. McGown, E. L. and Hafeman, D. G. 'Multichannel Pipettor Performance Verified by Measuring Pathlength of Reagent Dispensed into a Microplate'. Vol. 258(1) (1998), pp. 155–157 (cit. on p. 22).
121. Lampinen, J., Raitio, M., Perälä, A., Oranen, H., and Harinen, R.-R. 'Microplate Based Pathlength Correction Method for Photometric DNA Quantification Assay'. *Thermo Scientific Appl. Note*, vol. (ANMR MUGO 0412) (2012) (cit. on p. 22).
122. Hansen, S. K., Jamali, B., and Hubbuch, J. 'Selective high throughput protein quantification based on UV absorption spectra'. *Biotechnology and Bioengineering*, vol. 110(2) (Feb. 2013), pp. 448–460 (cit. on p. 30).

5.2 Photoinitiated Miniemulsion Polymerization in Microfluidic Chips on Automated Liquid Handling Stations: Proof of Concept

Carsten P. Radtke*, Michèle Delbè*, Michael Wörner, Jürgen Hubbuch

Institute of Engineering in Life Sciences, Section IV: Biomolecular Separation Engineering, Karlsruhe Institute of Technology (KIT), 76131 Karlsruhe, Germany

* These authors contributed equally to this work.



published in *Engineering in Life Sciences* 16 (2016): 505–514.
DOI: 10.1002/elsc.201500186

Abstract

Photoinitiated polymerization is usually applied in the area of specialty chemicals and UV curing but can also be employed in the production of bifunctional polymers and nanocapsules. A promising approach for the preparation of those polymers is the photoinitiated polymerization of miniemulsions. Here, the mild reaction conditions are beneficial for the integration of sensitive biomaterials into the process. The optimal combination of different varied cause variables like irradiance, irradiation time, and height of the irradiated volume is crucial for an appropriate polymerization result. For the presented proof of concept study, a microfluidic tool was established to screen these cause variables in an automated high throughput manner on a liquid handling station (LHS). The experiments are planned and executed by means of a design of experiments (DoE) approach to investigate the effect of the variables on the residual monomer content (RMC) within the stated design space. As the RMC is considered as crucial for bioapplications, the optimal parameter combinations for the complete monomer conversion have been determined. The model-based evaluation of the executed experiments resulted a channel height respectively optical path of 200–400 μm , an irradiance of 65% (equals 44.2 mW/cm^2) and an irradiation time of 30 s for complete styrene conversion.

Keywords: *DoE; liquid-handling station; microfluidics; miniemulsion; photopolymerization*

Introduction

The employment of polymer networks for applications in the biological, biomedical, or biochemical field is common standard [123]. Most of these biomaterial-based networks can be prepared by photoinitiated polymerization [124]. The huge potential of the photopolymerization of bio compatible materials is exploited for a broad range of applications, for instance tissue engineering [125, 126], dental applications [127], drug delivery [107, 108], cell encapsulation [128, 129], biomimetic coatings [130], and nano-patterned surfaces [131].

The selected biomaterials can be directly implemented into polymer networks, e.g. by stereolithographic methods to build functional 3D structures as reported by Arcaute et al. [132]. Biofunctionalized polymers can also be achieved by subsequent modification. Pierre et al. presented a method to immobilize enzymes on photopolymerized monoliths [133]. In addition, the employment of click-chemistry was shown to be an efficient method to generate biofunctional polymers [134].

Applying these methods the integrity of the bioactive materials has to be preserved throughout the whole process. Therefore, the photoinitiated polymerization provides a good technology for the generation of polymer networks under mild reaction conditions. Photopolymerization can be executed at room temperature that is preferable for biological material. One of the main advantages of the photopolymerization is the spatial and temporal control of the reaction by turning on the light for defined time spans and at specified locations to produce radicals at this particular spot [135]. Also the irradiation condition of the reaction system can be varied by employing different monochromatic light sources that allows specific excitation of the dedicated photoinitiator and optimization of the initiation rate, respectively [136].

To produce nanoparticles for coatings or for the encapsulation of drugs and biomaterials, the (photo-) polymerization of miniemulsions is the method of choice [137]. Miniemulsions consist of small, homogeneous, and stable monomer droplets that behave as autonomous reaction compartments [138]. The photopolymerization of miniemulsions takes place in an aqueous environment, avoiding the use of organic solvents, which is another benefit for the processing of biomaterials.

Due to the opaque appearance of those miniemulsions, the limiting parameter of the photopolymerization process is the limited penetration depth of the photons into the reaction volume. Light attenuation (extinction) in heterogeneous systems arises not only from absorption of photons but also from scattering effects. Monomer miniemulsions are highly scattering media, the optical properties are known to be strongly dependent on the droplet size and the chemical nature of the oil phase [139]. In case of diluted miniemulsions, a droplet size increase causes a progressive increase of the scattering coefficient, but without affecting the absorption coefficient of the miniemulsion and the photoinitiator itself. The use of concentrated miniemulsions may give rise to significant loss of photons by multiple scattering due to the high density of droplets. The increased scattering contribution increases extinction and reduces light penetration depth. However, photons can be scattered several times by the monomer droplets and be subsequently absorbed by the photoinitiator that may compensate the consequences of considerably shorter optical path length [140]. Nevertheless, the effective extent of the loss of photons due

to out-scattering and its impact on photopolymerization of monomer miniemulsions remain to be investigated. One strategy to overcome possible limitations of the photochemical reaction system is to optimize the reactor layer thickness with respect to the penetration depth of the UV light in the dispersed media.

This approach was adopted regarding the development of continuous operating photopolymerization reactors for the polymerization of miniemulsions in tubular reactors and microfluidic devices. To identify the influence of different parameters on the polymerization result, a number of parameters like residence time or droplet size have been varied [67, 136]. These studies revealed that reactors with an optical path of 1 mm are suitable for continuous flow photopolymerization with a high polymer yield. Another conclusion is that a systematic investigation of the different influencing parameters is needed to obtain optimal reaction conditions for the intended application.

Nevertheless, preserving the functionality of biomaterials in photopolymerization processes is still a challenging task and requires further understanding and optimization of the technology [124]. The application of high energy photons due to UV radiation recommends the control and dosing of irradiance and irradiation time. Likewise, a crucial parameter is the almost complete monomer conversion to minimize toxic contaminants without the need of complex and expensive purification steps [141].

To investigate several cause variables of the photoinitiated miniemulsion photopolymerization and their impact on the monomer conversion, a method has to be established that allows a fast screening procedure with low sample consumption in a preferably large parameter space.

The presented screening study provides versatile methods for the characterization of photopolymerization processes that will contribute to an improved understanding of these processes. It combines established techniques for high throughput experimentation with a newly developed microfluidic platform for photopolymerization. As a proof of concept study the Design of Experiments (DoE) methodology was selected for a systematic examination of different and mutual-dependent parameters like irradiance, irradiation time, and channel height (optical path) regarding to their impact on the monomer conversion. The DoE permits to detect the correlation and impact of the cause variables on the target value in the selected design space [142]. To accelerate and simplify the exploration within the design space a strategy to increase the sample throughput was developed by adopting a microfluidic (μF) device on a liquid handling station (LHS), which has been introduced by Waldbaur et al. [79]. This approach allows a high throughput screening process with low sample consumption and less manual operation due to automation. The use of microfluidic chips that can be designed highly variable permits, e.g. the study of the effect of various channel heights respectively reactor layer thickness or optical path on the monomer conversion. In addition to the optical path, the concentration of photoinitiator, the time of irradiation and the irradiance was varied to explore the impact of these parameters on the photoinitiated polymerization in regard to minimize the residual monomer content (RMC).

In practice, for the miniemulsion photopolymerization styrene was selected as model monomer for various reasons. A particular feature is the ability to form copolymers with a high variability of other monomers that permits the adjustment of different polymer properties. A further advantage is the implementation of chemical substitution on the

aromatic core (nucleus) allowing simple introduction of additional chemical functionalities during homo- or copolymerization. Further, employing styrene as a comonomer the synthesized polymer can be easily secondary functionalized, for example introducing ion exchange capabilities by sulfonation. In addition, using alkyne styrene as a comonomer, which is chemically easily accessible, the obtained polymer can be (bio-) functionalized by click chemistry [143]. Bis(acylphosphine) oxide (Irgacure 819, BAPO) has been selected as photoinitiator for several reasons, in particular due to the excellent absorption properties in the near UV region and fast photolysis under bleaching, combined with high initiation quantum yields [144]. Thereby it was possible to excite the photoinitiator efficiently employing quasi monochromatic LEDs without appreciable absorption by the monomer styrene, permitting fast, and deep-through initiation of frontal polymerization. In addition, BAPO is capable of multiple photo-induced decomposition (“snowballing” radical generation), leading to multiple growing radicals within a polymerizing chain, and is attributed to the formation of ultrahigh molecular weight polymers [145].

Materials and Methods

Chemicals

For the presented proof of concept study styrene was chosen as monomer and used as received ($\geq 99\%$, Sigma-Aldrich, St. Lois, USA). The miniemulsions were stabilized with the nonionic surfactant Lutensol® AT 50, obtained from BASF SE (Ludwigshafen, Germany), and the hydrophobic n-hexadecane (Alfa Aesar, Ward Hill, USA) against coalescence and Ostwald ripening. Bis(2,4,6-trimethylbenzoyl)-phenylphosphineoxide (Irgacure® 819) from BASF SE (Ludwigshafen, Germany) was employed as oil-soluble photoinitiator without any further purification. Ethanol ($\geq 99.9\%$, Carl Roth, Karlsruhe, Germany) was applied for the sample preparation for GC analysis of RMC. Ultrapure water was used throughout all experiments (Elga LabWater, Celle, Germany). The two component curing PDMS Elastosil 601 RT (Wacker Chemie, Burghausen, Germany) was employed for molding the microfluidic chips.

Preparation of miniemulsions

The miniemulsions in this study are composed of 10 wt% styrene as dispersed phase in the continuous phase water. The content of Lutensol® AT 50 (1.4 wt%) and hexadecane (4 wt%) remained constant for all miniemulsions while weight percentage of Irgacure® 819 (photoinitiator) was adjusted according to the experimental design between 0.5 and 3 wt% with respect to the dispersed phase. The two phases were preemulsified under mechanical stirring at 1800 rpm (Ultra Turrax® Tube Drive, IKA-Werke, Staufen im Breisgau, Germany) for 30 min followed by ultrasonication (Branson Sonifier S-450D, Branson Ultrasonics Corp., USA) over 4 min at 90 % amplitude to prepare the miniemulsions.

Manufacturing of microfluidic devices

The fabrication of the microfluidic replication master, the molding and the manufacturing of the microfluidic chip was executed as described by Waldbaur et al. [79]. The replication master for the introduced application was designed with seven inlet channels and one outlet channel (see figure 5.6). The seven channels differed in width and heights of their

individual sections. For the presented proof of concept study, inlet channel No. 2 (IN-2) and the outlet channel (OUT) were utilized. The width of the channel between the inlet and the outlet port is kept constant with 1 mm. The bottom plate of the chip was made of silicone with a thickness of 1.5 mm. The used inlet channel has three sections with different heights (1000, 500, and 200 μm) and each about 29 mm long. By irradiating the channel from the bottom up, the irradiated volume could be varied by these different optical path lengths to evaluate the effect of the penetration depth of irradiation in miniemulsions.

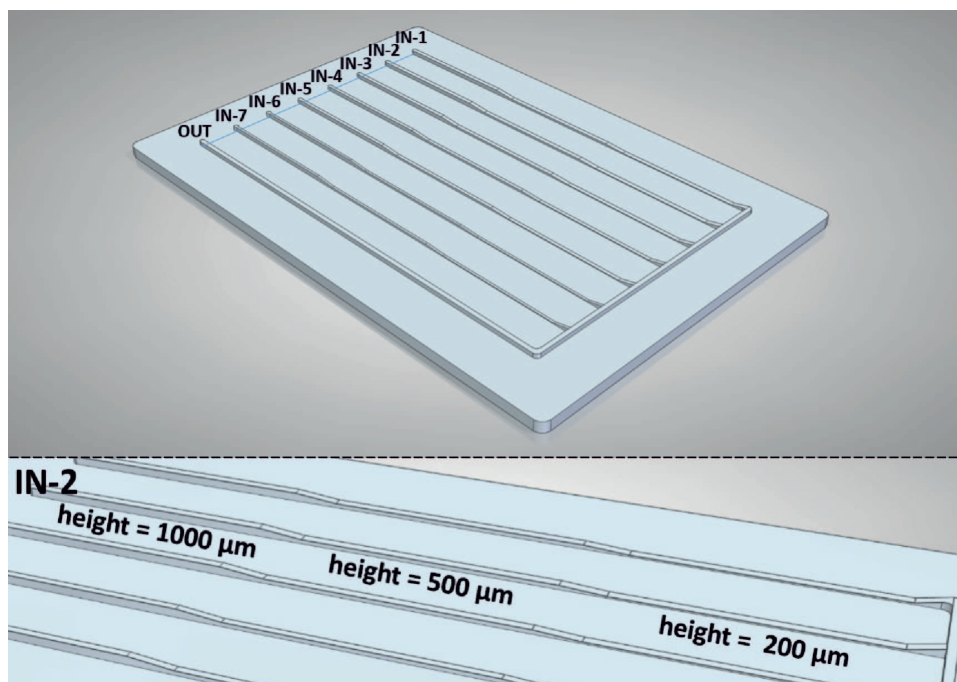


Figure 5.6: Part (A) of this figure shows the replication master for the molding of the microfluidic chips used for the presented experiments. The channel system consists of one outlet channel (OUT) and seven inlet channels (IN 1–7) that differ in width and are decreasing in height. Part (B) of the picture, this step-wise decrease is shown at the example of the channel 2 that allows experiments with different optical path length.

The microfluidic chip setup

A conventional disposable tip (DiTi) carrier from Tecan (Crailsheim, Germany) provides as base-module for the chip system. A custom made insert was placed in the carrier that serves as positioning site for the chip. The insert was designed with a gap, which allows the mounting of the monochromatic UV LED-spot (NVSU233A, 365 nm, Nichia, Japan) with a maximum irradiance of 68 mW/cm^2 under the microfluidic chip and thereby a irradiation from below. This LED-based irradiation system was equipped with a condenser and power supply by macrolenses (Dr.-Ing. Klaus Schmitt, Weinheim, Germany). An overview photograph of the setup on the liquid handling station is shown in figure 5.7. To control the irradiated reaction volume, a mask with a 7 mm \times 1 mm slit in direction of the channel was placed between the chip and the diode to create a defined irradiation slot.

The UV radiation coming out of the chip was weakened by mounting a piece of acrylic glass on top of the chip. With additional equipment from Tecan-like carriers for centrifuge tubes, microtiter plates, and troughs placed on the desk of the LHS an integration of the microfluidic chip in an automated screening procedure was possible. The liquid handling station used in this work was a Freedom EVO 200 (Tecan, Crailsheim, Germany) equipped with 1000 μL syringes and controlled by EVOware Standard (provided with the LHS).

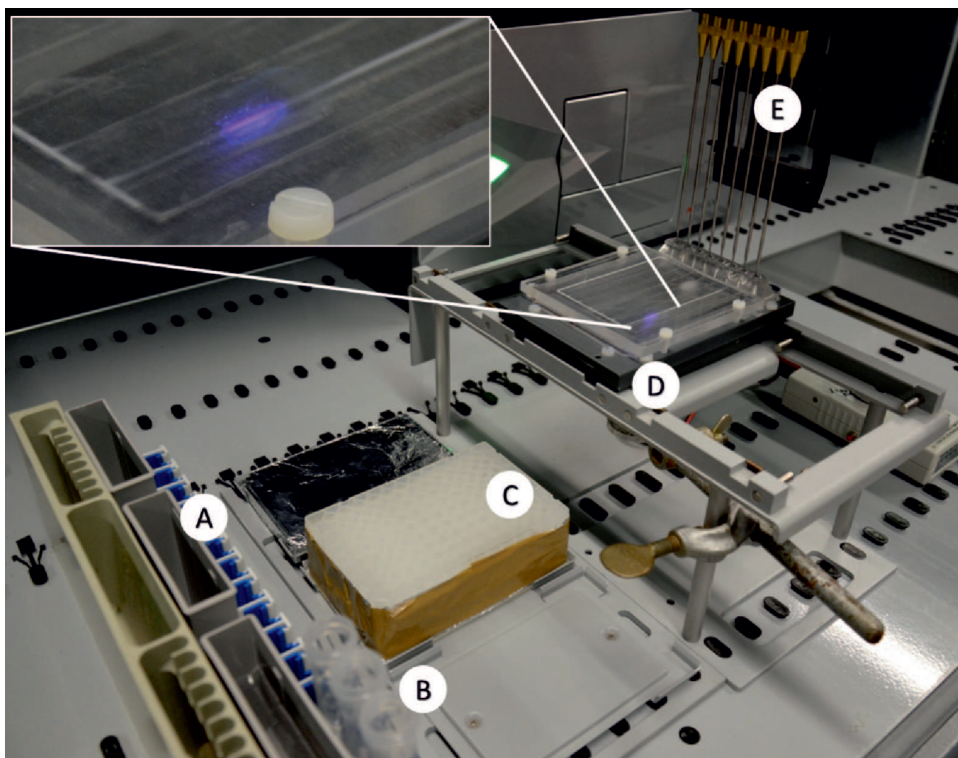


Figure 5.7: Photograph of the experimental setup on the liquid handling station. Shown here are troughs for the reagents (A), centrifugal tubes (B), and deep-well plate (C) for the storage and processing of the polymer samples. The modified carrier (D) for the microfluidic chip that allows the fixation of the LED-spot underneath the chip and a reversible connection between the channel system and the pipetting needles of the liquid handling arm (E). The magnified detail shows the irradiated channel section.

Design of experiments

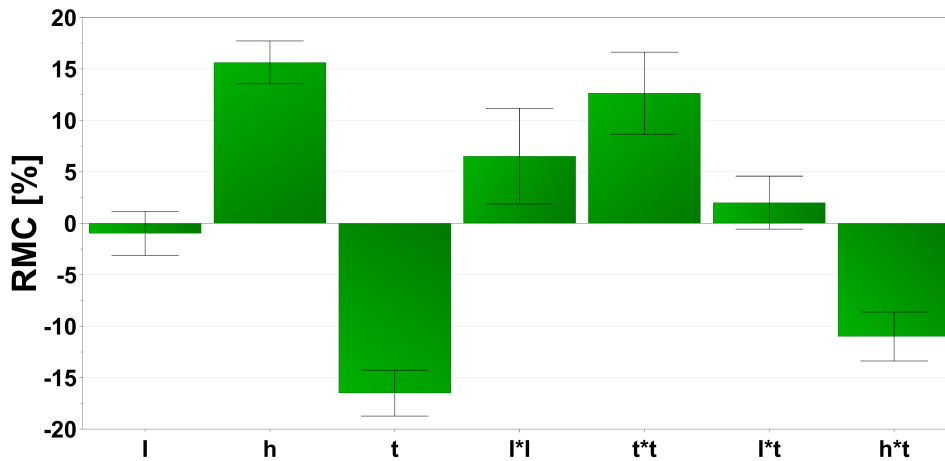
The experimental design was created by the use of MODDE (Version 10.1, Umetrics, Umeå, Sweden). Thus, four parameters with a critical influence on the miniemulsion photopolymerization in microfluidic channels were identified and set as factors with defined variation ranges. The considered variation ranges of the factors irradiation time t , irradiance I , initiator concentration c , and height of the microfluidic channel h (optical path) are presented in table 5.1.

Based on a D-optimal design a fractional factorial experimental matrix with 26 experi-

Table 5.1: Variation of the cause variables for the photopolymerization of styrene in microfluidic channels with irradiation at 365 nm ($I = 100$ % equals 68 mW/cm²)

Cause variable	Variation range
Irradiation time (t)	10-60 s
Irradiance (I)	25, 50, 75, 100 %
Initiator concentration (c)	0.5-3.0 wt%
Channel height (h)	20, 500, 1000 μm

ments was obtained. The experimental design included a threefold determination of the center point to affirm the experimental repeatability. The produced polymer lattices have been analyzed regarding the residual monomer content (RMC in %), their particle size distribution and the morphology of the polymer particles. The experimental results for the RMC were fitted with a quadratic model using the response-surface-method in MODDE consisting of 14 coefficients (including four linear, six interaction, and four quadratic terms). To discuss the influence of the factors on the RMC a model discrimination was performed to identify nonsignificant coefficients. The remaining coefficients are shown in figure 5.8 and the modeling results for RMC are depicted as contour plots.

**Figure 5.8:** Coefficient plot to illustrate the impact of irradiation time t , irradiance I , channel height h (optical path), and combined factors on the residual monomer content (RMC in %) for the 26 executed experiments of photoinitiated miniemulsion polymerization in microfluidic channels. The error bars represent the ± 95 % confidence interval.

Automated screening procedure

To explore the impact of different variable factors on the photopolymerization of miniemulsions in microfluidic channels a screening in the variation range of the cause variables was executed in an automated manner on a liquid handling station. Therefore, the chip setup was placed on the deck of the LHS and troughs with 25 mL miniemulsion of different compositions were put next to the chip carrier. For the sample preparation, a deep-well

microtiter plate and 15 mL centrifugal tubes, each with 100 mL ultrapure water, and a trough with Ethanol were provided on the platform (see figure 5.7). The mounting and irradiance of the LED-spot was adjusted manually.

For the polymerization runs, an amount of 800 μL of the prepared miniemulsion was aspirated by a pipetting needle. After the liquid handling arm (LiHa) was reversibly connected to the channel system, the miniemulsion was pumped semicontinuously in steps of 7 μL , which correlates with the irradiated volume through the mask. The pause between two steps allowed the control of the irradiation time. The time needed for the volume exchange was negligible. As soon as the complete volume of the irradiated miniemulsion was aspirated by the pipetting needle in the outlet port, the needles were elevated to unplug the connection and the sample was then dispensed in the microwell plate provided. A part of the sample was used to prepare a dilution with ethanol for GC-analysis. To protect the samples in the wells from light, the plate was wrapped in aluminum foil and covered with a lightproof lid. The dilution for the PCCS analysis (photon cross-correlation spectroscopy) was achieved by mixing 100 μL of the sample with 100 mL of ultrapure water in a centrifugal tube.

Before the following polymerization experiment could be executed, the channel was purged with water and dried with streaming air pumped by the LHS. After every polymerization cycle, the diluted samples could be taken off the LHS and were transferred to the subsequent analytics.

Analytics

For the determination of the residual monomer content, processed samples were analyzed via gas chromatography (Agilent 6890 plus, Agilent Technologies, Santa Clara, USA). The samples were mixed with ethanol (ratio of 1:4) in a microwell plate, followed by filtration through Nylon filter (0.2 μm pore size). The samples were analyzed at 200°C on a highly polar capillary column (Agilent INNOWax, 30 m length, 0.32 mm inner diameter, 0.25 μm film thickness). The chromatograms of the individual analyses were evaluated with the ChemStation Software (Agilent, REV. A10.02).

The samples for the determination of the particle size distribution via photon cross-correlation spectroscopy (PCCS) and for the study of the morphology of the polymer particles via SEM have been diluted with ultrapure water (ratio of 1:100). The photon cross-correlation spectroscopy was conducted in the NANOPHOX sensor system (Sympatec, Clausthal-Zellerfeld, Germany) and evaluated with the corresponding software (WINDOX, Version 5.6, Sympatec, Germany). The scanning electron microscope LEO1530 (LEO/Zeiss, Jena, Germany) has been used for the shape characterization of the polymer particle morphology.

Results & discussion

Coefficient plot

To validate the concept of screening photopolymerization in miniemulsions by employing the μF -on-LHS concept, styrene miniemulsions with varying Irgacure[®] 819 content were polymerized under the conditions brought out by the experimental design. These 26 experiments carried out within the stated factor ranges resulted in residual styrene concentrations

between 0 and 74 % with respect to the initial monomer concentration. Thus a wide range of response values could be discussed as model output. A response surface modeling approach was employed to identify sensitive process parameters to the residual monomer concentration and to identify the optimal parameter set leading to a complete conversion of styrene miniemulsions. The response surface methodology including all 14 coefficients of the four residual styrene concentration (RMC) defining factors predicted the experimental data very well with a coefficient of determination (R^2) of about 0.99, a model validity of 0.84 and a reproducibility of 0.98. Analyzing the significance of each factor to the response showed that the initial concentration of Irgacure[®] 819 had no perceptible impact on the residual styrene concentration after polymerization within the stated factor ranges. The selected range of photoinitiator variation might be too small for a noticeable impact, in connection with an overestimated minimum concentration. Figure 3 shows the coefficient plot with scaled and centered coefficients comparable with confidence intervals. In this plot the Irgacure[®] 819 concentration and its interaction terms have been excluded due to their nonsignificant influence on the model. The seven remaining coefficients simplify the response surface model with no lack of fit ($R^2 = 0.98$, model validity 0.83). The values of the coefficients (see figure 5.8) are indicators for the significance of the factors and interaction terms and their impact on the response. Thereby, factors with positive coefficient values make a contribution to higher residual styrene concentrations, while factors with negative ones are indicative for enhanced styrene conversion. Especially the coefficient of the irradiance itself is negative and nonsignificant, but the term of $I * I$ will lead to a remarkable effect at higher irradiance in the direction of higher residual styrene concentrations. This may be explained by depolymerization that becomes dominant at higher irradiance especially with increasing irradiation time. The comparatively limited effect of the irradiance can be explained in connection with the small impact of the interaction term $I * t$, which can be attributed to the fast bleaching of the photoinitiator even for the lowest investigated irradiance and highest investigated photoinitiator concentration (c.f. ongoing discussion in the following section). Keeping all other factors constant, the residual styrene concentration increases if the polymerization is carried out in higher channels. This dependency depicts that the influence of the penetration depth of the photons has to be considered even in photoreactors with optical path lengths between 200 and 1000 μm . Furthermore, the term $h * t$ predicts a positive interaction to the styrene conversion, thus a certain combination of channel height and irradiation time could enhance the polymerization results in regard to high monomer conversion. In addition, the factor time is represented in the negative factor t and in the positive term $t * t$, meaning that the longer the styrene miniemulsion is irradiated the smaller the residual styrene content after polymerization is. This effect will be counterbalanced at higher irradiation times by the positive term of $I * I$ that predicts higher residual styrene concentrations.

Response surface modeling

The results of the four-dimensional response surface modeling will be discussed on the basis of two sets of contour plots (figure 5.9). The negative values for the residual monomer content RMC at the limits of the response surfaces are extrapolated of the empiric modeling approach and are therefore taken as full conversion.

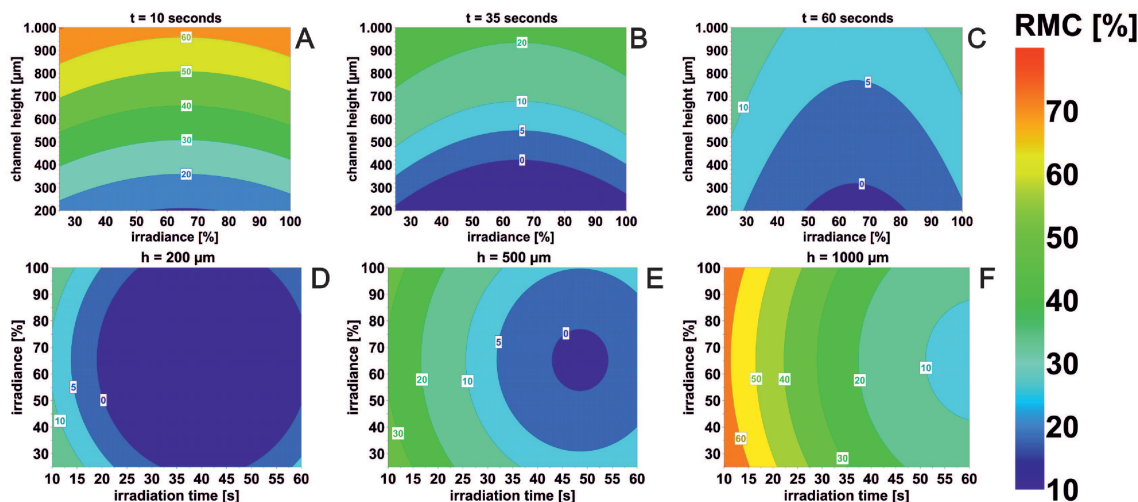


Figure 5.9: Contour plot set to illustrate the predicted development of the residual monomer content (RMC). (A–C) depending on the irradiance (25–100 %) and the channel height (200–1000 μm) for three different irradiation times (from left to right: $t = 10, 35, 60$ s). (D–F) Depending on the irradiation time (10–60 s) and the irradiance (25–100 %) for three different channel heights (from left to right: $h = 200, 500, 1000$ μm).

Figure 5.9A–C shows the RMC as a function of irradiance and channel height after 10, 35, and 60 s of irradiation. This sequence of subplots demonstrates that the monomer conversion increases with irradiation time from 10 to 60 s as expected for free radical polymerization mechanism among ongoing initiation steps and subsequent monomer addition to growing polymer radicals. For short irradiation times a RMC from 10 to 70 % can be achieved, in comparison with 0–30 % for intermediate and 0–15 % for the highest irradiation time. The negative influence of increasing channel height to the RMC is particularly distinctive for 10 s of irradiation and becomes much smaller in the case of 35 and 60 s. After irradiation with 50 % irradiance over 10 s, an increase in the optical path from 200 to 400 μm has more than doubled the RMC from 11 to 24 %, whereas for $t = 60$ s, the RMC is only increased by about 2 %. These results must be linked to the heterogeneity of the photochemical reactions system. The penetration depth of photons in monomer miniemulsions can be highly restricted due to scattering. According to Lobry et al. [146], droplets in the front layers have a higher probability of being nucleated than those in the rear. At high optical attenuation, initiation is highly localized leading to low conversion rates. The smaller the channel height and thus the optical path is, the more miniemulsion droplets are penetrated by incident photons and thus the polymerization reaction can be initiated within the whole reaction volume more equally. The penetration of photons in every droplet is a requirement in miniemulsion photopolymerization to achieve complete monomer conversion. Consequently, controlling the height with respect to the penetration depth of irradiation in a reactor for photopolymerization of miniemulsions, allows to reach quasi homogeneous reaction conditions for a rather heterogeneous system. This could be critical especially for continuous reactors in which turbulent flow is negligible. According to

figure 5.9A–C, a reduced effect of the channel height is predicted for 35 s of irradiation and is hardly present for 60 s. In summary, a positive interaction between channel height and irradiation time causes low RMC that means in effect that an increasing channel height demands an extension of the irradiation time simultaneously. The styrene concentration drops to less than 15 % after 60 s of irradiation in all channels up to 1000 μm . This appears surprisingly, since the expected penetration of UV radiation into photoinitiator-free monomer miniemulsions would not exceed 100 μm , with the consequence that only in a small fraction of droplets close to the irradiated surface polymerization could be initiated [147]. In addition, the presence of a photoinitiator will be further reduce the penetration depth of photons, leading to an enhanced heterogeneity between irradiated and nonirradiated volume. Nevertheless, employing a bleachable photoinitiator like BAPO, with longer irradiation times more photons are penetrating deeper into the reaction volume, as long as the “shielding” effect due to scattering phenomena becomes dominant. In fact, the observed transmission through the microfluidic chips increases with time for all channels heights and photoinitiator concentrations, in particular within the first 20 s for channel heights of 200 and 500 μm , which we attribute to the bleaching of the photoinitiator. This would imply that within this period the photoinitiator is completely consumed in the volume penetrated well with photons when scattering determine the optical properties of the miniemulsions only. As a consequence, for increasing optical path lengths, especially for the 1000 μm channel, other effects must be considered to explain the strong positive impact of the irradiation time on monomer conversion. On the basis of “shielding” due to scattering, only mixing effects by convection can cause that all the droplets of the miniemulsion are being nucleated within moderate time periods. This positive interaction can be exploited to enhance the photopolymerization performance by choosing maximal channel height and minimal irradiation time for complete monomer conversion. According to the subplots in figure 5.9A–C, the best performance regarding the throughput and monomer conversion with 0 % RMC would be achieved in a 200–400 μm channel, after 35 s of irradiation and 65 % irradiance. The curved contour levels depict that the irradiance passes through an optimum at a constant irradiation time. Moderate irradiance around 65 % result in a minimal RMC at channel heights up to 400 μm .

Tomovska et al. [148] discussed a comparable correlation between irradiance and the maximum conversion of styrene/butyl acrylate miniemulsions using irradiances of 2, 4, and 6 mW/cm^2 in a continuous photoreactor with 1 mm inner diameter after 30 min of irradiation. They explain the occurrence of a maximum in the monomer conversion in dependence of the irradiance with faster photoinitiator decomposition for higher irradiance and argue that the polymerization reaction stops after photoinitiator consumption. Taking this under consideration, an optimum for irradiance should be recognized in the modeling results for time and channel height dependency, because a complete exhaustion of the photoinitiator becomes unlikely for short irradiation times in combination with increased channel height. However, none of these dependencies can be recognized in the contour plots shown in figure 5.9. The course of the contour levels is similar within the subplots and only the absolute value of the RMC changes with irradiation time. Increasing the irradiance from 25 to about 65 % minimizes the RMC by approximately 7 % for all combinations of channel height and irradiation time, followed by a renewed increase of the RMC to a value

insignificantly lower at 100 % irradiance than at 25 %. According to the fundamentals of free radical polymerization mechanism, the active polymer chains (macro radicals) propagate further even if the photoinitiator is exhausted. This postpolymerization is attributed to the polymer radicals that continue to grow until bimolecular termination [149]. A more reasonable explanation for the occurrence of an optimum in irradiance refers to the primary radical generation and the competing recombination of primary with macro radicals. With increasing irradiance from 25 to 65 % more photoinitiator radicals (primary radicals) per time and volume are formed, because higher photon flux densities accelerate the initiation rate. Thus, the RMC decreases due to multiple chain initiation and propagation reactions running in parallel. If the irradiance is increased over 65 %, the concentration of photoinitiator radicals reached such a high level that the recombination of radicals becomes the dominating reaction, so either the reverse photolysis or the termination of chains by radicals are more likely to happen. Altogether, the polymerization rate decelerates at higher irradiances, because less primary radicals survive to be able to start the chain mechanism that results in higher RMC values. In conclusion, the contour plots depict that the RMC is basically controlled by factors time, channel height, and its interdependence with the irradiance, which appears to be optimal at about 65 %. The contour plots in figure 5.9D–F reveal additional information about the dependency of the predicted RMC on the irradiation time, which is plotted against irradiance for the three experimental channel heights in subplots, respectively. The RMC ranges from 17 to 0 % in 200 μm channels, for channels of 500 μm a RMC from 37 % up to complete conversion can be achieved and in 1000 μm channels values between 70 and 8 % are depicted for the RMC. The most remarkable characteristic shown in figure 5.9D–F is the occurrence of a minimum in the RMC with progressing irradiation time from 10 to 60 s. For a set combination of channel height and irradiance the RMC decreases with increasing irradiation time, since the ongoing decomposition of the photoinitiator leads to the formation of primary radicals able to initiate chain starts until exhaust of the photoinitiator. Subsequent and continuing propagation steps result into further consumption of monomer molecules. For the polymerization within 200 and 500 μm channels and intermediate irradiances, the values of the RMC are located in the dark plotted area of complete conversion. The shown subplots illustrate the shift of the RMC minimum with longer irradiation time and increasing channel height toward longer times of irradiation. The subplot on the right for the 1000 μm channel (figure 5.9F) gives reason to expect that the correspondent minimum will appear at irradiation times longer than 60 s, considering that an extrapolation beyond the limits of the design space is subject to considerable uncertainty. Nevertheless, under consideration of the heterogeneity of the reaction system again, one can assume/expect, that an irradiation time of 60 s is not sufficient in the 1000 μm channel to nucleate all miniemulsion droplets. It seems a matter of time that all droplets are able to reach the front layers, which are sufficient penetrated by photons. The negative influence on the RMC for longer irradiation times can be explained with depolymerization reactions leading to the reappearance of monomer molecules. The photodegradation and especially the photooxidation of polystyrene under UV irradiation are intensively discussed in the literature, e.g. in the review of Yousif et al. [150]. Depending on the chromophore groups existing in the reaction mixture and the irradiation conditions the absorption of photons

produce low molecular weight radicals and polymeric macro radicals that are able to accomplish chain scission leading to the reduction of the molecular weight of the polymer even in the absence of oxygen. In the presence of oxygen, which cannot be completely excluded in the conducted experiments, different photoproducts maybe formed during the photooxidation of polystyrene starting with the primary formation of hydroperoxides followed by several types of secondary reactions [151, 152]. Nevertheless, it is expected that for the employed microfluidic system oxygen contribution is very limited. Kaczmarek et al. [153] reported that small amounts (0.1–0.5 wt%) of photoinitiators like benzophenone accelerate photodestruction in polystyrene with breaking up of fragments from end chains under irradiation. The photolysis of benzophenone and Irgacure[®] 819 is characterized by the generation of benzoyl radicals, another potential species that could participate in depolymerization reactions at longer irradiation times. According to Kwant [154], depolymerization as the reverse reaction of chain propagation in styrene polymerization becomes significant in the range of rather high conversion, because diffusion limitations lower the rate constant of the propagation reaction significantly. These above-mentioned mechanistic aspects support the appearance of the RMC minimum in figure 5.9D–F due to depolymerization reactions that are effective at longer irradiation times.

REM analysis

The shape of the generated polymer particles were analyzed regarding the question if high monomer conversion has necessarily resulted in spherical polymer particles with a narrow particle size distribution as expected from miniemulsion polymerization mechanism. Conflicting this postulated narrow and monomodal polymer particle size distributions, PCCS measurements show broad monomodal or bimodal distributions (see figure 5.12). Nevertheless, the SEM images and PCCS measurements provide some information to support the discussed dependencies. The observed surface structures in the SEM images (see figure 5.10) vary from sharp spheres and half-shells over spherical particles covered with a cloudy layer of network-like polymer structures. In some experiments, usually in 1000 μm channels and with short irradiation times, no regular polymer structures are detected by SEM analysis. An interpretation of the images in correlation with corresponding RMC values illustrates that experimental conditions resulting in a low RMC do not necessarily result in spherical, equal-sized polymer particles consequently. Figure 5.10 shows exemplarily the differences in the surface appearances of generated polymer particles out of three experiments with 0 % RMC in each case. The spherical and hemispherical polymer particles as shown in the right image of figure 5.10 most closely correspond to the expected polymer structure and moreover to the optimal experimental conditions predicted by the response surface modeling. The deviation from the ideal spherical polymer structure in figure 5.10, thus the occurrence of half-shell particles, cloudy layer formation (figure 5.10, center image) and the sticking in network-like structures (figure 5.10, left image), can be explained by the formation of styrene dimers up to short oligomers in dependency of the selected polymerization conditions. For example, the cloudy layer in the center image indicates that 100 % irradiance compared with 75 % in the right image may be indicative for an excess of photons in channels with 200 μm height, so concurrently propagating chains are terminated to yield a high amount of small molecular weight polymers. As

possible explanation for the appearance of cloudy layers and different polymer particle shapes, the preparation conditions of the samples for SEM imaging and the formation of gel-type polymer structures has to be taken into account.

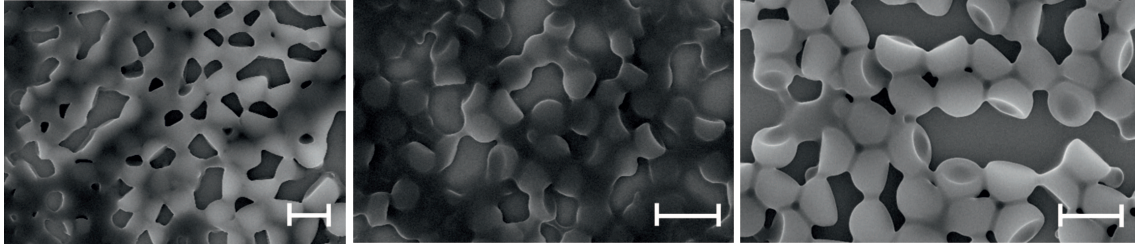


Figure 5.10: SEM images of the resulting polystyrene particles from experiments in the 200 μm channel with a RMC of 0 % but different configurations ((A): I = 50 %, t=60 s, 2.2wt% Irgacure[®] 819; (B): I = 100 %, t = 35 s, 1.8 wt% Irgacure[®] 819; (C): I = 75%, t = 60 s, 3.0 wt%) Irgacure[®] 819). Scale on the left image: 2000 nm, on the middle and right image: 1000 nm.

The polymer surface structures presented in figure 5.11 show considerable differences, although the shown particles were generated in experiments resulting in a RMC of around 17 %. The differences can be connected to different initial photoinitiator concentrations. The resulting particles shown in the left image clarify, that using a Irgacure[®] 819 concentration of 0.5 % is not sufficient in 1000 μm channels to form sharp, spherical polymer particles during 60 s of irradiation even at 100 % irradiance, whereas 3 % Irgacure[®] 819 provide well-defined structures like shown in the right image of figure 5.11.

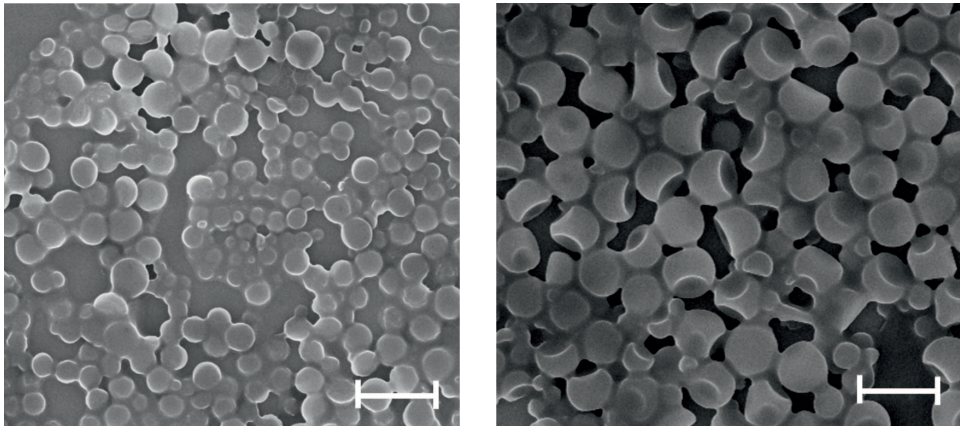


Figure 5.11: SEM images of the resulting polystyrene particles from experiments in the 1000 μm channel with an irradiation time of 60 s and an irradiance of 100 and 17 % RMC. The concentration of the initiator varies from 0.5 wt% on the (A) to 3.0 wt% on the (B). Scale: 1000 nm.

Particle size distribution

The measured particle size distributions of the polymer particles range from bimodal distributions to broad monomodal behavior (see figure 5.12). The main polymer fraction is located between 300 and 400 nm in diameter. This particle size is consistent with

the dominated particle size observed in SEM images for the well-defined spherical and hemispherical polymer structures. The second size is for all experiments either smaller than 120 nm or around 160 nm or not obvious. Particle sizes beneath 120 nm seem to be an artifact in these PCCS measurements, because correspondent polymer particles could not be confirmed by SEM image analysis. However, it should be noticed that polymer structures from these experiments were strongly sticking together and had no well-defined spherical shape. It can be assumed that PCCS analysis only provides reliable information for nearly spherical polymer particles and should not be applied if a sticky network of oligomers contributes to the scattered light signal as well.

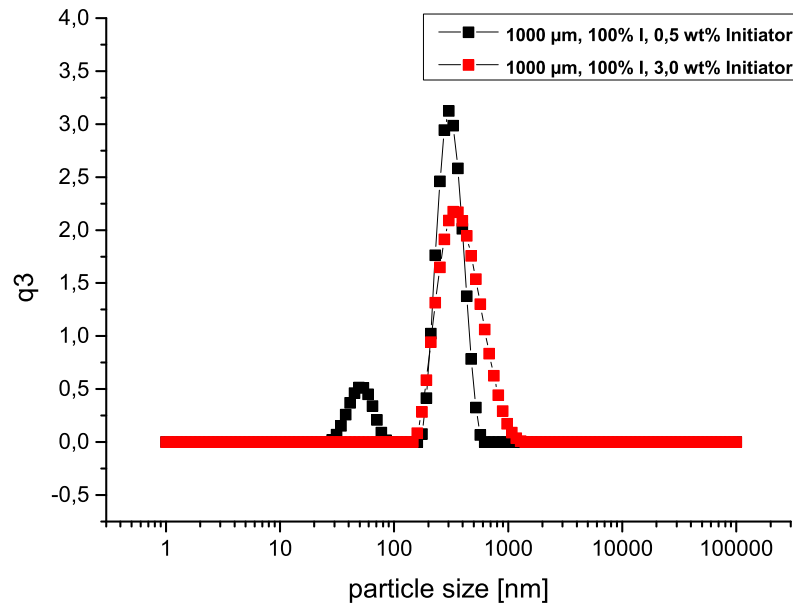


Figure 5.12: Particle size distribution of the resulting polystyrene particles from experiments in the 1000 μm channel with 100 % irradiance and a photoinitiator concentration of 0.5 wt% (black squares) respectively 3.0 wt% (red squares).

Concluding remarks

The reported combination of microfluidics and liquid handling stations ($\mu\text{F-on-LHS}$) was successfully adapted to the screening of photoinitiated miniemulsion polymerization. The concept was validated by styrene miniemulsion photopolymerization under variation of the cause variables like irradiance, irradiation time, and optical pathway. Employing statistical methods (DoE) this concept is a promising tool for the investigation of complex interdependencies with automated execution and low sample consumption.

It was shown that complete monomer conversion as required for bioapplications can be reached in channels with an optical path length smaller than 1000 μm . An increase in irradiation time led to a decrease of the residual monomer content. A linkage of complete monomer conversion to spherical particles in principle could not be deduced by the analysis of SEM images.

Probably, the molecular weight distribution of the formed polymers is another topic

for the comprehensive understanding of the photoinitiated miniemulsion polymerization, which has to be the subject of further investigations. In this context, a reconsideration of the impact of the photoinitiator concentration on the molecular weight has to be taken into account. Thus, the design space will be expanded for the consideration of the impact of the cause variables on the polymer shape and characteristics. To conduct the required experiments the presented strategy is expected to be very suitable.

Acknowledgments

This research work is part of the project “Molecular Interaction Engineering: From Nature’s Toolbox to Hybrid Technical Systems,” which is funded by the German Federal Ministry of Education and Research (BMBF), funding code 031A095B. The authors bear the complete responsibility for the content of this publication. Special thanks go to Volker Zibat from the Laboratory for Electron Microscopy at the Karlsruhe Institute of Technology (LEM – KIT) for recording the SEM images.

References

67. Lobry, E., Jasinski, F., Penconi, M., Chemtob, A., Croutxé-Barghorn, C., Oliveros, E., Braun, A. M., and Criqui, A. ‘Continuous-flow synthesis of polymer nanoparticles in a microreactor via miniemulsion photopolymerization’. *RSC Advances*, vol. 4(82) (2014), pp. 43756–43759 (cit. on pp. 4, 37).
79. Waldbaur, A., Kittelmann, J., Radtke, C. P., Hubbuch, J., and Rapp, B. E. ‘Microfluidics on liquid handling stations (μ F-on-LHS): an industry compatible chip interface between microfluidics and automated liquid handling stations’. *Lab on a Chip*, vol. 13(12) (2013), pp. 2337–2343 (cit. on pp. 5, 20, 37, 38, 59, 60, 68, 78).
107. Mellott, M. B., Searcy, K., and Pishko, M. V. ‘Release of protein from highly cross-linked hydrogels of poly (ethylene glycol) diacrylate fabricated by UV polymerization’. *Biomaterials*, vol. 22(9) (2001), pp. 929–941 (cit. on pp. 10, 36, 78, 96, 101, 103, 105).
108. Quick, D. J. and Anseth, K. S. ‘DNA delivery from photocrosslinked PEG hydrogels: encapsulation efficiency, release profiles, and DNA quality’. *Journal of Controlled Release*, vol. 96(2) (2004), pp. 341–351 (cit. on pp. 10, 36).
123. Ramakrishna, S., Mayer, J., Wintermantel, E., and Leong, K. W. ‘Biomedical applications of polymer-composite materials: a review’. *Composites science and technology*, vol. 61(9) (2001), pp. 1189–1224 (cit. on p. 36).
124. Baroli, B. ‘Photopolymerization of biomaterials: issues and potentialities in drug delivery, tissue engineering, and cell encapsulation applications’. *Journal of Chemical Technology and Biotechnology*, vol. 81(4) (2006), pp. 491–499 (cit. on pp. 36, 37).
125. Fisher, J. P., Dean, D., and Mikos, A. G. ‘Photocrosslinking characteristics and mechanical properties of diethyl fumarate/poly (propylene fumarate) biomaterials’. *Biomaterials*, vol. 23(22) (2002), pp. 4333–4343 (cit. on p. 36).
126. Davis, K. A., Burdick, J. A., and Anseth, K. S. ‘Photoinitiated crosslinked degradable copolymer networks for tissue engineering applications’. *Biomaterials*, vol. 24(14) (2003), pp. 2485–2495 (cit. on p. 36).
127. Anseth, K., Goodner, M., Reil, M., Kannurpatti, A., Newman, S., and Bowman, C. ‘The influence of comonomer composition on dimethacrylate resin properties for dental composites’. *Journal of dental research*, vol. 75(8) (1996), pp. 1607–1612 (cit. on p. 36).
128. Lu, M., Lan, H., Wang, F., and Wang, Y. ‘A novel cell encapsulation method using photosensitive poly (allylamine alpha-cyanocinnamylideneacetate)’. *Journal of microencapsulation*, vol. 17(2) (2000), pp. 245–251 (cit. on p. 36).
129. Quek, C.-H., Li, J., Sun, T., Chan, M. L. H., Mao, H.-Q., Gan, L. M., Leong, K. W., and Yu, H. ‘Photo-crosslinkable microcapsules formed by polyelectrolyte copolymer

- and modified collagen for rat hepatocyte encapsulation'. *Biomaterials*, vol. 25(17) (2004), pp. 3531–3540 (cit. on p. 36).
130. Gobin, A. S. and West, J. L. 'Effects of epidermal growth factor on fibroblast migration through biomimetic hydrogels'. *Biotechnology progress*, vol. 19(6) (2003), pp. 1781–1785 (cit. on p. 36).
 131. Yokoyama, S., Nakahama, T., Miki, H., and Mashiko, S. 'Fabrication of three-dimensional microstructure in optical-gain medium using two-photon-induced photopolymerization technique'. *Thin Solid Films*, vol. 438 (2003), pp. 452–456 (cit. on p. 36).
 132. Arcaute, K., Mann, B. K., and Wicker, R. B. 'Stereolithography of three-dimensional bioactive poly (ethylene glycol) constructs with encapsulated cells'. *Annals of biomedical engineering*, vol. 34(9) (2006), pp. 1429–1441 (cit. on p. 36).
 133. Pierre, S. J., Thies, J. C., Dureault, A., Cameron, N. R., Hest, J. C. van, Carette, N., Michon, T., and Weberskirch, R. 'Covalent enzyme immobilization onto photopolymerized highly porous monoliths'. *Advanced Materials*, vol. 18(14) (2006), pp. 1822–1826 (cit. on p. 36).
 134. Li, L., Zhao, N., and Liu, S. 'Versatile surface biofunctionalization of poly (ethylene terephthalate) by interpenetrating polymerization of a butynyl monomer followed by "Click Chemistry"'. *Polymer*, vol. 53(1) (2012), pp. 67–78 (cit. on p. 36).
 135. Chemtob, A., Kunstler, B., Croutxé-Barghorn, C., and Fouchard, S. 'Photoinduced miniemulsion polymerization'. *Colloid and Polymer Science*, vol. 288(5) (2010), pp. 579–587 (cit. on p. 36).
 136. Daniloska, V., Tomovska, R., and Asua, J. M. 'Hybrid miniemulsion photopolymerization in a continuous tubular reactor—A way to expand the characteristics of polyurethane/acrylics'. *Chemical Engineering Journal*, vol. 184 (2012), pp. 308–314 (cit. on pp. 36, 37).
 137. Landfester, K. 'Miniemulsion polymerization and the structure of polymer and hybrid nanoparticles'. *Angewandte Chemie International Edition*, vol. 48(25) (2009), pp. 4488–4507 (cit. on p. 36).
 138. Antonietti, M. and Landfester, K. 'Polyreactions in miniemulsions'. *Progress in Polymer Science*, vol. 27(4) (2002), pp. 689–757 (cit. on p. 36).
 139. Jasinski, F., Lobry, E., Chemtob, A., Croutxé-Barghorn, C., and Criqui, A. 'Photopolymerizable monomer miniemulsions: why does droplet size matter?' *Macromolecular Chemistry and Physics*, vol. 214(15) (2013), pp. 1669–1676 (cit. on p. 36).
 140. Penconi, M., Lobry, E., Jasinski, F., Chemtob, A., Croutxé-Barghorn, C., Criqui, A., Braun, A. M., and Oliveros, E. 'The use of chemical actinometry for the evaluation of the light absorption efficiency in scattering photopolymerizable miniemulsions'.

- Photochemical & Photobiological Sciences*, vol. 14(2) (2015), pp. 308–319 (cit. on p. 36).
141. Patel, H., Raval, D., Madamwar, D., and Patel, S. ‘Polymeric prodrug: Synthesis, release study and antimicrobial property of poly (styrene-co-maleic anhydride)-bound acriflavine’. *Macromolecular Materials and Engineering*, vol. 263(1) (1998), pp. 25–30 (cit. on p. 37).
 142. Montgomery, D. C., Peck, E. A., and Vining, G. G. *Introduction to linear regression analysis*. John Wiley & Sons, 2012 (cit. on p. 37).
 143. Malkoch, M., Thibault, R. J., Drockenmuller, E., Messerschmidt, M., Voit, B., Russell, T. P., and Hawker, C. J. ‘Orthogonal approaches to the simultaneous and cascade functionalization of macromolecules using click chemistry’. *Journal of the American Chemical Society*, vol. 127(42) (2005), pp. 14942–14949 (cit. on p. 38).
 144. Decker, C., Zahouily, K., Decker, D., Nguyen, T., and Viet, T. ‘Performance analysis of acylphosphine oxides in photoinitiated polymerization’. *Polymer*, vol. 42(18) (2001), pp. 7551–7560 (cit. on p. 38).
 145. Laurino, P., Hernandez, H. F., Bräuer, J., Krüger, K., Grützmacher, H., Tauer, K., and Seeberger, P. H. ‘Snowballing radical generation leads to ultrahigh molecular weight polymers’. *Macromolecular rapid communications*, vol. 33(20) (2012), pp. 1770–1774 (cit. on p. 38).
 146. Lobry, E., Jasinski, F., Penconi, M., Chemtob, A., Ley, C., Croutxé-Barghorn, C., Oliveros, E., Braun, A. M., and Criqui, A. ‘Absorption and scattering in concentrated monomer miniemulsions: static and dynamic investigations’. *Macromolecular Chemistry and Physics*, vol. 215(12) (2014), pp. 1201–1211 (cit. on p. 44).
 147. Hoijemberg, P. A., Chemtob, A., Croutxé-Barghorn, C., Poly, J., and Braun, A. M. ‘Radical photopolymerization in miniemulsions. Fundamental investigations and technical development’. *Macromolecules*, vol. 44(22) (2011), pp. 8727–8738 (cit. on p. 45).
 148. Tomovska, R., Cal, J. C. de la, and Asua, J. M. ‘Miniemulsion photo-copolymerization of styrene/butyl acrylate in a continuous tubular reactor’. *Industrial & Engineering Chemistry Research*, vol. 53(18) (2013), pp. 7313–7320 (cit. on p. 45).
 149. Decker, C. ‘Kinetic study and new applications of UV radiation curing’. *Macromolecular Rapid Communications*, vol. 23(18) (2002), pp. 1067–1093 (cit. on p. 46).
 150. Yousif, E. and Haddad, R. ‘Photodegradation and photostabilization of polymers, especially polystyrene: review’. *SpringerPlus*, vol. 2(1) (2013), p. 398 (cit. on p. 46).
 151. Bottino, F. A., Cinquegrani, A. R., Di Pasquale, G., Leonardi, L., and Pollicino, A. ‘Chemical modifications, mechanical properties and surface photo-oxidation of films of polystyrene (PS)’. *Polymer testing*, vol. 23(4) (2004), pp. 405–411 (cit. on p. 47).

152. Gardette, J.-L., Mailhot, B., and Lemaire, J. 'Photooxidation mechanisms of styrenic polymers'. *Polymer degradation and stability*, vol. 48(3) (1995), pp. 457–470 (cit. on p. 47).
153. Kaczmarek, H., Kamińska, A., Świątek, M., and Sanyal, S. 'Photoinitiated degradation of polystyrene in the presence of low-molecular organic compounds'. *European polymer journal*, vol. 36(6) (2000), pp. 1167–1173 (cit. on p. 47).
154. Kwant, P. 'Kinetics of styrene polymerization at ultrahigh conversion'. *Journal of Polymer Science: Polymer Chemistry Edition*, vol. 17(10) (1979), pp. 3397–3410 (cit. on p. 47).

5.3 Fully Automated Method for Fluorescence *in situ* Hybridization for Biofilm Analysis

Silla H. Hansen^{1*}, Carsten P. Radtke^{2*}, Eva Krolitzki², Susanne Krause³, Tobias Kabbeck³, Michael Wagner⁴, Johannes Gescher³, Jürgen Hubbuch² and Christof M. Niemeyer¹

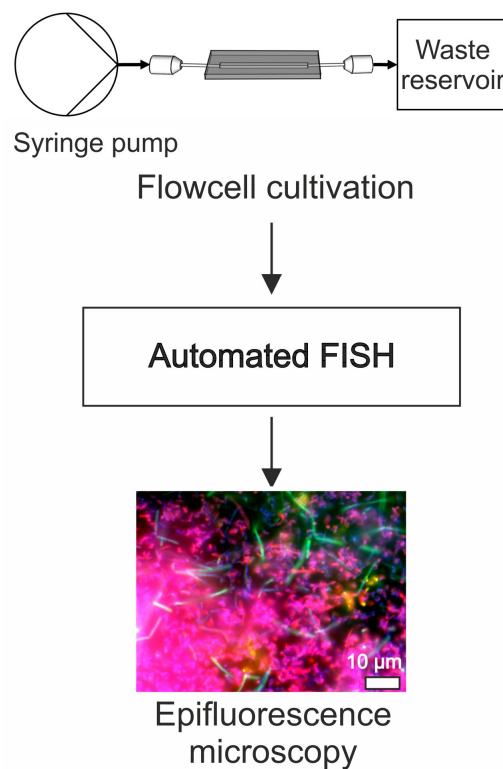
¹*Institute for Biological Interfaces 1, Karlsruhe Institute of Technology (KIT), 76344 Eggenstein-Leopoldshafen, Germany*

²*Institute of Engineering in Life Sciences, Section IV: Biomolecular Separation Engineering, Karlsruhe Institute of Technology (KIT), 76131 Karlsruhe, Germany*

³*Institute for Applied Biosciences, Department of Applied Biology, Karlsruhe Institute of Technology (KIT), 76131 Karlsruhe, Germany*

⁴*Engler-Bunte-Institut, Water Chemistry and Water Technology, Karlsruhe Institute of Technology (KIT), 76131 Karlsruhe, Germany*

* These authors contributed equally to this work.



Original manuscript is edited and extended for a publication in a wider context

Abstract

Fluorescence *in situ* hybridization (FISH) as well as catalyzed reporter deposition fluorescence *in situ* hybridization (CARD-FISH) are extremely powerful tools for microbiological research. Unfortunately, both techniques are highly time- and labour-consuming which complicates the analysis of multiple parallel experiments. Therefore, this study describes the development of an automated platform for FISH and CARD-FISH, which combines a cultivation flowcell with a commercially available liquid handling station to enable fully automated analysis of up to nine biofilm flowcells in parallel. The method was successfully applied for the identification and quantification of mixed model organisms and an acidophilic environmental biofilm from a pyrite mine. Owing to the standardized dimensions and formats of the newly designed modular platform, standard devices and equipment of the liquid handling station could be readily implemented including a microplate reader for fluorescence spectroscopic analysis of the labeled biofilms. This allowed us to establish a semi-quantitative read out of the fluorescence hybridization signals. The automated procedure enabled parallelization and high reproducibility of the analysis of fluidic cultivation systems.

Keywords: *FISH; CARD-FISH; biofilm; microfluidics; high-throughput experimentation*

Introduction

Biofilms are one of the most abundant form of microbial life in our ecosystems. This extremely robust class of living systems affects various areas of human life. On the one hand, biofilms are causing severe problems, like biofouling or hardly treatable infections [155]. On the other hand they are nowadays known to be essential for human health [156] and their potential for industrial processes is far from being exploited [157]. In the past decades, biofilm research was mainly focused on single species model systems, such as *Pseudomonas* and *Bacillus* species as well as various *E. coli* strains [155, 158]. However, to fully understand and effectively take advantage of biofilms, studies of multi-species biofilms are inevitable and therefore there is a growing interest in complex microbial communities [159, 160]. Multispecies biofilms are prevalent in nature and the study of spatially-dependent cell organization in biofilm development plays an important role in elucidating interspecies interactions in these systems [160]. To meet the requirements of modern biofilm research, novel tools are necessary to enable investigations in a highly parallel fashion with high throughput. To study biofilms *in vitro*, flowcells are often more favourable than static plate based methods because the hydrodynamic conditions in flowcells do much better resemble the natural environment of the majority of biofilms. This holds particularly true for fluidic shear forces, which strongly influence the microbial communities' behaviour [161, 162]. While there are several assays available for the parallel screening of the static growth of biofilms [163–165], to date only very few approaches have been reported which are suitable for the parallel screening of biofilms cultured in flowcells [62, 63, 166, 167]. For example, Benoit et al. [166] have used the commercially available Bio-Flux system for parallel viability screening of flow biofilms. This device enables the cultivation of up to 96 biofilms in microfluidic channels. More recently the same system was used to study biofilm formation and host-pathogen interactions of pathogenic *E. coli* [167]. As a drawback of this device, researchers are limited to the available channel geometries and an automated fluid exchange is not provided. Furthermore these studies have been restricted to single-species biofilms. To the best of our knowledge, no method is currently available for comparative screening studies of multispecies flow biofilms with high throughput. Flowcells have been combined with imaging techniques like confocal laser scanning microscopy (CLSM) to study the spatial structure and bacterial organisation under culturing conditions [168]. While this requires the expression of recombinant fluorescent proteins, end-point analyses can be achieved by fluorescence *in situ* hybridization (FISH), which is nowadays an established tool for the identification of single species within complex native microbial communities [169, 170]. Typically, ribosomal RNA (rRNA)-targeting oligonucleotide probes with specificities ranging from the species level to the level of phyla are used to identify single microbial cells. The so-called “catalysed reporter deposition fluorescence *in situ* hybridization (CARD-FISH)” provides a higher sensitivity than regular FISH because the catalytic signal amplification step with horseradish peroxidase (HRP) enables reliable detection of cells with low cellular ribosome content [171]. However, common drawbacks of the FISH methods stem from the time consuming and work-intensive procedures and the limited number of probes that can be used in a single experiment. As an approach to overcome the latter problem, flow-through systems have been tested for semi-automated

FISH protocols in the chromosomal analysis of eukaryotic cells [172]. However, they either require highly sophisticated fluidic chips to achieve semi-automation [~tai2013, 173] or they cannot avoid numerous manual handling steps [174–176]. For example, an automated procedure for quantitative cell characterization by FISH has recently been proposed [172], but its practical implementation remains to be demonstrated. Here we report on the development of an interface for the handling of biofilm flowcells and the implementation of a fully automated FISH procedure including analysis by fluorescence spectroscopy taking advantage of commercially available and widely established liquid handling stations (LHS). Our system is based on the platform proposed by Waldbaur et al. [79]. The dimensions, contact points and connections are compatible with standard microtiter plate equipment, such as thermocycler, shaker and plate readers, and offer full flexibility in the choice of the flowcells' geometry. As a proof of concept, we demonstrate the fully automated FISH analysis of single- and mixed-species biofilms of *Escherichia coli* and *Bacillus subtilis* grown in up to nine independent flow chambers with constant medium supply. Moreover, to demonstrate the scope of our system, we implemented the complex and sensitive CARD-FISH procedure, often used for reliable identification of slow growing species in complex natural biofilms. An acidophilic consortium derived from a former pyrite mine [177] was cultivated in the flowcell and automated CARD-FISH was conducted to screen for members from the groups of Archaea and Bacteria.

Materials and Methods

General workflow

Biofilms were cultivated under flow in the newly developed cultivation chips. The chips were tightly connected to the tubing via standard sterile cannulas. Since this connection is reversible, after cultivation the flowcells could easily be disconnected from the silicone tubing and reconnected to the chip-to-LHS interface described below. Fluorescence *in situ* hybridization was then carried out fully automated on a LHS type Tecan Freedom Evo 200 (Tecan, Switzerland) controlled by Evoware 2.5 (Tecan). Besides the custom made flowcells, cartridges and a modified holder only commercially available accessories were used for the procedure. The stained biofilms were automatically transferred to the integrated microplate reader for fluorescence analysis. Subsequently, the biofilm structure was examined manually by epifluorescence microscopy (cf. figure 5.13).

Flowcell fabrication and chip-to-LHS interface

The channel of the flowcell for biofilm cultivation was 3 mm wide, 1 mm high and 54 mm long giving a channel volume of 162 μL . The width was chosen in accordance with the lateral resolution and minimal spot size for fluorescence measurements of the Tecan microplate reader (Infinite M200 pro Tecan, Switzerland). The outer dimensions of the chips were 26x76 mm according to the standard format of microscope slides, to enable examination of the chips with all standard microscopes. The replication master used for molding of the flowcell was milled in brass with a computerized numerical control (CNC) machine. Cannulas (Sterican, B. Braun Melsungen AG, Germany), were inserted through horizontal holes in the mold before pouring the PDMS prepolymer (Sylgard 184, Dow Corning, USA) to serve as placeholders for the later connection channel. The PDMS was cured at 60°C

for at least 3h. The PDMS chip was bonded to a cover glass after activating both parts for two minutes with oxygen-plasma (2 minutes, 20 sccm, 300 W, Plasma Flecto 10, Plasma technology, Germany). The use of a cover glass for sealing the channel structure enabled microscopic observations through the bottom of the chip. Standard cannulas were inserted in the preformed connection channel to link the chip to the silicone tubing (figure 5.13). The chip-to-LHS interface consisted of the flowcells, the inlet and outlet structures, connecting cannulas and the three-part cartridge. One cartridge can hold up to three cultivation chips for automated handling on the LHS (Fig. 1). The PDMS structures for inlet and outlet were produced by solution casting of PDMS. The replication masters for this process as well as the flowcell cartridges were produced by 3D-printing (Sculpteo, France). During the casting process, as described for the fabrication of the flowcell, blunt cannulas inserted through horizontal holes served as placeholders for the later connection channels between flowcells and the respective structure. The flowcells were connected to these structures via standard stainless steel capillaries (Sterican, B. Braun Melsungen AG, Germany). The pipetting needles of the LHS could enter in the cone shaped connector ports of the inlet structure to establish the leak-free but reversible connection between the pipetting needles and the fluidic chip (Fig. 1). The design of the PDMS inlet structure was adopted from the “microfluidics-on-liquid handling station” (μ F-on-LHS) concept introduced by Waldbaur et al. [79]. The outlet structure was designed suitable for storage of up to 800 μ L liquid in each cavity. The accumulated liquid could be removed from the cavities by the pipetting needles. The fully assembled fluidic system (injection structure, up to three flowcells, outlet structure) was placed in the carrier to allow for automated transfer by the robotic manipulator arm (RoMa) of the LHS. The cartridge system comprised of the bottom plate with positioning recesses, a cover with access holes for the pipetting needles and a removable lid to enable optical analysis (Fig. 1). The cover provided light protection and prevented lifting of the fluidic system from the bottom plate.

Biofilm cultivation in flowcells

Prior to assembly, all parts were sterilized by UV-radiation for 1.5 h, subsequently the parts were connected under sterile conditions. The whole system was flushed with 70 % isopropyl alcohol and filled with lysogeny broth medium (LB) (5 g/l yeast extract, 10 g/l tryptone, 5 g/l NaCl) with a multichannel syringe pump (KDS Multi syringe infusion/withdrawal pump series 230, KD Scientific, USA). *E. coli* DH5 α and *B. subtilis* DSM1088 were cultured in LB medium. The system was equilibrated with the LB medium overnight. For inoculation, overnight cultures (LB, 37°C) of both species were diluted to an optical density of 0.1 at 600 nm (OD₆₀₀). For mixed species biofilms the overnight cultures were adjusted to an OD₆₀₀ of 0.2 and subsequently mixed in a ratio of 1:1. The cultivation channels were inoculated by injecting 300 μ L of the diluted precultures. The system was incubated without flow for one hour to allow initial attachment of the microorganisms. Subsequently, the biofilms were cultivated at 37°C for 12 h with a constant flowrate of 50 μ L/min. The acidophilic consortium was inoculated with a suspension of the native biofilm which was collected from the abandoned pyrite mine “Drei Kronen und Ehrt” in the Harz Mountains in Germany [177, 178] and stored at -80°C until usage. The biofilm was cultivated with an adopted Picrophilus medium (FeSO₄ 90 mM, 0.128 g/l yeast extract, 1.51 mM (NH₄)₂SO₄,

MgSO₄ 2 mM, CaCl 1.7 mM, Wolfe's mineral elixir, vitamin solution, [pH 2.5]) [179] at room temperature under constant medium flow for four weeks (10 μ L/min)

Automated Fluorescence *in situ* hybridization

For automated execution of the FISH protocol, the Tecan Freedom Evo 200 (Tecan, Switzerland) was equipped with two temperature control systems (F25-MC, Julabo, Germany) with coupled microplate/eppendorf tube carrier and a custom made modification for a microplate carrier which prevented the cartridge from lifting when the pipetting needles were retracted. One temperature control system was constantly cooled to 4°C and used for storage of heat-sensitive reagents (hybridization buffer, DAPI solution), the second temperature control system was initially cooled to 4°C for the fixation step of the FISH-assay and afterwards heated to 48°C for hybridization. Temperature adjustments and all other process steps were controlled by the Evoware software. Figure 1 displays a detailed scheme of the LHS deck. The automated FISH procedure followed the protocol from Pernthaler [171]. All reagents were injected to the channels by the LHS with a flowrate of 50 μ L/min.

Fixation and permeabilization of flow biofilms Flow biofilms were fixed by purging the channel with 660 μ L of 4 % formaldehyde in LB medium and incubation for 60 minutes at 4°C. Subsequently, the biofilms were washed with 660 μ L phosphate buffered saline (PBS) (137 mM NaCl, 2.7 mM KCl, 10 mM Na₂HPO₂, 1.76 mM KH₂PO₂, [pH 7.6]). Cells were then further permeabilized with 0.1 M HCl (660 μ L) for 10 minutes at room temperature. Afterwards, the channels were purged with 242 μ L ultrapure water (ISO 3696).

Hybridization *B. subtilis* was visualized by hybridization with Alexa Fluor 488 labeled LGC354B probe (5'-3' [A488]- CGGAAGATTCCTACTGC) (Sigma-Aldrich, USA). *E. coli* was stained with Alexa Fluor 546 labeled Ent probe (5'-3' [A546]- CCCC-CWCTTTGGTCTTGC) (Sigma-Aldrich, USA). The hybridization buffer (0.9 M NaCl, 20 mM Tris-HCl [pH 8.0], 0.01 % SDS, 35 % formamide) containing 0.5 pmol/ μ L of both probes was stored on deck at 4°C until usage. An amount of 400 μ L was injected into the channel. Hybridization was carried out at 46°C for 90 minutes.

Washing The excess probe was removed by purging the channel with 660 μ L of preheated washing buffer (70 mM NaCl, 20 mM TrisHCl [pH 8.0], 5 mM EDTA, 0.01 % SDS) followed by another incubation at 46°C for 15 minutes. Subsequently the biofilms were washed a second time with 440 μ L of saline and sodium citrate buffer (SSC) (150 mM NaCl, 15 mM trisodium citrate, [pH 7.0]), incubated again for 15 minutes at room temperature and finally rinsed with ultrapure water (440 μ L).

DAPI staining and embedding The biofilms were counterstained with 4',6-diamidin-2-phenylindole (DAPI) as follows. A solution of 1 μ g/mL DAPI (440 μ L) was injected into the channel, the biofilms were then incubated for 5 minutes at room temperature and washed with ultrapure water and ethanol (440 μ L each). Finally the channels were filled

with 300 μL of citifluor AF 3 (Citifluor, Great Britain) which provided protection against bleaching.

CARD-FISH

The procedure for permeabilization and hybridization for CARD-FISH was similar as described for FISH, besides the hybridization temperature which was set to 48°C. Bacteria were visualized with the HRP-labeled EUB 338-I probe (5'-3' GCTGCCTCCCGTAG-GAGT), archaea with HRP-labeled Arch 915 (5'-3' GTGCTCCCCCGCCAATTCCT). For hybridization with multiple probes, the hybridization and amplification (including all washing steps) was carried out separately for each probe. Excess probe and tyramide conjugate were removed and the remaining HRP was inhibited with 0.1 M hydrochloric acid.

Washing step I The channel was washed with 660 μL of preheated washing buffer (70 mM NaCl, 20 mM TrisHCl [pH 8.0], 5 mM EDTA, 0.01 % SDS), followed by 15 minutes incubation at 48°C. After incubation, the channel was washed a second time with 440 μL washing buffer and subsequently rinsed with 440 μL 1x SSC and incubated again for 15 minutes at room temperature.

Signal amplification The channel was filled with 400 μL of freshly prepared amplification mix (2 M NaCl, 0.2x PBS, 2.5 M dextran sulphate, 0.1 % blocking agent, 1 $\mu\text{g}/\text{mL}$ tyramide conjugate, 15 ppm H₂O₂). Tyramide signal amplification was carried out for 20 minutes at 37°C. Bacteria were visualized in red (Alexa 546), Archaea in green (Alexa 488).

Washing step II In the second washing step the remaining amplification mix was removed by purging the channel with 660 μL 1 x SSC (pH 6). Subsequently, the chip was incubated at room temperature (total time, including purging and incubation, 30 minutes). The channel was then rinsed with 660 μL ultrapure water.

Fluorescence analysis in multiplate reader

The fluorescence of the stained biofilms was measured with the on-deck microplate reader Tecan Infinite M200 pro (Tecan, Switzerland). The detachable lid of the carrier system was opened by the RoMa and a predefined measurement protocol was executed automatically. A modified protocol was used for the imaging of 13 measuring points in each chip uniformly distributed along the flow path (Fig. 1). The excitation wavelengths for detection of the probes were 490 nm and 556 nm for Alexa 488 and Alexa 546, respectively. The emission was determined at 530 nm and 588 nm for Alexa 488 and Alexa 546, respectively. The gain was set to 150 and 50 flashes were applied per measurement. DAPI was excited at 358 nm, emission was detected at 461 nm. For DAPI the gain was set to 80 and 25 flashes were used per measurement. For each individual chip the background values for the 13 measurement points were recorded beforehand and subtracted from the raw signal. The mean value of all 13 measurement points yielded the signal of one cultivation channel which was then normalized to the mean background value of the respective chip. The average signal and the standard deviation of three parallel cultivated chips were determined (Fig.

3). The average signal and the standard deviation of three parallel cultivated chips were determined.

Microscopic analysis

Fluorescence microscope images were taken to confirm successful staining of the cells and to observe the structure of the single and mixed species biofilms. An inverted fluorescence microscope (ApoTome, Zeiss, Germany), a digital camera (AxioCam MRm, Zeiss, Germany) and the AxioVision Rel. 4.7 software were used to obtain images of the stained biofilms. Exposure times were kept constant for examination of various biofilms. For the overview pictures nine sequential micrographs were recorded separately and composed afterwards [180].

Optical coherence tomography (OCT)

Briefly, OCT is an interferometric imaging modality capable of visualizing biofilms completely [181, 182]. In this study a GANYMEDE-II spectral domain OCT was applied (Thorlabs GmbH, Dachau, Germany). It acquires three-dimensional structural datasets at the mesoscale (mm-range) with high lateral ($\leq 12 \mu\text{m}/\text{pixel}$) and axial ($\leq 3.1 \mu\text{m}/\text{pixel}$) resolution at high speed, *in situ*, and without any sample treatment directly inside the cultivation device. Thus, the biofilm structure after each step of the automated FISH procedure was acquired and stored in a three-dimensional dataset. These datasets were analysed using ImageJ [183]. After cropping the datasets to the flow channel of the microfluidic device and binarization using Otsu's method [184] a topographic representation of the bulk-biofilm interface was calculated.

Results

Automated flow through FISH protocol development and parallelization

Different procedures were initially tested to identify suitable conditions for the flow-through FISH protocol. The objective was to handle as many flowcells in parallel as possible by maintaining identical incubation times for all individual flowcells. With a nested procedure it was possible to handle up to nine chips in parallel on three individual cartridges (Fig. 5.13 1/2/3) without major differences in incubation times. In general, we found that the introduction of air into the microfluidic system must be strictly avoided to preclude high shear forces arising from bubbles traveling through the cultivation channel. Therefore, drying steps were excluded to avoid biofilm ablation and were compensated by a continuous flow of reagents. For the flowcells used in the present study, three channel volumes (CV) of liquid were necessary for complete liquid replacement. The whole procedure for nine biofilm flowcells took 10 hours and could be carried out completely automated overnight.

Biofilm cultivation in flowcells and fluorescence *in situ* hybridization

The selected model bacteria representing a gram-positive and gram-negative bacterium formed thick biofilms after cultivation in the flowcells at 37°C with LB medium for 12 h. The permeabilization of the biofilm with 0.1 M hydrochloric acid was sufficient for the used model bacteria. The chosen FISH probes showed the anticipated specificity for *B. subtilis* and *E. coli*. Although the hybridization signal of *B. subtilis* was weaker than that of *E. coli*, it was well suited for both manual microscopic analysis (Fig. 5.14) and automated

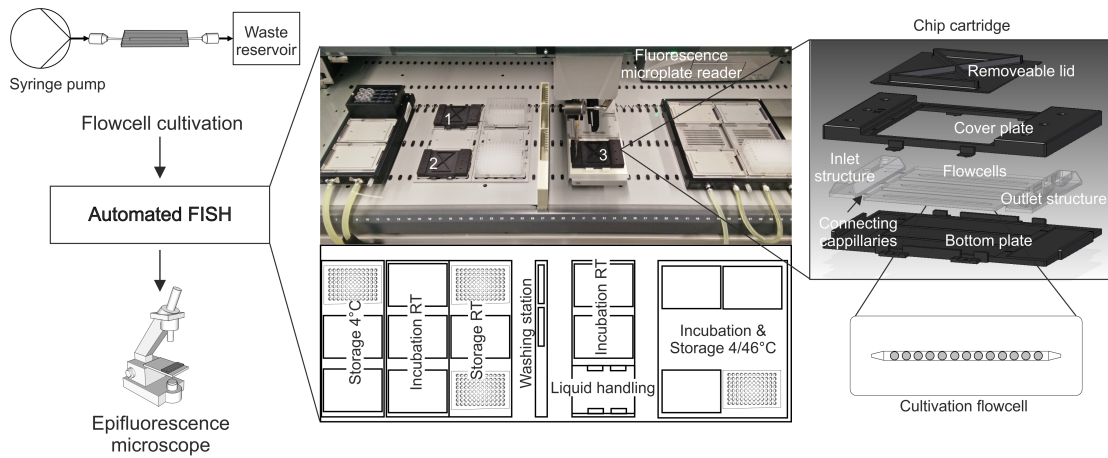


Figure 5.13: Workflow of automated FISH labeling of biofilms cultivated in flowcells. *E. coli* and *B. subtilis* biofilms were grown in a PDMS/glass hybrid cultivation flowcell. The PDMS channel structure was sealed with a coverglass to enable microscopic examination of the biofilms. The flowcell was connected to the tubing via standard cannulas. A medium flow of 50 $\mu\text{L}/\text{min}$ was applied with a syringe pump. The various steps of FISH labeling procedure were carried out fully automated with up to nine flowcells in parallel on a liquid handling station (LHS). The center shows a photograph and a schematic representation of the working deck equipped with the various stations necessary for the FISH procedure. The fluorescence signal of the labeled cells in the channel was measured with the on-deck microplate reader on the LHS. Afterwards, the results were additionally confirmed by epifluorescence microscopy. An exploded view of the newly developed interface is shown on the right. One cartridge hosts up to three chips which are connected to the inlet and outlet structures via stainless steel capillaries. The pipetting needles form a tight but reversible connection to the inlet structure. The scheme below shows the cultivation flowcell with the 13 measurement points for automated fluorescence analysis in the microplate reader indicated as circles.

fluorescence analysis with the microplate reader (Fig. 5.15). The former allowed observing the biofilm structure on different length scales. Figure 5.14 shows a number of fluorescence micrographs with magnifications ranging from 50-fold displaying the whole channel width to 1000-fold resolving the single cells of the biofilm structure. The *E. coli* D5 α strain formed mainly flat films (Fig. 5.14 B) whereas *B. subtilis* was also able to form filamentous streamers (Fig. 5.14 A). In the co-cultivation this behaviour seemed not to be altered significantly (Fig. 5.14 C). With higher magnification a cloudy structure in the *E. coli* biofilms could be observed, which hampered the visualization of individual cells in some areas (Fig. 5.14 E/H). In contrary, *B. subtilis* created a dense mesh of individual cells. In mixed biofilms *E. coli* cells seemed to spread all over the *Bacillus* mesh (Fig. 5.14 B/C/F) and only the streamer parts of the biofilm appeared to be dominated by *B. subtilis* cells.

Fluorescence analysis in the microplate reader

The *E. coli* and *B. subtilis* cultures could be reliably identified by an automated fluorescence measurement following the hybridization protocol. A standard microplate reader integrated

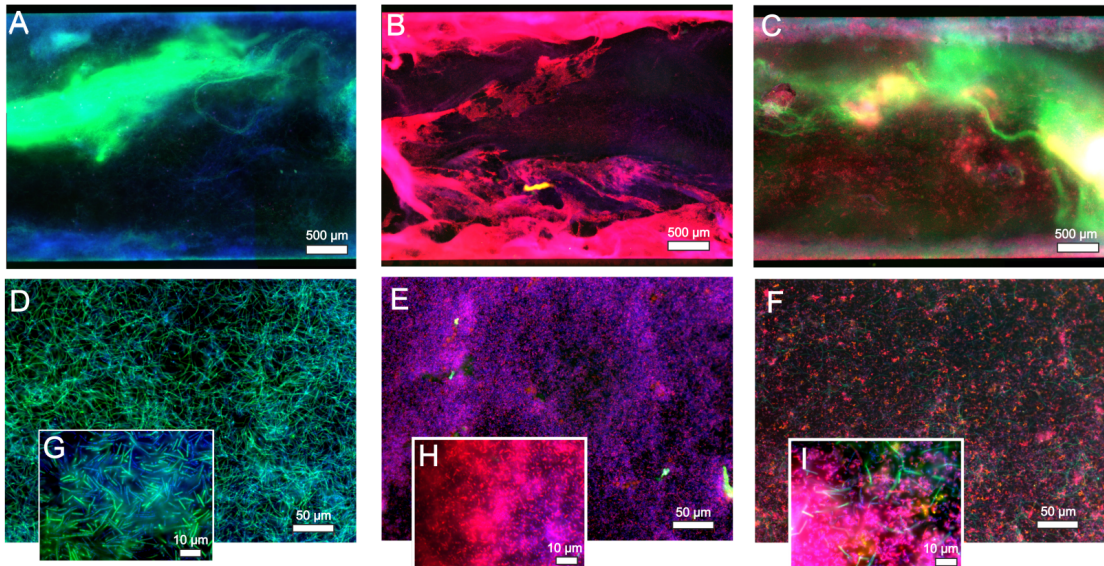


Figure 5.14: Epifluorescence micrograph of *B. subtilis* (A, D, G), *E. coli* (B, E, H) and mix species (C, F, I) biofilms. *B. subtilis* and *E. coli* were hybridized with probes LGC354B-A488 (colored in green) and Ent-A546 (red), respectively. Each of images A-C is a composition of nine micrographs which were recorded sequentially and composed afterwards [180]. As a consequence, the entire channel width is depicted in the images giving an overview of the macroscopic structure of the flowcell biofilms. *E. coli* was forming a flat biofilm particularly at the walls of the flow cell, whereas *B. subtilis* grew in filamentous streamers. In the mixed species biofilms the individual structures seemed not to be strongly affected by co-cultivation. (D) Detailed view of a *B. subtilis* biofilm. The Bacillus cells formed a dense network structure. (G) The biofilm structure could be resolved at the single cell level with the 1000-fold magnification. (E) Cloudy *E. coli* biofilm in 200-fold magnification. Larger particles sometimes stuck in the biofilms interfering with the photometric fluorescence measurement (B and E). (F) Mixed species biofilm with *Bacillus* cells forming a dense mesh and *E. coli* cells growing inside the network. (I) Close up of the mixed species biofilm clearly demonstrating a successful one-step double hybridization of the gram positive *B. subtilis* and the gram negative *E. coli* in a mixed species biofilm.

on the LHS was used for the analysis. More distant excitation and emission wavelengths were used to compensate for the distorting effect of light scattering by the PDMS. Figure 5.15 depicts the results of the fluorescence measurement of nine flowcells, which were cultivated and stained in parallel. The chips were inoculated with *E. coli*, *B. subtilis* or a co-culture of both organisms. The detected variations of the hybridization signals between three flowcells were comparable for all cultures. The signals from the gram-negative *E. coli* were about five-fold higher than those obtained from the gram-positive *B. subtilis* cultures although signals from unspecific DAPI stain were comparable for both.

Optical coherence tomography (OCT)

To proof that the structural integrity of the biofilms during the automated FISH procedure we monitored the mesoscopic structure of the developing biofilms (*E. coli*, *B. subtilis*,

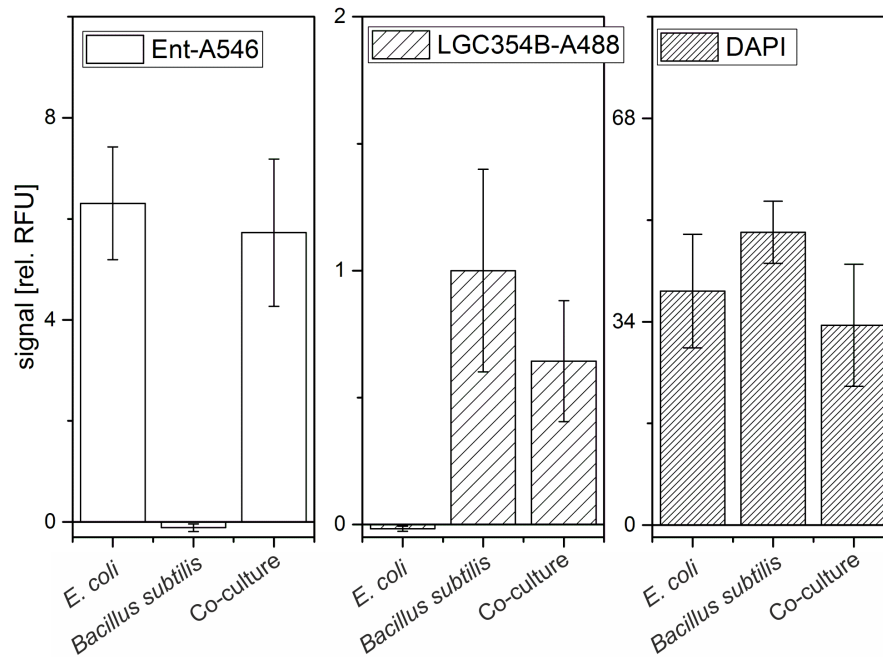


Figure 5.15: Mean fluorescence values of three parallel cultivated biofilms normalized to the respective mean background value. For each flowcell the signal was averaged over the 13 measurement points. Error bars reflect the deviation between three cultivation flowcells. The excitation wavelengths for detection of the dyes were 490 nm, 556 nm and 358 nm for Alexa 488, Alexa 546 and DAPI, respectively. The emission was determined at 530 nm, 588 nm, and 461 nm for Alexa 488, Alexa 546 and DAPI, respectively. Note that the *E. coli* and *B. subtilis* cultures could be reliably identified by the automated fluorescence measurements.

E. coli + *B. subtilis*) by means of optical coherence tomography (OCT) during the entire experiment. Figure 5.16 shows the subsequent OCT images during automated FISH procedure as well as an example of an OCT image in conjunction to the FISH images itself. Especially for the mixed species biofilm there were a lot of planktonic cells visible before the protocol was started (green, loose parts), which were washed out in the fixation step. Subsequently there was no obvious association between biomass loss and one specific step, rather than a continuous slight erosion of biofilm throughout the whole procedure. Due to partly strong reflexion effects on the glass bottom of the cultivation channel a quantification of the biofilm was difficult.

CARD-FISH

Slowly growing archaea and bacteria from an acidophilic native biofilm were successfully cultivated over long periods of up to four weeks in the microfluidic channels and visualized with an automated CARD-FISH procedure for flowcell biofilms. The complex protocol took approx. 10 hours for one cartridge with three flowcells and could be conducted overnight in a fully automated manner. Figure 5.17 shows an epifluorescence micrograph of stained archaea cells in green and neighbouring bacteria cells in red with 1000-fold magnification. The

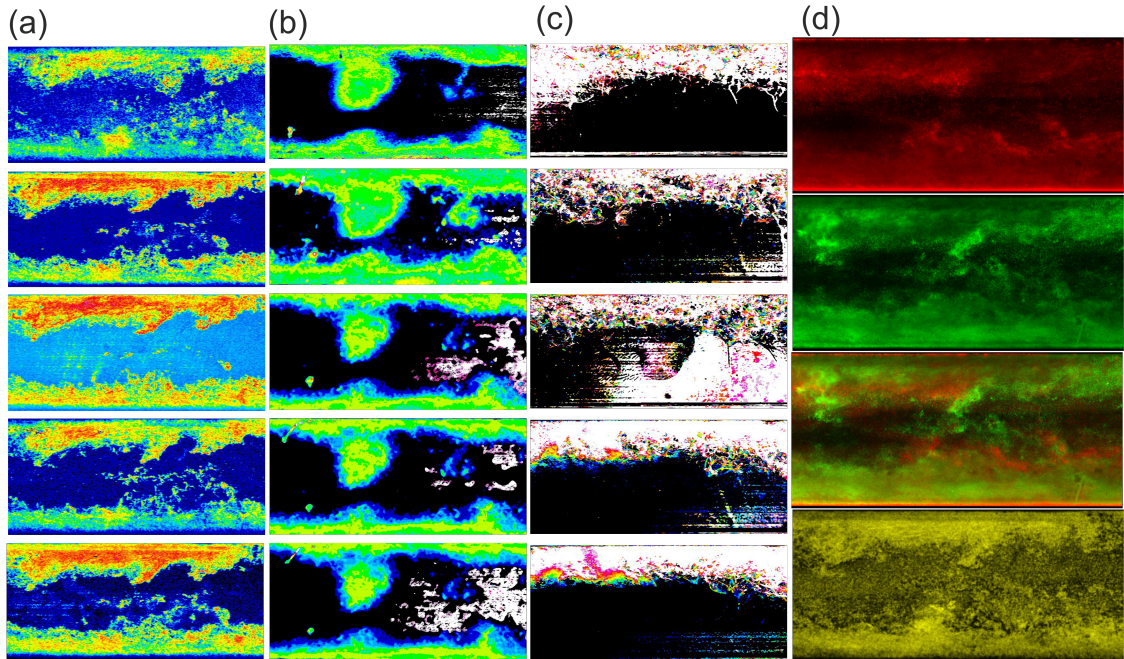


Figure 5.16: (a)/(b)/(c) Topographic representation (6.7 mm x 3 mm, height = 100 μm (red colored)) of the 3D structure of mixed species (a), *E. coli* (b) and *B. subtilis* (c) biofilms captured by means of OCT during automated FISH procedure. For each biofilm images were acquired right before FISH was conducted, after fixation, permeabilization, hybridization and washing. Slight biofilm detachment was observed throughout the whole procedure. But altogether the structural integrity could be preserved for all three model biofilms. (d) Epi-fluorescence micrograph of mix species biofilm. Biofilm features visualized by OCT are easily recognizable by epi-fluorescence microscopy after FISH.

bacterial activity induced the formation of insoluble minerals, probably Fe(III) species which result from the oxidation of Fe(II) in the medium by chemolithoautotrophic microorganisms.

Discussion

Fluorescence *in situ* hybridization (FISH) is an established, widely used and powerful tool for the identification of single cells or the analysis of complex microbial consortia [171, 185]. For conventional FISH staining as well as the more sensitive catalysed reporter deposition fluorescence *in situ* hybridization (CARD-FISH) various slightly different methods have been reported depending on the target species [171]. They all have in common the numerous labour-intensive and time consuming steps which make the FISH method a complex process for routine analysis. This is especially true for all CARD-FISH protocols. This study describes the development of a platform for the fully automated handling of flowcells for biofilm cultivation and established methods for FISH of up to nine flowcells in parallel as well as CARD-FISH of up to three flowcells in parallel. Thus, one person can analyse nine biofilm samples in parallel with high reproducibility and a hands-on-time of approximately only 1.5 hours. Full automation of the FISH method in a flow-through format required

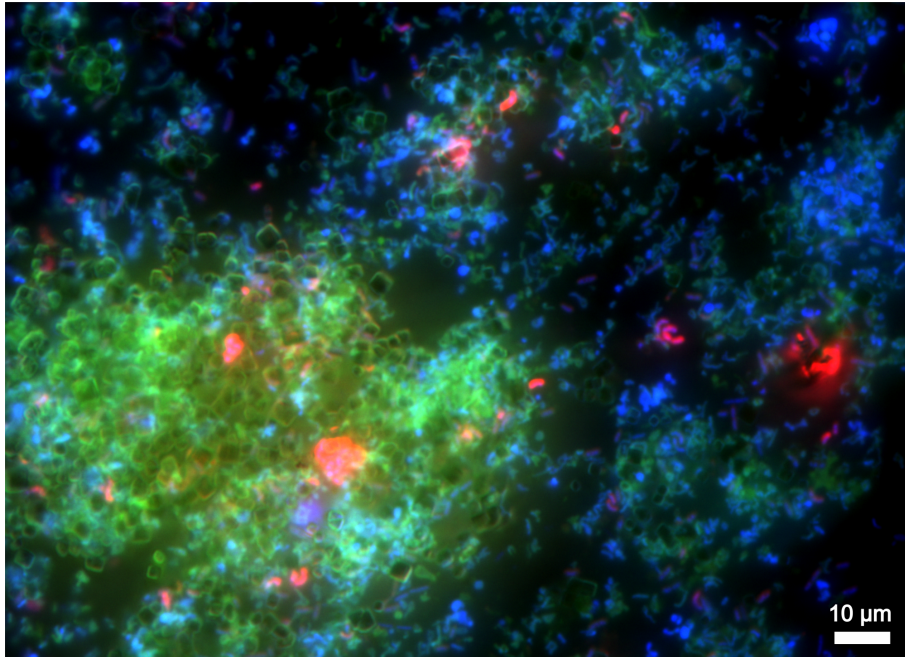


Figure 5.17: Catalysed reporter deposition fluorescence *in situ* hybridization (CARD-FISH) image of a cultivation flowcell, inoculated with native biofilm and cultivated for four weeks. Archaea (ARCH 915) are visualized in green (Alexa 488), bacteria (EUB 338-I) in red (Alexa 546) and DAPI blue.

an automated manner of liquid replacement. The here described solution is characterized by its minimal design using a standard robotic pipetting platform instead of a previously suggested complex valving system, which usually provides a limited number of available supply lines [173]. The small dead volume of the here adopted μ F-on-LHS platform [79] reduces loss of expensive reagents because the required reagent volumes only depend on channel volume and geometry. With this set-up, it was possible to successfully hybridize oligonucleotide probes with a mixed-species biofilm consisting of *E. coli* and *B. subtilis* cells. Fixation with formaldehyde combined with 0.1 M hydrochloric acid treatment for 10 minutes was well suited for the permeabilization of both cell types. However, quantitative results of the photometric fluorescence measurements obtained with the microplate reader should be handled with caution because the signals are affected by many different factors such as light scattering by the PDMS, traces of lint or dirt inside the channels, brightness and photostability of the various fluorophores as well as a lack of suitable calibration standards. Nevertheless, this simple and very fast method allowed for unequivocal assignment of the different organisms building up the biofilms. Furthermore, the results provided first indications for hybridization efficiencies and composition of the mixed species biofilms. The unspecific DAPI staining resulted in a 1.25-fold higher signal for the *Bacillus* biofilms, while with the fluorescently labeled hybridization probes it was about 6-fold lower than those observed for *E. coli*, thereby indicating a lower labeling efficacy for *B. subtilis*. The latter can most likely be attributed to limited permeabilization of the gram-positive cell

wall by the hydrochloric acid treatment. Therefore, further optimization of the automated FISH-protocol will concern, in particular, optimization of the cell wall permeabilization of gram-positive cells. In general, the permeabilization step has been identified as crucial for successful FISH of mixed species biofilms [186]. This step has to reach an optimal compromise between sufficient permeabilization of rather rigid cells and the integrity of more sensitive cell-types. Since enzymatic methods like lysozyme treatment, as suggested by Thurnheer et al. [186], are less robust and very sensitive to exact timing, we believe that careful optimization of the hydrochloric acid treatment with respect to incubation time and concentration will be suitable to attain higher labeling efficiencies. Microscopic investigation of FISH stained biofilms enables a detailed analysis of the microbial community especially with regard to spatial organisation on the cellular level without the need of genetically modified strains. Therefore, the presented method is particularly suitable for analysis of environmental or complex technologically relevant biofilms [160, 185]. For the used model community, the biofilm structure could be visualized on different length scales and different taxa could be specifically identified. The drawback of the method, a limitation all FISH experiments have in common, is the number of available fluorescent colors. The intensity of the FISH signal strongly depends on the cellular ribosome content, which, on the one hand, can be a beneficial for determination of cellular activity [187]. On the other hand, small or slowly growing microorganisms cannot be easily detected by conventional FISH [171, 185]. In the present study, an acidophilic consortium with chemolithoautotrophic organisms as primary producers was cultivated in the flowcell system for very long time periods of up to four weeks without any sign of contaminations. The consortium was subsequently screened for members from the domains of Bacteria and Archaea by automated CARD-FISH. This successful demonstration of long-term cultivation and automated high-sensitivity analysis complements the application spectrum of our automation platform to the characterization of all kinds of extremophilic and/or oligotrophic biofilms. There are a number of review studies proposing fluidic or microfluidic structures as a promising tool to target new questions in microbiology [188, 189] and particularly in biofilm research [190]. While the number of parallel cultivations is primarily limited to the number of available pumps and valves, the subsequent analytical methods require a lot of manual work and, hence, this becomes the bottleneck of throughput in experimentation. In the present study we introduced a system which is suitable for automated handling of microfluidic chips independent of the channel geometries. The system could be easily adopted to smaller flowcell geometries and up to eight channels per cartridge could be operated. Accordingly, a total of [175] flow biofilms could be readily analysed in parallel with our newly established procedure. To conclude, we developed a platform for the automated handling of fluidic biofilm cultivation chips. We established the procedures for automated execution of FISH and CARD-FISH analyses of flowcell biofilms on this platform and successfully applied the method to a mixed species biofilm with a gram-positive as well as a gram-negative member. Furthermore, the hybridized biofilms could be analysed by means of a microplate reader and epifluorescence microscopy. In addition to the applications shown in the present study, our platform could be used for various analytical assays in biofilm research. For instance, Hennig et al. developed a method for the functional analysis of immune cells by combining microfluidic chips for cell immobilization with an automated microscopic

read-out [191]. Pernthaler et al. [192] provided a system for the automated counting of double-stained microbial cells to determine the relative abundance of specific microbial taxa in marine picoplankton after FISH. Following these examples, a next step for widening the scope of the here presented platform would concern the implementation of automated microscopy, which could be easily achieved due to the standard dimensions and formats of our cultivation chips.

Acknowledgments

We gratefully acknowledge financial support of this work by the Helmholtz programme BioInterfaces in Technology and Medicine and the project „Molecular Interaction Engineering: From Nature’s Toolbox to Hybrid Technical Systems“ which is funded by the German Federal Ministry of Education and Research (BMBF), funding code 031A095B.

References

62. Kim, J., Hegde, M., Kim, S. H., Wood, T. K., and Jayaraman, A. 'A microfluidic device for high throughput bacterial biofilm studies'. *Lab on a Chip*, vol. 12(6) (2012), pp. 1157–1163 (cit. on pp. 4, 58).
63. Lee, J.-H., Kaplan, J. B., and Lee, W. Y. 'Microfluidic devices for studying growth and detachment of *Staphylococcus epidermidis* biofilms'. *Biomedical microdevices*, vol. 10(4) (2008), pp. 489–498 (cit. on pp. 4, 58).
79. Waldbaur, A., Kittelmann, J., Radtke, C. P., Hubbuch, J., and Rapp, B. E. 'Microfluidics on liquid handling stations (μ F-on-LHS): an industry compatible chip interface between microfluidics and automated liquid handling stations'. *Lab on a Chip*, vol. 13(12) (2013), pp. 2337–2343 (cit. on pp. 5, 20, 37, 38, 59, 60, 68, 78).
155. Hall-Stoodley, L., Costerton, J. W., and Stoodley, P. 'Bacterial biofilms: from the natural environment to infectious diseases'. *Nature reviews microbiology*, vol. 2(2) (2004), pp. 95–108 (cit. on p. 58).
156. De Vos, W. M. 'Microbial biofilms and the human intestinal microbiome'. *npj Biofilms and Microbiomes*, vol. 1 (2015), p. 15005 (cit. on p. 58).
157. Verstraete, W. 'The technological side of the microbiome'. *npj Biofilms and Microbiomes*, vol. 1 (2015), p. 15001 (cit. on p. 58).
158. Parsek, M. R. and Greenberg, E. P. 'Sociomicrobiology: the connections between quorum sensing and biofilms'. *Trends in microbiology*, vol. 13(1) (2005), pp. 27–33 (cit. on p. 58).
159. Zengler, K. and Palsson, B. O. 'A road map for the development of community systems (CoSy) biology'. *Nature Reviews Microbiology*, vol. 10(5) (2012), pp. 366–372 (cit. on p. 58).
160. Burmølle, M., Ren, D., Bjarnsholt, T., and Sørensen, S. J. 'Interactions in multispecies biofilms: do they actually matter?' *Trends in microbiology*, vol. 22(2) (2014), pp. 84–91 (cit. on pp. 58, 69).
161. Kirisits, M. J., Margolis, J. J., Purevdorj-Gage, B. L., Vaughan, B., Chopp, D. L., Stoodley, P., and Parsek, M. R. 'Influence of the hydrodynamic environment on quorum sensing in *Pseudomonas aeruginosa* biofilms'. *Journal of bacteriology*, vol. 189(22) (2007), pp. 8357–8360 (cit. on p. 58).
162. Purevdorj, B., Costerton, J., and Stoodley, P. 'Influence of hydrodynamics and cell signaling on the structure and behavior of *Pseudomonas aeruginosa* biofilms'. *Applied and environmental microbiology*, vol. 68(9) (2002), pp. 4457–4464 (cit. on p. 58).
163. Mariscal, A., Carnero-Varo, M., Gutierrez-Bedmar, M., Garcia-Rodriguez, A., and Fernandez-Crehuet, J. 'A fluorescent method for assessing the antimicrobial efficacy of disinfectant against *Escherichia coli* ATCC 35218 biofilm'. *Applied microbiology and biotechnology*, vol. 77(1) (2007), pp. 233–240 (cit. on p. 58).

164. Repp, K. K., Menor, S. A., and Pettit, R. K. 'Microplate Alamar blue assay for susceptibility testing of *Candida albicans* biofilms'. *Medical mycology*, vol. 45(7) (2007), pp. 603–607 (cit. on p. 58).
165. Junker, L. M. and Clardy, J. 'High-throughput screens for small-molecule inhibitors of *Pseudomonas aeruginosa* biofilm development'. *Antimicrobial agents and chemotherapy*, vol. 51(10) (2007), pp. 3582–3590 (cit. on p. 58).
166. Benoit, M. R., Conant, C. G., Ionescu-Zanetti, C., Schwartz, M., and Matin, A. 'New device for high-throughput viability screening of flow biofilms'. *Applied and environmental microbiology*, vol. 76(13) (2010), pp. 4136–4142 (cit. on p. 58).
167. Tremblay, Y. D., Vogeleeer, P., Jacques, M., and Harel, J. 'High-throughput microfluidic method to study biofilm formation and host-pathogen interactions in pathogenic *Escherichia coli*'. *Applied and environmental microbiology*, vol. 81(8) (2015), pp. 2827–2840 (cit. on p. 58).
168. Pamp, S. J., Sternberg, C., and Tolker-Nielsen, T. 'Insight into the microbial multi-cellular lifestyle via flow-cell technology and confocal microscopy'. *Cytometry Part A*, vol. 75(2) (2009), pp. 90–103 (cit. on p. 58).
169. Amann, R. I., Ludwig, W., and Schleifer, K.-H. 'Phylogenetic identification and *in situ* detection of individual microbial cells without cultivation.' *Microbiological reviews*, vol. 59(1) (1995), pp. 143–169 (cit. on p. 58).
170. Stewart, P. S. and Franklin, M. J. 'Physiological heterogeneity in biofilms'. *Nature Reviews Microbiology*, vol. 6(3) (2008), pp. 199–210 (cit. on p. 58).
171. Pernthaler, A. e. a. 'Sensitive multi-color fluorescence *in situ* hybridization for the identification of environmental microorganisms'. *Molecular microbial ecology manual*. Vol. 1 and 2 (2004), pp. 711–725 (cit. on pp. 58, 61, 67, 69).
172. Perez-Toralla, K., Mottet, G., Guneri, E. T., Champ, J., Bidard, F.-C., Pierga, J.-Y., Klijanienko, J., Draskovic, I., Malaquin, L., Viovy, J.-L., et al. 'FISH in chips: turning microfluidic fluorescence *in situ* hybridization into a quantitative and clinically reliable molecular diagnosis tool'. *Lab on a Chip*, vol. 15(3) (2015), pp. 811–822 (cit. on p. 59).
173. Sieben, V. J., Debes-Marun, C. S., Pilarski, L. M., and Backhouse, C. J. 'An integrated microfluidic chip for chromosome enumeration using fluorescence *in situ* hybridization'. *Lab on a Chip*, vol. 8(12) (2008), pp. 2151–2156 (cit. on pp. 59, 68).
174. Zanardi, A., Bandiera, D., Bertolini, F., Corsini, C. A., Gregato, G., Milani, P., Barborini, E., and Carbone, R. 'Miniaturized FISH for screening of onco-hematological malignancies'. *Biotechniques*, vol. 49(1) (2010), pp. 497–504 (cit. on p. 59).
175. Liu, Y., Kirkland, B., Shirley, J., Wang, Z., Zhang, P., Stembridge, J., Wong, W., Takebayashi, S.-i., Gilbert, D. M., Lenhert, S., et al. 'Development of a single-cell

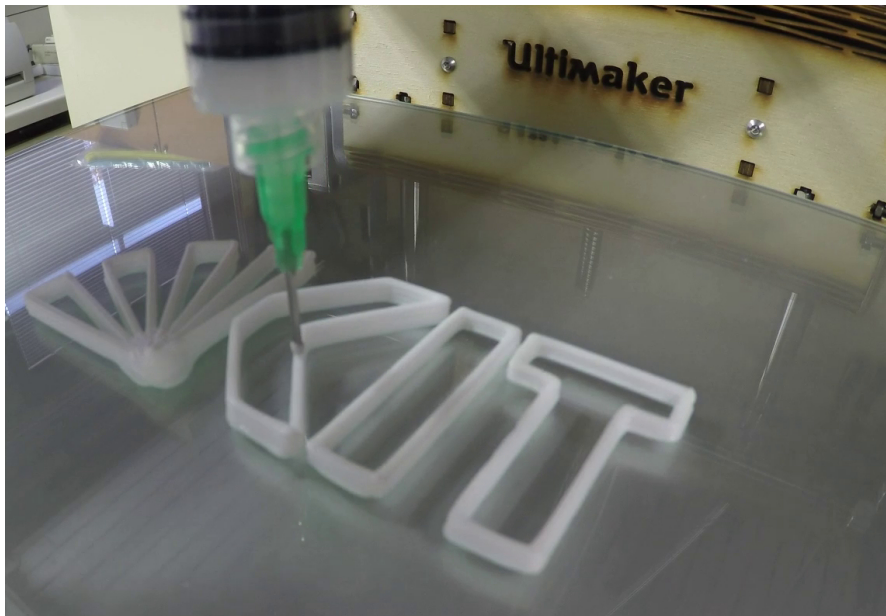
- array for large-scale DNA fluorescence *in situ* hybridization'. *Lab on a Chip*, vol. 13(7) (2013), pp. 1316–1324 (cit. on pp. 59, 69).
176. Vedarethinam, I., Shah, P., Dimaki, M., Tumer, Z., Tommerup, N., and Svendsen, W. E. 'Metaphase FISH on a chip: miniaturized microfluidic device for fluorescence *in situ* hybridization'. *Sensors*, vol. 10(11) (2010), pp. 9831–9846 (cit. on p. 59).
 177. Ziegler, S., Ackermann, S., Majzlan, J., and Gescher, J. 'Matrix composition and community structure analysis of a novel bacterial pyrite leaching community'. *Environmental microbiology*, vol. 11(9) (2009), pp. 2329–2338 (cit. on pp. 59, 60).
 178. Ziegler, S., Dolch, K., Geiger, K., Krause, S., Asskamp, M., Eusterhues, K., Kriews, M., Wilhelms-Dick, D., Goettlicher, J., Majzlan, J., et al. 'Oxygen-dependent niche formation of a pyrite-dependent acidophilic consortium built by archaea and bacteria'. *The ISME journal*, vol. 7(9) (2013), pp. 1725–1737 (cit. on p. 60).
 180. Preibisch, S., Saalfeld, S., and Tomancak, P. 'Globally optimal stitching of tiled 3D microscopic image acquisitions'. *Bioinformatics*, vol. 25(11) (2009), pp. 1463–1465 (cit. on pp. 63, 65).
 181. Haisch, C. and Niessner, R. 'Visualisation of transient processes in biofilms by optical coherence tomography'. *Water research*, vol. 41(11) (2007), pp. 2467–2472 (cit. on p. 63).
 182. Wagner, M., Taherzadeh, D., Haisch, C., and Horn, H. 'Investigation of the mesoscale structure and volumetric features of biofilms using optical coherence tomography'. *Biotechnology and bioengineering*, vol. 107(5) (2010), pp. 844–853 (cit. on p. 63).
 183. Schindelin, J., Arganda-Carreras, I., Frise, E., Kaynig, V., Longair, M., Pietzsch, T., Preibisch, S., Rueden, C., Saalfeld, S., Schmid, B., et al. 'Fiji: an open-source platform for biological-image analysis'. *Nature methods*, vol. 9(7) (2012), pp. 676–682 (cit. on p. 63).
 184. Otsu, N. 'An automatic threshold selection method based on discriminate and least squares criteria'. *Denshi Tsushin Gakkai Ronbunshi*, vol. 63 (1979), pp. 349–356 (cit. on p. 63).
 185. Amann, R. and Fuchs, B. M. 'Single-cell identification in microbial communities by improved fluorescence *in situ* hybridization techniques'. *Nature Reviews Microbiology*, vol. 6(5) (2008), pp. 339–348 (cit. on pp. 67, 69).
 186. Thurnheer, T., Gmür, R., and Guggenheim, B. 'Multiplex FISH analysis of a six-species bacterial biofilm'. *Journal of Microbiological Methods*, vol. 56(1) (2004), pp. 37–47 (cit. on p. 69).
 187. Regan, J., Oldenburg, P., Park, H.-D., Harrington, G., and Noguera, D. 'Simultaneous determination of bacterial viability and identity in biofilms using ethidium monoazide and fluorescent *in situ* hybridization'. *Water Science and Technology*, vol. 47(5) (2003), pp. 123–128 (cit. on p. 69).

188. Hol, F. J. and Dekker, C. ‘Zooming in to see the bigger picture: Microfluidic and nanofabrication tools to study bacteria’. *Science*, vol. 346(6208) (2014), p. 1251821 (cit. on p. 69).
189. Weibel, D. B., DiLuzio, W. R., and Whitesides, G. M. ‘Microfabrication meets microbiology’. *Nature Reviews Microbiology*, vol. 5(3) (2007), pp. 209–218 (cit. on p. 69).
190. Kim, J., Park, H.-D., and Chung, S. ‘Microfluidic approaches to bacterial biofilm formation’. *Molecules*, vol. 17(8) (2012), pp. 9818–9834 (cit. on p. 69).
191. Hennig, C., Adams, N., and Hansen, G. ‘A versatile platform for comprehensive chip-based explorative cytometry’. *Cytometry Part A*, vol. 75(4) (2009), pp. 362–370 (cit. on p. 70).
192. Pernthaler, J., Pernthaler, A., and Amann, R. ‘Automated enumeration of groups of marine picoplankton after fluorescence *in situ* hybridization’. *Applied and environmental microbiology*, vol. 69(5) (2003), pp. 2631–2637 (cit. on p. 70).

5.4 The *Biomaker*: An entry-level bioprinting device for biotechnological applications

Carsten P. Radtke, Nils Hillebrandt and Jürgen Hubbuch

*Institute of Engineering in Life Sciences, Section IV: Biomolecular Separation Engineering,
Karlsruhe Institute of Technology (KIT), 76131 Karlsruhe, Germany*



published in *Journal of Chemical Technology and Biotechnology* 93 (2018): 792-799.
DOI: 10.1002/jctb.5429

Abstract

BACKGROUND: 3D printing and bioprinting in particular are emerging technologies in the field of biotechnology. The developments of bioprinters and applications lie mostly in the highly observed working fields of tissue engineering and regenerative medicine. Until now only little attention has been paid to the application of 3D bioprinting for the investigation of hydrogel - liquid phase interactions in biotechnological applications. This can mostly be attributed to the need for complex and expensive equipment.

RESULTS: In this work, an entry-level bioprinter on the base of a commercially available Fused-Filament-Fabrication 3D printer and an easy to handle user interface was designed. This newly developed bioprinter allowed the structuring of bioinks and hydrogels in microwell plates and even complex models were printed. The applicability of the presented printer setup in the field of biotechnology was shown by the encapsulation of β -galactosidase (EC 3.2.1.23) in poly(ethylene glycol) diacrylate based hydrogels. Subsequently, an automated screening of the biocatalytic conversion of the substrate ONPG by the encapsulated enzyme was executed on a liquid handling station. Under varied pH conditions in the surrounding liquid phase highest substrate turnover rates were detected at pH 3 and pH 5 which is in good accordance with previously reported pH optima of β -galactosidase.

CONCLUSION: This approach shows an easy access to 3D bioprinting in the field of biotechnology and the implementation of 3D printed hydrogels in high-throughput experimentation.

Keywords: *3D bioprinting; hydrogels; encapsulated enzymes; high-throughput screening*

Introduction

Printing in three dimensions is one of the most aspiring technologies in various industrial and scientific sectors. In many industrial fields 3D printing is already an established technology for rapid prototyping or product manufacturing. Whenever new and more effective shapes need to be developed, 3D printing provides an unrivalled fast and cheap manufacturing technique.[84, 193] In biotechnological research at present, 3D printing is mainly used for the manufacturing of molds for microfluidic devices [79, 194] or the direct printing of the devices itself [49, 195, 196]. Furthermore, 3D printing technologies are applied for tailor-made fabrication of labware [12, 87, 197] and opens simple and fast access for new scientific approaches [89, 198, 199]. However, most attention is certainly paid to the upcoming field of bioprinting. The concept of bioprinting is commonly defined as the construction of three dimensional structures of biological or biocompatible materials. Bioprinting is considered as key technology in the field of biofabrication for tissue engineering (TE) and regenerative medicine.[200] Thus many researchers focus on adapting techniques and materials for this intended purpose.[100, 201] In TE the use of hydrogels as scaffold material to generate cell-friendly environments is a well-established method. [102, 202–204] Bioprinting techniques are applied in the preparation of scaffolds with subsequent cell seeding [205–207], for development of medical applications [208], personalized drug screening [209] and the engineering of tumor [210], skin [211] and organ models [212]. Further functionalities can be implemented by the combination of 3D printed hydrogels and conducting polymers, which led to bionic approaches.[213] Yet, 3D printing of hydrogels is not only of interest in the context of tissue engineering and regenerative medicine but also other sectors in the biotechnological spectrum profit from this technology including 'green bioprinting' [15] and printing of bacterial cells [16]. Further versatile hydrogel printing applications can be developed as hydrogels are already in use for different kind of experimental approaches. For example, the entrapment of biopharmaceutical proteins in hydrogel structures is part of investigations in a new methodology of drug release.[110, 214, 215] Furthermore, the encapsulation or even immobilization of enzymes in and on hydrogels is of huge interest as reusable matrix in biocatalysis or analytical applications.[109] Functional biological composite materials can be incorporated in microreactors and microfluidic devices [216–218], biosensors [219, 220] or as beads in diverse applications [221, 222]. For these and other applications the move towards three dimensional structures could open new possibilities in industry and academics. In particular, the interaction of the hydrogel and the encapsulated protein with the surrounding liquid phase is a crucial issue in regards to unwanted leaching, controlled release and penetration of other molecules [107, 111]. To investigate the multitude of variable parameters in hydrogel or liquid phase experimental approaches in established automated high-throughput instrumentations provide a promising concept.

The vast majority of commercially available bioprinters, which are capable of printing hydrogels, are designed for the application in tissue engineering. To address the challenges of cell printing applications, they provide sterile environments and cell-friendly printing conditions which makes them expensive, complex and difficult to access. To lower the hurdle for scientists to establish 3D printing technologies in their laboratories entry-level solutions

with a user-friendly interface are required. To date, only a few studies are available that provide a possibility for a more easy entry to bioprinting by the modification of commercially available non-bioprinters.[106, 223, 224] These studies present printers specially adapted for the application in the field of TE. The particular focus of these works was establishing cell-friendly printing conditions and the preservation of the viability of the printed cells. But further applications in other biotechnological fields have hardly been investigated so far. By transferring the tools and methods developed for tissue engineering to other biotechnological applications, promising opportunities could arise. For example, the implementation of the 'mold and fill' strategy [225] enables the three dimensional structuring of low viscosity bioinks, which are preferred for applications in microfluidic devices [216, 217] or for coating procedures [226, 227]. What is currently missing are a range of entry-level 3D bioprinters for simple hydrogel printing in biotechnological applications, which fulfill the demands of respective laboratory environments, are operated in ambient conditions and are open and easy to access for researchers. The here presented study introduces a combinatorial approach for the implementation of 3D printed hydrogels in automated high-throughput experimentation on liquid handling stations (LHS) adapting printing strategies known from tissue engineering. For this purpose we created the *Biomaker*, a modified low-cost commercially available fused filament fabrication (FFF) printer with full and easy access via G-code. The *Biomaker* is equipped with a custom-made syringe extrusion unit that allowed the deposition of hydrogels on various printing substrates including multiwell plates. These hydrogel-loaded plates could be readily implemented in automated processes on well-established liquid handling stations. As a proof of principle we applied the presented combination of bioprinting and automated high-throughput experimentation to encapsulate β -galactosidase (EC 3.2.1.23) in poly(ethylene glycol) diacrylate based hydrogels with a mold and fill printing process. The use of sacrificial ink as a 3D printed mold could circumvent the inherent issues generating 3D structures of low viscosity bioinks. Subsequent to the printing procedure, the activity of the encapsulated enzyme is determined by the automated execution of a screening assay. Various concentrations of 2-Nitrophenyl β -D-galactopyranoside as substrate and three different pH values of the surrounding buffer are tested. The method could be particularly suitable for the investigation of the influence of varying parameters in a design of experiments approach.

Experimental

Modification of an Ultimaker Original+ for bioprinting

A commercially available 3D printer (Ultimaker Original+, Ultimaker, The Netherlands) was equipped with a custom-made syringe extruder. The wooden body of the printer was replaced with laser cut acrylic glass parts (Formulor, Germany) by modifying the open use design laser files which are shared online (<https://github.com/Ultimaker/Ultimaker-Original-Plus>). The syringe extruder was inspired by the work of Marry Bassa and Jelle Boomstra (<http://www.thingiverse.com/thing:31210>). It was mounted on the print head, which preserved the possibility of fused filament fabrication of various materials. The CAD files for the construction of the extrusion unit were created using Solid Edge (ST7, Siemens

PLM Software, USA). The extrusion unit consists of a housing, a NEMA 17 stepper motor with threaded rod (Thingibox, Spain), two linear bearings and rods (Thingibox, Spain) leading extrusion movements, printed connectors between the threaded rod and the plunger and a printed cartridge for the syringe. The installed stepper motor is identical in construction with the provided motors of the Ultimaker which enables the control of the extrusion unit by the Ultimaker main board. The rotation of the motor drives the movement of the syringe plunger for extrusion. The connector between the rod and the cartridge stabilized syringe allowed the implementation of withdrawal commands. According to the Ultimaker specifications (see <https://ultimaker.com/en/products/ultimaker-original/specifications>), the positioning accuracy is 12.5 μm in X- and Y-direction and 5 μm in Z-direction. The print head travels with a velocity up to 300 mm/s, which corresponds to the potential maximum velocity during extrusion. The actual print speed and extrusion rate to be set for a proper and precise printing result are strongly dependent on the characteristics of the printing material and the dispensing tip geometry (length and inner diameter).[228] Furthermore, the printing platform of the *Biomaker* can be heated up to 100°C if necessary for the printing process. The commands for the printer were provided as a G-code file. For creation of G-code files a user interface (UI) consisting of multiple Excel sheets (V15.0, Microsoft, USA) was created. This UI allowed to specify various printing conditions and parameters like the kind of printing substrate (multiwell plates, microscope slides, petri dishes), the number of printed structures (up to 96, depending on chosen printing substrate), the shape of the structures from a selection of predefined geometries (circle or square) and the number of layers. Other entries in this UI affect the crucial printing parameters like printing speed and extrusion rate which have to be adopted for a change in material or size of the dispensing tip. From this entered data a G-code file is generated and send to the printer by the open source software Pronterface (part of printrun, licensed under GNU General Public License, version 3). More complex structures in the STL file format could be printed with the use of the slicing and printing software Cura (V2.1, Ultimaker, The Netherlands). Modified filament classes which control the printing parameters have been created to enable Cura controlled extrusion of hydrogels.

Printing and polymerization process for the β -galactosidase encapsulation

For the sacrificial ink a solution of 30 %(w/w) Kolliphor P 407 (Sigma-Aldrich, USA) in ultrapure water (Purelab Ultra, Elga Labwater, GB) was prepared. To achieve a homogeneous solution, the mixture was stirred for several hours in the refrigerator. The sacrificial ink was then filled in 10 mL syringes (Omnifix Luer lock Solo, B. Braun, Germany) for the use in the extrusion unit of the printer. The Poly(ethylene glycol) diacrylate (PEG-DA) based bioinks were prepared with a ratio of 50 %(w/w) PEG-DA (average Mn 575, Sigma-Aldrich, USA), 1 %(w/w) 2-Hydroxy-2-metylpropiophenone (HMPP, Sigma-Aldrich, USA) as photoinitiator and ultrapure water respectively a solution of β -galactosidase from *Aspergillus oryzae* (EC 3.2.1.23, Sigma-Aldrich, USA) in ultrapure water. The final amount of encapsulated β -galactosidase in one hydrogel-loaded well was 0.4 mg. As depicted in the process scheme in figure figure 5.18, steps A-E the printing procedure was as follows. In each well of a costar® 48 well plate (Corning, USA) ten layers of the sacrificial ink were printed as hollow cylinders with a diameter of 7 mm using a dispensing tip with an inner

diameter of 0.84 mm and a length of 1 inch (Vieweg, Germany). The printing process was executed with an extrusion velocity of 500 mm/min and an extrusion rate of 0.41 mL/min (respectively 0.82 μL per mm printing distance), with the heated platform turned off. The gap between well rim and the printed molding structure was filled with 320 μL of the PEG-DA based bioinks and polymerized with a UV-diode (LC-L2, Hamamatsu, Japan) at 365 nm for 20 seconds with an irradiance of 14 W/cm² (figure 5.18, step A). After the polymerization, the multiwell plate was transferred to a liquid handling station (Freedom Evo 200, Tecan, Switzerland) and a cleaning protocol was executed. At lower temperatures, the sacrificial Kolliphor ink became liquid and could be washed out. Hence, the plate was gently shaken on a cooled shaker (4°C) and filled with ultrapure water of the same temperature (figure 5.18, step B). The water was renewed every two minutes for a total of ten cleaning cycles. After this automated cleaning procedure the wells were filled with 800 μL of ultrapure water and stored in the refrigerator overnight.

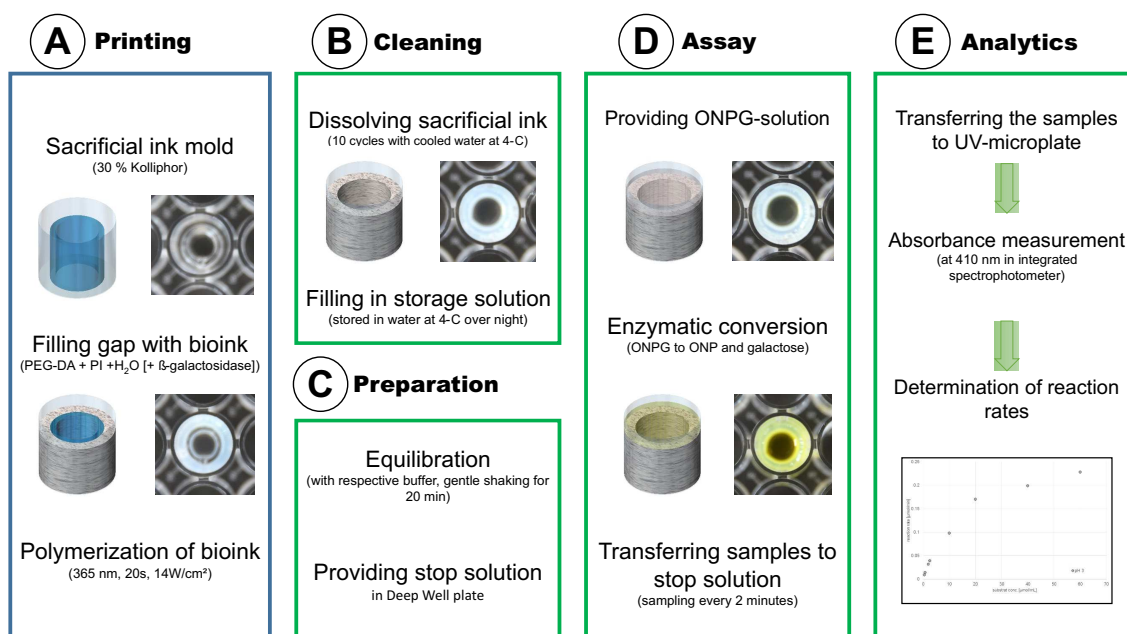


Figure 5.18: Schematic representation of the process steps for the execution of the case study. Step A – Printing procedure with the production of a printed sacrificial mold. The resultant gap was filled with bioink, followed by UV-polymerization. From this point on, the process was executed on the liquid handling station. Step B – Removal of the sacrificial mold with cooled water in a cleaning procedure. Step C – Preparation of polymerized and cleaned hydrogels for the assay by equilibration. Meanwhile the stop solution was provided in a deep well plate. Step D – The execution of the enzymatic assay was started with the filling of the hydrogel-loaded wells with ONPG solution. Samples were drawn and transferred to the provided stop solution. Step E – The samples were transferred to a UV microplate and the absorption is measured at 410 nm. The gained data leads to the determination of reaction rates.

Automated preparation and execution of enzyme assay

For the execution of the case study, the enzyme β -galactosidase was chosen as model enzyme because of the colorimetric activity assay with the small substrate ONPG which is transformed to ONP. The enzyme assay was executed according to previously published protocols [229, 230], slightly adapted for kinetic investigations on the liquid handling station. As buffer system a 25 mM multicomponent buffer (after Kroener and Hubbuch [231]) was applied consisting of MOPSO (3-Morpholino-2-hydroxypropanesulfonic acid, AppliChem, Germany) and L-(-)-Malic acid (Sigma-Aldrich, USA). The buffer was split in three portions with the pH set to 3, 5 and 7 by titration using 4 M sodium hydroxide solution (NaOH, Merck, USA). The five-point calibrated pH-meter HI-3220 (Hanna Instruments, USA) with a SenTix R 62 pH electrode (Xylem Inc., USA) was used for the adjustment of the pH. For the enzyme assay the substrate 2-Nitrophenyl β -D-galactopyranoside (ONPG, Sigma-Aldrich, USA) was dissolved in different concentrations in the pH-variants of the mentioned multicomponent buffer. To quantify the turnover of the substrate, a calibration with 2-Nitrophenol (ONP, Sigma-Aldrich, USA) was performed. The stop solution was prepared by dissolving 4 M sodium carbonate (Sigma-Aldrich, USA) in ultrapure water. For each substrate concentration two multiwell plates with hydrogels were prepared, one with and one without β -galactosidase to execute and blank the activity assay. To investigate the stability of the encapsulated enzyme in a dry and moist storing condition, one pair of plates (with and without β -galactosidase) was dried at 37°C and one pair of plates was filled with ultrapure water. These plates were stored in the refrigerator at 4°C for 30 days until the execution of the enzyme assay. The enzyme assay was performed fully automated on the LHS. The storage solution was removed prior to an equilibration step. The hydrogel cylinders in the wells were filled with the buffer of the same pH as the assay would be executed and gently shaken for 20 min to equilibrate (figure 5.18, step C). Meanwhile, 300 μ L of stop solution were provided for each sample in a deep well plate (VWR, Germany). The dried hydrogels were re-hydrated with ultrapure water before the equilibration. Subsequently, the liquid was discarded and the wells were filled with ONPG solution of defined concentration and pH (figure 5.18, step D). For every sampling point and every pH a duplicate was prepared. The hydrolysis of ONPG to ONP and galactose was monitored over a time span of 16 minutes by retrieving liquid samples every two minutes. The samples were transferred to the deep well plate with provided stop solution. The use of the alkaline stop solution tautomerized the produced ONP which gave it the yellow color detectable at 410 nm, also for the samples of lower pH.⁴⁰ Subsequently, the samples were transferred to a 96 well UV-microplate (Greiner Bio-One, Germany) and the absorption at 410 nm was measured in the integrated spectrophotometer (infinite® M200 pro, Tecan, Germany) to obtain the substrate turnover (figure 5.18, step E). The turnover rate of the encapsulated β -galactosidase was determined for eight different ONPG concentrations in the range from 0.5 to 60 μ mol/mL at three different pH values (3, 5 and 7) on a tempered shaker at 37°C.

Results and discussion

Printer modification and printing process

A 3D printer for bioprinting applications in the field of biotechnology should be easy to implement in present biological laboratory environments and therefore has to fulfil common biotechnological lab standards. Furthermore a low price-tag and the possibility for uncomplicated adaptations and refinements in soft- and hardware are highly preferable. This need for simple and entry-level 3D printers for bioink printing in the field of biotechnology was addressed by the modification of a commercially available fused filament fabrication printer as could be seen in figure 5.19A. The open-source pedigree of the Ultimaker original+ printer allowed the well-functioning transformation into a bioprinter. The mounting of the extrusion unit (see figure 5.19B) on the print head also reduced the actual dead volume which would have been occurred by an external installation and a tubing connection to the print head. The first prototype parts for the extrusion unit were printed by the printer itself using PLA. In a progressed stage the housing parts of the extrusion unit and the original wooden parts of the printer were replaced by acrylic glass cuttings. The implementation of an equivalent stepper motor for the extrusion unit simplified the operation and the control by means of G-code files. With the help of simple positioning tools for the determination of the starting point of the print and with known geometrical parameters of the multiwell plate and its wells, the printing pattern for up to 96 wells at once or individually could be set up. For the use of automated generated G-Code files from the slicer and printing software Cura the predefined filament classes were adapted for bioink application.

The replacement of the wooden housing parts fulfilled the requirements for the integration of the printer in the bio lab working environment. The acrylic glass parts conforming to lab safety standards and are easy to clean. Through the ability to withdraw the plunger after the completion of a print a proper outcome of the structures and the tidy and leak-free travel of the print head between the printing spots were ensured. Providing a fixation of the syringe in the cartridge on the extrusion unit together with the linear guidance minimized the influence of occurring leverage effects while extruding. This resulted in a good position precision for the entire printing process which could not been achieved without the constructive optimization. The presented setup could print inks with a viscosity up to 5000 Pa*s (measured at a shear rate of 0.1 s^{-1}) which sufficiently covers the usual viscosity range of extruded bioinks. [232, 233] The opportunities for manipulating the G-code by the various variables entered in the UI allowed a fast adaption on changed printing substrate geometries, inks or nozzle types. The created filament classes for various bioinks enabled the print of complex structures like scaffolds as used in tissue engineering or even challenging models like body parts (shown in figure 5.20) by importing files in the STL-format into Cura. Although the biomarker is not intended to be employed for tissue engineering, this feature could serve well for the production of preliminary research objects, proof of concept studies and definitely as demonstration system for educational purposes.

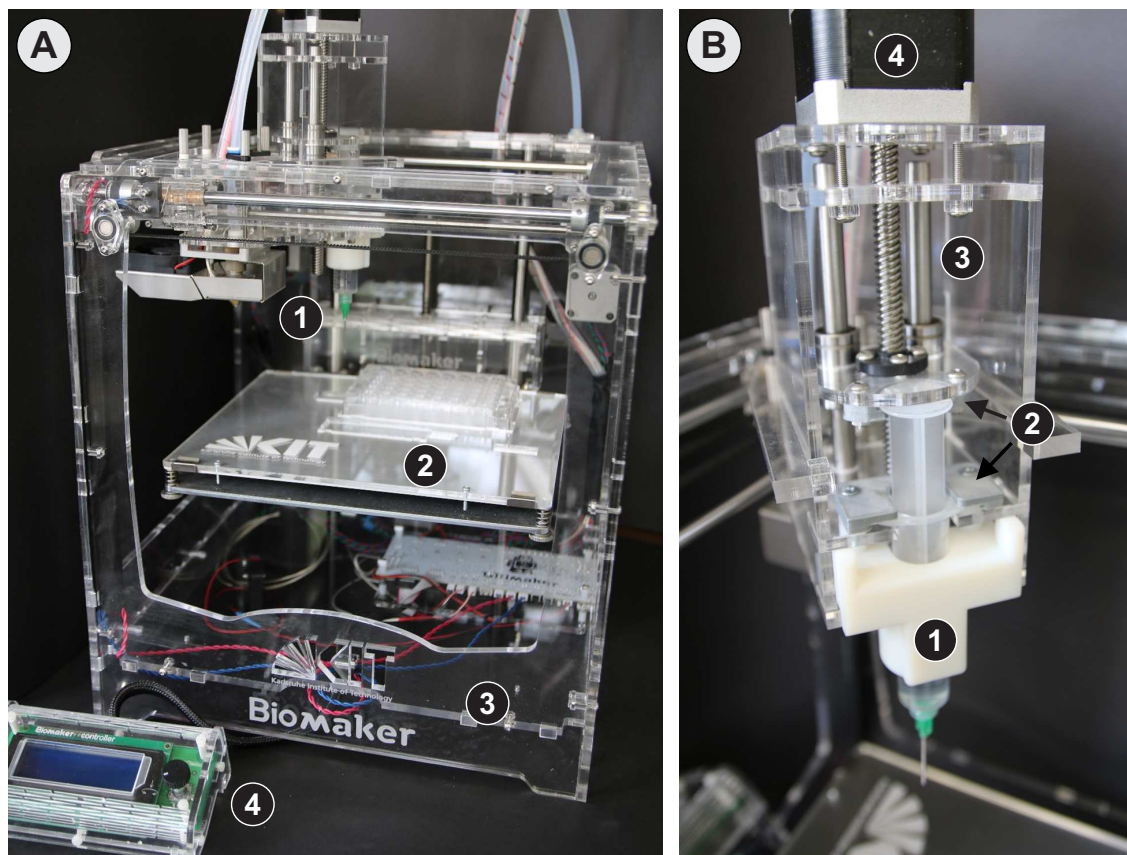


Figure 5.19: Photographs of the *Biomaker* and the extrusion unit. (A) Overview of the modified printer named *Biomaker* with the extrusion unit mounted on the printhead (1), a template for the positioning of the multiwell plate (2) and the acrylic glass body which replaces the original wooden body. The “ulticontroller” (4) can be used for direct control of the printing process. (B) Close-up view of the extrusion unit. The syringe is fixated in a cartridge (1) on the extruder. The additional printed parts (2) enclose the plunger of the syringe and enabled retraction movements. Together with the cartridge, the linear bearings and rods (3) allowed the precise printing position. The extrusion was executed by the movement of the stepper motor (4).

Automated execution of enzyme assay with encapsulated β -galactosidase

In the field of biotechnology, the interactions between liquid phases of various compositions and hydrogels with incorporated biologically active components is of great interest. For this investigative challenge of manifold combinations, automated high-throughput screenings are a promising and already established strategy. Such screening approaches facilitate the preparatory hydrogel research especially for applications which are difficult to automate or to parallelize and will profit from uncomplicated preliminary tests.

To demonstrate the applicability of the developed bioprinter in the field of biotechnology, a screening study for optimal process parameters of hydrogel encapsulated β -galactosidase was conducted. The enzyme containing, UV-curable bioink which is usually not printable

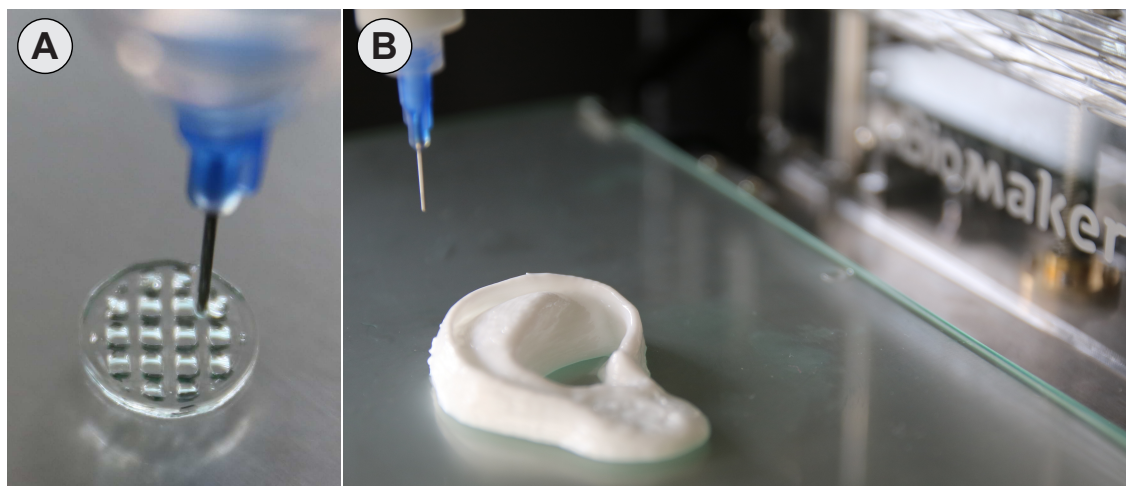


Figure 5.20: Photographs of printed models generated from STL files, both models were printed with a dispensing tip of 0.41 mm inner diameter (A) Scaffold printed with 30 % (w/w) Kolliphor (B) model of a human ear (after: <http://www.thingiverse.com/thing:105808>) printed with Nivea Soft Creme.

in three dimensions by extrusion-based systems, was 3D structured by a two-step printing process using a sacrificial ink (see figure 5.18, step A). By producing these structures in multiwell plates, a LHS based high-throughput screening of the hydrogel-enzyme composite and its interaction with the liquid surrounding was enabled without changing the original composition of the bioink. Hence, the transferability to the later applications in microfluidics or coatings was preserved. The easy setup and control of the printing process and the precise deposition of the sacrificial ink in the multiwell plate allowed the manufacturing of hollow hydrogel cylinders with a good positioning accuracy of the sacrificial structures. The resulting polymerized hydrogel cylinders were approximately 8 mm in height, had a wall thickness of approximately 1.6 mm and kept their shape over the entire experimental period of 30 days. The activity of the encapsulated β -galactosidase was determined by monitoring the production of the yellow-colored ONP, which was detected by absorption measurements at 410 nm. The calculated values of produced ONP were plotted over time to determine the turnover rate by the initial slope of the data points. An example of the turnover kinetics for an ONPG concentration of 40 $\mu\text{mol}/\text{mL}$ for all three pH values is shown in figure 5.21A. The determined turnover rates were 0.199 $\mu\text{mol}/\text{min}$ for pH 3, 0.201 $\mu\text{mol}/\text{min}$ for pH 5 and 0.117 $\mu\text{mol}/\text{min}$ for pH 7. Except for one outlier the shown standard deviations were ranged between 0.05 % and 8 % which indicates a satisfactory reproducibility in the measured duplicates. This emphasizes the good precision of the printer which results in the production of hydrogel cylinders of consistent quality. The established turnover rates from the multiple experiments were then merged to plot the dependency of the turnover on the substrate concentration as depicted in figure 5.21B. For each pH, the gained data points fit perfectly in the expected scheme of a typical Michaelis-Menten saturation curve of an enzyme reaction. The reaction rates at pH 7 were always smaller than the rates at pH 5 and pH 3, which showed a performance comparable to each other. These obtained findings

matched well the pH optimum of the ONPG conversion of β -galactosidase from *Aspergillus oryzae* which is reported to be in the range of pH 4-5. [234–236] From the measured kinetics also the enzymatic parameters K_m and v_{max} could be calculated which permit a comparison of the influence of different hydrogel compositions and identical liquid phase conditions.

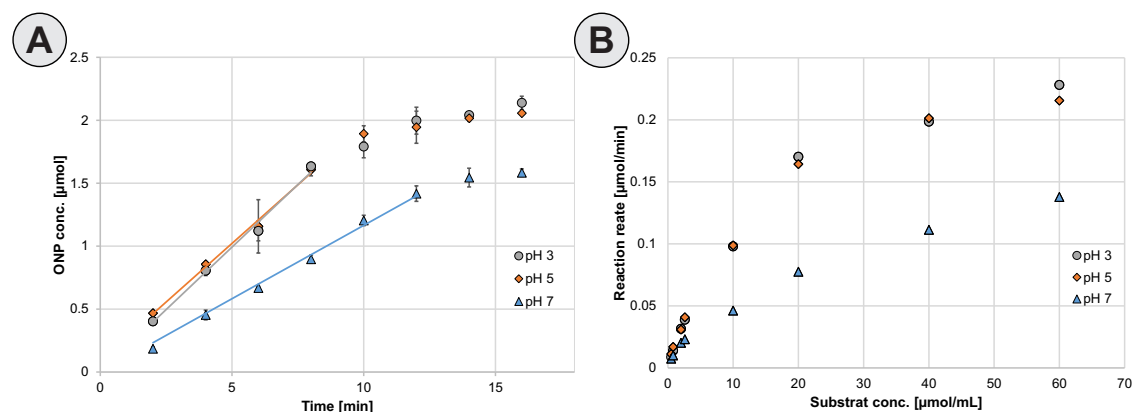


Figure 5.21: Representation of the reaction rate determination and the resulting Michaelis-Menten plot. (A) The initial slope of the measured production of ONP over the observed time span corresponds to the reaction rate of the encapsulated enzyme for the present condition. In the shown example, an initial ONPG concentration of 40 $\mu\text{mol}/\text{mL}$ at pH 3, 5 and 7 was examined. (B) The calculated reaction rates were plotted over the respective ONPG concentration which leads to a typical Michaelis-Menten saturation curve for all examined pH values.

The used PEG-DA based hydrogel could also preserve between 60-65 % of the activity of the encapsulated enzyme over a period of 30 days regarding the reaction rates measured after the overnight storage as 100 % for each pH individually. This could be determined for dry as well as for moist storing conditions (see figure 5.22). The enzyme assay for this investigation was executed with an ONPG concentration of 10 $\mu\text{mol}/\text{mL}$. The observed influence on the activity of stored hydrogel-encapsulated enzyme could be beneficial for the use as storage matrix in biocatalytic applications.

To check if the observed substrate conversion was triggered by the encapsulated β -galactosidase or by unintentionally released enzyme, hydrogels were equilibrated with buffer instead of incubating with ONPG solution. The gained samples were then examined on their potential enzyme activity with ONPG solution. The turnover of the substrate was observed at 410 nm in the spectrophotometer but no significant activity could be determined. Likewise, the storage solution from the overnight and the 30 days storage as well as the water which was used to rehydrate the dried hydrogels were examined by the same procedure. In all tested samples low activity was detected, slightly increasing with the contact time of water and hydrogel but was insignificantly small in all cases in terms of the activities detected within the actual assay of the encapsulated enzymes. The described case study was successfully executed to encapsulate the enzyme β -galactosidase in hollow cylinder shaped, PEG-DA based hydrogels in 48 well plates. The washing out of

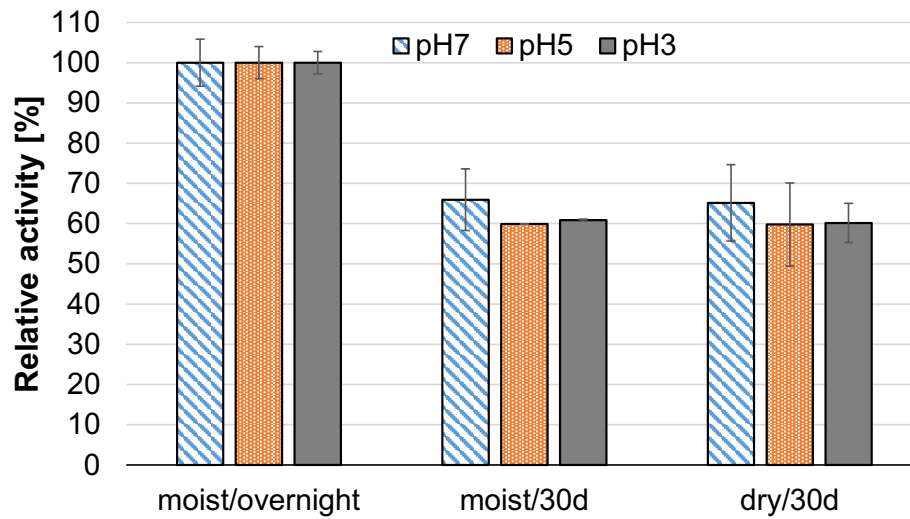


Figure 5.22: Comparison of the enzyme activity after different storage conditions. The assay was executed with 10 $\mu\text{mol}/\text{mL}$ ONPG. Storing the hydrogels up to 30 days in moist or dry conditions preserved up to 65 % of the activity determined after one night of moist storage.

the sacrificial ink with ultrapure water under cooled conditions and the execution of the enzyme assay in hydrogel-loaded wells could be successfully implemented in an automated screening process on the liquid handling station (see process scheme in figure 5.18, steps A and B). This included the scheduling and performance of the hydrogel equilibration (figure 5.18, step C), the providing of the stop solution and the ONPG solution as well as the sampling and measurement of the gained samples (figure 5.18, steps D and E).

Conclusion

The presented study established the combination of an entry-level bioprinter for the production of 3D hydrogel structures followed by the automated execution of the hydrogel – liquid phase interaction investigation in multiwell plates on a liquid handling station.

The *Biomaker* is easy to operate through a user friendly interface, is ready to implement in biological laboratory environments and offers a very good price-performance ratio. The suitability of the printer for an application in the field of biotechnology was shown by the encapsulation of β -galactosidase in poly(ethylene glycol) diacrylate based hydrogels. The two-step printing process ('mold-and-fill') was adapted from tissue engineering for the production of hollow hydrogel cylinders from low viscous bioinks in multiwell plates. This allowed the subsequent execution of an enzymatic activity assay on an automated liquid handling station. The enzymatic turnover of various substrate concentrations was monitored which resulted in the typical Michaelis-Menten curves for the three tested pH values of the surrounding liquid phase.

The introduced setup is suggested to open new possibilities for the biotechnological research and as a highly promising educational tool. It facilitates the access to 3D bioprinting with an easy to handle user interface and an open source environment for the simple adaption

to following demands without compromising equipment dedicated for the delicate working field of cell applications. It can be employed to screen bioink components, their influence on the resulting hydrogel and on the interaction with liquid phases of different compositions.

Acknowledgments

This research work is part of the project „Molecular Interaction Engineering: From Nature’s Toolbox to Hybrid Technical Systems“, which is funded by the German Federal Ministry of Education and Research (BMBF), funding code 031A095B.

References

12. Baden, T., Chagas, A. M., Gage, G., Marzullo, T., Prieto-Godino, L. L., and Euler, T. ‘Open Labware: 3-D Printing Your Own Lab Equipment’. *PLoS Biol.* Vol. 13(3) (Mar. 2015), e1002086 (cit. on pp. 2, 78).
15. Lode, A., Krujatz, F., Brüggemeier, S., Quade, M., Schütz, K., Knaack, S., Weber, J., Bley, T., and Gelinsky, M. ‘Green bioprinting: Fabrication of photosynthetic algae-laden hydrogel scaffolds for biotechnological and medical applications’. *Engineering in Life Sciences*, vol. 15(2) (2015), pp. 177–183 (cit. on pp. 2, 78).
16. Rodriguez-Dévora, J. I., Zhang, B., Reyna, D., Shi, Z.-d., and Xu, T. ‘High throughput miniature drug-screening platform using bioprinting technology’. *Biofabrication*, vol. 4(3) (2012), p. 035001 (cit. on pp. 2, 78).
49. Waldbaur, A., Rapp, H., Länge, K., and Rapp, B. E. ‘Let there be chip—towards rapid prototyping of microfluidic devices: one-step manufacturing processes’. *Anal. Methods*, vol. 3(12) (2011), pp. 2681–2716 (cit. on pp. 4, 6, 78).
79. Waldbaur, A., Kittelmann, J., Radtke, C. P., Hubbuch, J., and Rapp, B. E. ‘Microfluidics on liquid handling stations (μ F-on-LHS): an industry compatible chip interface between microfluidics and automated liquid handling stations’. *Lab on a Chip*, vol. 13(12) (2013), pp. 2337–2343 (cit. on pp. 5, 20, 37, 38, 59, 60, 68, 78).
84. Panda, B., Tan, M. J., Gibson, I., and Chua, C. K. ‘The Disruptive Evolution Of 3D Printing’. *Proc. 2nd Int. Conf. Prog. Addit. Manuf. (Pro-AM 2016)*, vol. (2016), pp. 152–157 (cit. on pp. 6, 78).
100. Jose, R. R., Rodriguez, M. J., Dixon, T. A., Omenetto, F., and Kaplan, D. L. ‘Evolution of Bioinks and Additive Manufacturing Technologies for 3D Bioprinting’. *ACS Biomater. Sci. Eng.* Vol. 2(10) (Oct. 2016), pp. 1662–1678 (cit. on pp. 7, 10, 78).
102. Malda, J., Visser, J., Melchels, F. P., Jüngst, T., Hennink, W. E., Dhert, W. J. A., Groll, J., and Huttmacher, D. W. ‘25th Anniversary Article: Engineering Hydrogels for Biofabrication’. *Adv. Mater.* Vol. 25(36) (Sept. 2013), pp. 5011–5028 (cit. on pp. 9, 10, 78).
106. Reid, J. A., Mollica, P. A., Johnson, G. D., Ogle, R. C., Bruno, R. D., and Sachs, P. C. ‘Accessible bioprinting: adaptation of a low-cost 3D-printer for precise cell placement and stem cell differentiation’. *Biofabrication*, vol. 8(2) (June 2016), p. 025017 (cit. on pp. 9, 79).
107. Mellott, M. B., Searcy, K., and Pishko, M. V. ‘Release of protein from highly cross-linked hydrogels of poly (ethylene glycol) diacrylate fabricated by UV polymerization’. *Biomaterials*, vol. 22(9) (2001), pp. 929–941 (cit. on pp. 10, 36, 78, 96, 101, 103, 105).

109. Sheldon, R. A. and Pelt, S. van. 'Enzyme immobilisation in biocatalysis: why, what and how'. *Chem. Soc. Rev.* Vol. 42(15) (Mar. 2013), pp. 6223–6235 (cit. on pp. 10, 78).
111. Russell, R., Axel, A., Shields, K., and Pishko, M. 'Mass transfer in rapidly photopolymerized poly(ethylene glycol) hydrogels used for chemical sensing'. *Polymer (Guildf)*. Vol. 42(11) (May 2001), pp. 4893–4901 (cit. on pp. 10, 78).
193. Savastano, M., Amendola, C., D'Ascenzo, F., and Massaroni, E. '3-D Printing in the Spare Parts Supply Chain: An Explorative Study in the Automotive Industry'. *Digit. Support. Innov. Lect. Notes Inf. Syst. Organ.* Ed. by Caporarello, L., Cesaroni, F., Giesecke, R., and Missikoff, M. Springer, Cham, 2016, pp. 153–170 (cit. on p. 78).
194. McDonald, J. C., Chabinyk, M. L., Metallo, S. J., Anderson, J. R., Stroock, A. D., and Whitesides, G. M. 'Prototyping of Microfluidic Devices in Poly(dimethylsiloxane) Using Solid-Object Printing'. *Anal. Chem.* Vol. 74(7) (Apr. 2002), pp. 1537–1545 (cit. on p. 78).
195. Chen, C., Wang, Y., Lockwood, S. Y., and Spence, D. M. '3D-printed fluidic devices enable quantitative evaluation of blood components in modified storage solutions for use in transfusion medicine'. *Analyst*, vol. 139(13) (2014), pp. 3219–3226 (cit. on p. 78).
197. Su, C.-K. and Chen, J.-C. 'Reusable, 3D-printed, peroxidase mimic-incorporating multi-well plate for high-throughput glucose determination'. *Sensors Actuators B Chem.* Vol. 247 (Aug. 2017), pp. 641–647 (cit. on p. 78).
199. Gross, B. C., Erkal, J. L., Lockwood, S. Y., Chen, C., and Spence, D. M. 'Evaluation of 3D Printing and Its Potential Impact on Biotechnology and the Chemical Sciences'. *Anal. Chem.* Vol. 86(7) (Apr. 2014), pp. 3240–3253 (cit. on p. 78).
200. Groll, J. et al. 'Biofabrication: reappraising the definition of an evolving field'. *Biofabrication*, vol. 8(1) (Jan. 2016), p. 013001 (cit. on p. 78).
201. Patra, S. and Young, V. 'A Review of 3D Printing Techniques and the Future in Biofabrication of Bioprinted Tissue'. *Cell Biochem. Biophys.* Vol. 74(2) (June 2016), pp. 93–98 (cit. on p. 78).
202. Drury, J. L. and Mooney, D. J. 'Hydrogels for tissue engineering: scaffold design variables and applications'. *Biomaterials*, vol. 24(24) (Nov. 2003), pp. 4337–4351 (cit. on p. 78).
203. Nguyen, K. T. and West, J. L. 'Photopolymerizable hydrogels for tissue engineering applications'. *Biomaterials*, vol. 23(22) (Nov. 2002), pp. 4307–4314 (cit. on p. 78).
204. Langer, R. and Peppas, N. A. 'Advances in biomaterials, drug delivery, and bionanotechnology'. *AIChE J.* Vol. 49(12) (Dec. 2003), pp. 2990–3006 (cit. on p. 78).
205. Derby, B. 'Printing and prototyping of tissues and scaffolds'. *Science*, vol. 338(6109) (2012), pp. 921–926 (cit. on p. 78).

206. Hollister, S. J. 'Porous scaffold design for tissue engineering.' *Nature materials*, vol. 4(7) (2005) (cit. on p. 78).
207. Ouyang, L., Highley, C. B., Rodell, C. B., Sun, W., and Burdick, J. A. '3D Printing of Shear-Thinning Hyaluronic Acid Hydrogels with Secondary Cross-Linking'. *ACS Biomaterials Science & Engineering*, vol. 2(10) (2016), pp. 1743–1751 (cit. on p. 78).
208. Ventola, C. L. 'Medical applications for 3D printing: current and projected uses'. *Pharmacy and Therapeutics*, vol. 39(10) (2014), p. 704 (cit. on p. 78).
209. Ma, X., Qu, X., Zhu, W., Li, Y.-S., Yuan, S., Zhang, H., Liu, J., Wang, P., Lai, C. S. E., Zanella, F., et al. 'Deterministically patterned biomimetic human iPSC-derived hepatic model via rapid 3D bioprinting'. *Proceedings of the National Academy of Sciences*, vol. 113(8) (2016), pp. 2206–2211 (cit. on p. 78).
210. Zhao, Y., Yao, R., Ouyang, L., Ding, H., Zhang, T., Zhang, K., Cheng, S., and Sun, W. 'Three-dimensional printing of HeLa cells for cervical tumor model in vitro'. *Biofabrication*, vol. 6(3) (2014), p. 035001 (cit. on p. 78).
211. MacNeil, S. 'Progress and opportunities for tissue-engineered skin'. *Nature*, vol. 445(7130) (2007), pp. 874–880 (cit. on p. 78).
212. Marga, F., Jakab, K., Khatiwala, C., Shepherd, B., Dorfman, S., Hubbard, B., Colbert, S., and Forgacs, G. 'Toward engineering functional organ modules by additive manufacturing'. *Biofabrication*, vol. 4(2) (2012), p. 022001 (cit. on p. 78).
213. Mannoor, M. S., Jiang, Z., James, T., Kong, Y. L., Malatesta, K. A., Soboyejo, W. O., Verma, N., Gracias, D. H., and McAlpine, M. C. '3D printed bionic ears'. *Nano letters*, vol. 13(6) (2013), p. 2634 (cit. on p. 78).
214. Leonard, M., De Boisseson, M., Hubert, P., Dalençon, F., and Dellacherie, E. 'Hydrophobically modified alginate hydrogels as protein carriers with specific controlled release properties'. *J. Control. Release*, vol. 98(3) (Aug. 2004), pp. 395–405 (cit. on p. 78).
215. Gil, M. S., Cho, J., Thambi, T., Giang Phan, V., Kwon, I., and Lee, D. S. 'Bioengineered robust hybrid hydrogels enrich the stability and efficacy of biological drugs'. *J. Control. Release*, vol. (Apr. 2017), DOI: 10.1016/j.jconrel.2017.04.009 (cit. on p. 78).
216. Heo, J. and Crooks, R. M. 'Microfluidic Biosensor Based on an Array of Hydrogel-Entrapped Enzymes'. *Anal. Chem.* Vol. 77(21) (Nov. 2005), pp. 6843–6851 (cit. on pp. 78, 79).
218. Kerby, M. B., Legge, R. S., and Tripathi, A. 'Measurements of Kinetic Parameters in a Microfluidic Reactor'. *Anal. Chem.* Vol. 78(24) (Dec. 2006), pp. 8273–8280 (cit. on p. 78).

219. Brahim, S., Narinesingh, D., and Guiseppi-Elie, A. 'Polypyrrole-hydrogel composites for the construction of clinically important biosensors'. *Biosens. Bioelectron.* Vol. 17(1-2) (Jan. 2002), pp. 53–59 (cit. on p. 78).
220. Podual, K., Doyle, F. J., and Peppas, N. A. 'Glucose-sensitivity of glucose oxidase-containing cationic copolymer hydrogels having poly(ethylene glycol) grafts'. *J. Control. Release*, vol. 67(1) (June 2000), pp. 9–17 (cit. on p. 78).
222. Park, T. G. and Hoffman, A. S. 'Immobilization and characterization of β -galactosidase in thermally reversible hydrogel beads'. *J. Biomed. Mater. Res.* Vol. 24(1) (Jan. 1990), pp. 21–38 (cit. on p. 78).
223. Hinton, T. J., Jallerat, Q., Palchesko, R. N., Park, J. H., Grodzicki, M. S., Shue, H.-J., Ramadan, M. H., Hudson, A. R., and Feinberg, A. W. 'Three-dimensional printing of complex biological structures by freeform reversible embedding of suspended hydrogels'. *Sci. Adv.* Vol. 1(9) (Oct. 2015), e1500758–e1500758 (cit. on p. 79).
224. Yang, F., Tadepalli, V., and Wiley, B. J. '3D Printing of a Double Network Hydrogel with a Compression Strength and Elastic Modulus Greater than those of Cartilage'. *ACS Biomater. Sci. Eng.* Vol. 3(5) (May 2017), pp. 863–869 (cit. on p. 79).
227. Liu, J., Agarwal, M., and Varahramyan, K. 'Glucose sensor based on organic thin film transistor using glucose oxidase and conducting polymer'. *Sensors Actuators B Chem.* Vol. 135(1) (2008), pp. 195–199 (cit. on p. 79).
228. He, Y., Yang, F., Zhao, H., Gao, Q., Xia, B., and Fu, J. 'Research on the printability of hydrogels in 3D bioprinting'. *Scientific reports*, vol. 6 (2016), p. 29977 (cit. on p. 80).
230. Griffiths, M. W. and Muir, D. D. 'Properties of a thermostable β -galactosidase from a thermophilic *Bacillus*: Comparison of the enzyme activity of whole cells, purified enzyme and immobilised whole cells'. *J. Sci. Food Agric.* Vol. 29(9) (Sept. 1978), pp. 753–761 (cit. on p. 82).
231. Kröner, F. and Hubbuch, J. 'Systematic generation of buffer systems for pH gradient ion exchange chromatography and their application'. *J. Chromatogr. A*, vol. 1285 (Apr. 2013), pp. 78–87 (cit. on pp. 82, 98).
232. Hölzl, K., Lin, S., Tytgat, L., Van Vlierberghe, S., Gu, L., and Ovsianikov, A. 'Bioink properties before, during and after 3D bioprinting'. *Biofabrication*, vol. 8(3) (Sept. 2016), p. 032002 (cit. on p. 83).
233. Markstedt, K., Mantas, A., Tournier, I., Martínez Ávila, H., Hägg, D., and Gatenholm, P. '3D Bioprinting Human Chondrocytes with Nanocellulose–Alginate Bioink for Cartilage Tissue Engineering Applications'. *Biomacromolecules*, vol. 16(5) (May 2015), pp. 1489–1496 (cit. on p. 83).

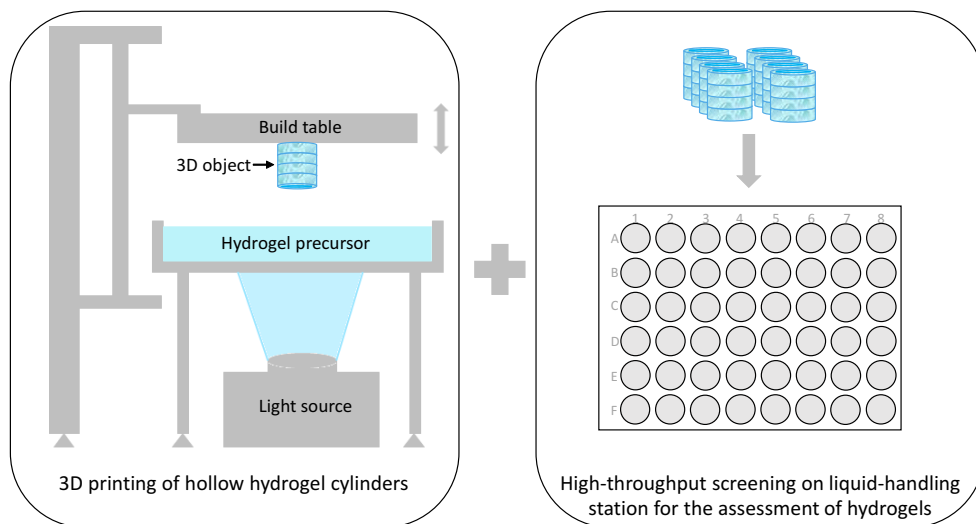
234. Haider, T. and Husain, Q. 'Calcium alginate entrapped preparations of *Aspergillus oryzae* β galactosidase: Its stability and applications in the hydrolysis of lactose'. *Int. J. Biol. Macromol.* Vol. 41(1) (June 2007), pp. 72–80 (cit. on p. 86).
235. Sarto, V., Marzetti, A., and Focher, B. ' β -d-Galactosidases immobilized on soluble matrices: Kinetics and stability'. *Enzyme Microb. Technol.* Vol. 7(10) (Oct. 1985), pp. 515–520 (cit. on p. 86).
236. Tanaka, Y., Kagamiishi, A., Kiuchi, A., and Horiuchi, T. 'Purification and Properties of β -Galactosidase from *Aspergillus oryzae*'. *J. Biochem.* Vol. 77(1) (1975), pp. 241–247 (cit. on p. 86).

5.5 Assessment of hydrogels for biopharmaceutical purposes using a combination of 3D printing and high-throughput screening

Josefine Morgenstern*, Carsten P. Radtke*, Cathrin Dürr and Jürgen Hubbuch

Institute of Engineering in Life Sciences, Section IV: Biomolecular Separation Engineering, Karlsruhe Institute of Technology (KIT), 76131 Karlsruhe, Germany

* *These authors contributed equally to this work.*



manuscript in preparation

Abstract

Synthetic hydrogels provide an effective and convenient way to administer high molecular weight protein drugs. However, the release kinetics of these proteins from hydrogels depend on the highly complex physical and chemical properties of the hydrogel, the surrounding solution conditions and the protein itself. The objective of this work was the development of an rapid and cost-effective tool for the investigation of the influences of these variables on occurring interactions. The fulfilment and realization of this aim was successfully achieved by a combination of hydrogel 3D printing and high-throughput screening techniques. In a case study, the lysozyme uptake and release profiles of hydrogel structures with different compositions (poly(ethylene glycol) diacrylate and acrylic acid) under the influence of varying surrounding buffer conditions was investigated. In comparison with literature data, it was shown that the approach presented here leads to verisimilar data for the used materials and thus constitutes a helpful tool for the development of hydrogel based drug delivery systems.

Keywords: *3D printing; photopolymerization; controlled drug delivery; protein uptake and release*

Introduction

Advances in medical technology and the pharmaceutical sector have created a better understanding of the root cause of a variety of diseases in recent years. Biopharmaceuticals based on recombinant proteins, such as monoclonal antibodies or therapeutic enzymes, promise highly effective therapies with minimal side effects due to their high selectivity for certain cells or metabolic pathways in the human body. Moreover, recombinant proteins can treat diseases resulting from insufficient or deficient production of endogenous proteins [237]. The increasing use of pharmaceutical proteins has created a need for new methods of controlled administration of these compounds [107]. In this context, polymeric carrier systems arouse the interest of academia and industry for the controlled spatial and temporal release of biotherapeutics [238, 239]. For use in the clinical field, these polymers must meet the requirements of biocompatibility and immunological acceptance while integrating elements of responsive behavior to give a well-defined reaction to external conditions [238]. Proteins are found in human tissues mainly in aqueous environments. In order to mimic this natural environment and thus to preserve the native protein conformation, hydrophilic polymers are suitable to administer pharmaceutical proteins. These polymers are capable of absorbing large amounts of water or biological fluids and can be interlinked to three-dimensional networks. Therefore those hydrophilic networks are often referred to as hydrogels. The presence of chemical and/or physical crosslinks renders hydrogels insoluble in water after network formation. [240]

Hydrogels are already used as a matrix for the oral administration of small molecule drugs [241]. Also, hydrogel based formulations present a promising approach for the oral administration of protein drugs since the molecule is protected from harsh conditions and degradation by endogenous enzymes in the gastrointestinal tract [107]. Thus, for example, considerable efforts for the development and clinical testing of oral delivery forms for insulin have been made [242–244]. Further, hydrogels may be applied directly to a wound or implanted near the site of action. This approach results in a depot formulation from which the drug slowly elutes and thus maintains a high local concentration in the surrounding tissues over an extended period of time [245].

The network structure and the thermodynamic nature of all compounds involved determine the protein release profile of these networks [246]. The molecular weight and content of the polymer as well as the addition of crosslinking agents determine the density of crosslinks in the gel matrix and thus the mesh size [107]. The mesh size of the swollen network affects the physical properties of the gel, such as mechanical strength, degradation and diffusion of captured molecules [237]. By the addition of ionizable or hydrophobic hydrogel monomers, additional interactions of the proteins with the polymer network can be promoted [107]. On the protein side, mainly the molecular weight, the composition of the amino acids and thus the distribution of charged and hydrophobic residues on the surface of the protein as well as the three-dimensional structure of the protein affect the release properties from the hydrogel [107]. The interaction based uptake and release of biomolecules is determined by the ratio of the interaction between the hydrogel and the protein as well as the protein and the surrounding solution [238].

There are many theoretical approaches to describe network structure, mesh size, swelling

behavior and mass transport of biomolecules in hydrogels [240]. The high number of variables, however, makes a comprehensive mechanistic understanding of protein-hydrogel interaction difficult. Furthermore, the theoretical predictability of the uptake and release profiles is aggravated by the multiplicity of combinable proteins and hydrogel materials [247]. A sound experimental data base is essential for theoretical knowledge building of the various interactions occurring between the hydrogels, proteins and the liquid environment. In this context, high-throughput screenings (HTS) may help to understand the complexity affecting the drug delivery result [248]. HTS offer an accurate, rapid, and cost-saving method to study hydrogel-protein interactions and the influence of surrounding solution conditions while covering a high number of potential process parameters at the same time. The standard HTS-format in biotechnology are multi-well plates, which are handled by highly automated pipetting stations [24, 35, 36, 249]. For hydrogels, however, a fast and reproducible method to crosslink precursor solutions into a HTS-compatible shape is still missing. 3D printing offers the heretofore needed outstanding possibility to polymerize precursor solutions to any shape [250]. In case of 3D bioprinting, the printing materials, or bioinks, are composed of biocompatible matrix materials such as hydrogels or their precursors, additives and biological components.

This study aims to implement three dimensional hydrogel structures into multi-well plates for the investigation of hydrogel-protein interactions on liquid-handling stations. Therefore, hollow hydrogel cylinders fitting into standard 48-well plates were produced using 3D bioprinting. This shape provides a large surface to volume ratio for the observation of transport phenomena while ensuring a non-destructive operation of the automated pipetting tips. Lysozyme from chicken egg white was used as a model protein to study the drug uptake and release behavior from poly(ethylene glycol) diacrylate (PEG-DA) based hydrogels. PEG-DA was photochemically crosslinked using a DLP (digital light processing) based stereolithography system. Two approaches for the incorporation of proteins in hydrogels are compared. In the first approach, the hydrogel was printed without protein and subsequently loaded with protein (PostFabLoading). This approach increases the probability of preserving the biological activity of the protein, reduces, however, the maximum utilization of the protein due to partitioning limitations [251]. In order to maximize the protein uptake different polymer contents and pH values as well as the addition of the co-monomer acrylic acid (AA) were investigated. For the second approach, the protein was part of the bioink and consequently present during the polymerization process (PrintLoading). This approach may result in activity loss due to potential reactions with the hydrogel polymer, resulting radicals or the energy input necessary for crosslinking. After hydrogel formation and protein loading, the release was examined under different solution conditions (pH and ionic strength). In order to ensure protein integrity after the release, an activity assay was performed.

Materials and Methods

All solutions were prepared with ultra-pure water ($0.55 \mu\text{S}/\text{cm}$) obtained from a PURELAB Ultra water purification system (ELGA Labwater, Germany). The 25 mM multicomponent buffer with a linear buffering range from pH 3 to pH 9 consisted of the buffer substances AMPSO (2-hydroxy-3-[(1-hydroxy-2-methylpropan-2-yl)amino]propane-1-sulfonic

acid) (Sigma-Aldrich), TAPSO (3-[[1,3-dihydroxy-2-(hydroxymethyl)propan-2-yl]amino]-2-hydroxypropane-1-sulfonic acid)(Sigma-Aldrich), MES 1-hydrate (2-morpholinoethane-sulfonic acid) (AppliChem), sodium acetate trihydrate (Sigma-Aldrich, USA) and formic acid (Merck Millipore). The buffer recipe is summarized in Table 5.2.

Table 5.2: Composition of 25 mM multicomponent buffer with a linear buffering range from pH 3 to pH 9 calculated according to [231]. The used buffer substances are displayed with the corresponding pKa value and molarity.

Buffer component	pKa-value [-]	molarity [mM]
AMPSO	9.14	42.44
TAPSO	7.64	33.90
MES 1-hydrate	6.10	38.03
Sodium acetate trihydrate	4.76	27.56
Formic acid	3.75	37.43

Potassium chloride (KCl) and di-potassium hydrogen phosphate (K_2HPO_4) for the size exclusion chromatography running buffer were purchased from VWR. Dulbecco's Phosphate buffered saline (PBS) (ThermoFisher Scientific) and sodium chloride (Merck Millipore) were used for protein release studies. pH adjustment of all buffers within a range of ± 0.05 units was performed using a five-point calibrated pH-meter HI-3220 (Hanna Instruments, USA) with a SenTix[®] 62 pH electrode (Xylem Inc., USA). For pH correction hydrochloric acid and sodium hydroxide were obtained from Merck (Germany). All buffers were filtered using a 0.2 μ m cellulose-acetate filter (Sartorius, Germany) and degassed for chromatographic purposes.

Poly(ethylene glycol) diacrylate (PEG-DA, average MW 575), 2,2-Dimethoxy-2-phenylacetophenone (DMPA) and acrylic acid for bioink preparation were obtained from Sigma-Aldrich. Protein solutions were prepared using chicken egg-white lysozyme (subsequently referred to as lysozyme) from Hampton Research.

3D printing of PEG-DA based hydrogels

Preparation of bioinks The used mass concentrations of all components are summarized in Table 5.3 for all studied bioinks. To prevent premature polymerization, all ink components were weighed in and stored in lightproof centrifuge tubes (50 ml Tube Cellstar[®], Greiner Bio-One). The ink was mixed on an overhead shaker for at least 24 hours to ensure complete dissolution of the photoinitiator.

3D fabrication of hydrogels A commercially available B9Creator DLP 3D printer (version 1.2, B9Creations) equipped with an modified projector (D912HD, vivitek) as light source was used to polymerize the bioinks. The CAD model of the hollow cylinder was created in Solid Edge ST7 (Siemens PLM Software) and exported as a stereolithography file (.stl) into the 3D printer software (B9Creator). The hollow cylinders have an outer diameter of 9.45 mm, a wall thickness of 0.82 mm and a height of 7 mm. This results in a total volume of the hollow cylinder of 155.6 mm³ before being swollen in water. The model was

Table 5.3: Composition of bioinks. The percentage of a component %(w/w) refers to the total weight of all components. The lysozyme stock solution was prepared by dissolving 6.45 %(w/w) in ultrapure water.

	PEG-DA (MW 575)	ultra-pure water	acrylic acid	DMPA	lysozyme stock solution
PEG-DA ₅₀	50	49	-	1	-
PEG-DA ₇₅	75	24	-	1	-
PEG-DA ₉₀	90	9	-	1	-
PEG-DA ₇₅ AA _{7.5}	75	16.5	7.5	1	-
PEG-DA ₇₅ AA ₁₅	75	9	15	1	-
PEG-DA ₇₅ Ly _{81.55}	75	-	-	1	9.6

sliced to layers of 200 μm thickness and the configuration of the printer was set to an x, y resolution of 30 μm . Before printing, calibration of the build table and automatic focusing of the projector was performed. Depending on the ink composition printer settings were adjusted in order to achieve complete polymerization and 3D objects free from defects. The applied settings for the different bioinks are summarized in Table 5.4.

Table 5.4: Adapted printing parameters for the various ink compositions (see Table 5.3).

	Exposure settings base	Exposure settings over	Attach layers	Attach base	Attach Over
PEG-DA ₅₀	25	1	1	20	1
PEG-DA ₇₅	20	1	1	15	1
PEG-DA ₉₀	20	1	1	15	1
PEG-DA ₇₅ AA _{7.5}	20	1	1	30	1
PEG-DA ₇₅ AA ₁₅	28	1	1	50	1
PEG-DA ₇₅ Ly _{81.55}	11	1	2	12	1

Except the changes stated here, the bioinks were printed with the default settings for the commercial ink B9R-1-Red from B9Creations. Since a complete filling of the tank with bioink was too material-consuming, the ink was gradually applied manually. The necessary time for ink application was achieved by setting the post-release delay to 10 seconds. Four cylinders were produced simultaneously in one printing run.

The irradiation by the projector led to a clouding of the silicone layer which is built-in to prevent adhesion of the printed structure to the resin vat. This effect was amplified by increasing the content of AA in the bioinks. Therefore, the silicone layer was exchanged at regular intervals according to the specification of B9Creations using Elastosil[®] RT 601 (Wacker Chemie).

Determination of protein uptake and release by 3D printed hydrogel cylinders

Loading of hydrogels with protein For PrintLoading, the protein is present during the printing process. The fabrication of the protein containing hydrogel cylinders is already described in section 5.5. The amount of lysozyme that was entrapped within the hydrogel was determined by assuming the same weight percent of lysozyme in the precursor solution to be also present in the polymerized hydrogel.

To perform the PostFabLoading of the printed hydrogel cylinders, a lysozyme solution of 40 mg/ml was prepared using the 25 mM multicomponent buffer of respective pH. Protein concentration measurements were conducted using a NanoDrop2000c UV-Vis spectrophotometer (Thermo Fisher Scientific) and an extinction coefficient of $\epsilon_{280\text{ nm, lysozyme}}^{1\%} = 22.00$ [252]. The 3D-printed cylinders were stored in ultra-pure water for at least 24 h in order to deplete unpolymerized bioink components. For the uptake experiments, the cylinders were drained, patted dry and placed in the wells of a 48-well plate (48 Well Cell Culter Cluster, Costar®). Using a fully automated pipetting station Freedom EVO® 200 (Tecan) the cylinders were equilibrated for 30 min in 400 μl multicomponent buffer of the respective pH. After equilibration, 300 μl of the buffer were withdrawn and replaced by the 40 mg/ml protein solution yielding a concentration of 30 mg/ml for the uptake experiments. During incubation, the 48-well plates were covered to avoid evaporation and shaken at 200 rpm on a Te-Shake orbital mixer (Tecan). After 0, 2, 4, 6, 8, 10 and 12 hours, the supernatant was removed from a triplet of cylinders of equal composition and examined by analytical size exclusion chromatography (SEC) for the remaining protein concentration. For all experiments carried out, only one measurement value is generated from the supernatant of each hydrogel cylinder of a 48-well plate. Thus, the multiple determination of a data point as well as the different time steps within a protein uptake series result from different cylinders.

The chromatography runs were performed using a Dionex UltiMate® 3000 liquid chromatography system (ThermoFisher Scientific) equipped with a HPG-3400RS pump, a WPS-3000TFC analytical autosampler, a TCC3000RS column thermostat and a DAD3000RS detector. As stationary phase, an Acquity UPLC® BEH200 SEC 1.7 μm (4.6 x 30mm) column (Waters) was used. Analysis was performed at a flow rate of 0.2 ml/min using a 200 mM K_2HPO_4 buffer at pH 7 containing 250 mM KCl. The injection volume was set to 20 μl using double loop overfill.

Protein release from hydrogels Protein release was studied using the 25 mM multicomponent buffer at three different pH values (3, 7 and 9) and under the influence of three different sodium chloride concentrations (0 M, 0.15 M and 0.5 M). Furthermore, the protein release under physiological conditions was tested using phosphate buffered saline (PBS). To study the protein release from the loaded hydrogels, cylinders were incubated for 12 h with protein solution for PostFabLoading as described in section 5.5. After incubation, the protein solution was withdrawn and the hydrogels were washed with 1 ml ultra-pure water by single-time uptake and dispensing with a pipette. The PrintLoaded cylinders were rinsed with ultra-pure water for 10 s after the printing process.

For the protein release studies, 500 μl of the release buffer to be screened was added to each cylinder. During incubation, the 48-well plates was shaken at 200 rpm. Kinetics were recorded using a NanoDrop2000c UV-Vis spectrophotometer and an extinction coefficient of $\epsilon_{280\text{ nm}, \text{lysozyme}}^{1\%} = 22.00$. For each time point, 3 μl of sample were withdrawn and analyzed. The multiple determination of a data point within one protein release series results from three independent cylinders.

In order to evaluate biological integrity after the fabrication process, the released protein was analyzed for residual activity using *Micrococcus lysodeikticus* based activity assay according to [253]. This method was slight modified by measuring the activities only at a protein concentration of 0.3 mg/ml. The slope of the absorption at 450 nm over time was used as activity and related to the activity of reference sample containing native lysozyme at pH 7. Moreover, samples were analyzed by analytical SEC in order to monitor the formation of aggregates (c.f. section 5.5).

Results and discussion

PEG-DA based hydrogels were fabricated by photopolymerization with a DLP based stereolithography system using DMPA as a photoinitiator. DMPA photofragments to highly reactive methyl radicals, which initiate photopolymerization by attacking the carbon-carbon double (C=C) bonds present in the acrylate groups of PEG-DA and acrylic acid [107, 254]. This radical photopolymerization leads to linear chain growth as well as to branched and crosslinked structures forming a three-dimensional network [254]. The two components PEG-DA and acrylic acid absorb water in an aqueous environment and thus create an ideal environment to incorporate biomolecules in this three-dimensional network. In this study, two methods to introduce the biomolecule into the hydrogels are investigated. Firstly, the hydrogel is polymerized and subsequently incubated in concentrated drug solutions (post-fabrication equilibrium partitioning = PostFabLoading) [251] and secondly, the protein is present in the bioink during the polymerization (PrintLoading) [107]. The hydrogels loaded in both ways are tested for their release behavior and the residual activity of the incorporated protein.

3D printing of PEG-DA based hydrogels

The presented setup with the B9Creator and the modified projector was well suited to produce hydrogel structures from all prepared ink compositions. With the UV filter removed from the projector the emission spectra and the irradiance was adequate to polymerize hydrogel layers of 200 μm and hollow cylinders could be build up. To ensure a proper print result, the applied printing parameters (c.f. Table 5.4) had to be adapted for the varying bioink formulations (c.f. Table 5.3). The aim of the adaptations was the production of hydrogel structures with a minimum of reject and waste. Furthermore, the duration of light exposure was optimized in regard to print result, total print time, and in the specific case preventing inadequate irradiation of the protein. Adjusting the suitable print settings as well as the application of the ink were the most crucial steps for a successful printing procedure. Insufficient exposure settings for the attaching layer concluded in poor attachment and the occurring of polymerized parts in the applied ink (see Fig. 5.23A).

Also incomplete structures were developing when the freshly printed layer had no contact

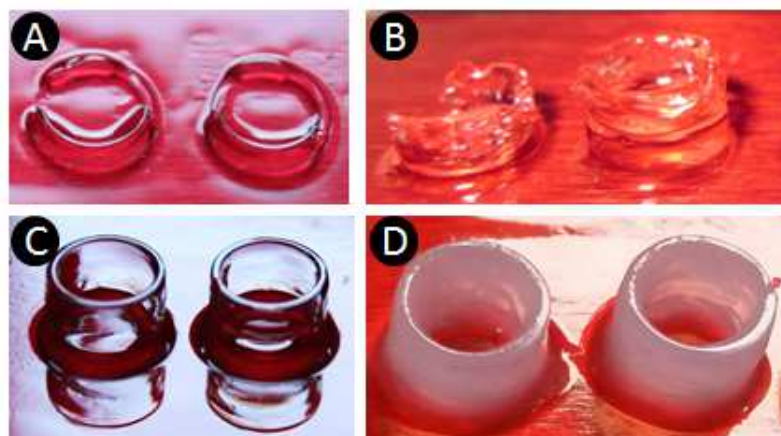


Figure 5.23: Photographs of printed hydrogel structures from PEG-DA₇₅ (A-C) and PEG-DA₇₅Lys_{1.55} (D). Underexposure led to insufficient adherence of the hydrogel at the build platform (A). Unbalanced ink application and air bubbles resulted in partially defective structures (B). Flawless hollow hydrogel cylinders as they have been used in the presented study (C). PrintLoading cylinders with noticeable turbidity due to incorporated protein (D).

to the already consisting layer. In the later printing process, air bubbles or the lack of applied ink could disrupt the resulting hydrogel structure as shown in Fig. 5.23B. It is in the nature of this printing technique, that unintended absence of polymerizable material during the printing process inevitably causes malformations in the resulting structure. Nonetheless, commensurate ink application in combination with the adapted printing parameters (c.f. Table 5.4) resulted in a high repeatability in the production of flawless hydrogel cylinders for the further use in this study (see Fig. 5.23C). An increasing amount of PEG-DA in the bioink resulted in shorter exposure times needed for good printing outcomes. This need for lower energy input at the given layer height can be explained by the concentration dependent amount of possible crosslinking sites [255]. To generate flawless hydrogel structures from bioinks containing 75 % PEG-DA and additional acrylic acid an increase in the exposure time was required compared to bioinks without acrylic acid. The reaction rate of this copolymerization seems to be slowed down with increasing percentage of acrylic acid. Different reactivities of PEG-DA and acrylic acid can be used as an explanation for this shift. The applied exposure times could be reduced for the bioink PEG-DA₇₅Lys_{1.55}. This was influenced by the noticeable turbidity (see Fig. 5.23D), which was already visible before the polymerization and probably occurred due to precipitated lysozyme in this ink. The turbidity increased the absorbance of luminous energy which resulted in a faster polymerization process.

Protein uptake during post-fabrication equilibrium partitioning

Post-fabrication equilibrium partitioning (PostFabLoading) of lysozyme to PEG-DA based hydrogels was studied using the bioinks PEG-DA₅₀, PEG-DA₇₅, PEG-DA₉₀, PEG-DA₇₅AA_{7.5} and PEG-DA₇₅AA₁₅. The protein uptake was determined by measuring the

lysozyme concentration in the supernatant of incubated hydrogel cylinders at regular time intervals by analytical SEC. The amount of loaded protein was calculated by the difference between the amount of protein in the protein stock solution and in the supernatant. The relative protein uptake was defined by Eq. 5.4, where m_{loaded} and m_{stock} are the mass of the loaded protein and the mass of the total protein in the stock solution, respectively.

$$Relative\ protein\ uptake = \frac{m_{loaded}}{m_{stock}} \cdot 100\% \quad (5.4)$$

In Fig. 5.24, the relative protein uptake is displayed for different bioink compositions and loading conditions. The error bars indicate the standard deviation of a triple determination from the supernatant of three independent hydrogel cylinders. In Fig. 5.24A, the influence of PEG-DA mass fraction in the bioink on the relative protein uptake at pH 7 is shown. Over a time of 12 hours, the hydrogels with an initial PEG-DA mass fraction of 50 % exhibit the highest uptake of up to 40 % of the initial applied protein mass. The course of the protein uptake curve for the hydrogels with 75 % and 90 % PEG-DA are very similar and achieve a maximum of approximately 20 % in the studied 12 h. These observations are consistent with the work of Zhang and coworkers [256] who describe that a higher PEG-DA concentration leads to a more compact hydrogel structure with higher crosslinking density. A higher crosslinking density restricts the swelling of the hydrogel and results in a reduced meshsize which in turn hinders protein diffusion into and out of the hydrogel. For all three curves, the increase in protein uptake is highest during the first 6 h and almost reaches a plateau value after 10 h. The plateau value reflects the maximal protein absorption capacity of the hydrogel, which is denoted as protein uptake at saturation [257]. Zaho et al. [257] have observed similar results for the uptake of lysozyme by glycerol diglycidylether crosslinked oxidized starch microgels. They found a absorption time of 4 h to be sufficient for the microgel to reach saturation during protein absorption.

In Fig. 5.24B it is demonstrated, how the relative protein uptake of PEG-DA based hydrogels can be increased by addition of the co-monomer acrylic acid. Firstly, it can be seen that the protein uptake rises more steeply in the first 4 h than without acrylic acid. This indicates that lysozyme absorbs with higher affinity to hydrogels containing acrylic acid. This observation can be explained by the introduction of an ionic character to the hydrogel by the addition of acrylic acid [107]. At pH 7, acrylic acid is negatively charged due to its pKa of 4.25 [258] while the net charge of lysozyme is positive (pI=11.3 [259]). Therefore, electrostatic interactions occur between protein and ionized acrylic acid. Secondly, the protein uptake at saturation increases approximately linearly with increasing mass fraction of acrylic acid. This linear increase can be explained by the introduction of exactly one negative charge per molecule acrylic acid into the hydrogel. Doubling the acrylic acid content therefore leads to a doubling of the binding sites for the protein. An unlimited increase in the acrylic acid content is, however, not possible, because the molecule has only one free double bond and thus weakens the network structure of the hydrogel.

In Fig. 5.24C, the effect of the solution pH on the protein uptake is shown for the bioink PEG-DA₇₅AA₁₅ containing 75 % PEG-DA and 15 % acrylic acid. When comparing the

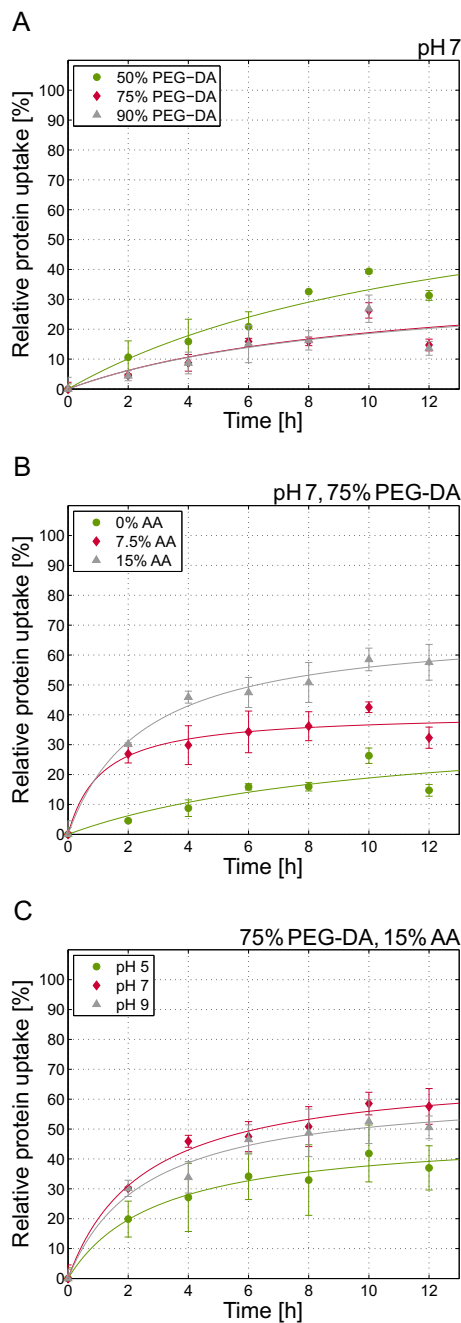


Figure 5.24: PostFabLoading of PEG-DA based hydrogels with lysozyme: Relative protein uptake of hydrogels with varying mass fraction of PEG-DA at pH 7 (A), with 75 % PEG-DA and varying mass fraction of the co-monomer acrylic acid at pH 7 (B) and different loading pH values for 75 % PEG-DA and 15 % acrylic acid (C)

three pH values, the lowest protein uptake is achieved at pH 5. The curves of pH 7 and pH 9 are identical within the error bars. Since pH 7 and pH 9 are more than two pH-steps

higher than the pKa-value of acrylic acid, a complete deprotonation of all acid groups can be assumed for both pH values. According to the calculation of the protein charge with H^+ [260], the net charge of lysozyme is +8 at pH 7 and pH 9. These assumptions apply to the identical protein uptake curves at pH 7 and pH 9. In contrast, pH 5 is very close to the pKa-value of the acrylic acid. Since the pKa-value indicates the pH-value at which 50 % of the acid groups are deprotonated, it is possible that not all acid groups are deprotonated at pH 5. This would result in a reduced number of negative charges available to the protein for the interactions, and thus can explain the lower protein uptake.

Protein release from loaded hydrogels

To study the release profiles for the protein-loaded hydrogels, the hollow cylinders were incubated in different release buffers for 150 min. During this period, samples were regularly taken and the contained protein was quantified by means of absorption measurements. The resulting release profiles are displayed in Fig. 5.25 for 0 M and 0.15 M NaCl in the release buffer.

In all experiments, PBS behaves as the multicomponent buffer at pH 7 containing 0.15 M sodium chloride. In Fig. 5.25A-D, the lysozyme release profiles for hydrogel cylinders consisting of 75 % PEG-DA and 0 % AA (in the bioink) are displayed. These hydrogels are uncharged since they are formed exclusively by crosslinking uncharged PEG-DA chains. For the two loading methods PostFabLoading (Fig. 5.25A and B) and PrintLoading (Fig. 5.25C and D), neither the pH of the surrounding solution nor the salt concentration has any influence on the release profile. The transport of the protein therefore appears to be driven exclusively by diffusive processes. When comparing PostFabLoading and PrintLoading for a given solution condition, it is noticeable that the maximum protein released is higher for PrintLoaded hydrogels. This difference can not be attributed to different concentration gradients since hydrogel cylinders of both loading methods contain the same amount of protein after the loading process. The most probable cause for the difference in the maximum protein release between PostFabLoaded and PrintLoaded hydrogels is an unequal swelling state at the beginning of the release experiments. Hydrogel water content will affect the release profile because water in the matrix is the medium through which proteins will diffuse [107]. The PostFabLoaded hydrogels are already completely swollen due to their storage, equilibrium and protein loading and have thus reached their equilibrium water content (EWC) [107]. In contrast, the PrintLoaded hydrogels were only washed for 10 s in ultra-pure water immediately after printing to reduce uncontrolled protein release during the washing process. The addition of buffer during the release experiments induced the swelling process and thus led to an increasing mesh size during the release process. An increased gel mesh size allows more protein to diffuse out of the hydrogel [256]. The generally low release rates indicate the existence of intermolecular interactions such as hydrogen bonds or Van-der-Waals forces which appear to be stronger between lysozyme and PEG-DA than between lysozyme and the surrounding solution. In case of PrintLoaded hydrogels, covalent binding of the protein to the gel is also possible by free radical addition or Michael addition between lysine residues and acrylate groups of the polymer [107, 261]. Since being present during the printing process, the

5.5 Assessment of hydrogels using a combination of 3D printing and high-throughput screening

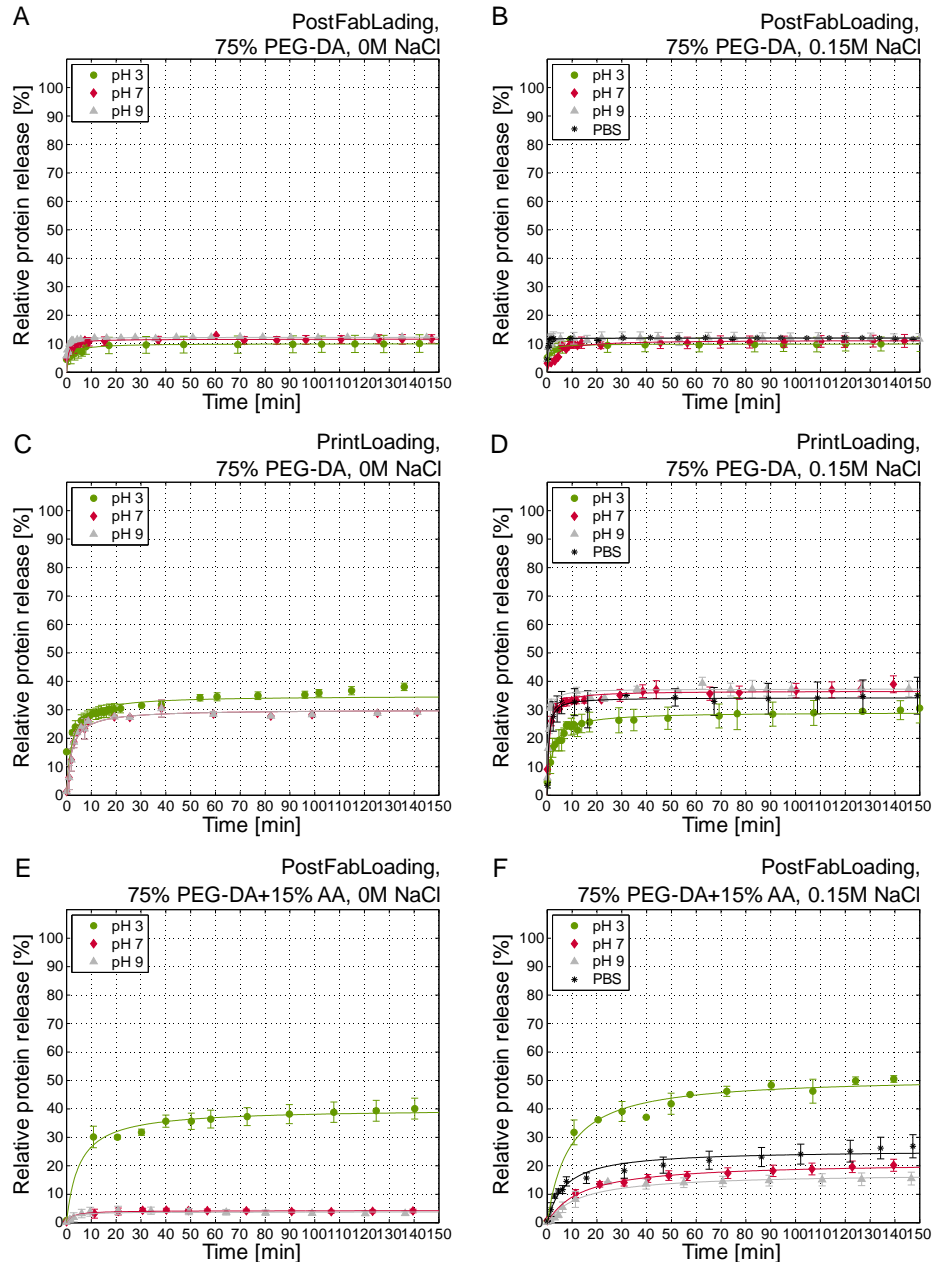


Figure 5.25: Relative protein release under the influence of 0 M NaCl in the release buffer (PostFabLoaded hydrogels from 75 % PEG-DA (A), PrintLoaded hydrogels from 75 % PEG-DA (C) and PostFabLoaded hydrogels from 75 % PEG-DA and 15 % AA (E)) and under the influence of 0.15 M NaCl in the release buffer (PostFabLoaded hydrogels from 75 % PEG-DA (B), PrintLoaded hydrogels from 75 % PEG-DA (D) and PostFabLoaded hydrogels from 75 % PEG-DA and 15 % AA (F))

protein may additionally be enclosed inaccessibly in closed or too narrow pores. In Fig. 5.25E and F, lysozyme release profiles from hydrogels containing 75 % PEG-DA

and 15 % AA are shown. Comparing Fig. 5.25E and F with Fig. 5.25A and B, it can be seen that the release of lysozyme from acrylic acid containing hydrogels is slower than from acrylic acid-free hydrogels. These observations suggest an affinity based mechanism of release, as is was already discussed for the protein uptake experiments. For 0 M sodium chloride in the release buffer (Fig. 5.25E), a clear dependency of the protein release on the pH value of the surrounding solution can be seen. At pH 3, the maximum protein release is 10 fold greater than at pH 7 and pH 9. Since pH 3 is below the pKa of acrylic acid, the acid groups in the hydrogel are protonated and thus uncharged. Due to the pH change of pH 7 during the loading to pH 3 during release, the protein which was absorbed via electrostatic attraction is released. These results are in accordance with the work of Zhang and coworkers [256], who have described a fast initial burst release of proteins at pH 2.0 due to a squeezing mechanism. Since there are no electrostatic attractions between hydrogel and lysozyme at pH 3, the addition of salt ions (compare Fig. 5.25F) also has no significant effect on the release. At pH 7 and pH 9, the acid groups of acrylic acid, however, are deprotonated and thus negatively charged. Since lysozyme has a net charge of +8 (calculated with H ++ [260]) at both pH 7 and pH 9, the protein is equally retained in the hydrogel by means of electrostatic interactions. When salt is added (compare Fig. 5.25F), the salt ions compete with the proteins for the charges of the hydrogel and displace the proteins. This effect has been discussed by various authors including Brooks and Cramer [262] in the context of ion exchange chromatography.

Activity examination of the released lysozyme

Following the release studies, the gained samples were examined regarding their residual enzyme activity compared to native lysozyme. In Fig. 5.26, the determined relative activity of all samples is shown. The way of carrying out the assay could have led to partially pronounced standard deviations. Therefore, we defined a relative activity of 100 % \pm 10 % as unimpaired preservation of activity. It can be seen, that the buffer conditions of the release procedure also had an influence on the activity of the released lysozyme in the diluted assay conditions. For the lysozyme released from PostFabLoading PEG-DA₇₅ a slightly positive effect can be seen for the presence of NaCl in the release buffer but no reliable statement can be made due to the standard deviations. The positive influence of the salt could definitely be observed for the release at pH 3 PrintLoading and even more clearly at pH 7 and pH 9 PostFabLoading PEG-DA₇₅AA₁₅. The salt significantly alleviated the negative impact on the activity initiated by the loading into acrylic acid containing hydrogels and the subsequent release with buffers at pH 7 and pH 9. The lysozyme released in PBS showed a slightly smaller activity than the comparable multicomponent buffer at pH 7 with 0.15 M NaCl. Comparing the two executed approaches PostFabLoading and PrintLoading at given pH, a negative impact of the PrintLoading procedure could be determined. This impact was strongly evident for the released lysozyme at pH 9.

In order to further investigate the reduced activity, released protein samples from Post-FabLoaded and PrintLoaded hydrogels without acrylic acid at pH 9 and 0 M NaCl were analyzed using analytical SEC. The results are displayed in Fig. 5.27. The protein sample from PostFabLoading resulted in a single peak which could be attributed to a reference

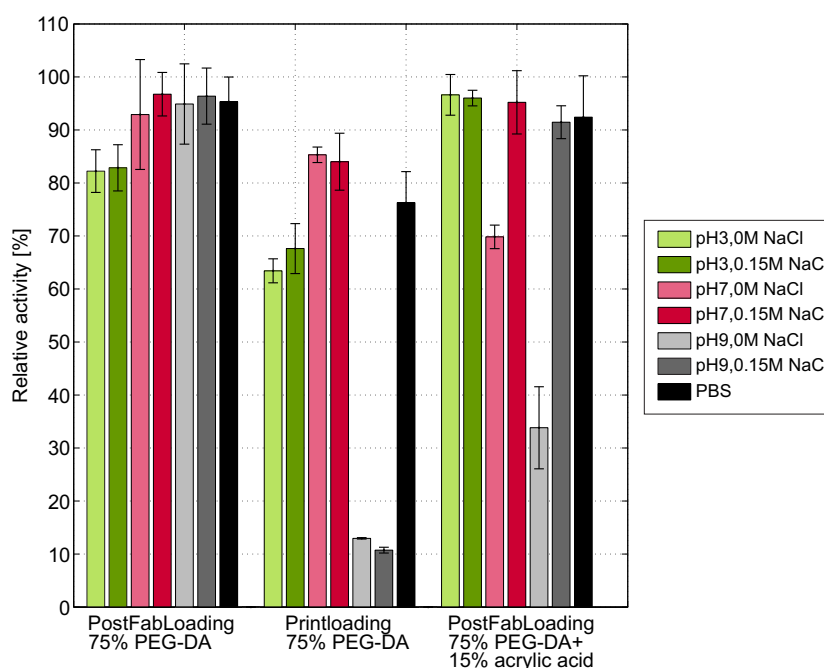


Figure 5.26: Comparison of the relative activities of released lysozyme relating to the loading method and ink composition.

sample of native lysozyme. The protein sample from PrintLoading, however, contained larger and smaller protein species, which eluted earlier and later than native lysozyme, respectively. The loss in activity during the PrintLoading process may therefore be attributed to the formation of precipitate and fragments of lysozyme due to the bioink composition and effects triggered by irradiation. The turbidity of the applied bioink and resulting hydrogels could serve as a first indication of protein aggregation during the printing process.

Conclusion

Protein uptake and release of hydrogels depends on the right combination of hydrogel materials, protein and surrounding solution conditions. This study has demonstrated that mechanisms and effects of protein adsorption and release by hydrogels already described in the literature could be reproduced reliably by the presented combination of 3D printing and high-throughput screening. Thus, a helpful tool was developed for the rapid and cost-effective optimization of new hydrogel materials with regard to the physical, biological and material transport requirements at the site of action. The development of oral delivery products and implanted reservoir systems for biopharmaceutical proteins may profit from the here presented approach. In order to further qualify this approach for high-throughput studies, we are in the process of automating the printing procedure.

Furthermore, the results demonstrated that the direct incorporation of proteins into the

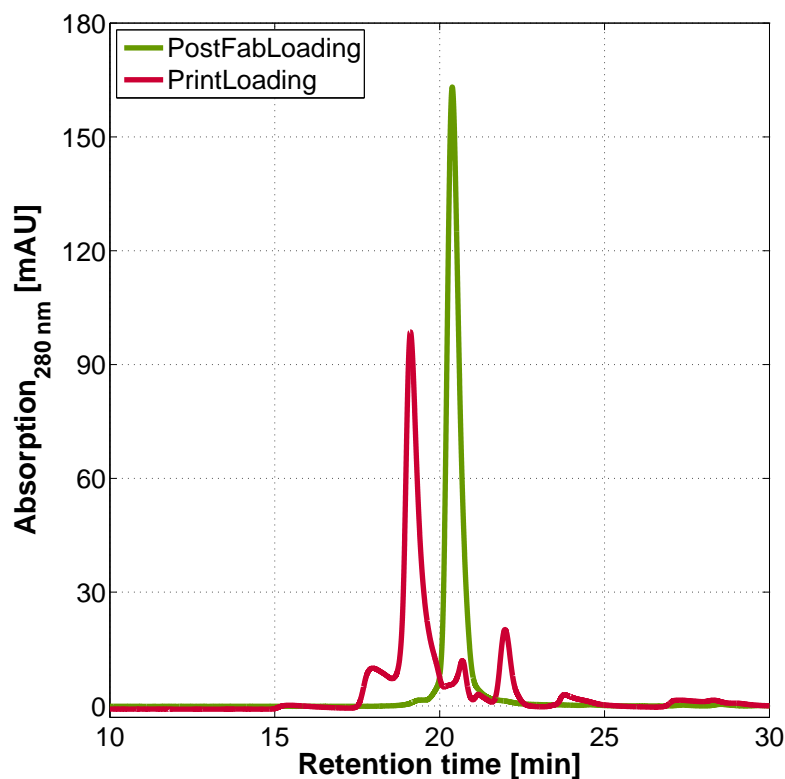


Figure 5.27: Analytical SEC comparing released lysozyme form PostFabLoading and Print-Loading for PEG-DA based hydrogels without acrylic acid at pH 9 and 0 M NaCl

bioinks may lead to the formation of inactive species during the printing process. The development of suitable stabilization strategies for hydrogel based biopharmaceutical products are therefore of the utmost interest to meet this challenge.

Acknowledgments

We gratefully acknowledge the financial support by the German Federal Ministry of Education and Research (BMBF). This research work is part of the project 'Molecular Interaction Engineering: From Nature's Toolbox to Hybrid Technical Systems', funding code 031A095B. The authors further acknowledge Rebecca L. Hoffman, Dominik S. G. Hiltmann and Nicolai Bluthardt for their support in the laboratory.

References

24. Hertzberg, R. P. and Pope, A. J. 'High-throughput screening: new technology for the 21st century'. *Current Opinion in Chemical Biology*, vol. 4(4) (2000), pp. 445–451 (cit. on pp. 2, 18, 97).
35. Kittelmann, J., Ottens, M., and Hubbuch, J. 'Robust high-throughput batch screening method in 384-well format with optical in-line resin quantification'. *Journal of Chromatography B*, vol. 988 (2015), pp. 98–105 (cit. on pp. 3, 97).
36. Bensch, M., Schulze Wierling, P., Lieres, E. von, and Hubbuch, J. 'High Throughput Screening of Chromatographic Phases for Rapid Process Development'. *Chemical Engineering & Technology*, vol. 28(11) (2005), pp. 1274–1284 (cit. on pp. 3, 18, 97).
79. Waldbaur, A., Kittelmann, J., Radtke, C. P., Hubbuch, J., and Rapp, B. E. 'Microfluidics on liquid handling stations (μ F-on-LHS): an industry compatible chip interface between microfluidics and automated liquid handling stations'. *Lab on a Chip*, vol. 13(12) (2013), pp. 2337–2343 (cit. on pp. 5, 20, 37, 38, 59, 60, 68, 78).
107. Mellott, M. B., Searcy, K., and Pishko, M. V. 'Release of protein from highly cross-linked hydrogels of poly (ethylene glycol) diacrylate fabricated by UV polymerization'. *Biomaterials*, vol. 22(9) (2001), pp. 929–941 (cit. on pp. 10, 36, 78, 96, 101, 103, 105).
231. Kröner, F. and Hubbuch, J. 'Systematic generation of buffer systems for pH gradient ion exchange chromatography and their application'. *J. Chromatogr. A*, vol. 1285 (Apr. 2013), pp. 78–87 (cit. on pp. 82, 98).
237. Sharpe, L. A., Daily, A. M., Horava, S. D., and Peppas, N. A. 'Therapeutic applications of hydrogels in oral drug delivery'. *Expert opinion on drug delivery*, vol. 11(6) (2014), pp. 901–915 (cit. on p. 96).
238. Liechty, W. B., Kryscio, D. R., Slaughter, B. V., and Peppas, N. A. 'Polymers for drug delivery systems'. *Annual review of chemical and biomolecular engineering*, vol. 1 (2010), pp. 149–173 (cit. on p. 96).
239. Langer, R. and Tirrell, D. A. 'Designing materials for biology and medicine'. *Nature*, vol. 428(6982) (2004), pp. 487–492 (cit. on p. 96).
240. Peppas, N. A., Bures, P., Leobandung, W. S., and Ichikawa, H. 'Hydrogels in pharmaceutical formulations'. *European journal of pharmaceuticals and biopharmaceutics*, vol. 50(1) (2000), pp. 27–46 (cit. on pp. 96, 97).
241. Ferreira, L., Vidal, M. M., and Gil, M. H. 'Evaluation of poly (2-hydroxyethyl methacrylate) gels as drug delivery systems at different pH values'. *International journal of pharmaceuticals*, vol. 194(2) (2000), pp. 169–180 (cit. on p. 96).
242. Hari, P. R., Chandy, T., and Sharma, C. P. 'Chitosan/calcium–alginate beads for oral delivery of insulin'. *Journal of Applied Polymer Science*, vol. 59(11) (1996), pp. 1795–1801 (cit. on p. 96).

243. Chaturvedi, K., Ganguly, K., Nadagouda, M. N., and Aminabhavi, T. M. 'Polymeric hydrogels for oral insulin delivery'. *Journal of controlled release*, vol. 165(2) (2013), pp. 129–138 (cit. on p. 96).
244. Zou, X., Zhao, X., and Ye, L. 'Synthesis of cationic chitosan hydrogel with long chain alkyl and its controlled glucose-responsive drug delivery behavior'. *RSC Advances*, vol. 5(116) (2015), pp. 96230–96241 (cit. on p. 96).
245. Hoare, T. R. and Kohane, D. S. 'Hydrogels in drug delivery: progress and challenges'. *Polymer*, vol. 49(8) (2008), pp. 1993–2007 (cit. on p. 96).
246. Hoffman, A. S. 'Hydrogels for biomedical applications'. *Advanced drug delivery reviews*, vol. 64 (2012), pp. 18–23 (cit. on p. 96).
247. Brandl, F., Hammer, N., Blunk, T., Tessmar, J., and Goepferich, A. 'Biodegradable hydrogels for time-controlled release of tethered peptides or proteins'. *Biomacromolecules*, vol. 11(2) (2010), pp. 496–504 (cit. on p. 97).
248. Oliveira, M. B. and Mano, J. F. 'High-throughput screening for integrative biomaterials design: exploring advances and new trends'. *Trends in biotechnology*, vol. 32(12) (2014), pp. 627–636 (cit. on p. 97).
249. Capelle, M. A. H., Gurny, R., and Arvinte, T. 'High throughput screening of protein formulation stability: practical considerations'. *European journal of pharmaceuticals and biopharmaceutics*, vol. 65(2) (2007), pp. 131–148 (cit. on p. 97).
250. Wang, J., Goyanes, A., Gaisford, S., and Basit, A. W. 'Stereolithographic (SLA) 3D printing of oral modified-release dosage forms'. *International journal of pharmaceuticals*, vol. 503(1) (2016), pp. 207–212 (cit. on p. 97).
251. Lin, C.-C. and Anseth, K. S. 'PEG hydrogels for the controlled release of biomolecules in regenerative medicine'. *Pharmaceutical research*, vol. 26(3) (2009), pp. 631–643 (cit. on pp. 97, 101).
252. Galm, L., Morgenstern, J., and Hubbuch, J. 'Manipulation of lysozyme phase behavior by additives as function of conformational stability'. *International journal of pharmaceuticals*, vol. 494(1) (2015), pp. 370–380 (cit. on p. 100).
253. Morgenstern, J., Baumann, P., Brunner, C., and Hubbuch, J. 'Effect of PEG molecular weight and PEGylation degree on the physical stability of PEGylated lysozyme'. *International journal of pharmaceuticals*, vol. 519(1) (2017), pp. 408–417 (cit. on p. 101).
254. Sirkar, K. and Pishko, M. V. 'Amperometric biosensors based on oxidoreductases immobilized in photopolymerized poly (ethylene glycol) redox polymer hydrogels'. *Analytical Chemistry*, vol. 70(14) (1998), pp. 2888–2894 (cit. on p. 101).
255. Arcaute, K., Mann, B. K., and Wicker, R. B. 'Practical use of hydrogels in stereolithography for tissue engineering applications'. *Stereolithography*. Springer, 2011, pp. 299–331 (cit. on p. 102).

256. Zhang, L., Ma, Y., Zhao, C., Zhu, X., Chen, R., and Yang, W. ‘Synthesis of pH-responsive hydrogel thin films grafted on PCL substrates for protein delivery’. *Journal of Materials Chemistry B*, vol. 3(39) (2015), pp. 7673–7681 (cit. on pp. 103, 105, 107).
257. Zhao, L., Chen, Y., Li, W., Lu, M., Wang, S., Chen, X., Shi, M., Wu, J., Yuan, Q., and Li, Y. ‘Controlled uptake and release of lysozyme from glycerol diglycidyl ether cross-linked oxidized starch microgel’. *Carbohydrate polymers*, vol. 121 (2015), pp. 276–283 (cit. on p. 103).
258. Morris, G. E., Vincent, B., and Snowden, M. J. ‘Adsorption of Lead Ions onto N-Isopropylacrylamide and Acrylic Acid Copolymer Microgels’. *Journal of colloid and interface science*, vol. 190(1) (1997), pp. 198–205 (cit. on p. 103).
259. Maiser, B., Kröner, F., Dismar, F., Brenner-Weiß, G., and Hubbuch, J. ‘Isoform separation and binding site determination of mono-PEGylated lysozyme with pH gradient chromatography’. *Journal of Chromatography A*, vol. 1268 (2012), pp. 102–108 (cit. on p. 103).
260. VirginiaTech. *H++*. Date Accessed 06 July 2017. URL: <http://biophysics.cs.vt.edu/index.php> (cit. on pp. 105, 107).
261. Hammer, N., Brandl, F. P., Kirchhof, S., Messmann, V., and Goepferich, A. M. ‘Protein Compatibility of Selected Cross-linking Reactions for Hydrogels’. *Macromolecular bioscience*, vol. 15(3) (2015), pp. 405–413 (cit. on p. 105).
262. Brooks, C. A. and Cramer, S. M. ‘Steric mass-action ion exchange: displacement profiles and induced salt gradients’. *AIChE Journal*, vol. 38(12) (1992), pp. 1969–1978 (cit. on p. 107).

CHAPTER 6

Conclusion & Outlook

The focus of this thesis was the implementation of novel tools in the high-throughput process development. This was achieved by the adaptation of techniques from the fields of microfluidics and bioprinting to meet the requirements of automated experimental workflow.

The μ F-on-LHS system was successfully applied in studies from different research areas. For the absorption-based protein analysis, a microfluidic device was developed and established. This device allows the quantitative determination of protein concentrations in a wide concentration range. The dimensions of the device allow its implementation in experimental procedures on liquid-handling stations (LHS) including automated filling and handling. Additionally, the material used for the manufacturing of the chips enabled a read-out with the integrated spectrophotometer in the UV/Vis spectrum. Up to 96 samples on a microfluidic device can be measured with proven accuracy and repeatability. The applicability of this tool was shown on the basis of the sample measurement of a microscale chromatographic separation procedure. This tool especially is a significant improvement for the measurement of highly concentrated protein solutions which have nowadays to be analyzed as standard in biopharmaceutical processes.

Further, the beneficial use of microfluidic channels in combination with automated process management for the investigation of complex interdependencies could be demonstrated. The impact of various cause variables on the monomer conversion of photoinitiated miniemulsion polymerization has been studied. The low volume needed for a single experiment allowed the increase of information gained from one batch of miniemulsion. The screening concept was supported by a design of experiments approach for the systematical investigation of the different influencing factors. This strategy was shown to be a promising tool for the characterization and optimization of photopolymerization processes. This is of great interest for the introduction of biological material and their interactions with the produced nanoparticles and possible toxic reaction residues.

In addition, the ability of the μ F-on-LHS system to perform highly sensitive microbiological experiments was shown. In this context, the automation of the complex fluorescence *in situ* hybridization protocol was demonstrated by its implementation in a LHS procedure. The developed concept allowed the handling of up to 9 cultivation flowcells in an interlaced process for the reliable experimentation without further manual work. Besides the automated execution of all protocol steps also the semi-quantitative read-out of the fluorescence signal was accomplished. The developed platform enabled the successful hybridization of biofilms which could be verified through microplate reader analysis and epifluorescence microscopy.

Apart from the implementation of the FISH protocol, the feasibility of a CARD-FISH procedure was successfully shown. Therefore, the automation of this methods contributes to the simplification of the analysis of microbial communities in complex biofilms.

In the field of bioprinting, two different printing techniques have been investigated for the build-up of hydrogel structures. The adaptation of these structures to the size of the wells of a multiwell plate allowed their integration in automated screening procedures. The structure and the incorporated biological material was investigated on interactions with liquid surroundings of various compositions. The first approach was the conversion of a conventional fused filament fabrication 3D-printer to an entry-level bioprinter capable of extruding paste-like bioinks. In combination with a simple user interface for the generation of printing command sets, an easy access to bioprinting could be presented. In a case study, a printing method from tissue engineering research was adapted for the encapsulation of enzymes. The preserved activity of the enzymes was subsequently tested by an automated assay execution. The resulting substrate conversion rates have been in good accordance to Michaelis-Menten enzyme kinetics.

Furthermore, a stereolithographic printing device was adjusted for the production of multiwell plate compatible hydrogel structures. This approach was applied for the investigation of the behavior of hydrogels with respect to the uptake and release of lysozyme. The influence of the variation of hydrogel and liquid surrounding composition could be determined in a high-throughput screening. With this method, a novel strategy for the investigation of hydrogel materials for their application in drug delivery systems was demonstrated.

The developed approaches have demonstrated excellent applicability concerning applications in preparatory procedures and actual bioprinting strategies. The presented applications for the combination of microfluidics and liquid-handling stations are well suited for the further integration in process development and workflows. Preliminary studies have been deployed for the execution of self-interaction chromatography and flow-through aqueous two phase systems to investigate protein interactions. The bioprinting approaches demonstrate an auspicious strategy for the implementation of hydrogel 3D-printing in automated screening procedures. Investigations on the interaction of proteins and hydrogels in various liquid surroundings could be performed. The open source pedigree of both applied printers provides an good starting point for further add-on components and research tasks.

In summary, the adapted workflows highly benefit from the practicable miniaturization and automation. Thus, the application spectrum of LHS-based experiments has been extended by additional tools and possibilities.

Bibliography

1. Nissani, M. 'Ten cheers for interdisciplinarity: The case for interdisciplinary knowledge and research'. *The social science journal*, vol. 34(2) (1997), pp. 201–216 (cit. on p. 1).
2. Repko, A. F. *Interdisciplinary research: Process and theory*. Sage, 2008 (cit. on p. 1).
3. Bothast, R. and Schlicher, M. 'Biotechnological processes for conversion of corn into ethanol'. *Applied microbiology and biotechnology*, vol. 67(1) (2005), pp. 19–25 (cit. on p. 1).
4. Woodward, J., Orr, M., Cordray, K., and Greenbaum, E. 'Biotechnology: enzymatic production of biohydrogen'. *Nature*, vol. 405(6790) (2000), p. 1014 (cit. on p. 1).
5. Gupta, R., Gigras, P., Mohapatra, H., Goswami, V. K., and Chauhan, B. 'Microbial α -amylases: a biotechnological perspective'. *Process biochemistry*, vol. 38(11) (2003), pp. 1599–1616 (cit. on p. 1).
6. Roque, A. C. A., Lowe, C. R., and Taipa, M. Â. 'Antibodies and genetically engineered related molecules: production and purification'. *Biotechnology progress*, vol. 20(3) (2004), pp. 639–654 (cit. on p. 1).
7. Hollenberg, C. P. and Gellissen, G. 'Production of recombinant proteins by methylotrophic yeasts'. *Current opinion in biotechnology*, vol. 8(5) (1997), pp. 554–560 (cit. on p. 1).
8. Wittmann, C. *Industrial Biotechnology: Products and Processes*. Vol. 4. John Wiley & Sons, 2017 (cit. on p. 1).
9. Mayr, L. M. and Bojanic, D. 'Novel trends in high-throughput screening'. *Current opinion in pharmacology*, vol. 9(5) (2009), pp. 580–588 (cit. on p. 1).
10. Gibson, I., Rosen, D., and Stucker, B. *Additive manufacturing technologies: Rapid prototyping to direct digital manufacturing*. cited By 987. 2010, pp. 1–459 (cit. on p. 1).
11. Pearce, J. M. *Open-source lab: How to build your own hardware and reduce research costs*. Newnes, 2013 (cit. on p. 1).
12. Baden, T., Chagas, A. M., Gage, G., Marzullo, T., Prieto-Godino, L. L., and Euler, T. 'Open Labware: 3-D Printing Your Own Lab Equipment'. *PLOS Biol.* Vol. 13(3) (Mar. 2015), e1002086 (cit. on pp. 2, 78).

13. Bishop, G. W., Satterwhite-Warden, J. E., Kadimisetty, K., and Rusling, J. F. '3D-printed bioanalytical devices'. *Nanotechnology*, vol. 27(28) (2016), p. 284002 (cit. on pp. 2, 4).
14. Chua, C. K. and Yeong, W. Y. *Bioprinting: principles and applications*. Vol. 1. World Scientific Publishing Co Inc, 2014 (cit. on p. 2).
15. Lode, A., Krujatz, F., Brüggemeier, S., Quade, M., Schütz, K., Knaack, S., Weber, J., Bley, T., and Gelinsky, M. 'Green bioprinting: Fabrication of photosynthetic algae-laden hydrogel scaffolds for biotechnological and medical applications'. *Engineering in Life Sciences*, vol. 15(2) (2015), pp. 177–183 (cit. on pp. 2, 78).
16. Rodriguez-Dévora, J. I., Zhang, B., Reyna, D., Shi, Z.-d., and Xu, T. 'High throughput miniature drug-screening platform using bioprinting technology'. *Biofabrication*, vol. 4(3) (2012), p. 035001 (cit. on pp. 2, 78).
17. Hungarian Center for Epidemiology. *Medical doctor, microbiologist, inventor*. Date Accessed 06 Sept 2017. URL: www.oek.hu/oek.web?nid=499&pid=1 (cit. on p. 2).
18. Manns, R. *History of Microplates*. Date Accessed 06 Sept 2017. URL: http://plastiquarian.com/?page_id=14361 (cit. on p. 2).
19. Hardy, A. and Feldman, J. *ANSI Approves Microplate Standards Drafted by SBS Committee: New Universal Standards Expected to Accelerate and Streamline Industry*. Date Accessed 06 Sept 2017. URL: <http://www.businesswire.com/news/home/20040115005770/en/ANSI-Approves-Microplate-Standards-Drafted-SBS-Committee> (cit. on p. 2).
20. Kong, F., Yuan, L., Zheng, Y. F., and Chen, W. 'Automatic liquid handling for life science: a critical review of the current state of the art'. *Journal of laboratory automation*, vol. 17(3) (2012), pp. 169–185 (cit. on pp. 2, 3).
21. Lander, E. S., Linton, L. M., Birren, B., Nusbaum, C., Zody, M. C., Baldwin, J., Devon, K., Dewar, K., Doyle, M., FitzHugh, W., et al. 'Initial sequencing and analysis of the human genome'. Vol. (2001) (cit. on p. 2).
22. Meldrum, D. 'Automation for genomics, part one: preparation for sequencing'. *Genome Research*, vol. 10(8) (2000), pp. 1081–1092 (cit. on p. 2).
23. Bhambure, R., Kumar, K., and Rathore, A. S. 'High-throughput process development for biopharmaceutical drug substances'. *Trends in Biotechnology*, vol. 29(3) (2011), pp. 127–135 (cit. on pp. 2, 3, 18).
24. Hertzberg, R. P. and Pope, A. J. 'High-throughput screening: new technology for the 21st century'. *Current Opinion in Chemical Biology*, vol. 4(4) (2000), pp. 445–451 (cit. on pp. 2, 18, 97).
25. Lye, G. J., Ayazi-Shamlou, P., Baganz, F., Dalby, P. A., and Woodley, J. M. 'Accelerated design of bioconversion processes using automated microscale processing techniques'. *Trends in biotechnology*, vol. 21(1) (2003), pp. 29–37 (cit. on p. 3).

26. Meldrum, D. 'Automation for genomics, part two: sequencers, microarrays, and future trends'. *Genome Research*, vol. 10(9) (2000), pp. 1288–1303 (cit. on p. 3).
27. Baumann, P. and Hubbuch, J. 'Downstream process development strategies for effective bioprocesses: Trends, progress, and combinatorial approaches'. *Engineering in Life Sciences*, vol. (2016) (cit. on p. 3).
28. Huber, R., Ritter, D., Hering, T., Hillmer, A.-K., Kensy, F., Müller, C., Wang, L., and Büchs, J. 'Robo-Lector—a novel platform for automated high-throughput cultivations in microtiter plates with high information content'. *Microbial cell factories*, vol. 8(1) (2009), p. 42 (cit. on p. 3).
29. Stevens, R. C. 'High-throughput protein crystallization'. *Current opinion in structural biology*, vol. 10(5) (2000), pp. 558–563 (cit. on p. 3).
30. Nfor, B. K., Hylkema, N. N., Wiedhaup, K. R., Verhaert, P. D., Van der Wielen, L. A., and Ottens, M. 'High-throughput protein precipitation and hydrophobic interaction chromatography: salt effects and thermodynamic interrelation'. *Journal of Chromatography A*, vol. 1218(49) (2011), pp. 8958–8973 (cit. on p. 3).
31. Vincentelli, R., Canaan, S., Campanacci, V., Valencia, C., Maurin, D., Frassinetti, F., Scappucini-Calvo, L., Bourne, Y., Cambillau, C., and Bignon, C. 'High-throughput automated refolding screening of inclusion bodies'. *Protein Science*, vol. 13(10) (2004), pp. 2782–2792 (cit. on p. 3).
32. Oelmeier, S. A., Dismer, F., and Hubbuch, J. 'Application of an aqueous two-phase systems high-throughput screening method to evaluate mAb HCP separation'. *Biotechnology and bioengineering*, vol. 108(1) (2011), pp. 69–81 (cit. on p. 3).
33. Effio, C. L., Wenger, L., Ötes, O., Oelmeier, S. A., Kneusel, R., and Hubbuch, J. 'Downstream processing of virus-like particles: Single-stage and multi-stage aqueous two-phase extraction'. *Journal of Chromatography A*, vol. 1383 (2015), pp. 35–46 (cit. on p. 3).
34. Schuldt, S. and Schembecker, G. 'A fully automated ad-and desorption method for resin and solvent screening'. *Chemical Engineering & Technology*, vol. 36(7) (2013), pp. 1157–1164 (cit. on p. 3).
35. Kittelmann, J., Ottens, M., and Hubbuch, J. 'Robust high-throughput batch screening method in 384-well format with optical in-line resin quantification'. *Journal of Chromatography B*, vol. 988 (2015), pp. 98–105 (cit. on pp. 3, 97).
36. Bensch, M., Schulze Wierling, P., Lieres, E. von, and Hubbuch, J. 'High Throughput Screening of Chromatographic Phases for Rapid Process Development'. *Chemical Engineering & Technology*, vol. 28(11) (2005), pp. 1274–1284 (cit. on pp. 3, 18, 97).
37. Wiendahl, M., Schulze Wierling, P., Nielsen, J., Fomsgaard Christensen, D., Krarup, J., Staby, A., and Hubbuch, J. 'High Throughput Screening for the Design and Optimization of Chromatographic Processes - Miniaturization, Automation and

- Parallelization of Breakthrough and Elution Studies'. *Chemical Engineering & Technology*, vol. 31(6) (2008), pp. 893–903 (cit. on pp. 3, 22).
38. Hansen, S. K., Skibsted, E., Staby, A., and Hubbuch, J. 'A label-free methodology for selective protein quantification by means of absorption measurements.' *Biotechnology and bioengineering*, vol. 108(11) (2011), pp. 2661–2669 (cit. on pp. 3, 30).
 39. Whitesides, G. M. 'The origins and the future of microfluidics'. *Nature*, vol. 442(7101) (2006), p. 368 (cit. on p. 4).
 40. Cho, S.-W., Kang, D.-K., Choo, J.-B., Demllo, A. J., and Chang, S.-I. 'Recent advances in microfluidic technologies for biochemistry and molecular biology'. *BMB reports*, vol. 44(11) (2011), pp. 705–712 (cit. on p. 4).
 41. Huang, H. and Densmore, D. 'Integration of microfluidics into the synthetic biology design flow'. *Lab on a Chip*, vol. 14(18) (2014), pp. 3459–3474 (cit. on p. 4).
 42. Tian, W.-C. and Finehout, E. *Microfluidics for biological applications*. Vol. 16. Springer Science & Business Media, 2009 (cit. on p. 4).
 43. Squires, T. M. and Quake, S. R. 'Microfluidics: Fluid physics at the nanoliter scale'. *Reviews of modern physics*, vol. 77(3) (2005), p. 977 (cit. on p. 4).
 44. Stroock, A. D. and Whitesides, G. M. 'Components for integrated poly (dimethylsiloxane) microfluidic systems'. *Electrophoresis*, vol. 23(20) (2002), pp. 3461–3473 (cit. on p. 4).
 45. Hong, C.-C., Choi, J.-W., and Ahn, C. H. 'A novel in-plane passive microfluidic mixer with modified Tesla structures'. *Lab on a Chip*, vol. 4(2) (2004), pp. 109–113 (cit. on p. 4).
 46. Williams, M. S., Longmuir, K. J., and Yager, P. 'A practical guide to the staggered herringbone mixer'. *Lab on a Chip*, vol. 8(7) (2008), pp. 1121–1129 (cit. on p. 4).
 47. Laser, D. J. and Santiago, J. G. 'A review of micropumps'. *Journal of micromechanics and microengineering*, vol. 14(6) (2004), R35 (cit. on p. 4).
 48. Oh, K. W. and Ahn, C. H. 'A review of microvalves'. *Journal of micromechanics and microengineering*, vol. 16(5) (2006), R13 (cit. on p. 4).
 49. Waldbaur, A., Rapp, H., Länge, K., and Rapp, B. E. 'Let there be chip—towards rapid prototyping of microfluidic devices: one-step manufacturing processes'. *Anal. Methods*, vol. 3(12) (2011), pp. 2681–2716 (cit. on pp. 4, 6, 78).
 50. Becker, H. and Gärtner, C. 'Polymer microfabrication methods for microfluidic analytical applications'. *Electrophoresis*, vol. 21(1) (2000), pp. 12–26 (cit. on p. 4).
 51. Jo, B.-H., Van Lerberghe, L. M., Motsegood, K. M., and Beebe, D. J. 'Three-dimensional micro-channel fabrication in polydimethylsiloxane (PDMS) elastomer'. *Journal of microelectromechanical systems*, vol. 9(1) (2000), pp. 76–81 (cit. on p. 4).

52. Carlborg, C. F., Haraldsson, T., Öberg, K., Malkoch, M., and Wijngaart, W. van der. ‘Beyond PDMS: off-stoichiometry thiol–ene (OSTE) based soft lithography for rapid prototyping of microfluidic devices’. *Lab on a Chip*, vol. 11(18) (2011), pp. 3136–3147 (cit. on p. 4).
53. Ren, K., Chen, Y., and Wu, H. ‘New materials for microfluidics in biology’. *Current opinion in biotechnology*, vol. 25 (2014), pp. 78–85 (cit. on p. 4).
54. Roy, E., Pallandre, A., Zribi, B., Horny, M.-C., Delapierre, F. D., Cattoni, A., Gamby, J., and Haghiri-Gosnet, A.-M. ‘Overview of Materials for Microfluidic Applications’. *Advances in Microfluidics-New Applications in Biology, Energy, and Materials Sciences*. InTech, 2016 (cit. on p. 4).
55. Guckenberger, D. J., Groot, T. E. de, Wan, A. M., Beebe, D. J., and Young, E. W. ‘Micromilling: a method for ultra-rapid prototyping of plastic microfluidic devices’. *Lab on a Chip*, vol. 15(11) (2015), pp. 2364–2378 (cit. on p. 4).
56. Bhattacharjee, N., Urrios, A., Kang, S., and Folch, A. ‘The upcoming 3D-printing revolution in microfluidics’. *Lab on a Chip*, vol. 16(10) (2016), pp. 1720–1742 (cit. on p. 4).
57. Yager, P., Edwards, T., Fu, E., Helton, K., Nelson, K., Tam, M. R., and Weigl, B. H. ‘Microfluidic diagnostic technologies for global public health’. *Nature*, vol. 442(7101) (2006), p. 412 (cit. on p. 4).
58. Sackmann, E. K., Fulton, A. L., and Beebe, D. J. ‘The present and future role of microfluidics in biomedical research’. *Nature*, vol. 507(7491) (2014), p. 181 (cit. on pp. 4, 5).
59. Kong, D. S., Carr, P. A., Chen, L., Zhang, S., and Jacobson, J. M. ‘Parallel gene synthesis in a microfluidic device’. *Nucleic acids research*, vol. 35(8) (2007), e61 (cit. on p. 4).
60. Kopp, M. U., De Mello, A. J., and Manz, A. ‘Chemical amplification: continuous-flow PCR on a chip’. *Science*, vol. 280(5366) (1998), pp. 1046–1048 (cit. on p. 4).
61. Noort, D. van, Ong, S. M., Zhang, C., Zhang, S., Arooz, T., and Yu, H. ‘Stem cells in microfluidics’. *Biotechnology progress*, vol. 25(1) (2009), pp. 52–60 (cit. on p. 4).
62. Kim, J., Hegde, M., Kim, S. H., Wood, T. K., and Jayaraman, A. ‘A microfluidic device for high throughput bacterial biofilm studies’. *Lab on a Chip*, vol. 12(6) (2012), pp. 1157–1163 (cit. on pp. 4, 58).
63. Lee, J.-H., Kaplan, J. B., and Lee, W. Y. ‘Microfluidic devices for studying growth and detachment of *Staphylococcus epidermidis* biofilms’. *Biomedical microdevices*, vol. 10(4) (2008), pp. 489–498 (cit. on pp. 4, 58).
64. Teh, S.-Y., Lin, R., Hung, L.-H., and Lee, A. P. ‘Droplet microfluidics’. *Lab on a Chip*, vol. 8(2) (2008), pp. 198–220 (cit. on p. 4).

65. Cygan, Z. T., Cabral, J. T., Beers, K. L., and Amis, E. J. 'Microfluidic platform for the generation of organic-phase microreactors'. *Langmuir*, vol. 21(8) (2005), pp. 3629–3634 (cit. on p. 4).
66. He, M., Edgar, J. S., Jeffries, G. D., Lorenz, R. M., Shelby, J. P., and Chiu, D. T. 'Selective encapsulation of single cells and subcellular organelles into picoliter-and femtoliter-volume droplets'. *Analytical chemistry*, vol. 77(6) (2005), pp. 1539–1544 (cit. on p. 4).
67. Lobry, E., Jasinski, F., Penconi, M., Chemtob, A., Croutxé-Barghorn, C., Oliveros, E., Braun, A. M., and Criqui, A. 'Continuous-flow synthesis of polymer nanoparticles in a microreactor via miniemulsion photopolymerization'. *RSC Advances*, vol. 4(82) (2014), pp. 43756–43759 (cit. on pp. 4, 37).
68. Yeh, C.-H. and Lin, Y.-C. 'Using a cross-flow microfluidic chip for monodisperse UV-photopolymerized microparticles'. *Microfluidics and nanofluidics*, vol. 6(2) (2009), pp. 277–283 (cit. on p. 4).
69. SooHoo, J. R. and Walker, G. M. 'Microfluidic aqueous two phase system for leukocyte concentration from whole blood'. *Biomedical microdevices*, vol. 11(2) (2009), pp. 323–329 (cit. on p. 4).
70. Yamada, M., Kasim, V., Nakashima, M., Edahiro, J., and Seki, M. 'Continuous cell partitioning using an aqueous two-phase flow system in microfluidic devices'. *Biotechnology and bioengineering*, vol. 88(4) (2004), pp. 489–494 (cit. on p. 4).
71. Gossett, D. R., Weaver, W. M., Mach, A. J., Hur, S. C., Tse, H. T. K., Lee, W., Amini, H., and Di Carlo, D. 'Label-free cell separation and sorting in microfluidic systems'. *Analytical and bioanalytical chemistry*, vol. 397(8) (2010), pp. 3249–3267 (cit. on p. 4).
72. Hu, R., Feng, X., Chen, P., Fu, M., Chen, H., Guo, L., and Liu, B.-F. 'Rapid, highly efficient extraction and purification of membrane proteins using a microfluidic continuous-flow based aqueous two-phase system'. *Journal of Chromatography A*, vol. 1218(1) (2011), pp. 171–177 (cit. on p. 4).
73. Silva, D., Azevedo, A., Fernandes, P., Chu, V., Conde, J., and Aires-Barros, M. 'Design of a microfluidic platform for monoclonal antibody extraction using an aqueous two-phase system'. *Journal of Chromatography A*, vol. 1249 (2012), pp. 1–7 (cit. on p. 4).
74. Kutter, J. P. 'Liquid phase chromatography on microchips'. *Journal of Chromatography a*, vol. 1221 (2012), pp. 72–82 (cit. on p. 5).
75. Becker, H. 'One size fits all?' *Lab on a Chip*, vol. 10(15) (2010), pp. 1894–1897 (cit. on p. 5).
76. Klapperich, C. M. 'Microfluidic diagnostics: time for industry standards'. *Expert review of medical devices*, vol. 6(3) (2009), pp. 211–213 (cit. on p. 5).

77. Heeren, H. van. ‘Standards for connecting microfluidic devices?’ *Lab on a Chip*, vol. 12(6) (2012), pp. 1022–1025 (cit. on p. 5).
78. El-Ali, J., Sorger, P. K., and Jensen, K. F. ‘Cells on chips’. *Nature*, vol. 442(7101) (2006), p. 403 (cit. on p. 5).
79. Waldbaur, A., Kittelmann, J., Radtke, C. P., Hubbuch, J., and Rapp, B. E. ‘Microfluidics on liquid handling stations (μ F-on-LHS): an industry compatible chip interface between microfluidics and automated liquid handling stations’. *Lab on a Chip*, vol. 13(12) (2013), pp. 2337–2343 (cit. on pp. 5, 20, 37, 38, 59, 60, 68, 78).
80. Hull, C. W. *Apparatus for production of three-dimensional objects by stereolithography*. US Patent 4,575,330. Mar. 1986 (cit. on p. 6).
81. Horvath, J. ‘A brief history of 3D printing’. *Mastering 3D Printing*. Springer, 2014, pp. 3–10 (cit. on p. 6).
82. Gibson, I., Rosen, D., and Stucker, B. *Additive manufacturing technologies: 3D printing, rapid prototyping, and direct digital manufacturing*. Springer, 2014 (cit. on p. 6).
83. Berman, B. ‘3-D printing: The new industrial revolution’. *Business horizons*, vol. 55(2) (2012), pp. 155–162 (cit. on p. 6).
84. Panda, B., Tan, M. J., Gibson, I., and Chua, C. K. ‘The Disruptive Evolution Of 3D Printing’. *Proc. 2nd Int. Conf. Prog. Addit. Manuf. (Pro-AM 2016)*, vol. (2016), pp. 152–157 (cit. on pp. 6, 78).
85. Bak, D. ‘Rapid prototyping or rapid production? 3D printing processes move industry towards the latter’. *Assembly Automation*, vol. 23(4) (2003), pp. 340–345 (cit. on p. 6).
86. Wijnen, B., Hunt, E. J., Anzalone, G. C., and Pearce, J. M. ‘Open-source syringe pump library’. *PloS one*, vol. 9(9) (2014), e107216 (cit. on p. 6).
87. Lücking, T. H., Sambale, F., Beutel, S., and Scheper, T. ‘3D-printed individual labware in biosciences by rapid prototyping: A proof of principle’. *Eng. Life Sci.* Vol. 15(1) (Jan. 2015), pp. 51–56 (cit. on pp. 6, 78).
88. Shukla, M. R., Singh, A. S., Piunno, K., Saxena, P. K., and Jones, A. M. P. ‘Application of 3D printing to prototype and develop novel plant tissue culture systems’. *Plant Methods*, vol. 13(1) (2017), p. 6 (cit. on p. 6).
89. Amrhein, S., Bauer, K. C., Galm, L., and Hubbuch, J. ‘Non-invasive high throughput approach for protein hydrophobicity determination based on surface tension’. *Biotechnol. Bioeng.* Vol. 112(12) (Dec. 2015), pp. 2485–2494 (cit. on pp. 6, 78).
90. Kazenwadel, F., Biegert, E., Wohlgemuth, J., Wagner, H., and Franzreb, M. ‘A 3D-printed modular reactor setup including temperature and pH control for the

- compartmentalized implementation of enzyme cascades'. *Engineering in Life Sciences*, vol. 16(6) (2016), pp. 560–567 (cit. on p. 6).
91. Bártolo, P. J. *Stereolithography: materials, processes and applications*. Springer Science & Business Media, 2011 (cit. on p. 7).
 92. Stratasys. *PolyJet Technology*. Date Accessed 09 Sept 2017. URL: <http://www.stratasys.com/3d-printers/technologies/polyjet-technology> (cit. on p. 7).
 93. Dacey, E. J. *Method, apparatus, and article of manufacture for a control system in a selective deposition modeling system*. US Patent 6,490,496. Dec. 2002 (cit. on p. 7).
 94. Sachs, E. M., Haggerty, J. S., Cima, M. J., and Williams, P. A. *Three-dimensional printing techniques*. US Patent 5,340,656. Aug. 1994 (cit. on p. 7).
 95. Kruth, J.-P., Wang, X., Laoui, T., and Froyen, L. 'Lasers and materials in selective laser sintering'. *Assembly Automation*, vol. 23(4) (2003), pp. 357–371 (cit. on p. 7).
 96. Agarwala, M., Bourell, D., Beaman, J., Marcus, H., and Barlow, J. 'Direct selective laser sintering of metals'. *Rapid Prototyping Journal*, vol. 1(1) (1995), pp. 26–36 (cit. on p. 7).
 97. Tian, X., Liu, T., Yang, C., Wang, Q., and Li, D. 'Interface and performance of 3D printed continuous carbon fiber reinforced PLA composites'. *Composites Part A: Applied Science and Manufacturing*, vol. 88 (2016), pp. 198–205 (cit. on p. 7).
 98. Le Duigou, A., Castro, M., Bevan, R., and Martin, N. '3D printing of wood fibre biocomposites: From mechanical to actuation functionality'. *Materials & Design*, vol. 96 (2016), pp. 106–114 (cit. on p. 7).
 99. Mitchell, M. G. *Bioprinting: Techniques and Risks for Regenerative Medicine*. Academic Press, 2017 (cit. on p. 7).
 100. Jose, R. R., Rodriguez, M. J., Dixon, T. A., Omenetto, F., and Kaplan, D. L. 'Evolution of Bioinks and Additive Manufacturing Technologies for 3D Bioprinting'. *ACS Biomater. Sci. Eng.* Vol. 2(10) (Oct. 2016), pp. 1662–1678 (cit. on pp. 7, 10, 78).
 101. Campbell, P. G. and Weiss, L. E. 'Tissue engineering with the aid of inkjet printers'. *Expert opinion on biological therapy*, vol. 7(8) (2007), pp. 1123–1127 (cit. on p. 7).
 102. Malda, J., Visser, J., Melchels, F. P., Jüngst, T., Hennink, W. E., Dhert, W. J. A., Groll, J., and Huttmacher, D. W. '25th Anniversary Article: Engineering Hydrogels for Biofabrication'. *Adv. Mater.* Vol. 25(36) (Sept. 2013), pp. 5011–5028 (cit. on pp. 9, 10, 78).
 103. Klebe, R. J. 'Cytoscribing: a method for micropositioning cells and the construction of two- and three-dimensional synthetic tissues'. *Experimental cell research*, vol. 179(2) (1988), pp. 362–373 (cit. on p. 9).

104. Dababneh, A. B. and Ozbolat, I. T. ‘Bioprinting technology: a current state-of-the-art review’. *Journal of Manufacturing Science and Engineering*, vol. 136(6) (2014), p. 061016 (cit. on p. 9).
105. Landers, R. and Mülhaupt, R. ‘Desktop manufacturing of complex objects, prototypes and biomedical scaffolds by means of computer-assisted design combined with computer-guided 3D plotting of polymers and reactive oligomers’. *Macromolecular Materials and Engineering*, vol. 282(1) (2000), pp. 17–21 (cit. on p. 9).
106. Reid, J. A., Mollica, P. A., Johnson, G. D., Ogle, R. C., Bruno, R. D., and Sachs, P. C. ‘Accessible bioprinting: adaptation of a low-cost 3D-printer for precise cell placement and stem cell differentiation’. *Biofabrication*, vol. 8(2) (June 2016), p. 025017 (cit. on pp. 9, 79).
107. Mellott, M. B., Searcy, K., and Pishko, M. V. ‘Release of protein from highly cross-linked hydrogels of poly (ethylene glycol) diacrylate fabricated by UV polymerization’. *Biomaterials*, vol. 22(9) (2001), pp. 929–941 (cit. on pp. 10, 36, 78, 96, 101, 103, 105).
108. Quick, D. J. and Anseth, K. S. ‘DNA delivery from photocrosslinked PEG hydrogels: encapsulation efficiency, release profiles, and DNA quality’. *Journal of Controlled Release*, vol. 96(2) (2004), pp. 341–351 (cit. on pp. 10, 36).
109. Sheldon, R. A. and Pelt, S. van. ‘Enzyme immobilisation in biocatalysis: why, what and how’. *Chem. Soc. Rev.* Vol. 42(15) (Mar. 2013), pp. 6223–6235 (cit. on pp. 10, 78).
110. Hoffman, A. S. ‘Hydrogels for biomedical applications’. *Adv. Drug Deliv. Rev.* Vol. 64 (Dec. 2012), pp. 18–23 (cit. on pp. 10, 78).
111. Russell, R., Axel, A., Shields, K., and Pishko, M. ‘Mass transfer in rapidly photopolymerized poly(ethylene glycol) hydrogels used for chemical sensing’. *Polymer (Guildf)*. Vol. 42(11) (May 2001), pp. 4893–4901 (cit. on pp. 10, 78).
112. Walsh, G. ‘Biopharmaceutical benchmarks 2014’. *Nature Biotechnology*, vol. 32(10) (Oct. 2014), pp. 992–1000 (cit. on p. 18).
113. Lowe, C. R., Lowe, A. R., and Gupta, G. ‘New developments in affinity chromatography with potential application in the production of biopharmaceuticals’. *Journal of Biochemical and Biophysical Methods*, vol. 49(1) (2001), pp. 561–574 (cit. on p. 18).
114. Nfor, B. K., Verhaert, P. D., Wielen, L. A. van der, Hubbuch, J., and Ottens, M. ‘Rational and systematic protein purification process development: the next generation’. *Trends in Biotechnology*, vol. 27(12) (2009), pp. 673–679 (cit. on p. 18).
115. Nfor, B. K., Ahamed, T., Dedem, G. W. van, Wielen, L. A. van der, Sandt, E. J. van de, Eppink, M. H., and Ottens, M. ‘Design strategies for integrated protein purification processes: challenges, progress and outlook’. *Journal of Chemical Technology & Biotechnology*, vol. 83(2) (2008), pp. 124–132 (cit. on p. 18).

116. Wiendahl, M., Völker, C., Husemann, I., Krarup, J., Staby, A., Scholl, S., and Hubbuch, J. 'A novel method to evaluate protein solubility using a high throughput screening approach'. *Chemical Engineering Science*, vol. 64(17) (2009), pp. 3778–3788 (cit. on p. 18).
117. Robertson, C. 'Liquid photometer using surface tension to contain sample'. US6628382 B2. 2003 (cit. on p. 18).
118. Thakkar, S. V., Allegre, K. M., Joshi, S. B., Volkin, D. B., and Middaugh, C. R. 'An Application of Ultraviolet Spectroscopy to Study Interactions in Proteins Solutions at High Concentrations'. *Journal of Pharmaceutical Sciences*, vol. 101(9) (2012), pp. 3051–3061 (cit. on p. 19).
119. Baber, N. 'International conference on harmonisation of technical requirements for registration of pharmaceuticals for human use (ICH)'. *British Journal of Clinical Pharmacology*, vol. 37(5) (May 1994), pp. 401–404 (cit. on p. 21).
120. McGown, E. L. and Hafeman, D. G. 'Multichannel Pipettor Performance Verified by Measuring Pathlength of Reagent Dispensed into a Microplate'. Vol. 258(1) (1998), pp. 155–157 (cit. on p. 22).
121. Lampinen, J., Raitio, M., Perälä, A., Oranen, H., and Harinen, R.-R. 'Microplate Based Pathlength Correction Method for Photometric DNA Quantification Assay'. *Thermo Scientific Appl. Note*, vol. (ANMR MUGO 0412) (2012) (cit. on p. 22).
122. Hansen, S. K., Jamali, B., and Hubbuch, J. 'Selective high throughput protein quantification based on UV absorption spectra'. *Biotechnology and Bioengineering*, vol. 110(2) (Feb. 2013), pp. 448–460 (cit. on p. 30).
123. Ramakrishna, S., Mayer, J., Wintermantel, E., and Leong, K. W. 'Biomedical applications of polymer-composite materials: a review'. *Composites science and technology*, vol. 61(9) (2001), pp. 1189–1224 (cit. on p. 36).
124. Baroli, B. 'Photopolymerization of biomaterials: issues and potentialities in drug delivery, tissue engineering, and cell encapsulation applications'. *Journal of Chemical Technology and Biotechnology*, vol. 81(4) (2006), pp. 491–499 (cit. on pp. 36, 37).
125. Fisher, J. P., Dean, D., and Mikos, A. G. 'Photocrosslinking characteristics and mechanical properties of diethyl fumarate/poly (propylene fumarate) biomaterials'. *Biomaterials*, vol. 23(22) (2002), pp. 4333–4343 (cit. on p. 36).
126. Davis, K. A., Burdick, J. A., and Anseth, K. S. 'Photoinitiated crosslinked degradable copolymer networks for tissue engineering applications'. *Biomaterials*, vol. 24(14) (2003), pp. 2485–2495 (cit. on p. 36).
127. Anseth, K., Goodner, M., Reil, M., Kannurpatti, A., Newman, S., and Bowman, C. 'The influence of comonomer composition on dimethacrylate resin properties for dental composites'. *Journal of dental research*, vol. 75(8) (1996), pp. 1607–1612 (cit. on p. 36).

128. Lu, M., Lan, H., Wang, F., and Wang, Y. ‘A novel cell encapsulation method using photosensitive poly (allylamine alpha-cyanocinnamylideneacetate)’. *Journal of microencapsulation*, vol. 17(2) (2000), pp. 245–251 (cit. on p. 36).
129. Quek, C.-H., Li, J., Sun, T., Chan, M. L. H., Mao, H.-Q., Gan, L. M., Leong, K. W., and Yu, H. ‘Photo-crosslinkable microcapsules formed by polyelectrolyte copolymer and modified collagen for rat hepatocyte encapsulation’. *Biomaterials*, vol. 25(17) (2004), pp. 3531–3540 (cit. on p. 36).
130. Gobin, A. S. and West, J. L. ‘Effects of epidermal growth factor on fibroblast migration through biomimetic hydrogels’. *Biotechnology progress*, vol. 19(6) (2003), pp. 1781–1785 (cit. on p. 36).
131. Yokoyama, S., Nakahama, T., Miki, H., and Mashiko, S. ‘Fabrication of three-dimensional microstructure in optical-gain medium using two-photon-induced photopolymerization technique’. *Thin Solid Films*, vol. 438 (2003), pp. 452–456 (cit. on p. 36).
132. Arcaute, K., Mann, B. K., and Wicker, R. B. ‘Stereolithography of three-dimensional bioactive poly (ethylene glycol) constructs with encapsulated cells’. *Annals of biomedical engineering*, vol. 34(9) (2006), pp. 1429–1441 (cit. on p. 36).
133. Pierre, S. J., Thies, J. C., Dureault, A., Cameron, N. R., Hest, J. C. van, Carette, N., Michon, T., and Weberskirch, R. ‘Covalent enzyme immobilization onto photopolymerized highly porous monoliths’. *Advanced Materials*, vol. 18(14) (2006), pp. 1822–1826 (cit. on p. 36).
134. Li, L., Zhao, N., and Liu, S. ‘Versatile surface biofunctionalization of poly (ethylene terephthalate) by interpenetrating polymerization of a butynyl monomer followed by “Click Chemistry”’. *Polymer*, vol. 53(1) (2012), pp. 67–78 (cit. on p. 36).
135. Chemtob, A., Kunstler, B., Croutxé-Barghorn, C., and Fouchard, S. ‘Photoinduced miniemulsion polymerization’. *Colloid and Polymer Science*, vol. 288(5) (2010), pp. 579–587 (cit. on p. 36).
136. Daniloska, V., Tomovska, R., and Asua, J. M. ‘Hybrid miniemulsion photopolymerization in a continuous tubular reactor—A way to expand the characteristics of polyurethane/acrylics’. *Chemical Engineering Journal*, vol. 184 (2012), pp. 308–314 (cit. on pp. 36, 37).
137. Landfester, K. ‘Miniemulsion polymerization and the structure of polymer and hybrid nanoparticles’. *Angewandte Chemie International Edition*, vol. 48(25) (2009), pp. 4488–4507 (cit. on p. 36).
138. Antonietti, M. and Landfester, K. ‘Polyreactions in miniemulsions’. *Progress in Polymer Science*, vol. 27(4) (2002), pp. 689–757 (cit. on p. 36).

139. Jasinski, F., Lobry, E., Chemtob, A., Croutxé-Barghorn, C., and Criqui, A. ‘Photopolymerizable monomer miniemulsions: why does droplet size matter?’ *Macromolecular Chemistry and Physics*, vol. 214(15) (2013), pp. 1669–1676 (cit. on p. 36).
140. Penconi, M., Lobry, E., Jasinski, F., Chemtob, A., Croutxé-Barghorn, C., Criqui, A., Braun, A. M., and Oliveros, E. ‘The use of chemical actinometry for the evaluation of the light absorption efficiency in scattering photopolymerizable miniemulsions’. *Photochemical & Photobiological Sciences*, vol. 14(2) (2015), pp. 308–319 (cit. on p. 36).
141. Patel, H., Raval, D., Madamwar, D., and Patel, S. ‘Polymeric prodrug: Synthesis, release study and antimicrobial property of poly (styrene-co-maleic anhydride)-bound acriflavine’. *Macromolecular Materials and Engineering*, vol. 263(1) (1998), pp. 25–30 (cit. on p. 37).
142. Montgomery, D. C., Peck, E. A., and Vining, G. G. *Introduction to linear regression analysis*. John Wiley & Sons, 2012 (cit. on p. 37).
143. Malkoch, M., Thibault, R. J., Drockenmuller, E., Messerschmidt, M., Voit, B., Russell, T. P., and Hawker, C. J. ‘Orthogonal approaches to the simultaneous and cascade functionalization of macromolecules using click chemistry’. *Journal of the American Chemical Society*, vol. 127(42) (2005), pp. 14942–14949 (cit. on p. 38).
144. Decker, C., Zahouily, K., Decker, D., Nguyen, T., and Viet, T. ‘Performance analysis of acylphosphine oxides in photoinitiated polymerization’. *Polymer*, vol. 42(18) (2001), pp. 7551–7560 (cit. on p. 38).
145. Laurino, P., Hernandez, H. F., Bräuer, J., Krüger, K., Grützmacher, H., Tauer, K., and Seeberger, P. H. ‘Snowballing radical generation leads to ultrahigh molecular weight polymers’. *Macromolecular rapid communications*, vol. 33(20) (2012), pp. 1770–1774 (cit. on p. 38).
146. Lobry, E., Jasinski, F., Penconi, M., Chemtob, A., Ley, C., Croutxé-Barghorn, C., Oliveros, E., Braun, A. M., and Criqui, A. ‘Absorption and scattering in concentrated monomer miniemulsions: static and dynamic investigations’. *Macromolecular Chemistry and Physics*, vol. 215(12) (2014), pp. 1201–1211 (cit. on p. 44).
147. Hoijemberg, P. A., Chemtob, A., Croutxé-Barghorn, C., Poly, J., and Braun, A. M. ‘Radical photopolymerization in miniemulsions. Fundamental investigations and technical development’. *Macromolecules*, vol. 44(22) (2011), pp. 8727–8738 (cit. on p. 45).
148. Tomovska, R., Cal, J. C. de la, and Asua, J. M. ‘Miniemulsion photo-copolymerization of styrene/butyl acrylate in a continuous tubular reactor’. *Industrial & Engineering Chemistry Research*, vol. 53(18) (2013), pp. 7313–7320 (cit. on p. 45).
149. Decker, C. ‘Kinetic study and new applications of UV radiation curing’. *Macromolecular Rapid Communications*, vol. 23(18) (2002), pp. 1067–1093 (cit. on p. 46).

150. Yousif, E. and Haddad, R. 'Photodegradation and photostabilization of polymers, especially polystyrene: review'. *SpringerPlus*, vol. 2(1) (2013), p. 398 (cit. on p. 46).
151. Bottino, F. A., Cinquegrani, A. R., Di Pasquale, G., Leonardi, L., and Pollicino, A. 'Chemical modifications, mechanical properties and surface photo-oxidation of films of polystyrene (PS)'. *Polymer testing*, vol. 23(4) (2004), pp. 405–411 (cit. on p. 47).
152. Gardette, J.-L., Mailhot, B., and Lemaire, J. 'Photooxidation mechanisms of styrenic polymers'. *Polymer degradation and stability*, vol. 48(3) (1995), pp. 457–470 (cit. on p. 47).
153. Kaczmarek, H., Kamińska, A., Świątek, M., and Sanyal, S. 'Photoinitiated degradation of polystyrene in the presence of low-molecular organic compounds'. *European polymer journal*, vol. 36(6) (2000), pp. 1167–1173 (cit. on p. 47).
154. Kwant, P. 'Kinetics of styrene polymerization at ultrahigh conversion'. *Journal of Polymer Science: Polymer Chemistry Edition*, vol. 17(10) (1979), pp. 3397–3410 (cit. on p. 47).
155. Hall-Stoodley, L., Costerton, J. W., and Stoodley, P. 'Bacterial biofilms: from the natural environment to infectious diseases'. *Nature reviews microbiology*, vol. 2(2) (2004), pp. 95–108 (cit. on p. 58).
156. De Vos, W. M. 'Microbial biofilms and the human intestinal microbiome'. *npj Biofilms and Microbiomes*, vol. 1 (2015), p. 15005 (cit. on p. 58).
157. Verstraete, W. 'The technological side of the microbiome'. *npj Biofilms and Microbiomes*, vol. 1 (2015), p. 15001 (cit. on p. 58).
158. Parsek, M. R. and Greenberg, E. P. 'Sociomicrobiology: the connections between quorum sensing and biofilms'. *Trends in microbiology*, vol. 13(1) (2005), pp. 27–33 (cit. on p. 58).
159. Zengler, K. and Palsson, B. O. 'A road map for the development of community systems (CoSy) biology'. *Nature Reviews Microbiology*, vol. 10(5) (2012), pp. 366–372 (cit. on p. 58).
160. Burmølle, M., Ren, D., Bjarnsholt, T., and Sørensen, S. J. 'Interactions in multispecies biofilms: do they actually matter?' *Trends in microbiology*, vol. 22(2) (2014), pp. 84–91 (cit. on pp. 58, 69).
161. Kirisits, M. J., Margolis, J. J., Purevdorj-Gage, B. L., Vaughan, B., Chopp, D. L., Stoodley, P., and Parsek, M. R. 'Influence of the hydrodynamic environment on quorum sensing in *Pseudomonas aeruginosa* biofilms'. *Journal of bacteriology*, vol. 189(22) (2007), pp. 8357–8360 (cit. on p. 58).
162. Purevdorj, B., Costerton, J., and Stoodley, P. 'Influence of hydrodynamics and cell signaling on the structure and behavior of *Pseudomonas aeruginosa* biofilms'. *Applied and environmental microbiology*, vol. 68(9) (2002), pp. 4457–4464 (cit. on p. 58).

-
163. Mariscal, A., Carnero-Varo, M., Gutierrez-Bedmar, M., Garcia-Rodriguez, A., and Fernandez-Crehuet, J. 'A fluorescent method for assessing the antimicrobial efficacy of disinfectant against *Escherichia coli* ATCC 35218 biofilm'. *Applied microbiology and biotechnology*, vol. 77(1) (2007), pp. 233–240 (cit. on p. 58).
 164. Repp, K. K., Menor, S. A., and Pettit, R. K. 'Microplate Alamar blue assay for susceptibility testing of *Candida albicans* biofilms'. *Medical mycology*, vol. 45(7) (2007), pp. 603–607 (cit. on p. 58).
 165. Junker, L. M. and Clardy, J. 'High-throughput screens for small-molecule inhibitors of *Pseudomonas aeruginosa* biofilm development'. *Antimicrobial agents and chemotherapy*, vol. 51(10) (2007), pp. 3582–3590 (cit. on p. 58).
 166. Benoit, M. R., Conant, C. G., Ionescu-Zanetti, C., Schwartz, M., and Matin, A. 'New device for high-throughput viability screening of flow biofilms'. *Applied and environmental microbiology*, vol. 76(13) (2010), pp. 4136–4142 (cit. on p. 58).
 167. Tremblay, Y. D., Vogeleeer, P., Jacques, M., and Harel, J. 'High-throughput microfluidic method to study biofilm formation and host-pathogen interactions in pathogenic *Escherichia coli*'. *Applied and environmental microbiology*, vol. 81(8) (2015), pp. 2827–2840 (cit. on p. 58).
 168. Pamp, S. J., Sternberg, C., and Tolker-Nielsen, T. 'Insight into the microbial multicellular lifestyle via flow-cell technology and confocal microscopy'. *Cytometry Part A*, vol. 75(2) (2009), pp. 90–103 (cit. on p. 58).
 169. Amann, R. I., Ludwig, W., and Schleifer, K.-H. 'Phylogenetic identification and in situ detection of individual microbial cells without cultivation.' *Microbiological reviews*, vol. 59(1) (1995), pp. 143–169 (cit. on p. 58).
 170. Stewart, P. S. and Franklin, M. J. 'Physiological heterogeneity in biofilms'. *Nature Reviews Microbiology*, vol. 6(3) (2008), pp. 199–210 (cit. on p. 58).
 171. Pernthaler, A. e. a. 'Sensitive multi-color fluorescence in situ hybridization for the identification of environmental microorganisms'. *Molecular microbial ecology manual*. Vol. 1 and 2 (2004), pp. 711–725 (cit. on pp. 58, 61, 67, 69).
 172. Perez-Toralla, K., Mottet, G., Guneri, E. T., Champ, J., Bidard, F.-C., Pierga, J.-Y., Klijanienko, J., Draskovic, I., Malaquin, L., Viovy, J.-L., et al. 'FISH in chips: turning microfluidic fluorescence in situ hybridization into a quantitative and clinically reliable molecular diagnosis tool'. *Lab on a Chip*, vol. 15(3) (2015), pp. 811–822 (cit. on p. 59).
 173. Sieben, V. J., Debes-Marun, C. S., Pilarski, L. M., and Backhouse, C. J. 'An integrated microfluidic chip for chromosome enumeration using fluorescence in situ hybridization'. *Lab on a Chip*, vol. 8(12) (2008), pp. 2151–2156 (cit. on pp. 59, 68).

174. Zanardi, A., Bandiera, D., Bertolini, F., Corsini, C. A., Gregato, G., Milani, P., Barbarini, E., and Carbone, R. ‘Miniaturized FISH for screening of onco-hematological malignancies’. *Biotechniques*, vol. 49(1) (2010), pp. 497–504 (cit. on p. 59).
175. Liu, Y., Kirkland, B., Shirley, J., Wang, Z., Zhang, P., Stenbridge, J., Wong, W., Takebayashi, S.-i., Gilbert, D. M., Lenhart, S., et al. ‘Development of a single-cell array for large-scale DNA fluorescence in situ hybridization’. *Lab on a Chip*, vol. 13(7) (2013), pp. 1316–1324 (cit. on pp. 59, 69).
176. Vedarethinam, I., Shah, P., Dimaki, M., Tumer, Z., Tommerup, N., and Svendsen, W. E. ‘Metaphase FISH on a chip: miniaturized microfluidic device for fluorescence in situ hybridization’. *Sensors*, vol. 10(11) (2010), pp. 9831–9846 (cit. on p. 59).
177. Ziegler, S., Ackermann, S., Majzlan, J., and Gescher, J. ‘Matrix composition and community structure analysis of a novel bacterial pyrite leaching community’. *Environmental microbiology*, vol. 11(9) (2009), pp. 2329–2338 (cit. on pp. 59, 60).
178. Ziegler, S., Dolch, K., Geiger, K., Krause, S., Asskamp, M., Eusterhues, K., Kriews, M., Wilhelms-Dick, D., Goettlicher, J., Majzlan, J., et al. ‘Oxygen-dependent niche formation of a pyrite-dependent acidophilic consortium built by archaea and bacteria’. *The ISME journal*, vol. 7(9) (2013), pp. 1725–1737 (cit. on p. 60).
179. Huber, R. and Stetter, K. *The prokaryotes: An Evolving Electronic Resource for the Microbiological Community*. 2001 (cit. on p. 61).
180. Preibisch, S., Saalfeld, S., and Tomancak, P. ‘Globally optimal stitching of tiled 3D microscopic image acquisitions’. *Bioinformatics*, vol. 25(11) (2009), pp. 1463–1465 (cit. on pp. 63, 65).
181. Haisch, C. and Niessner, R. ‘Visualisation of transient processes in biofilms by optical coherence tomography’. *Water research*, vol. 41(11) (2007), pp. 2467–2472 (cit. on p. 63).
182. Wagner, M., Taherzadeh, D., Haisch, C., and Horn, H. ‘Investigation of the mesoscale structure and volumetric features of biofilms using optical coherence tomography’. *Biotechnology and bioengineering*, vol. 107(5) (2010), pp. 844–853 (cit. on p. 63).
183. Schindelin, J., Arganda-Carreras, I., Frise, E., Kaynig, V., Longair, M., Pietzsch, T., Preibisch, S., Rueden, C., Saalfeld, S., Schmid, B., et al. ‘Fiji: an open-source platform for biological-image analysis’. *Nature methods*, vol. 9(7) (2012), pp. 676–682 (cit. on p. 63).
184. Otsu, N. ‘An automatic threshold selection method based on discriminate and least squares criteria’. *Denshi Tsushin Gakkai Ronbunshi*, vol. 63 (1979), pp. 349–356 (cit. on p. 63).
185. Amann, R. and Fuchs, B. M. ‘Single-cell identification in microbial communities by improved fluorescence in situ hybridization techniques’. *Nature Reviews Microbiology*, vol. 6(5) (2008), pp. 339–348 (cit. on pp. 67, 69).

186. Thurnheer, T., Gmür, R., and Guggenheim, B. 'Multiplex FISH analysis of a six-species bacterial biofilm'. *Journal of Microbiological Methods*, vol. 56(1) (2004), pp. 37–47 (cit. on p. 69).
187. Regan, J., Oldenburg, P., Park, H.-D., Harrington, G., and Noguera, D. 'Simultaneous determination of bacterial viability and identity in biofilms using ethidium monoazide and fluorescent in situ hybridization'. *Water Science and Technology*, vol. 47(5) (2003), pp. 123–128 (cit. on p. 69).
188. Hol, F. J. and Dekker, C. 'Zooming in to see the bigger picture: Microfluidic and nanofabrication tools to study bacteria'. *Science*, vol. 346(6208) (2014), p. 1251821 (cit. on p. 69).
189. Weibel, D. B., DiLuzio, W. R., and Whitesides, G. M. 'Microfabrication meets microbiology'. *Nature Reviews Microbiology*, vol. 5(3) (2007), pp. 209–218 (cit. on p. 69).
190. Kim, J., Park, H.-D., and Chung, S. 'Microfluidic approaches to bacterial biofilm formation'. *Molecules*, vol. 17(8) (2012), pp. 9818–9834 (cit. on p. 69).
191. Hennig, C., Adams, N., and Hansen, G. 'A versatile platform for comprehensive chip-based explorative cytometry'. *Cytometry Part A*, vol. 75(4) (2009), pp. 362–370 (cit. on p. 70).
192. Pernthaler, J., Pernthaler, A., and Amann, R. 'Automated enumeration of groups of marine picoplankton after fluorescence in situ hybridization'. *Applied and environmental microbiology*, vol. 69(5) (2003), pp. 2631–2637 (cit. on p. 70).
193. Savastano, M., Amendola, C., D'Ascenzo, F., and Massaroni, E. '3-D Printing in the Spare Parts Supply Chain: An Explorative Study in the Automotive Industry'. *Digit. Support. Innov. Lect. Notes Inf. Syst. Organ.* Ed. by Caporarello, L., Cesaroni, F., Giesecke, R., and Missikoff, M. Springer, Cham, 2016, pp. 153–170 (cit. on p. 78).
194. McDonald, J. C., Chabinyk, M. L., Metallo, S. J., Anderson, J. R., Stroock, A. D., and Whitesides, G. M. 'Prototyping of Microfluidic Devices in Poly(dimethylsiloxane) Using Solid-Object Printing'. *Anal. Chem.* Vol. 74(7) (Apr. 2002), pp. 1537–1545 (cit. on p. 78).
195. Chen, C., Wang, Y., Lockwood, S. Y., and Spence, D. M. '3D-printed fluidic devices enable quantitative evaluation of blood components in modified storage solutions for use in transfusion medicine'. *Analyst*, vol. 139(13) (2014), pp. 3219–3226 (cit. on p. 78).
196. Au, A. K., Huynh, W., Horowitz, L. F., and Folch, A. '3D-Printed Microfluidics'. *Angew. Chemie Int. Ed.* Vol. 55(12) (Mar. 2016), pp. 3862–3881 (cit. on p. 78).
197. Su, C.-K. and Chen, J.-C. 'Reusable, 3D-printed, peroxidase mimic-incorporating multi-well plate for high-throughput glucose determination'. *Sensors Actuators B Chem.* Vol. 247 (Aug. 2017), pp. 641–647 (cit. on p. 78).

198. Kazenwadel, F., Biegert, E., Wohlgemuth, J., Wagner, H., and Franzreb, M. 'A 3D-printed modular reactor setup including temperature and pH control for the compartmentalized implementation of enzyme cascades'. *Eng. Life Sci.* Vol. 16(6) (Sept. 2016), pp. 560–567 (cit. on p. 78).
199. Gross, B. C., Erkal, J. L., Lockwood, S. Y., Chen, C., and Spence, D. M. 'Evaluation of 3D Printing and Its Potential Impact on Biotechnology and the Chemical Sciences'. *Anal. Chem.* Vol. 86(7) (Apr. 2014), pp. 3240–3253 (cit. on p. 78).
200. Groll, J. et al. 'Biofabrication: reappraising the definition of an evolving field'. *Biofabrication*, vol. 8(1) (Jan. 2016), p. 013001 (cit. on p. 78).
201. Patra, S. and Young, V. 'A Review of 3D Printing Techniques and the Future in Biofabrication of Bioprinted Tissue'. *Cell Biochem. Biophys.* Vol. 74(2) (June 2016), pp. 93–98 (cit. on p. 78).
202. Drury, J. L. and Mooney, D. J. 'Hydrogels for tissue engineering: scaffold design variables and applications'. *Biomaterials*, vol. 24(24) (Nov. 2003), pp. 4337–4351 (cit. on p. 78).
203. Nguyen, K. T. and West, J. L. 'Photopolymerizable hydrogels for tissue engineering applications'. *Biomaterials*, vol. 23(22) (Nov. 2002), pp. 4307–4314 (cit. on p. 78).
204. Langer, R. and Peppas, N. A. 'Advances in biomaterials, drug delivery, and bionanotechnology'. *AIChE J.* Vol. 49(12) (Dec. 2003), pp. 2990–3006 (cit. on p. 78).
205. Derby, B. 'Printing and prototyping of tissues and scaffolds'. *Science*, vol. 338(6109) (2012), pp. 921–926 (cit. on p. 78).
206. Hollister, S. J. 'Porous scaffold design for tissue engineering.' *Nature materials*, vol. 4(7) (2005) (cit. on p. 78).
207. Ouyang, L., Highley, C. B., Rodell, C. B., Sun, W., and Burdick, J. A. '3D Printing of Shear-Thinning Hyaluronic Acid Hydrogels with Secondary Cross-Linking'. *ACS Biomaterials Science & Engineering*, vol. 2(10) (2016), pp. 1743–1751 (cit. on p. 78).
208. Ventola, C. L. 'Medical applications for 3D printing: current and projected uses'. *Pharmacy and Therapeutics*, vol. 39(10) (2014), p. 704 (cit. on p. 78).
209. Ma, X., Qu, X., Zhu, W., Li, Y.-S., Yuan, S., Zhang, H., Liu, J., Wang, P., Lai, C. S. E., Zanella, F., et al. 'Deterministically patterned biomimetic human iPSC-derived hepatic model via rapid 3D bioprinting'. *Proceedings of the National Academy of Sciences*, vol. 113(8) (2016), pp. 2206–2211 (cit. on p. 78).
210. Zhao, Y., Yao, R., Ouyang, L., Ding, H., Zhang, T., Zhang, K., Cheng, S., and Sun, W. 'Three-dimensional printing of HeLa cells for cervical tumor model in vitro'. *Biofabrication*, vol. 6(3) (2014), p. 035001 (cit. on p. 78).
211. MacNeil, S. 'Progress and opportunities for tissue-engineered skin'. *Nature*, vol. 445(7130) (2007), pp. 874–880 (cit. on p. 78).

212. Marga, F., Jakab, K., Khatiwala, C., Shepherd, B., Dorfman, S., Hubbard, B., Colbert, S., and Forgacs, G. 'Toward engineering functional organ modules by additive manufacturing'. *Biofabrication*, vol. 4(2) (2012), p. 022001 (cit. on p. 78).
213. Mannoor, M. S., Jiang, Z., James, T., Kong, Y. L., Malatesta, K. A., Soboyejo, W. O., Verma, N., Gracias, D. H., and McAlpine, M. C. '3D printed bionic ears'. *Nano letters*, vol. 13(6) (2013), p. 2634 (cit. on p. 78).
214. Leonard, M., De Boisseson, M., Hubert, P., Dalençon, F., and Dellacherie, E. 'Hydrophobically modified alginate hydrogels as protein carriers with specific controlled release properties'. *J. Control. Release*, vol. 98(3) (Aug. 2004), pp. 395–405 (cit. on p. 78).
215. Gil, M. S., Cho, J., Thambi, T., Giang Phan, V., Kwon, I., and Lee, D. S. 'Bioengineered robust hybrid hydrogels enrich the stability and efficacy of biological drugs'. *J. Control. Release*, vol. (Apr. 2017), DOI: 10.1016/j.jconrel.2017.04.009 (cit. on p. 78).
216. Heo, J. and Crooks, R. M. 'Microfluidic Biosensor Based on an Array of Hydrogel-Entrapped Enzymes'. *Anal. Chem.* Vol. 77(21) (Nov. 2005), pp. 6843–6851 (cit. on pp. 78, 79).
217. Koh, W.-G. and Pishko, M. 'Immobilization of multi-enzyme microreactors inside microfluidic devices'. *Sensors Actuators B Chem.* Vol. 106(1) (Apr. 2005), pp. 335–342 (cit. on pp. 78, 79).
218. Kerby, M. B., Legge, R. S., and Tripathi, A. 'Measurements of Kinetic Parameters in a Microfluidic Reactor'. *Anal. Chem.* Vol. 78(24) (Dec. 2006), pp. 8273–8280 (cit. on p. 78).
219. Brahim, S., Narinesingh, D., and Guiseppi-Elie, A. 'Polypyrrole-hydrogel composites for the construction of clinically important biosensors'. *Biosens. Bioelectron.* Vol. 17(1-2) (Jan. 2002), pp. 53–59 (cit. on p. 78).
220. Podual, K., Doyle, F. J., and Peppas, N. A. 'Glucose-sensitivity of glucose oxidase-containing cationic copolymer hydrogels having poly(ethylene glycol) grafts'. *J. Control. Release*, vol. 67(1) (June 2000), pp. 9–17 (cit. on p. 78).
221. Grosová, Z., Rosenberg, M., Rebroš, M., Šipocz, M., and Sedláčková, B. 'Entrapment of β -galactosidase in polyvinylalcohol hydrogel'. *Biotechnol. Lett.* Vol. 30(4) (Apr. 2008), pp. 763–767 (cit. on p. 78).
222. Park, T. G. and Hoffman, A. S. 'Immobilization and characterization of β -galactosidase in thermally reversible hydrogel beads'. *J. Biomed. Mater. Res.* Vol. 24(1) (Jan. 1990), pp. 21–38 (cit. on p. 78).
223. Hinton, T. J., Jallerat, Q., Palchesko, R. N., Park, J. H., Grodzicki, M. S., Shue, H.-J., Ramadan, M. H., Hudson, A. R., and Feinberg, A. W. 'Three-dimensional printing

- of complex biological structures by freeform reversible embedding of suspended hydrogels'. *Sci. Adv.* Vol. 1(9) (Oct. 2015), e1500758–e1500758 (cit. on p. 79).
224. Yang, F., Tadepalli, V., and Wiley, B. J. '3D Printing of a Double Network Hydrogel with a Compression Strength and Elastic Modulus Greater than those of Cartilage'. *ACS Biomater. Sci. Eng.* Vol. 3(5) (May 2017), pp. 863–869 (cit. on p. 79).
225. Chang, C. C., Boland, E. D., Williams, S. K., and Hoying, J. B. 'Direct-write bioprinting three-dimensional biohybrid systems for future regenerative therapies'. *J. Biomed. Mater. Res. Part B Appl. Biomater.* Vol. 98B(1) (July 2011), pp. 160–170 (cit. on p. 79).
226. Riegel, A.-L., Borzenkova, N., Haas, V., Scharfer, P., and Schabel, W. 'Activity determination of FAD-dependent glucose dehydrogenase immobilized in PEDOT:PSS-PVA composite films for biosensor applications'. *Eng. Life Sci.* Vol. 16(6) (Sept. 2016), pp. 577–585 (cit. on p. 79).
227. Liu, J., Agarwal, M., and Varahramyan, K. 'Glucose sensor based on organic thin film transistor using glucose oxidase and conducting polymer'. *Sensors Actuators B Chem.* Vol. 135(1) (2008), pp. 195–199 (cit. on p. 79).
228. He, Y., Yang, F., Zhao, H., Gao, Q., Xia, B., and Fu, J. 'Research on the printability of hydrogels in 3D bioprinting'. *Scientific reports*, vol. 6 (2016), p. 29977 (cit. on p. 80).
229. Lederberg, J. 'The beta-d-galactosidase of Escherichia coli, strain K-12.' *J. Bacteriol.* Vol. 60(4) (Oct. 1950), pp. 381–92 (cit. on p. 82).
230. Griffiths, M. W. and Muir, D. D. 'Properties of a thermostable β -galactosidase from a thermophilic Bacillus: Comparison of the enzyme activity of whole cells, purified enzyme and immobilised whole cells'. *J. Sci. Food Agric.* Vol. 29(9) (Sept. 1978), pp. 753–761 (cit. on p. 82).
231. Kröner, F. and Hubbuch, J. 'Systematic generation of buffer systems for pH gradient ion exchange chromatography and their application'. *J. Chromatogr. A*, vol. 1285 (Apr. 2013), pp. 78–87 (cit. on pp. 82, 98).
232. Hölzl, K., Lin, S., Tytgat, L., Van Vlierberghe, S., Gu, L., and Ovsianikov, A. 'Bioink properties before, during and after 3D bioprinting'. *Biofabrication*, vol. 8(3) (Sept. 2016), p. 032002 (cit. on p. 83).
233. Markstedt, K., Mantas, A., Tournier, I., Martínez Ávila, H., Hägg, D., and Gatenholm, P. '3D Bioprinting Human Chondrocytes with Nanocellulose–Alginate Bioink for Cartilage Tissue Engineering Applications'. *Biomacromolecules*, vol. 16(5) (May 2015), pp. 1489–1496 (cit. on p. 83).
234. Haider, T. and Husain, Q. 'Calcium alginate entrapped preparations of *Aspergillus oryzae* β galactosidase: Its stability and applications in the hydrolysis of lactose'. *Int. J. Biol. Macromol.* Vol. 41(1) (June 2007), pp. 72–80 (cit. on p. 86).

235. Sarto, V., Marzetti, A., and Focher, B. ' β -d-Galactosidases immobilized on soluble matrices: Kinetics and stability'. *Enzyme Microb. Technol.* Vol. 7(10) (Oct. 1985), pp. 515–520 (cit. on p. 86).
236. Tanaka, Y., Kagamiishi, A., Kiuchi, A., and Horiuchi, T. 'Purification and Properties of β -Galactosidase from *Aspergillus oryzae*'. *J. Biochem.* Vol. 77(1) (1975), pp. 241–247 (cit. on p. 86).
237. Sharpe, L. A., Daily, A. M., Horava, S. D., and Peppas, N. A. 'Therapeutic applications of hydrogels in oral drug delivery'. *Expert opinion on drug delivery*, vol. 11(6) (2014), pp. 901–915 (cit. on p. 96).
238. Liechty, W. B., Kryscio, D. R., Slaughter, B. V., and Peppas, N. A. 'Polymers for drug delivery systems'. *Annual review of chemical and biomolecular engineering*, vol. 1 (2010), pp. 149–173 (cit. on p. 96).
239. Langer, R. and Tirrell, D. A. 'Designing materials for biology and medicine'. *Nature*, vol. 428(6982) (2004), pp. 487–492 (cit. on p. 96).
240. Peppas, N. A., Bures, P., Leobandung, W. S., and Ichikawa, H. 'Hydrogels in pharmaceutical formulations'. *European journal of pharmaceuticals and biopharmaceutics*, vol. 50(1) (2000), pp. 27–46 (cit. on pp. 96, 97).
241. Ferreira, L., Vidal, M. M., and Gil, M. H. 'Evaluation of poly (2-hydroxyethyl methacrylate) gels as drug delivery systems at different pH values'. *International journal of pharmaceuticals*, vol. 194(2) (2000), pp. 169–180 (cit. on p. 96).
242. Hari, P. R., Chandy, T., and Sharma, C. P. 'Chitosan/calcium–alginate beads for oral delivery of insulin'. *Journal of Applied Polymer Science*, vol. 59(11) (1996), pp. 1795–1801 (cit. on p. 96).
243. Chaturvedi, K., Ganguly, K., Nadagouda, M. N., and Aminabhavi, T. M. 'Polymeric hydrogels for oral insulin delivery'. *Journal of controlled release*, vol. 165(2) (2013), pp. 129–138 (cit. on p. 96).
244. Zou, X., Zhao, X., and Ye, L. 'Synthesis of cationic chitosan hydrogel with long chain alkyl and its controlled glucose-responsive drug delivery behavior'. *RSC Advances*, vol. 5(116) (2015), pp. 96230–96241 (cit. on p. 96).
245. Hoare, T. R. and Kohane, D. S. 'Hydrogels in drug delivery: progress and challenges'. *Polymer*, vol. 49(8) (2008), pp. 1993–2007 (cit. on p. 96).
246. Hoffman, A. S. 'Hydrogels for biomedical applications'. *Advanced drug delivery reviews*, vol. 64 (2012), pp. 18–23 (cit. on p. 96).
247. Brandl, F., Hammer, N., Blunk, T., Tessmar, J., and Goepferich, A. 'Biodegradable hydrogels for time-controlled release of tethered peptides or proteins'. *Biomacromolecules*, vol. 11(2) (2010), pp. 496–504 (cit. on p. 97).

248. Oliveira, M. B. and Mano, J. F. ‘High-throughput screening for integrative biomaterials design: exploring advances and new trends’. *Trends in biotechnology*, vol. 32(12) (2014), pp. 627–636 (cit. on p. 97).
249. Capelle, M. A. H., Gurny, R., and Arvinte, T. ‘High throughput screening of protein formulation stability: practical considerations’. *European journal of pharmaceuticals and biopharmaceutics*, vol. 65(2) (2007), pp. 131–148 (cit. on p. 97).
250. Wang, J., Goyanes, A., Gaisford, S., and Basit, A. W. ‘Stereolithographic (SLA) 3D printing of oral modified-release dosage forms’. *International journal of pharmaceuticals*, vol. 503(1) (2016), pp. 207–212 (cit. on p. 97).
251. Lin, C.-C. and Anseth, K. S. ‘PEG hydrogels for the controlled release of biomolecules in regenerative medicine’. *Pharmaceutical research*, vol. 26(3) (2009), pp. 631–643 (cit. on pp. 97, 101).
252. Galm, L., Morgenstern, J., and Hubbuch, J. ‘Manipulation of lysozyme phase behavior by additives as function of conformational stability’. *International journal of pharmaceuticals*, vol. 494(1) (2015), pp. 370–380 (cit. on p. 100).
253. Morgenstern, J., Baumann, P., Brunner, C., and Hubbuch, J. ‘Effect of PEG molecular weight and PEGylation degree on the physical stability of PEGylated lysozyme’. *International journal of pharmaceuticals*, vol. 519(1) (2017), pp. 408–417 (cit. on p. 101).
254. Sirkar, K. and Pishko, M. V. ‘Amperometric biosensors based on oxidoreductases immobilized in photopolymerized poly (ethylene glycol) redox polymer hydrogels’. *Analytical Chemistry*, vol. 70(14) (1998), pp. 2888–2894 (cit. on p. 101).
255. Arcaute, K., Mann, B. K., and Wicker, R. B. ‘Practical use of hydrogels in stereolithography for tissue engineering applications’. *Stereolithography*. Springer, 2011, pp. 299–331 (cit. on p. 102).
256. Zhang, L., Ma, Y., Zhao, C., Zhu, X., Chen, R., and Yang, W. ‘Synthesis of pH-responsive hydrogel thin films grafted on PCL substrates for protein delivery’. *Journal of Materials Chemistry B*, vol. 3(39) (2015), pp. 7673–7681 (cit. on pp. 103, 105, 107).
257. Zhao, L., Chen, Y., Li, W., Lu, M., Wang, S., Chen, X., Shi, M., Wu, J., Yuan, Q., and Li, Y. ‘Controlled uptake and release of lysozyme from glycerol diglycidyl ether cross-linked oxidized starch microgel’. *Carbohydrate polymers*, vol. 121 (2015), pp. 276–283 (cit. on p. 103).
258. Morris, G. E., Vincent, B., and Snowden, M. J. ‘Adsorption of Lead Ions onto N-Isopropylacrylamide and Acrylic Acid Copolymer Microgels’. *Journal of colloid and interface science*, vol. 190(1) (1997), pp. 198–205 (cit. on p. 103).
259. Maiser, B., Kröner, F., Dismar, F., Brenner-Weiß, G., and Hubbuch, J. ‘Isoform separation and binding site determination of mono-PEGylated lysozyme with pH

- gradient chromatography'. *Journal of Chromatography A*, vol. 1268 (2012), pp. 102–108 (cit. on p. 103).
260. VirginiaTech. *H++*. Date Accessed 06 July 2017. URL: <http://biophysics.cs.vt.edu/index.php> (cit. on pp. 105, 107).
261. Hammer, N., Brandl, F. P., Kirchhof, S., Messmann, V., and Goepferich, A. M. 'Protein Compatibility of Selected Cross-linking Reactions for Hydrogels'. *Macromolecular bioscience*, vol. 15(3) (2015), pp. 405–413 (cit. on p. 105).
262. Brooks, C. A. and Cramer, S. M. 'Steric mass-action ion exchange: displacement profiles and induced salt gradients'. *AIChE Journal*, vol. 38(12) (1992), pp. 1969–1978 (cit. on p. 107).

List of Figures

3.1	Microscale chromatography executed on a liquid-handling station	3
3.2	Photograph of μ F-on-LHS devices in an automated procedure on a liquid-handling station.	5
3.3	Schematic representation of the 3D-printing techniques fused filament fabrication, stereolithography and mutli-jet modeling (from top to bottom, illustrations taken from: www.additively.com)	8
3.4	Deposition-based bioprinting methods for the fabrication of three dimensional structers of bioinks. Illustration adapted with permission. [102]	9
5.1	(A) CAD model of the replication master for the manufacturing of the μ F-device. (B) Magnified channel structure with the four measuring chambers of varying channel height (100, 600, 1000, and 1500 μ m) (C) Photograph of the assembled device on the deck of the liquid handling station. The LHS-tips dispense the samples directly into the channel structures eight at a time. (D) Visualization of the absorption data gained in the four measuring chambers of one channel structure to illustrate the absorption gradient due to the differing channel heights.	20
5.2	(a) Lysozyme absorption values measured in the μ F-device plotted against the channel height. Exemplarily determination of the slope m of the regression line. The reference concentration of this sample measured in Nanodrop 2000 was 4.9 mg/mL. (b) Calculated lysozyme concentrations based on μ F-device absorption data plotted against set concentration values with corresponding standard deviations. (c) Tabular listing of theoretical lysozyme concentrations, concentrations based on Nanodrop measurements and concentrations based on μ F-device measurements with corresponding standard deviations.	23
5.3	Elution profiles of mAb and CytC with a gradient from 0–1.25 mM NaCl in 10 CV. Plotted are absorption values at 280 nm measured in the μ F-device in the four respective measuring chambers with a height of 100, 600, 1000 and 1500 μ m. Absorption values of mAb are plotted as blue circles, absorption values of CytC are plotted as red circles. The absorption values were fitted with a nonlinear Gaussian fit (blue and red lines).	25

5.4	Chromatograms of the four screened elution gradients of mAb and CytC absorption values. Illustrated are absorption values with related standard deviations measured in the μ F-device in a measuring chamber height of 1000 μ m and absorption values measured in MTP after dilution. (a) Gradient from 0 – 1.25 mM NaCl in 10 CV, highlighted are fraction 4, 9 and 13 which have been further investigated; (b) gradient from 0 – 1 mM NaCl in 10 CV; (c) gradient from 0 – 0.75 mM NaCl in 10 CV; (d) gradient from 0 – 0.5 mM NaCl in 10 CV.	26
5.5	Absorption values with related standard deviations of fraction 4, 9 and 13 from mAb (a) and CytC (b) measured in the μ F-device plotted against channel height with regression lines and related slope values m . The grey area depicts the allowed deviation of 3 %. (c, d) Protein concentrations with related standard deviations of F4, F9 and F13 calculated based on μ F-device absorption values (dark colored) and based on MTP absorption values (light colored). The concentrations based on absorption values measured in the μ F-device were calculated with the slope method (equation 5.3).	27
5.6	Part (A) of this figure shows the replication master for the molding of the microfluidic chips used for the presented experiments. The channel system consists of one outlet channel (OUT) and seven inlet channels (IN 1–7) that differ in width and are decreasing in height. Part (B) of the picture, this step-wise decrease is shown at the example of the channel 2 that allows experiments with different optical path length.	39
5.7	Photograph of the experimental setup on the liquid handling station. Shown here are troughs for the reagents (A), centrifugal tubes (B), and deep-well plate (C) for the storage and processing of the polymer samples. The modified carrier (D) for the microfluidic chip that allows the fixation of the LED-spot underneath the chip and a reversible connection between the channel system and the pipetting needles of the liquid handling arm (E). The magnified detail shows the irradiated channel section.	40
5.8	Coefficient plot to illustrate the impact of irradiation time t , irradiance I , channel height h (optical path), and combined factors on the residual monomer content (RMC in %) for the 26 executed experiments of photoinitiated miniemulsion polymerization in microfluidic channels. The error bars represent the \pm 95 % confidence interval.	41
5.9	Contour plot set to illustrate the predicted development of the residual monomer content (RMC). (A–C) depending on the irradiance (25–100 %) and the channel height (200–1000 μ m) for three different irradiation times (from left to right: $t = 10, 35, 60$ s). (D–F) Depending on the irradiation time (10–60 s) and the irradiance (25–100 %) for three different channel heights (from left to right: $h = 200, 500, 1000$ μ m).	44

-
- 5.10 SEM images of the resulting polystyrene particles from experiments in the 200 μm channel with a RMC of 0 % but different configurations ((A): I = 50 %, t=60 s, 2.2wt% Irgacure[®] 819; (B): I = 100 %, t = 35 s, 1.8 wt% Irgacure[®] 819; (C): I = 75%, t = 60 s, 3.0 wt%) Irgacure[®] 819). Scale on the left image: 2000 nm, on the middle and right image: 1000 nm. 48
- 5.11 SEM images of the resulting polystyrene particles from experiments in the 1000 μm channel with an irradiation time of 60 s and an irradiance of 100 and 17 % RMC. The concentration of the initiator varies from 0.5 wt% on the (A) to 3.0 wt% on the (B). Scale: 1000 nm. 48
- 5.12 Particle size distribution of the resulting polystyrene particles from experiments in the 1000 μm channel with 100 % irradiance and a photoinitiator concentration of 0.5 wt% (black squares) respectively 3.0 wt% (red squares). 49
- 5.13 Workflow of automated FISH labeling of biofilms cultivated in flowcells. E. coli and B. subtilis biofilms were grown in a PDMS/glass hybrid cultivation flowcell. The PDMS channel structure was sealed with a coverglass to enable microscopic examination of the biofilms. The flowcell was connected to the tubing via standard cannulas. A medium flow of 50 $\mu\text{L}/\text{min}$ was applied with a syringe pump. The various steps of FISH labeling procedure were carried out fully automated with up to nine flowcells in parallel on a liquid handling station (LHS). The center shows a photograph and a schematic representation of the working deck equipped with the various stations necessary for the FISH procedure. The fluorescence signal of the labeled cells in the channel was measured with the on-deck microplate reader on the LHS. Afterwards, the results were additionally confirmed by epifluorescence microscopy. An exploded view of the newly developed interface is shown on the right. One cartridge hosts up to three chips which are connected to the inlet and outlet structures via stainless steel capillaries. The pipetting needles form a tight but reversible connection to the inlet structure. The scheme below shows the cultivation flowcell with the 13 measurement points for automated fluorescence analysis in the microplate reader indicated as circles. 64

- 5.14 Epifluorescence micrograph of *B. subtilis* (A, D, G), *E. coli* (B, E, H) and mix species (C, F, I) biofilms. *B. subtilis* and *E. coli* were hybridized with probes LGC354B-A488 (colored in green) and Ent-A546 (red), respectively. Each of images A-C is a composition of nine micrographs which were recorded sequentially and composed afterwards [180]. As a consequence, the entire channel width is depicted in the images giving an overview of the macroscopic structure of the flowcell biofilms. *E. coli* was forming a flat biofilm particularly at the walls of the flow cell, whereas *B. subtilis* grew in filamentous streamers. In the mixed species biofilms the individual structures seemed not to be strongly affected by co-cultivation. (D) Detailed view of a *B. subtilis* biofilm. The Bacillus cells formed a dense network structure. (G) The biofilm structure could be resolved at the single cell level with the 1000-fold magnification. (E) Cloudy *E. coli* biofilm in 200-fold magnification. Larger particles sometimes stuck in the biofilms interfering with the photometric fluorescence measurement (B and E). (F) Mixed species biofilm with *Bacillus* cells forming a dense mesh and *E. coli* cells growing inside the network. (I) Close up of the mixed species biofilm clearly demonstrating a successful one-step double hybridization of the gram positive *B. subtilis* and the gram negative *E. coli* in a mixed species biofilm. 65
- 5.15 Mean fluorescence values of three parallel cultivated biofilms normalized to the respective mean background value. For each flowcell the signal was averaged over the 13 measurement points. Error bars reflect the deviation between three cultivation flowcells. The excitation wavelengths for detection of the dyes were 490 nm, 556 nm and 358 nm for Alexa 488, Alexa 546 and DAPI, respectively. The emission was determined at 530 nm, 588 nm, and 461 nm for Alexa 488, Alexa 546 and DAPI, respectively. Note that the *E. coli* and *B. subtilis* cultures could be reliably identified by the automated fluorescence measurements. 66
- 5.16 (a)/(b)/(c) Topographic representation (6.7 mm x 3 mm, height = 100 μm (red colored)) of the 3D structure of mixed species (a), *E. coli* (b) and *B. subtilis* (c) biofilms captured by means of OCT during automated FISH procedure. For each biofilm images were acquired right before FISH was conducted, after fixation, permeabilization, hybridization and washing. Slight biofilm detachment was observed throughout the whole procedure. But altogether the structural integrity could be preserved for all three model biofilms. (d) Epi-fluorescence micrograph of mix species biofilm. Biofilm features visualized by OCT are easily recognizable by epi-fluorescence microscopy after FISH. 67
- 5.17 Catalysed reporter deposition fluorescence *in situ* hybridization (CARD-FISH) image of a cultivation flowcell, inoculated with native biofilm and cultivated for four weeks. Archaea (ARCH 915) are visualized in green (Alexa 488), bacteria (EUB 338-I) in red (Alexa 546) and DAPI blue. . . . 68

5.18	Schematic representation of the process steps for the execution of the case study. Step A – Printing procedure with the production of a printed sacrificial mold. The resultant gap was filled with bioink, followed by UV-polymerization. From this point on, the process was executed on the liquid handling station. Step B – Removal of the sacrificial mold with cooled water in a cleaning procedure. Step C – Preparation of polymerized and cleaned hydrogels for the assay by equilibration. Meanwhile the stop solution was provided in a deep well plate. Step D – The execution of the enzymatic assay was started with the filling of the hydrogel-loaded wells with ONPG solution. Samples were drawn and transferred to the provided stop solution. Step E – The samples were transferred to a UV microplate and the absorption is measured at 410 nm. The gained data leads to the determination of reaction rates.	81
5.19	Photographs of the <i>Biomaker</i> and the extrusion unit. (A) Overview of the modified printer named <i>Biomaker</i> with the extrusion unit mounted on the printhead (1), a template for the positioning of the multiwell plate (2) and the acrylic glass body which replaces the original wooden body. The “ulticontroller” (4) can be used for direct control of the printing process. (B) Close-up view of the extrusion unit. The syringe is fixated in a cartridge (1) on the extruder. The additional printed parts (2) enclose the plunger of the syringe and enabled retraction movements. Together with the cartridge, the linear bearings and rods (3) allowed the precise printing position. The extrusion was executed by the movement of the stepper motor (4).	84
5.20	Photographs of printed models generated from STL files, both models were printed with a dispensing tip of 0.41 mm inner diameter (A) Scaffold printed with 30 %(w/w) Kolliphor (B) model of a human ear (after: http://www.thingiverse.com/thing:105808) printed with Nivea Soft Creme.	85
5.21	Representation of the reaction rate determination and the resulting Michaelis-Menten plot. (A) The initial slope of the measured production of ONP over the observed time span corresponds to the reaction rate of the encapsulated enzyme for the present condition. In the shown example, an initial ONPG concentration of 40 $\mu\text{mol/mL}$ at pH 3, 5 and 7 was examined. (B) The calculated reaction rates were plotted over the respective ONPG concentration which leads to a typical Michaelis-Menten saturation curve for all examined pH values.	86
5.22	Comparison of the enzyme activity after different storage conditions. The assay was executed with 10 $\mu\text{mol/mL}$ ONPG. Storing the hydrogels up to 30 days in moist or dry conditions preserved up to 65 % of the activity determined after one night of moist storage.	87

5.23	Photographs of printed hydrogel structures from PEG-DA ₇₅ (A-C) and PEG-DA ₇₅ Lys _{1.55} (D). Underexposure led to insufficient adherence of the hydrogel at the build platform (A). Unbalanced ink application and air bubbles resulted in partially defective structures (B) . Flawless hollow hydrogel cylinders as they have been used in the presented study (C). PrintLoading cylinders with noticeable turbidity due to incorporated protein (D).	102
5.24	PostFabLoading of PEG-DA based hydrogels with lysozyme: Relative protein uptake of hydrogels with varying mass fraction of PEG-DA at pH 7 (A), with 75 % PEG-DA and varying mass fraction of the co-monomer acrylic acid at pH 7 (B) and different loading pH values for 75 % PEG-DA and 15 % acrylic acid (C)	104
5.25	Relative protein release under the influence of 0 M NaCl in the release buffer (PostFabLoaded hydrogels from 75 % PEG-DA (A), PrintLoaded hydrogels from 75 % PEG-DA (C) and PostFabLoaded hydrogels from 75 % PEG-DA and 15 % AA (E)) and under the influence of 0.15 M NaCl in the release buffer (PostFabLoaded hydrogels from 75 % PEG-DA (B), PrintLoaded hydrogels from 75 % PEG-DA (D) and PostFabLoaded hydrogels from 75 % PEG-DA and 15 % AA (F))	106
5.26	Comparison of the relative activities of released lysozyme relating to the loading method and ink composition.	108
5.27	Analytical SEC comparing released lysozyme form PostFabLoading and PrintLoading for PEG-DA based hydrogels without acrylic acid at pH 9 and 0 M NaCl	109

List of Tables

5.1	Variation of the cause variables for the photopolymerization of styrene in microfluidic channels	41
5.2	Composition of 25 mM multicomponent buffer with a linear buffering range from pH 3 to pH 9 calculated according to [231]. The used buffer substances are displayed with the corresponding pKa value and molarity.	98
5.3	Composition of bioinks. The percentage of a component %(w/w) refers to the total weight of all components. The lysozyme stock solution was prepared by dissolving 6.45 %(w/w) in ultrapure water.	99
5.4	Adapted printing parameters for the various ink compositions (see Table 5.3).	99

A Publications

Paper

Carsten P. Radtke, Nils Hillebrandt, Jürgen Hubbuch (2017)

'The *Biomaker*: An entry-level Bioprinting Device for Biotechnological Applications'
Journal of Chemical Technology and Biotechnology. DOI: 10.1002/jctb.5429.

Carsten P. Radtke, Marie-Therese Schermeyer, Yün Claudia Zhai, Jacqueline Göpper, Jürgen Hubbuch (2016)

'Implementation of an analytical microfluidic device for the quantification of protein concentrations in a high-throughput format'
Engineering in Life Sciences. Vol. 16, pp. 515-524.

Carsten P. Radtke, Michèle Delbè, Michael Wörner, Jürgen Hubbuch (2016)

'Photoinitiated Miniemulsion Polymerization in Microfluidic Chips on Automated Liquid Handling Stations: Proof of Concept'
Engineering in Life Sciences. Vol. 16, pp. 505-514.

Jörg Kittelmann, **Carsten P. Radtke**, Ansgar Waldbaur, Christine Neumann, Jürgen Hubbuch, Bastian E. Rapp (2014)

'Microfluidics on liquid handling stations (μ F-on-LHS): A new industry-compatible microfluidic platform'
Proceedings of SPIE - The International Society for Optical Engineering. Vol. 8976.

Ansgar Waldbaur, Jörg Kittelmann, **Carsten P. Radtke**, Jürgen Hubbuch, Bastian E. Rapp (2013)

'Microfluidics on liquid handling stations (μ F-on-LHS): an industry compatible chip interface between microfluidics and automated liquid handling stations'
Lab on a Chip. Vol. 13, pp. 2337-2343.

Talks

Carsten P. Radtke, Nils Hillebrandt, Jürgen Hubbuch (2017)

'Entry-Level 3D-(Bio-)printing for LHS based HTE'

4th International Meeting on High-Throughput Process Development (HTPD)

Toledo, Spain.

Carsten P. Radtke, Jörg Kittelmann, Jürgen Hubbuch (2014)

' μ F-on-LHS – Integration of Microfluidics in high throughput Experimentation'

10th PhD Seminar on Chromatographic Separation Science (SOCS)

Egmond aan Zee, The Netherlands.